ELECTROSPINNING OF MILK PROTEINS WITH PULLULAN

By

SERIFE AKKURT

A dissertation submitted to the

School of Graduate Studies

Rutgers, The State University of New Jersey

In partial fulfillment of the requirements

For the degree of

Doctor of Philosophy

Graduate Program in Food Science

Written under the direction of

Kit L. Yam and Peggy M. Tomasula

And approved by

_____

_____

_____

_____

New Brunswick, New Jersey
October, 2018

ABSTRACT OF THE DISSERTATION

ELECTROSPINNING OF MILK PROTEINS WITH PULLULAN

by SERIFE AKKURT

Dissertation Directors:
Kit L. Yam and Peggy M. Tomasula

Electrospinning has been used to produce nonwoven mats from the nano- and microscale fibers by applying an electric field to a viscous polymer solution. Milk-based proteins (nonfat dry milk and caseinates) cannot be electrospun, they must incorporate with an electrospinnable, food- grade carrier polymer to produce edible fibers. To obtain the fibers, polymer solutions must meet some criteria specifically viscosity and molecular chain entanglement, which is a necessity for a successful electrospinning process. However, many proteins, which can self-assemble in 3-D structure by intermolecular interactions including hydrogen bonds, hydrophobic, and electrostatic interactions, have lack of chain entanglements that can be improved by their dissolution in organic polar solvents which is not for food use.

This study demonstrates the electrospinning of nonfat dry milk (NFDM) and caseinate proteins (CAS) blended with an electrospinnable polysaccharide, pullulan (PUL) to produce food-grade ultrafine fibers and fibrous mats. It also evaluates the theoretical mechanism behind the inability to electrospin these milk-based proteins by investigating the relationship between solution rheology and fiber formation and morphology. First, neat NFDM, CAS, and PUL have to fully dissolve in aqueous solutions and governing

parameters need to be optimized. Based on these optimized conditions, NFDM and CAS can be electrospun into the ultrafine fibers and fibrous mats as they blended with PUL.

The chemical and physical properties of NFDM and CAS blended with PUL fibers were examined using SEM micrograph, FTIR-ATR spectra, and the mechanical properties of their fibrous mats. Furthermore, bioactive living cell, *Lactobacillus Rhamnosus* GG, was chosen as a model application to encapsulate within the electrospun CAS: PUL blend fibrous mats to evaluate its recovery.

This study establishes the fundamental principles for the NFDM- and CAS-based nanofibers and nanofibrous mats for future studies. The nanofibrous mats possess smaller diameter fibers increasing the surface area-to-volume ratio and the porosity between the fibers. Therefore, the motivation of this study is to use these food-grade fibrous mats in many food applications including controlled nutrient delivery or flavor enhancement, sensitive bioactives encapsulation, texture improvement, functional foods, and beverages contribute to health-promoting foods.

ACKNOWLEDGEMENT

I better first express my special thanks and deep regards to, Dr. Kit L. YAM who began this journey with me as my advisor. He always made me aware of my progress during this doctoral journey. He taught me how to learn a lesson whenever I was not successful and not repeat mistakes. He has been a great research advisor who has coped with my stress, for inspiring me continuously with his guidance by teaching his scientific knowledge and sharing real-life experiences. Also, he always supported and encouraged me to design this dissertation. He helped me immensely to improve my critical thinking, communication, and writing skills. All of this has guided me to stick to my goal towards the right direction. I would not have accomplished my doctorate education without his guidance.

I appreciate the plentiful support and sincere thanks to Dr. Peggy M. Tomasula for being a co-advisor with her encouragement and critical feedback during my research. I have grown in various aspects through her instruction, enthusiasm, and standards in my academic career. Throughout my research, she has provided innovative ideas, specific models, and encouragements, which have all made me a self-starter and more organized. I am inspired by her valuable guidance to write this high-quality dissertation. This thesis would not have been possible without her help.

I am indebted and deep regards to Dr. LinShu Liu for all his support in both research and professional life. He has provided a great guidance by sharing his scientific knowledge as well as his real-life experiences. He always pushed me to be a better version of myself in my career and professional life.

I am also indebted to Dr. Laetitia Bonnaillie for providing me the necessary facilities and knowledge to complete the present work. I also appreciate her support and guidance. I sincerely thank her for the help provided anytime whenever I need to.

I would like to sincerely thank John Renye, Audrey Thomas, Raymond Kwoczak, John Mulherin, and Joseph Uknalis who helped me to conduct and make experiments and learn how to use machinery. They also provided their valuable guidance in a friendly work environment. I also appreciate the opportunity to work with the whole group in Dairy and Functional Foods Research Unit (Agricultural Research Service, USDA, Wyndmoor, PA). This group has been a source of friendships who provided their help and guidance in data interpretation, analysis, and guidance in the laboratory environment.

I would like to thank my research committee members, Dr. Kit L. Yam, Dr. Peggy M. Tomasula, Dr. LinShu Liu, and Dr. Paul Takhistov for their continuous help in all aspect of my research.

I am indebted to many of my colleagues for all their help, support, and inspiration to create a fun environment in which to learn and grow. I am especially grateful to Minqian Wang and Jamshed Bobokalanov. They have always been very supportive whenever I went through hard times.

Lastly, and most importantly, I would like to give special thanks and deep regards to my husband and my parents in Turkey for all their love, motivation, support, and continuously encouragement. There is no way I could have taken on this journey without their unconditional love and support. I would also like to thank my husband David, for offering endless positivity, incredible motivation, and encouragement. In addition, I cannot

forget the level of support I have received from all my loving, supportive, and encouraging friends, especially Esin, Hande, Hope, Humeyra, Kiswa, and Mualla.

This thesis is dedicated to people who touched my life and left many sweet reminiscences in my heart.

TABLE OF CONTENTS

LIST OF TABLES

LIST OF ILLUSTRATIONS

CHAPTER 1

Introduction

Electrospinning is a technology to produce a nonwoven mat from fibers on the micro- and nano-scale by applying an electric field to a polymer solution or polymer melt. It has become a versatile and valuable technique for the fabrication of long polymer fibers with diameters ranging from 0.01 μm to 10 μm. As the fibers have small pore sizes with an interconnected structure and a large surface area per unit volume, the technique has been employed in many applications such as air filtration (Chung et al., 2004), tissue engineering (Huang et al., 2003), drug delivery (Kenawy et al., 2002), and wound dressings (Katti et al., 2004).

The basic setup of electrospinning process consists of four main components which are a pump, a syringe to contain a polymer solution linked to a needle, an external voltage supply, and a grounded collector or counter electrode for collecting the fibers in a fibrous mat. The solution forms a pendant drop through a capillary tip of the syringe. The drop is balanced at the tip by the surface tension of the solution and is ejected when an electrostatic force overcomes the surface tension (Shenoy et al., 2005; Greiner and Wendorff, 2007). The applied electric field makes the pendant drop to form into a cone shape, called Taylor cone, which then forms a continuous jet. As the jet moves towards the grounded collector, it becomes narrower and forms an unstable whipping leading to continuous randomly oriented fibers in the form of a fibrous mat by accumulating on the grounded collector.

The electrospinning process is governed by both solution properties and processing parameters. To obtain nanofibers, polymer solution must meet several criteria. The polymers should be highly soluble and have random coil structure in the solvent and of

concentration in which the polymer chains can entangle and stretch. It must have a minimum viscosity to maintain an electrified jet through the molecular chain entanglements to form the continuous electrospun ultrafine fiber without a jet breakup (Greiner and Wendorff, 2007; Kriegel et al., 2008; Schiffman and Schauer, 2008). If the viscosity is too low, electrospraying occurs instead of the electrospinning, which is causing the solution to drip from the tip of the needle (Shenoy et al., 2005). If it is too high, the viscosity restricts the flow of the polymer solution from the tip of the syringe needle due to the solidification of the viscous solution (Subbiah et al., 2005). Surface tension and electrical conductivity may also affect the processing and the fiber morphology. The surface tension of the polymer solution determines the amount of charge repulsion needed to initiate the formation of the Taylor cone and the polymer jet (Alborzi et al., 2010; Liu et al., 2016). The electrical conductivity of the solution governs the stability of the static charge that develops on the surface of the pendant droplet, which establishes an adequate electrostatic force to overcome the surface tension of the droplet to form the polymer jet (Alborzi et al., 2010; Liu et al., 2016). In addition to the solution properties, some of the key parameters of the processing including voltage, distance from the tip of the needle to the collector, and the flow rate may affect the processing and the fiber morphology.

The electrospinning of synthetic and water-soluble polymers dissolving in organic solvents has been extensively studied and reviewed in the literature for biomedical and other applications (Huang et al., 2003; Tan et al., 2005; Wendorff, Agarwal, and Greiner, 2012). However, there are a few examples of food-based polymers including polysaccharides and proteins electrospun from their aqueous solutions for food use. Electrospinning of natural polymers requires to have a minimum viscosity which is a

function of concentration, thus in effect the molecular weight (M_w) of polymer which can facilitate the chain overlap and entanglements. For example, Stijnman et al (2011) reported that the aqueous solutions of polysaccharides produced electrospun fibers when the solutions have the concentrations ranging between 10 and 20 wt% and present a weak shear-thinning behavior at the shear rate less than 1000 s^{-1} (Stijnman, Bodnar, and Hans Tromp, 2011). Under these conditions, the food-grade, electrospun fibers were formed from dextran and pullulan (PUL) solutions, whereas pectin, gum arabic, alginate, and many more polysaccharides in aqueous solutions were not electrospun due to their strong shear thinning behavior, high viscosity, and compact, globular-like chains causing a lack of chain entanglements which play a crucial role in the electrospinning process (McKee et al., 2004; Stijnman et al., 2011).

Proteins dissolved in water are challenging to electrospin because of their 3-D structures including complex secondary (i.e. alpha-helix, βeta-sheets), tertiary structure, and/or globular structure, which have less and weak interactions with each other to stretch and entangle under an electric field. Specifically, nonfat dry milk (NFDM) and its derivatives, pure calcium (CaCAS) or sodium (NaCAS) caseinates dissolved in water cannot be electrospun alone due to their complex macromolecular and strong inter- and/or intramolecular forces (Xie and Hsieh, 2003; Nieuwland et al., 2013). CaCAS forms a colloidal structure in the presence of Ca^{2+} by hydrophobically linked phosphoserine groups (Pitkowski, Nicolai, and Durand, 2009; Thomar et al., 2012; Tomasula et al., 2016), causing the lack of molecular entanglements (Nieuwland et al., 2013). NaCAS dissolved in water exists as small protein strands and agglomerates, limiting the protein chain entanglements at lower viscosities (McMahon and Oommen, 2013). At higher viscosities,

it can form the jamming of the small protein pieces, which causes a sharp increase in viscosity, challenging its processing (Thomar et al., 2012; Tomasula et al., 2016). Also, their high electrical conductivities may constrain the formation of electrostatic forces among the protein molecules under the electric field.

To electrospin proteins, an approach is to use organic solvents which have a good solvent quality to interrupt both intra- and intermolecular interactions, dissolving in a random coil conformation. Using organic solvents including hexafluoro-2-propanol (HFIP), trifluoroethanol (TEE) and/or aqueous acids (40 % acetic acid or 98 % formic acid), collagen and gelatin (Huang et al., 2004; Ki et al., 2005; Zhang et al., 2006; Chong et al., 2007; Son et al., 2013; Aduba et al., 2013; Xue et al., 2014; Xu et al., 2015; Wang et al., 2016), silk (Kawahara et al., 2008), fibrinogen (Min et al., 2004), and hemoglobin (Barnes et al., 2006) produced electrospun fibers for the biomedical and other applications. However, using these solvents is not applicable for food applications.

To overcome the inability to electrospin aqueous protein solutions, another approach is an incorporation of a carrier polymer such as polyethylene oxide (PEO) or polyvinyl alcohol (PVA) for zein and NaCAS (Nieuwland et al., 2013), and PUL for both pectin (Liu et al., 2016) and CAS proteins (Tomasula et al., 2016), which such cannot be electrospun alone. The carrier polymers can disrupt the 3-D structure of proteins and promote the chain entanglements of the protein molecules along under the electric field. It is also assumed that they can lower the surface tension and electrical conductivity of the blended solutions to ease the electrospinning of protein molecules (Alborzi et al., 2010; Nieuwland et al., 2013). Also, non-food carrier polymer has to be used as low as possible to produce fibers from proteins to use. For example, PVA or PEO, as an electrospinnable

carrier, is employed with the ratio of proteins of 1:1 to 1:20 for protein-based nanofibers including collagen, whey protein isolate (WPI), elastin, soy protein, silk, and keratin in biomedical applications (Huang et al., 2001; Buttafoco et al., 2006; Vega-Lugo, Cristina, and Lim, 2009; Ramji and Shah, 2014). However, these nanofibers cannot be used in foods because of the incorporation of non-food carrier polymers.

A few proteins and polysaccharides dissolved in aqueous solutions can be readily electrospun and acceptable for food use. PUL, an electrospinnable polysaccharide (Kong and Ziegler, 2014), is used as electrospinning carrier for whey protein concentrate (López-Rubio et al., 2012), pectin (Liu et al., 2016), and caseinate (CAS) proteins (Tomasula et al., 2016). PUL is a linear and non-charged food-grade polysaccharide with repeating units of both maltotrioses linked by α-(1→6) linkages and glucopyranose connected by α-(1→4) glucosidic bonds (Kong and Ziegler, 2014; Tomasula et al., 2016). Tomasula et al (2016) shortly reported that edible electrospun nanofibrous mats were produced from aqueous CAS only by incorporating PUL (Tomasula et al., 2016). The impacts of solution properties on molecular configurations or entanglements and their correlation with electrospinnability of CAS have not been extensively studied. These studies both examined the microstructure, thermal properties, and fiber morphology but not the relationship between solution viscosity and the molecular entanglement as well as fiber formation.

Studies have been shown empirically that electrospun fiber formation is correlated with the amount of polymer chain entanglements which results from molecular weight and viscosity as a function of concentration. For the polymers with molecular weight, M, above the entanglement molecular weight, M_e, the entanglement concentration (c_e) is the minimum concentration required for the chain entanglements to facilitate the

electrospinning to observe the fiber. Wool (1993) theoretically predicted that zero shear viscosity (η_0) was proportional to $M^{3.4}$ and $c^{3.5}$ for linear and neutral random coil polymers (Wool, 1993). Morris et al (1981) reported that specific viscosity (η_{sp}) was proportional to $c^{3.3}$ for the random coil polysaccharides including dextran, alginate, lambda-carrageenan, and hyaluronate (Morris et al., 1981). Even though these experimental and theoretical studies are related to the association between the rheological properties of polymer solutions and the chain entanglement, any study regarding the relationship between the rheology of milk-based proteins blended with PUL solutions and the point at which molecular chain entanglements occur has been reported in the literature.

Our aim is to establish a correlation between viscosity and fiber formation in the electrospinning of aqueous NFDM and CAS solutions with and without PUL. We hypothesized that the concentrations of the milk proteins-based solutions must exceed the c_e for the fiber formation. A stable jet is needed for a successful electrospinning and it is only formed when the sufficient chain entanglements occur. The increase in the polymer concentration stabilizes the jet, and then fiber formation. Therefore, the chain entanglements increases with increasing the polymer concentration have been considered to correlate to the electrospinnability of polymers and their fiber structures. Because the electrospinning of NFDM and CAS solutions was challenging, the solutions were electrospun under a variety of conditions such as increasing concentration and pH with and without adding PUL carrier to establish the correlation between the solution rheology, specifically, viscosity and molecular entanglements, and the electrospinnability of neat milk-based proteins in aqueous solutions. The effect of PUL carrier on the solution viscosity, molecular entanglements, and fiber morphology of the proteins was examined.

1.1 Impact of this project

The thesis is expected to have the following impacts: extend the ability to electrospin milk proteins, NFDM and CAS. Tomasula et al (2016) reported that CAS blended with PUL produced nanofibrous mats with an average diameter of 172 nm. This means that if the hypothesis of this study is achieved, not only creating edible nanofibrous mats from milk-based proteins can be sharply boosted, but they can also be potential candidates for the encapsulation of bioactive compounds to contribute to health-promoting foods in addition to the nutrition properties of milk-based proteins by itself. The mats can carry more bioactive compounds than edible films and coatings because of their higher surface area-to-volume ratio and pores in their 3-D structures.

The importance of this technique: The surface area-to-volume ratio will be incredibly increased for the electrospun ultrafine fibers obtained from the polymers as the diameters of the fibers are reduced from the micrometers to the nanometers. Therefore, the encapsulation of the bioactive compounds within the nanofibrous mats for food use and their mechanical properties can be improved compared to other known forms of materials such edible films and coatings (Tomasula et al., 1998; Tomasula et al., 2003; Dangaran, Tomasula, and Qi, 2009; Bonnaillie et al., 2014). Researchers have reported that the electrospun fibers have a very high surface area-to-mass ratio ranging from 500 to 10 m^2/g for the diameters from 10 to 500 nm (Gibson et al., 2001; Zhang et al., 2005; Reneker and Fong, 2006), as well as surface area-to-volume ratio of about 1000 times than human hair (Greiner and Wendorff, 2007; Angammana and Jayaram, 2016). For instance, Figure 1 shows pullulan (PUL) nanofibers with diameters of 230 nm fabricated by the electrospinning of 12 wt% PUL in aqueous solution in this study, compared to a human

hair with a diameter of around 100 µm. If we calculated the surface area-to-volume ratio to demonstrate a rough minimum estimate, the ratio will be about 500 times increased compared to the human hair by assuming that the fiber has a cylindrical structure. The 3-D fibrous nature of these mats, with smaller diameter fibers increasing the ratio of surface area/volume and larger diameter fibers increasing the pore sizes between the fibers, is intriguing for their potential use in functional foods and beverages as ingredient carriers.

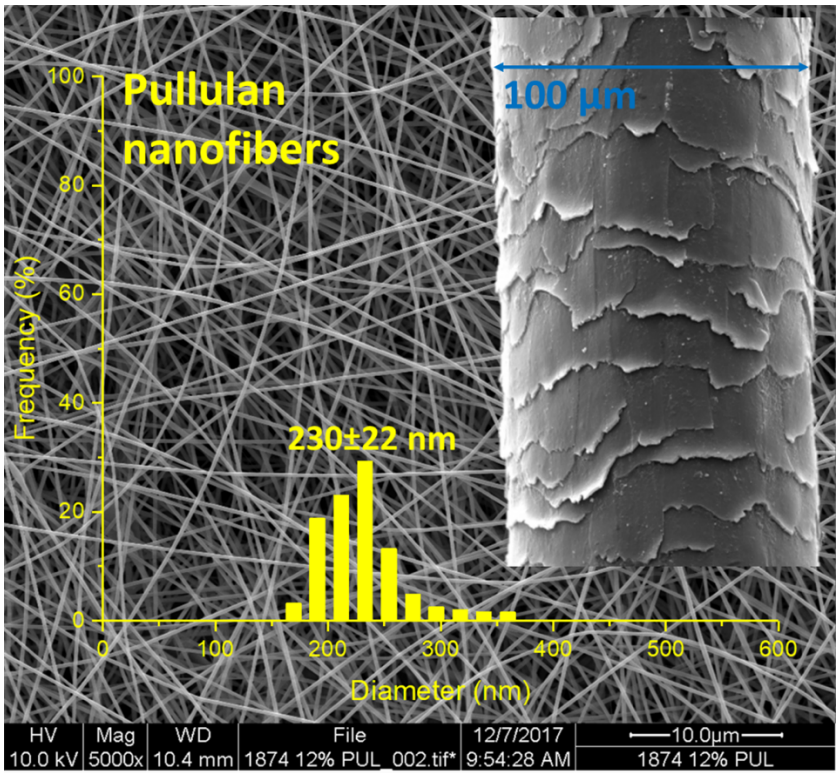

Figure 1: SEM images of polysaccharide fibers with a diameter of 230 nm obtained from 12 wt% pullulan (PUL) compared to a human hair piece with a diameter of about 100 µm (Magnified 5000×).

1.2 Overview of the thesis

The thesis is divided into 8 chapters which are Introduction (Chapter 1), theoretical background (Chapter 2), objectives of the study (Chapter 3), materials and methods (Chapter 4), results and discussion (Chapters 5, 6, and 7), and finally the conclusion and future work (Chapter 8).

- **In Chapter 2,** the theoretical background of the electrospinning technique and a basic electrospinning setup will be explained together with some mathematical equations of the process. A description of the proteins selected in this work are given and their electrospinning studies in the literature are reviewed.
  - ➢ This chapter supports the hypothesis and why the solution viscosity and the molecular chain entanglements are important for the electrospinning of milk-based protein solutions.
- **In Chapter 3,** the objectives and the sub-objectives of this study will be explained in detail.
- **In Chapter 4,** the methodology including materials, solution preparation, electrospinning setup, and characterization techniques will be mentioned.
- **In Chapter 5,** the first part of the experimental results on the electrospinning of the control samples including PUL, NFDM, and Ca- and NaCAS will be presented and discussed. Also, the correlation between the solution rheology, including concentration, viscosity, and molecular chain entanglements, and fiber morphology will be reported and discussed.
  - ➢ Objective 1 and Sub-objectives 1a and 1b will be explained in this chapter.
- ➢ **In Chapter 6,** the second part of the experimental results will cover the effect of PUL as a carrier on the electrospinnability of NFDM and CAS by considering the conclusion from Chapter 4.
  - ➢ Objective 2 will be explained in this chapter.

- **In Chapter 7,** the third part of the experimental results will be provided. It determines the effect of pH adjustment of CAS (pH 8, 9, and 10) blended with PUL on the solution viscosity and the fiber morphology.
  - Objective 3 and Sub-objectives 3a, 3b, and 3c will be presented in this chapter.
- **In Chapter 8,** conclusion and future work will be provided in this chapter.

CHAPTER 2

Theoretical Background

The principle, governing parameters, and setup system of the electrospinning technique are mentioned in the first two parts. A short review is provided a general idea how the system works, what parameters can influence the processing, as well as the importance of concentration dependence and polymer chain entanglements which play an important role for a successful electrospinning process. Electrospinning of food-grade biopolymers and their potential applications are summarized in the last part.

2.1 Ultrafine fibers

Ultrafine fibers are usually defined as fibers with diameters of less than 1000 nm with length-to-width ratios typically greater than 50. When the diameter of fibers is reduced, the ratio of surface area to volume of fibers will be increased. Their mechanical and surface functionalities can be improved compared to other forms produced from the same materials such as microfibers or films. Due to their unique properties, nanostructures have a wide range of use in biomedical applications such as wound dressings and tissue scaffolds, environmental applications such as filter media, as well as protective clothing. A research report on nanofibers was published that the global nanofiber market reached $203.2 and $276.8 million in 2013 and 2014, respectively, which represents the annual growth rate of 38 % between 2015 and 2020 (Business Communications Company, Inc. Research (BCC) report code NAN043D, 2016)

Ultrafine fibers can be fabricated by several techniques including template synthesis, drawing, phase separation, self-assembly, and electrospinning.

Template synthesis is similar to melt spinning or extrusion and produces polymer nanofibers by using a nanoporous membrane. In this method, molten polymer travels from an extruder and passes through a filter and spinneret (Tavares et al., 2014). After extruding the polymer, nanofibers are produced by solidifying solution. Nanometer tubules and fibrils of various materials including carbon, conducting polymers, metals and semiconductors can be produced by this technique. However, there are two disadvantages including small-scale production and discontinuous fibers.

Drawing, also known as cold drawing, is a simple technique to produce plastic fibers. The fibers are improved to have a higher tensile strength, lower elongation, and an increased oriented crystallization (Anton and Baird, 2001). In this process, an ultrafine fiber is pulled from a droplet of a polymer solution at a certain temperature and relative humidity and the solvent evaporates. To produce the fiber, the viscoelasticity of the polymer should have sufficient cohesiveness to support the deformation, following by the evaporation of solvent and solidification of fibers (Feng, 2003). However, this technique is limited to produce nanofibers only in laboratory scale because it forms discontinuous fibers.

Phase separation only produces a nanofiber matrix from limited specific polymers such as poly (L-lactic acid) (PLLA) (Ma and Zhang, 1999). In this technique, polymer gelation is the main mechanism and the solvent is extracted from the gel. Water is generally used to replace the solvent and removed by freeze-drying the gel. The porous structure of the membrane can be manipulated by controlling the polymer concentration, types of polymers and solvents, and temperature, whereas the fiber dimensions cannot be controlled because of the porous structure.

Self-assembly is a technique to produce a smaller nanofiber (even lower than 100 nm) by taking advantage of the intermolecular forces of polymers which can arrange themselves into different configurations such as hydrogen bonding, hydrophobic interactions. It can only produce the nanofibers on the laboratory scale and is limited to control the fiber diameters (Beachley and Wen, 2010).

These methods have various disadvantages. Drawing, for example, is the simplest method to produce ultrafine fibers, but the fibers are not formed continuously. Phase separation and self-assembly techniques require a longer preparation time compared to other methods. To overcome these downfalls, electrospinning technique has a potential to make a continuous nanofiber, of which dimension can be controlled, and it can be applicable for a large variety of polymers.

Electrospinning is a process or technique that allows production of fibers on micro-/or nano-scale by from an electrically charged jet of polymer solution or melt. This technique is very simple to operate, convenient, and has low operating cost (Huang et al., 2003; Greiner and Wendorff, 2007). Among the other techniques to produce ultrafine fibers mentioned previously, electrospinning has the only technique that can produce nanofibers with the length of several meters on an industrial scale. In addition, the diameter of fibers and fiber directions can be controlled to produce aligned fibers depending on solution properties, electrospinning setup, and process parameters.

The process was first patented by John F. Cooley (1902) and later by Anton Formhals in 1934 for commercial production of the filaments from polymers (Formhals, 1934). The early studies of electrospinning had been continued by many researchers (Taylor and Acrivos, 1964; Taylor, 1966; Baumgarten, 1971). In 1960's, the jet forming

process of a polymer solution was fundamentally studied by investigating the cone shape of the polymer droplets at the tip of the needle with the presence of the electric field (Taylor and Acrivos, 1964; Taylor, 1966). In following years, researchers focused on the characterization of electrospun nanofibers and the relationship between the process parameters and fiber morphology. For example, Baumgarten (1971) carried out the electrospinning of acrylic fibers and produced fibers with the diameter of 500 to 1000 nm (Baumgarten, 1971). Reneker's group and others reignited interest in electrospinning research (Chun and Reneker, 1996; Bosworth and Downes, 2011). Doshi and Reneker (1995) attempted to characterize the electrospinning of polyethylene oxide (PEO) by varying the solution concentration and applied voltage (Doshi and Reneker, 1995). Several applications developed soon after, mainly in biomedical, biosensor, encapsulation of bioactive compounds, and others (Kriegel et al., 2008; Sill and von Recum, 2008; Bhardwaj and Kundu, 2010; Haider, Haider, and Kang, 2015; Liu et al., 2016; Quirós et al., 2016; Mendes, Stephansen, and Chronakis, 2017; Mercante et al., 2017).

2.2 The Electrospinning Process

A basic laboratory electrospinning setup (Figure 2) requires four main components which are a pump, a syringe to contain the polymer solution linked to a needle, a power supply, and a grounded collector, which is usually a rotating drum for collecting the fiber in a fibrous mat. The drum is typically wrapped in an aluminum foil for collecting the fibrous mat. The syringe with the needle is attached to a base which moves horizontally from side to side to deposit the fiber onto the drum to a defined width. In the setup, the positive electrode is linked to the needle attached to the syringe filled with the polymer solution when the collector is grounded, as shown in Figure 2 (Tomasula et al., 2016).

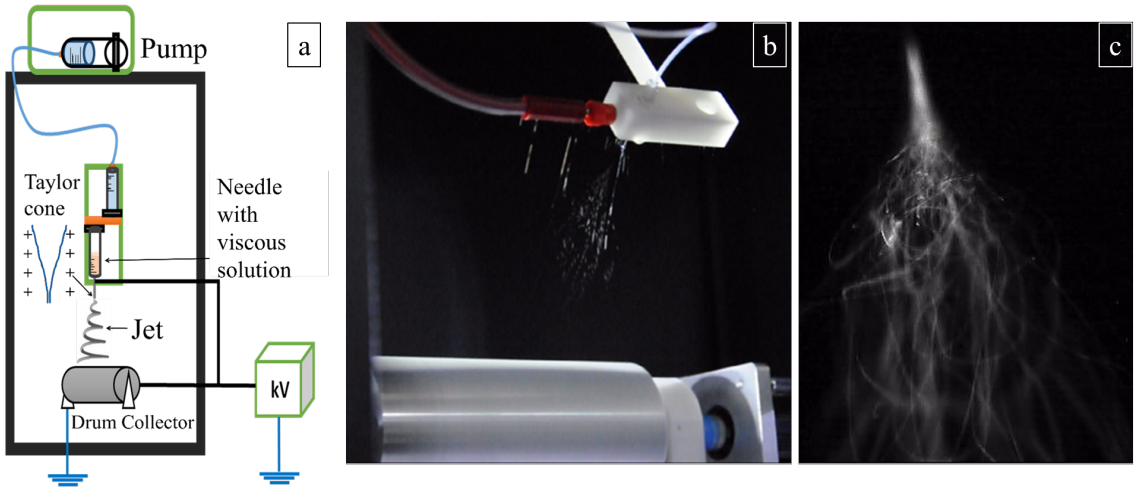

Figure 2: Diagram of electrospinning process (a), spinning taken by a high-speed camera (b and c).

A viscous polymer solution or melt is fed through a capillary tube or a small needle. Without applying the electric field, the viscous solution forms a pendant droplet at the tip of the needle or capillary tube due to the surface tension of the solution. The electrospinning process begins as the external voltage is applied to the solution. When the electrostatic force due to the applied voltage overcomes the surface tension of the pendant droplet, an electrified jet travels to the grounded collector. Then, it undergoes an instable bending and whipping occurs as it gets closer to the collector. This can be visually seen as spraying droplets or stretched strings of the solution, but it needs high-speed cameras to observe the rapid oscillation and bending, as shown in Figures 2b and 2c. During this journey through the distance, which is usually 10-20 cm, the solvent evaporates and leaves behind a charged fiber on the grounded collector (Deitzel et al., 2001; Huang et al., 2003).

The process can be divided into three regimes from the tip of the needle to the collector, as shown in Figure 3 (Taylor, 1966).

Regime I: The electrospinning process begins when a charged polymer solution or melt with sufficient molecular entanglements becomes a charged fluid jet in the presence

of an electric field. After the generation of the electric field, the conical formation occurs from a combination of charge repulsion of the droplet and the surface tension of the polymer liquid. When an electrical repulsion exceeds the surface tension of the solution, it leads to the formation of Taylor cone (Taylor 1964, 1966).

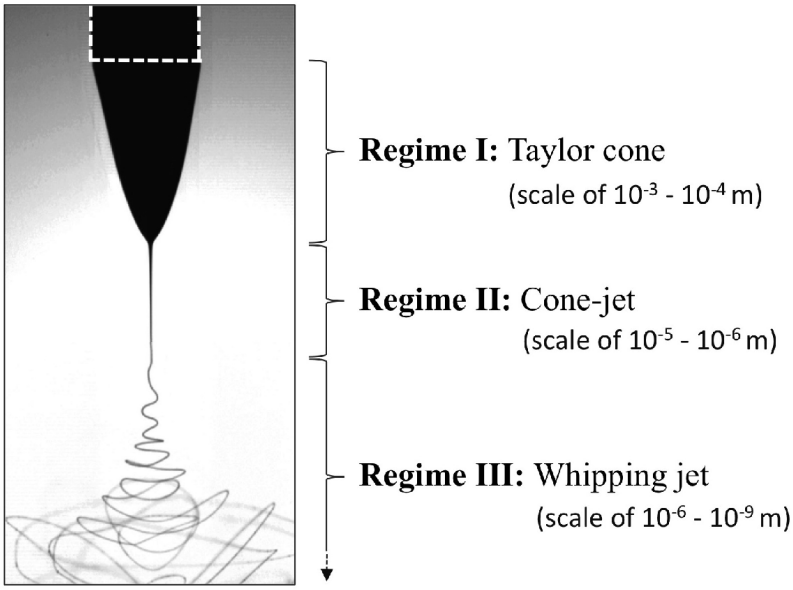

Figure 3: Three regimes, of the electrospinning process; (I) Taylor cone, (II) cone-jet and (III) whipping jet.

Regime II: Taylor cone shape turns into a continuous, stable jet due to the molecular chain entanglement and viscosity of the polymer solution. Then, the solution jet will remain stable for a certain distance following by a whipping motion. During the jet flight towards to the collector, the speed of the solution jet increases with the distance away from the needle tip and increasing with the applied voltage. Studies have been estimated the speed ranging from 0.5 to 5 m/s by either using the high-speed camera or laser doppler velocimetry (Bellan, Craighead, and Hinestroza, 2007; Reneker and Yarin, 2008).

Regime III: During the jet flight, the solvent evaporates and a coil with many turns is generated as the jet extensively stretches in response to the Coulomb repulsion of the

charge. Therefore, the evaporation of solvent along with the elongation of jet thins the jet when it closes to the counter electrode. Then, the jet leaves behind a charged and continuous fibrous nanofiber on the collector, and the fiber diameter is reduced to nanometer scale (Reneker et al., 2000; Shenoy et al., 2005; Reneker and Yarin, 2008).

The electrospinning process depends upon the combination of solution properties, processing conditions, and environmental conditions. The main factors of the polymer solution include viscosity which is a function of concentration and molecular weight of polymers, surface tension, and electrical conductivity. A jet formed from either low molecular weight fluid or less concentrated high molecular weight fluid breaks up into small droplets, known as electrospraying because less viscous solutions cannot provide enough polymer chain entanglement favoring the jet to elongate and stretch under the electric field (Greiner and Wendorff, 2007). However, the polymer solution with enough viscosity which in effect high molecular weight, which promotes molecular chain entanglements, does not break up and undergoes a bending instability that causes a whip-like motion between the capillary or needle tip and the grounded target. Some of the key parameters of processing involve voltage, the distance from the tip to the collector, and flow rate.

2.3 Effects of parameters on electrospinning

Even though the electrospinning setup and operating is straightforward, for widespread applications there are many unknown factors to be explained including: what parameters control the fiber formation, what/how fibers with uniform diameters can be obtained, how polymer molecular orientation can affect the electrospinnability of the polymer, what properties polymer solutions possess to fabricate nanofibers, and what other

parameters affect the resultant nanofibers. To form a continuous jet and ultrafine fiber during the electrospinning process is influenced by many interrelated variables, including solution properties, processing parameters, and environmental conditions. Solution properties include the polymer concentration and molecular weight, viscosity, electrical conductivity, surface tension, and the solvent ability, whereas processing conditions are usually the applied voltage, flow rate, and the spinning distance (Fong, Chun, and Reneker, 1999; Subbiah et al., 2005; Greiner and Wendorff, 2007) and is discussed in many reviews (Fong, Chun, and Reneker 1999; Subbiah et al., 2005; Greiner and Wendorff, 2007). Besides the solution and electrospinning parameters, temperature and humidity also affect the diameter and morphology of the nanofibers (Pelipenko et al., 2013; Huan et al., 2015).

There is a delicate balance between all these variables governing the electrospinning process and they are briefly discussed in the following sections.

2.3.1 Solution Properties

Rheological properties of the polymer solutions play a crucial role in determining the fiber forming ability of the polymer solution in the electrospinning process. The most important of the solution properties include the concentration dependence of viscosity, surface tension, and electrical conductivity which are varied by the types of polymers, their molecular weights, and solution concentration.

2.3.1.1 Solution viscosity

To achieve an effective electrospinning, the polymer must be highly soluble and have a random coil structure in the solvent. The random coil structure as a function of solution concentration is necessary for the polymer chains to entangle, and the solution concentration at which employs determines the rheological properties of solution (Wool,

1993; Shenoy et al., 2005). There is a concentration at which molecules can begin to overlap and entangle each other, which called critical concentration, and they sustain a continuous jet for fiber formation beyond this critical point. These critical concentrations for the electrospinning of common synthetic and water-soluble polymers have been extensively studied, but a few studies have been focused on detail for natural biopolymers such as proteins and polysaccharides.

The solution concentration should have a right viscosity forming a pendant drop at the tip of the needle to avoid restricting the flow of the solution from the syringe needle tip (Subbiah et al., 2005). The solution viscosity should be enough to maintain a jet formation in the electric field to form the continuous nanofiber (Tan et al., 2005; Greiner and Wendorff, 2007; Kriegel et al., 2008; Schiffman and Schauer, 2008). For example, Tomasula et al (2016) electrospun PUL solutions at the concentrations ranging from 5 to 15 wt% and reported their fiber morphology, as shown in Figure 4. PUL is a linear polysaccharide and have an ability to form electrospun fibers, described in detail in Section 2.4.4.2. Even though only droplets were generated from the electrospinning of the 5 wt% PUL solution, the 8 wt% PUL solution produced beaded fibers due to the electrospraying instead of electrospinning which results from the insufficient entanglement of the polymer chains, as shown in Figure 4B. However, increasing PUL concentration to 15 wt% favored the fiber morphology to have a bead-free and smooth structure compared to less viscous PUL solutions.

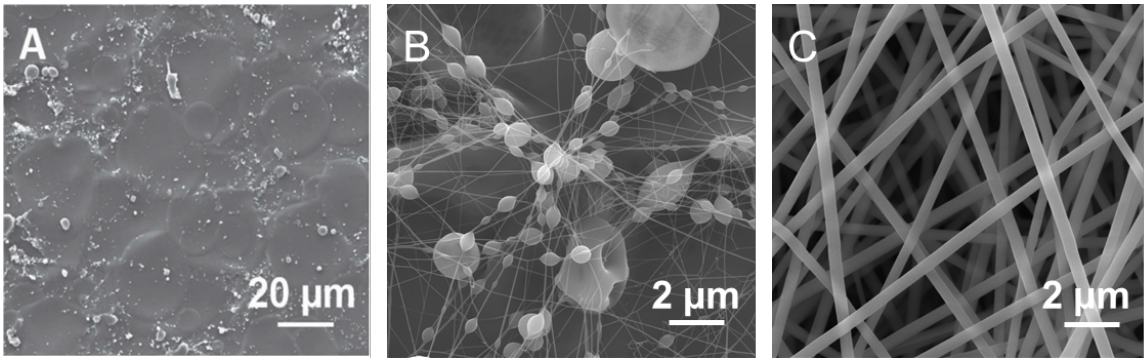

Figure 4: Scanning electron microscopy micrographs of the electrospun fibers obtained from 5, 8, and 15 wt% PUL solutions at 50 ºC. The processing conditions were the flow rate of 3 mL/h, the voltage of 20 kV. (A) 5 wt% PUL solution, (B) 8 wt% PUL solution, (C) 15 wt% PUL solution.

2.3.1.2 Molecular chain entanglement

Rheological properties of the polymer solutions play a crucial role in determining the ability of fiber formation of the polymer solution in the electrospinning process. Rheological behavior should be determined to decide whether the polymer solutions are in a viscosity range at where electrospinning process can be possible because the electrospinning process employs the polymer solutions or melts. Rheology is directly related to the polymer chain entanglements which are a function of the viscosity of polymer solutions. The number of entanglements (n_e) increases with increasing polymer chain length and molecular weight, M, due to the dependence of zero shear viscosity, η_0, which is attributed to the viscous electrospinning solutions (Lukáš et al., 2009). The η_0 is directly proportional to M or the polymer concentration (c), as shown in Figures 5A and 5B. The polymer solution without any entanglements shows Newtonian behavior.

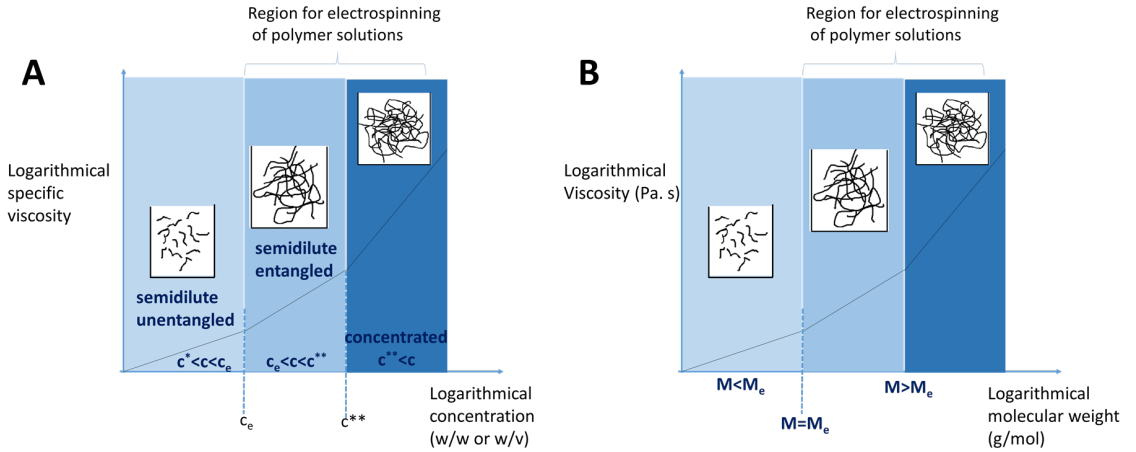

Figure 5: Concentration dependence of specific viscosity in polymer solutions with constant molecular weights (A); Molecular weight dependence of shear viscosity in polymer solutions or melts (Adapted from Agarwal et al., 2016).

It has been reported that a sharp upturn in the η_0 versus M plot occurs, resulting from corresponding to one entanglement per chain above critical molecular weight, M_c (Ferry, 1980; Wool, 1993). M_c relates to the molecular weight corresponding to the initiation of the chain entanglements at the η_0 and the entanglement molecular weight, M_e, referring to the average molecular weight between the entanglement junctions of the polymer chains. The M dependence of the η_0 changes from M^1 to $M^{3.4}$ for neutral, linear, random coil polymers (Wool, 1993). The details about the calculations and theoretical background are mentioned in the literature (Ferry, 1980; Wool, 1993). Bueche (1956) theoretically reported that the ratio of M_c to M_e also refers to the n_e which is about 2 (Bueche, 1956). The experimental results suggest that this ratio for many polymers ranges from 1.7 to 3 (Graessley, 1974).

Polymer solution concentration (c) or volume fraction (ϕ) and molecular weight influence the n_e. In dilute solutions resulting from the c below a critical concentration value, c^* ($c<c^*$), macromolecular chain overlap is absent due to low molecular weights, which is

not favorable for the electrospinning process. The dilute solution usually follows Newtonian behavior at low shear rates and the following equation is applied

$$\tau = \eta . \dot{\gamma} \qquad \text{Equation 1}$$

where τ shear stress (Pa), η is viscosity (Pa. s), and $\dot{\gamma}$ is the shear rate (s^{-1}). Pseudoplastic solutions which are entangled polymer solutions also show a Newtonian flow at very low shear rates, and its corresponding the solution viscosity, which is the η_0. As the c equals to c^* ($c=c^*$), the chain overlap is started. The overlap concentration can be determined from the viscosity as

$$c^* \sim [\eta]^{-1} \qquad \text{Equation 2}$$

The chain entanglement depends upon the c which is needed to exceed the c* as a crossover concentration between the dilute and the semidilute concentration regimes for a successful electrospinning process and nanofiber formation to occur (Ghorani and Tucker, 2015). Shenoy et al (2005) developed a semi-empirical theory related the n_e for the solution at $c \sim c^*$ or $c > c^*$, defined as

$$n_e = \frac{M}{M_e} = \frac{\emptyset_p M}{M_e} \qquad \text{Equation 3}$$

By assuming that the η_0 and M dependence are the same, the sharp turn in the η_0 ranging from M^1 to $M^{3.4}$ for $n_e \sim 2$ (Shenoy et al., 2005). The n_e of 2 for the solution refers to one entanglement per chain (n_e-1), but the formation of electrospun nanofibers is required the polymer solution with the n_e greater than 3.5 (Munir et al., 2009), but the entanglement per chain will be 2.5. At $2<n_e<3.5$, it is a transition from the beaded fibers to the smooth, bead-free fibers. If the n_e is less than 2, the electrospraying occurs (Shenoy et al., 2005; Munir et al., 2009).

Researchers have focused on the concentration dependence of the specific viscosity (η_{sp}) to determine the concentration regions and their influence on the electrospinning of the polymer solutions. The η_{sp} can be calculated by using the equation below

$$\eta_{sp} = (\eta_0 - \eta_{solvent})/\eta_{solvent} \quad \text{Equation 4}$$

where $\eta_{solvent}$ is the solvent viscosity (Millipore DI water in this study) and the η_0 is zero shear viscosity taken the shear viscosity at which starts to have a constant flow in the plot of shear viscosity versus shear rate (s^{-1}) (Kong and Ziegler, 2014; Liu et al., 2016).

From the plots of the η_{sp} as a function of the c for polymer solutions, four regions can be identified: the dilute ($c< c^*$), the semidilute unentangled ($c^*<c<c_e$), the semidilute entangled ($c_e<c<c^{**}$), and the concentrated regimes ($c^{**}<c$) (Morris et al., 1981; Colby et al., 1991; Kong and Ziegler 2014; Liu et al., 2016). Daoud and De Gennes (1979) reported that the double logarithmic plots of the η_{sp} against the c show a slight increase in the slope above the c^* while the plots show a pronounced increased in the slope above the c_e for the synthetic polymer solutions (Daoud and De Gennes, 1979). The solutions are attributed to the transition from the dilute solution conditions, which the individual polymer chains exist in isolated coils, to the concentrated polymer solutions where more polymer chains are present to overlap and entangle (Daoud and De Gennes, 1979). Thus, the c_e marks the onset of significant polymer chain overlaps and interpenetrations. The literature on the synthetic polymers, the term 'concentrated' is used for the polymer melts or solutions where the polymers dominates over the solvent, and the solutions at a lower concentration than the c_e are referred to the term 'semidilute' (Daoud and De Gennes, 1979). However, to reach such extreme concentration is experimentally difficult for all neutral polymer and biopolymers, instead four regions (the dilute, the semidilute unentangled, the semidilute entangled, and

the concentrated) are used to evaluate the concentration regimes for biopolymers (Morris et al., 1981; Colby et al., 1991; McKee et al., 2004). Morris et al (1981) reported that the η_{sp} was proportional to $c^{3.3}$ for the random coil polysaccharides including dextran, alginate, lambda-carrageenan, and hyaluronate (Morris et al., 1981).

Some researchers have reported the concentration dependence of the viscosity for neutral and natural polymers. Morris and coworkers (1981) experimentally reported that the transition from the dilute to the concentrated solution behavior occurs at the $c^*\sim4/[\eta]$ when $\eta_{sp}\sim10$ for a wide range of random coil polysaccharide solutions. In the dilute solutions, Morris et al (1981) reported that η_{sp} was proportional to $c^{1.4}$ for the random coil polysaccharides, whereas it was proportional to $c^{2.0}$ and $c^{3.3}$ in the semidilute entangled and the concentrated regimes, respectively (Morris et al., 1981). Daoud and De Gennes (1979) predicted the similar values that $\eta_{sp}\sim c^{1.25}$ in the semidilute unentangled regime, $\eta_{sp}\sim c^{4.8}$ in the semidilute entangled regime, and $\eta_{sp}\sim c^{3.6}$ in the concentrated regime for neutral and linear polymers in a good solvent (Daoud and De Gennes, 1979). Wool et al (1993) theoretically established a predicted model system which had the similar results ranging from 1.4 to 3.4 from the dilute to the concentrated solutions dissolved in a good solvent, respectively (Wool, 1993). Additionally, the concentration dependence of the η_{sp} of sodium hyaluronate in phosphate-buffered saline at 25 ºC was determined and found $\eta_{sp}\sim c^{4.0}$ in the semidilute entangled region, whereas $\eta_{sp}\sim c^{1.2}$ was found for the dilute and the semidilute unentangled regions (Berriaud, Milas, and Rinaudo, 1994; Krause, Bellomo, and Colby, 2001). McKee et al (2004) determined the adjustments of the concentration regimes for linear and branched poly(ethylene terephthalate-co-ethylene isophthalate) (PET-co-PEI) as a function of chain overlap and the c_e, and their relationship with electrospinnability

(McKee et al., 2004). It was mentioned that the polymer concentration should be 2-2.5 times the c_e (7 wt% polyesters for the study) to fabricate bead-free, smooth electrospun nanofibers (McKee et al., 2004). Even though there are many studies about the correlation between the rheological properties of synthetic and other polymers solutions and the formation and morphology of electrospun fibers, the evaluation of this relationship is lacking for food-grade biopolymers such as milk proteins, specifically nonfat dry milk and caseinates.

2.3.1.3 Surface tension and Electrical conductivity

One of the solution properties is surface tension because it eases the electrospinning process, which is related to the electrostatic charge needed to start the formation of the polymer jet. Under the electric field, the surface tension could be a factor leading the pendant droplet to collapse into the small droplets (Kriegel et al., 2008) or electrospraying (Ramakrishna, 2005).

Electrical conductivity makes the applied voltage to form charged ions among the molecules of the solutions leading to the formation of the electrostatic forces. The ions increase the charge density carrying the jet, and then overcome the surface tension of the pendant drop. The applied voltage results in pushing the solution away from the syringe tip into Taylor cone formation and leaving the fibers on the counter electrode (Shenoy et al., 2005; Greiner and Wendorff, 2007; Liu et al., 2016). Most polymers are conductive, and the charged ions in the polymer solution influence the jet formation.

2.3.2 Processing parameters

The processing conditions also affect the electrospinning process along with fiber morphology after the solution properties. These parameters are the applied external

voltage, the distance between the needle and the collector, flow rate, and needle diameter. Their effects have previously been reviewed in many publications (Huang et al., 2003; Bhardwaj and Kundu, 2010; Stijnman et al., 2011; Pillay et al., 2013; Ghorani and Tucker, 2015; Haider et al., 2015).

The most critical factor in terms of processing conditions is the applied voltage because the initiation of the Taylor cone can only occur if the applied voltage is sufficient to allow the electrostatic forces to overcome the surface tension. For example, an increase in the voltage forms the smaller diameter nanofibers due to charge repulsion within the jet, accelerates the jet and increases the polymer stretching as well as the mass ejected from the Taylor cone (Sill and von Recum, 2008; Weiss et al., 2012; Okutan, Terzi, and Altay, 2014). However, if the applied voltage is too high and flow rate at which the solution is removed from the tip of the needle may exceed the flow rate of the solution through the needle, which causes a breakdown of the Taylor cone and thus the formation of defects within the nanofiber structure (Yördem, Papila, and Menceloğlu, 2008). A lower applied voltage sometimes decreases the fiber diameter size because a decrease in the velocity causing the breakups of the polymer jet (Yang et al., 2004).

With the external voltage, the flow rate controls a stable Taylor cone and maintains the polymer jet stability (Ghorani and Tucker, 2015). When the flow rate increases, the amount of the solution withdrawn from the tip of the needle increases, leading to the formation of the fibers with larger diameters (Shin et al., 2001). A lower flow rate allows more time for the solvent to evaporate which prevents the formation of junctions or interconnected fibers.

As the external voltage is applied, the elongation of the polymer jet occurs between the tip and the counter electrode. Therefore, changing the distance from tip to collector affects the jet travel time and the strength of the electric field. The distance should be enough that provides a sufficient time for the evaporation of the solvent because a small distance accelerates the jet, which hinders the solvent evaporation (Bhardwaj and Kundu, 2010; Ghorani and Tucker, 2015).

Researchers have established a model of the electrospinning process by correlating it to the processing parameters. These models approach the electrospinning process as an electrohydrodynamic and are established to predict the jet diameter and the instability as a function of the processing parameters (Reneker et al., 2000; Yördem, Papila, and Menceloğlu, 2008). These models are also developed based on the assumption of an electrospinnable fluid and are mostly for synthetic polymers and biopolymers. Even though models based on the dynamic properties has given an accurate approach of the jet instability and the fiber diameters (Reneker et al., 2000; Shenoy et al., 2005), the morphologies of the electrospun nanofibers are not only the function of dynamic parameters but also depend upon the solution properties such as the type of polymer, viscosity, concentration, surface tension, electrical conductivity, and molecular weight (Feng, 2003).

2.3.3 Environment conditions

Besides the solution properties and processing parameters, the ambient parameters such as temperature and humidity also affect the diameter and morphology of nanofibers. Temperature has two opposite effects on the diameter size of electrospun nanofibers; increasing the rate of the solvent evaporation and decreasing the viscosity of the solutions.

Both outcomes can decrease the mean diameter of the electrospun fibers (Zhang et al., 2009). If temperature is increased more, it could cause the polymer solution dry at the tip of the needle, restricting the continuous flow of the solution (Weiss et al., 2012).

Humidity has an influence on the polymer solution during the electrospinning process. At a high humidity, water can likely condense on the fiber surface, which affects the fiber morphology as the process is employed under normal atmosphere (Megelski et al., 2002; Bognitzki et al., 2001). An increase in humidity during the electrospinning causes larger pores on the fiber surfaces while a volatile solvent dries very rapidly at a very low humidity, and its evaporation occurs faster than the distortion of solution from the tip of the needle, which may clog the needle tip (Casper et al., 2004). For example, Bak et al (2016) investigated the effects of humidity on the production of the collagen nanofibrous sheets in the solvent, consisting of 20× phosphate-buffered saline/ethanol (1:1, 1:1.3, and 1:1.5 ratios). The nanofibrous sheets were produced without beads in the 1:1.5 solvent at 30 % RH, whereas beaded sheets were produced at 60 % RH (Bak et al., 2016).

2.4 Electrospinning of Food-grade Biopolymers and Their Applications

Electrospinning of natural food-based polymers, which are also edible, are of interest by the food and pharmaceutical industries, for the creation of value-added products. They are nontoxic, digestible, biodegradable, and sustainable. However, production of nanofibrous mats from food-base polymers has many limitations because these polymers tend to have highly complex molecular structures, which without pH or salt adjustment; e.g., may not produce random coils to allow for electrospinning. They should also be soluble in water or ethanol, a requirement for edible food products. However, most natural

polymers may form micro or nanofibers if they are dissolved in a solvent other than water or ethanol or electrospun with a synthetic polymer, as summarized in Table 1.

Table 1: Overview of various electrospinning conditions for synthesis of food-based nanofibers.

Protein	Molecular weights (kDa)	Carrier/other compounds	Solvent	Viscosity at 100 s^{-1}, Pa. s	Surface Tension, mN/m	Fiber Mean Diameter, nm	References
Whey	>60 (Seralbumin) 23-32 (β-lactoglobulin) 13 (α-lactoalbumin)	PEO	Water	0.076-9.233	52-58	fibers/ 227-264	Colin-Orozco et al., 2014
			Acidic, glacial acetic acid	0.003	41	fibers/ 707	Vega-Lugo and Lim, 2012
			Neutral	0.0005	61	fibers/138-632	
			Alkaline, NaOH	0.001	60	fibers/ 191	
			Water	0.38-2.33	-	fibers/ 312-690	Sullivan et al., 2014
Calcium Caseinate	~19-24	Pullulan	Water	0.1	46-48	fibers/ 172-451	Tomasula et al., 2016
Sodium Caseinate	~19-24	Pullulan	Water	0.1-0.4	45	fibers/ 764	Tomasula et al., 2016
Egg albumen	~42	Cellulose acetate/ Tween 40	Formic acid, acetic acid	1.4-2.8	30-32	fibers/ 242-410	Wongsasulak et al., 2010
Gelatin	~20-100	-	Water, TFE, HFIP, acetic acid	-	-	fibers/ -	Zhang et al., 2009; Huang et al., 2003; Aduba et al., 2013; Gomes et al., 2015
Zein	~22-24	/Oleuropein	Ethanol	-	-	fibers/ 130-1440	Erdogan et al., 2015
		/Fish oil	Isopropanol	-	-	fibers/ 300-500	Moomand and Lim, 2014
Amaranth	~10-83	Pullulan/ Tween 80, curcumin	Formic acid, methanol, potassium persulfate and bile salts	*0.22-0.58	31-33	fibers/ 135-249	Blanco-Padilla et al., 2015
		Pullulan/ Tween 80, folic acid	Formic acid/potassium persulfate salt	0.36-0.59	-	fibers/ 305-378	Aceituno-Medina et al., 2015b
		Ferulic acid	formic acid,	0.36-0.60	-	fibers/ 261-390	Aceituno-Medina et al., 2015a
Soy	~140-170	PEO	Water, NaOH	*0.1-7.0	36-40	fibers/ 19-140	Ramji and Shah, 2014
Wheat protein	~10-1000	/urea	Acetic acid, ethanol, 2-mercaptoethanol, 2-proponal, acetone	-	-	fibers/ 683	Castro-Enríquez et al., 2012
		PVA	Water, HFIP	-	-	fibers/ 100-5000	Woerdeman et al., 2005; 2007

* viscosity - values at the unknown shear rate.

Continued: Overview of various electrospinning conditions for synthesis of food-based nanofibers.

Polysaccharide	Molecular weights (kDa)	Carrier/other compounds	Solvent	Viscosity at 100 s^{-1}, Pa. s	Surface Tension, mN/m	Fiber Mean Diameter, nm	References
Sodium Alginate	~46-100	-	Water, mixtures of glycerols	10.0-70.0	38-61	fibers with beads/ 120-300	Nie et al., 2008
		PEO/pectin, folic acid	Water, NaOH	-	-	fibers with few beads/ -	Alborzi et al., 2014
Dextran	~64-76	/crosslinked with glutaraldehyde	Water	0.33-4.40	61-63	fibers/ 291-1948	Ritcharoen et al., 2008
		-	Water, DMSO, DMF	*6.8-60.0	-	fibers/ 400-600	Jiang et al., 2004
Pectin	~260	Pullulan/ *Lactobacillus rhamnosus* GG	Water	-	76-86	fibers/ 38 - 148	Li et al., 2017
Pullulan	~100	/ $Na_3C_6H_5O_7$	Water	-	-	fibers/ 100–700	Sun et al., 2013
			Water (50°C)	0.082	61.8	fibers/218	Tomasula et al., 2016
		-	Water	19.0-333.0	63-75	fibers/ 27-492	Li et al., 2017

* viscosity - values at the unknown shear rate.

2.4.1 Solvents

Solvents are important for the formation of smooth and bead-free electrospun fibers. There are two factors to select a right solvent for the electrospinning process. First, the polymers should be highly soluble and have a random coil structure in the preferred solvent. Another factor is that the solvents should have a relative boiling point that enables the evaporation of the solvents before the fibers deposit on the collector (Haider et al, 2015).

This project is targeted to use water as a solvent for the formation of food-based nanofibers. However, many natural polymers dissolved in a number of polar organic solvents have been electrospun for non-food applications. These solvents include HFIP (Hexafluoroisopropanol, $(CF_3)_2CHOH$), TFE (2,2,2-Trifluoroethanol, CF_2CH_2OH), formic acid (HCOOH or HCO_2H), acetic acid, DMSO (Dimethyl sulfoxide, $(CH_3)_2SO$), TFA (Trifluoroacetic acid, CF_3CO_2H) and ethanol (C_2H_6O) have been used to dissolve many water-insoluble food-grade polymers (Haider and Haider, 2016; Akkurt, Liu, and Tomasula, 2018). They are discussed in many publications in detail (Haider and Haider, 2016; Mendes et al., 2017; Akkurt et al., 2018).

Even though using HFIP, TFE, formic acid, and others eases electrospinning of certain biopolymers, these toxic solvents and acids can cause a significant problem in electrospun nanofiber application when it comes into contact with food products (Li et al., 2006; Tomasula et al., 2016). Also, using concentrated acid or solvents may pose a problem for sensitive bioactive compounds including enzymes, genes, or antibiotic peptides.

2.4.2 Carrier polymers

In many applications, especially in biomedical, an electrospinnable synthetic polymer such as poly (vinyl alcohol (PVA), poly (ethylene oxide) (PEO) is often applied to stimulate electrospinnability of synthetic and water-insoluble polymers (Greiner and Wendorff, 2007; Mendes et al., 2017). An approach commonly used for the electrospinning of natural polymers is to use a carrier polymer such as PEO, polycaprolactone (PCL), poly (lactic-co-glycolic acid) (PLGA), PVA, and nylon-6, even though they are highly soluble in the solvent systems. The molecular weight of carrier polymers is an important factor to choose them for an effective electrospinning process. For example, when a blend prepared with PEO carrier with a molecular weight of 35 kDa produced sprayed drops so that PEO with 200 kDa was required to form beadless and uniform electrospun fibers from alginate and alginate-pectin blends (Bonino et al., 2011). These polymers and their uses in the electrospinning process of the natural polymers are discussed for non-food applications in many studies (Shao et al., 2003; Karim et al., 2009; Haider et al., 2015; Haider and Haider, 2016; Mendes et al., 2017).

This approach is also commonly used for the electrospinning of biopolymers, which are difficult to produce nanofibers. PVA and PEO are also used as a carrier for the electrospinning of proteins such as elastin, soy protein, collagen, silk and keratin from aqueous solution, without addition of other solvents (Buttafoco et al., 2006; Cho et al., 2010; Huang et al., 2003; Vega-Lugo, Cristina, and Lim, 2009). However, both PVA and PEO are undesirable in food when they are used in large quantities.

Besides the synthetic polymer carriers, electrospinnable food-grade biopolymer carriers such as pullulan, gelatin, and dextran have been used to produce edible electrospun

nanofibers from proteins by making use of natural protein-polysaccharides interactions. These electrospinnable and edible polymers either favors the viscosity of the solution to promote molecular entanglement of the polymer chains, maintaining a jet formation or decrease the electrical conductivity and surface tension of the solution to ease its electrospinning (Alborzi et al., 2014).

Because the synthetic polymer carriers are not intended for consumption, one of the objectives in this study is to use a food-based biopolymer carrier as an alternative for the natural carriers to produce edible food-grade proteins nanofibers such as milk proteins. In a previous study, Tomasula et al (2016) examined the use of pullulan (PUL), a food-grade polysaccharide, to electrospin milk caseinates (CAS), which are incapable of forming fibers from aqueous solution. They shortly reported that fibrous mats produced from either calcium caseinate or sodium caseinate at the range of caseinate content from 57 to 84 wt% in total solid mass of aqueous solution (Tomasula et al., 2016). Another research was conducted to produce food-based electrospun fibers from the blends of pectin (PEC) and PUL in aqueous solutions (Liu et al., 2016). They produced bead-free nanofibers from PEC blended PUL with the diameters ranging from 88 to 140 nm. While increasing PEC content from 1.8 to 2.4 wt% with decreasing PUL content from 6.0 to 3.0 wt% in their blend solutions, beaded fibers were obtained.

2.4.3 Protein-based Biopolymers

Even though there are many protein-based biopolymers that were studied to electrospin, this section will cover some animal-based and plant-based proteins: whey protein, casein and caseinates, egg albumen and gelatin as animal-based proteins and zein, amaranth, soy protein and wheat protein as plant-based proteins.

2.4.3.1 Animal-based Proteins

Whey protein

Whey proteins, one of two milk protein groups along with caseins, is the byproduct of cheese production. After the production of 1 kg of cheese, 9.5 kg of watery byproduct, whey, is produced. It can be also obtained when casein in milk precipitates at pH 4.6 (Morr and Ha, 1993). Whey contains less than 1 % whey proteins and approximately 6.3 % total solids. Therefore, it is concentrated to make both whey protein concentrates (WPC) with protein ranging from 35 to 90 % and whey protein isolates (WPI) with protein greater than 90 % used to exploit the nutritional and functional properties of its major proteins, beta-lactoglobulin (β-LG, MW 23-32 kDa) and alpha-lactalbumin(α-LA, MW 13 kDa) (Vega-Lugo and Lim, 2012). Whey protein contains mainly β-LG of 48-58 % and α-LA of 13-19 % and the rest is followed by bovine serum albumin (MW >60 kDa) and immunoglobulins (deWit and Klarenbeek 1984). β-LG is a small globular protein and consists of 162 amino acids (18 kDa) with secondary and tertiary structures, whereas α-La is composed of 123 amino acids (14 kDa) with eight cysteine groups (Corredig and Dalgleish, 1996; Fox and Kelly, 2006). β-LG has random coil conformations and consists of two disulfide bonds with one sulfhydryl group (Cys ^{121}) (deWit and Klarenbeek, 1984; Morr and Ha, 1993; Swaisgood, 2003; Vega-Lugo and Lim, 2012).

The whey proteins have been extensively studied for the formation of films and coatings and utilized for food and other edible applications, which are summarized in several review articles (Krochta and Mulder-Johnston, 1997; Jooyandeh, 2011; Ramos et al., 2012). To form edible films and coatings from WPI, its main proteins should be denatured to unfold the globular protein molecules via heating, pH adjustment or use of

denaturant. The denaturation favors the sulfhydryl (Cys^{121}) of β-LG to be available to interact with its two disulfide bonds to allow protein network formations for the films and coatings.

The electrospinning of WPI requires similar denaturation treatments because globular protein structure hinders the entanglements of protein chains which is important for the formation of a stable polymer jet during the electrospinning process. Even though denaturing WPI aqueous solutions by heating or other methods results in the protein network formation, the low viscosity of the solutions prevents the production of nanofibers due to the lack of molecular entanglement (Nie et al., 2008; Nieuwland et al., 2013).

Sullivan et al (2014) successfully electrospun WPI with PEO carrier polymer by heating the WPI in aqueous solutions to 70 °C to form disulfide bonds between neighboring chains, which sustain the electrified jet during the process (Sullivan et al., 2014). The nanofibers were obtained with the diameter ranged from 312 to 690 nm, depending on the composition and ratio of the PEO/WPI solutions. They used the small, hydrophobic molecule Rhodamine B (RhB) as a model flavonoid into the whey/PEO electrospun nanofiber mats to prove the encapsulation concept (Sullivan et al., 2014).

Electrospun nanofibers were produced from PEO/WPI solutions as a function of various mixing ratios to evaluate the dependence of morphology by testing viscosity, conductivity, surface tension, and thermal and vibrational properties (Colín-Orozco et al., 2015). The nanofibers with diameters ranging from 227 nm to 264 nm were formed at a high viscosity, whereas the bead formation occurred at both the lowest viscosity and surface tension along with high conductivity of the mixtures. The fibrous mats were used to encapsulate Rosmarinus officialis extract was encapsulated into the fibrous mats to

utilize the PEO/WPI nanofibers (Colín-Orozco et al., 2015). The effects of PEO addition and pH adjustment were tested to study the feasibility of aqueous WPI solutions. (Vega-Lugo and Lim, 2012). A uniform, bead-free fibers with a diameter of 707 nm were produced under acidic conditions along with the higher viscosity, lower surface tension and lower conductivity of PEO/WPI blend solutions. The fibers had ribbon-like structures with a diameter of 191 nm under alkaline conditions while the neutral pH allows the fibers to form with the diameter sizes varied from 138 to 632 nm (Vega-Lugo and Lim, 2012).

Casein and Caseinates

Casein is one of the milk proteins which exist in micelles and contains 80% of milk proteins with a molecular mass in the range between 19 to 24 kDa (Livney et al., 2010). These micelles are spherical colloids with a diameter ranging from 50 to 500 nm (Dickinson, 2006; Fox and Kelly, 2006). Casein proteins are differentiated by its calcium sensitivity and charge distribution (Dickinson 2006; Fox and Kelly, 2006; Varnam and Sutherland, 2001). It consists of α_{s1}-casein, α_{s2}-casein, and β-casein, which are calcium sensitive, and κ-casein, which is calcium insensitive (Uniacke-Lowe, Huppertz, and Fox, 2010). One model used to envision the structure of the casein micelles in milk is that of (Rebouillat and Ortega-requena, 2015) in which the micelles are composed of sub-micelles linked by $Ca_9(PO_4)_6$ as shown in Figure 6.

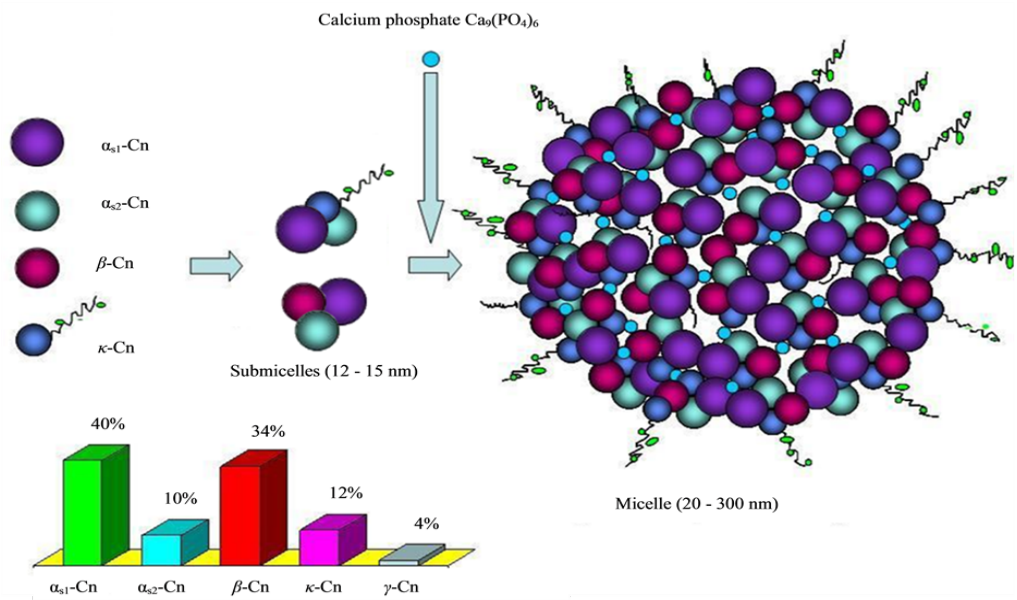

Figure 6: The formation of casein micelles in an aqueous medium. α_{s1}-Cn is alpha S1 casein, α_{s2}-Cn is alpha S2 casein, β-Cn is beta casein, and κ-Cn is kappa casein.

Casein micelles are naturally able to stabilize and transport essential nutrients such as calcium and protein (De Kruif and Holt, 2003). In milk, κ-caseins stabilize calcium-sensitive caseins avoiding precipitation with calcium ions (Ca^{2+}) (Walsh and Swaisgood, 1996; Horne, 2006). The calcium-sensitive caseins can bind Ca^{2+} by their phosphate groups located on the hydroxyl groups of serine. Phosphoserine residues correspond to the existence of hydrophilic areas with a high negative charge (Horne, 2006; Walsh and Swaisgood, 1996). These natural characteristics provide a unique biological activity and stability for casein in milk and its processing into dairy products (Tomasula et al., 1998; Fox, 2003; Swaisgood, 2003). Due to the casein micelle structure, Semo et al (2007) have proposed it as a carrier for the delivery of nutrients for nutraceutical applications (Semo et al., 2007). However, it has not been studied enough to take advantage of its unique property as a carrier vehicle for a nano-delivery system for added nutrients or bioactive compounds.

Casein proteins are stable at high temperatures, but they are unstable at pH below 5.0 which affects its structure and function. At pH, the casein aggregates by neutralizing negative charges on the casein to the isoelectric point of 4.6 with a decrease in the repulsions of side chains (Chakraborty and Basak, 2007). During the manufacturing of caseinates, acid casein gel is formed through hydrophobic interactions occurring when the protein becomes a colloidal particle. After such spherical particles are formed, native casein micelles in milk start to disappear (McHugh, Weller, and Krochta, 1994). Neutralization of the acid gel keeps net negative charges on the surface of colloidal particles leading the gel to disassociate as the particles repel each other. The protein continues to disintegrate without calcium ions until the steady state is reached. The supramolecular structures are converted into either calcium caseinate (CaCAS) or sodium caseinate (NaCAS) with pH ranging from 6.0-7.0 by addition of base solutions of either $Ca(OH)_2$ or NaOH, respectively. Calcium bridging occurs through individual proteins in colloidal particles which keeps them together to avoid further disintegration of supramolecular structure. As the net negative charge increases, numerous calcium bridges occurred leads to form subunit structures in caseinate dispersions (McMahon et al., 2009). Calcium ions make the proteins hold in close proximity which leads hydrophobic groups to self-associate. After this process, the mesh structure is formed by hydrophobically linked protein molecules with their polar groups on the surface of the mesh. The self-association results CaCAS in less soluble than NaCAS since Na^{1+} breaks calcium bridges and allows the protein to solubilize, instead of forming subunits as CaCAS (Hokes et al., 1982). Due to solubility and random coil structure properties, they have been used to form edible films and coatings by casting CaCAS and NaCAS solutions (Bonnaillie et al., 2014).

Caseinates as highly soluble proteins with a random coil structure may seem electrospinnable because they form protein building block necessary for the edible films and coatings. However, aqueous solutions of calcium and sodium caseinates (CaCAS and NaCAS) have not produced nanofibers without using organic solvents and a synthetic polymer as a processing aid (Xie and Hsieh, 2003; Kriegel et al., 2008; Nieuwland et al., 2013; Tomasula et al., 2016). The inability to electrospin neat CAS from aqueous solutions could be because of the aggregation of CAS protein molecules with mono- (Na) and divalent ions (Ca) which cause lack of molecular entanglement which is necessary for the formation of electrospun nanofibers (Pitkowski et al., 2008; Stijnman et al., 2011). To overcome this challenge, one of the approaches is to add a carrier polymer with excellent electrospinning properties into aqueous protein solutions to form electrospun nanofibers (Klimov et al., 2010; Choi et al., 2011; Friedemann et al., 2012). For proteins in non-food applications, usually, PEO is employed as processing carrier without the addition of other solvents (Buttafoco et al., 2006; Soffer et al., 2008; Varesano et al., 2008; Vega-Lugo and Lim 2008). However, using PEO with large quantities is undesirable in food applications.

Using this strategy of adding an edible carrier, PUL, Tomasula et al (2016) have successfully produced nanofibers from CAS in aqueous solutions. The food-based, electrospun nanofibers mats produced from aqueous CAS blended with PUL can be potential candidates for encapsulation of bioactive compounds for foods. As shown in Figure 7, increasing PUL concentration produced uniform, thinner fibers unlike increasing CaCAS in blends which produced thicker and less uniform fibers (Tomasula et al., 2016). Electrospun nanofibers with a mean diameter of 172±43 nm were produced from the

aqueous PUL: CaCAS solutions with a mixing ratio of 1:2 at 50 ℃, as shown in Figure 7A.

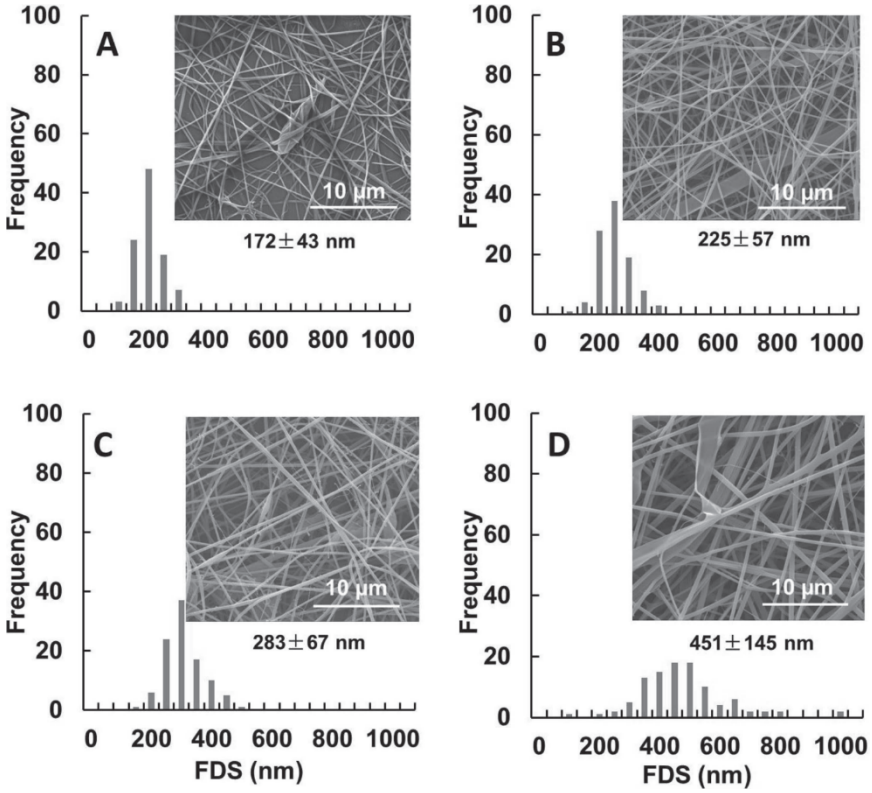

Figure 7: Scanning electron microscopy images and fiber diameter size (FDS) of electrospun fibers obtained from either 15 or 30 wt% pullulan (PUL) solutions and 20 wt% calcium caseinate (CaCAS) solutions in various mass ratios at 50 °C. Flow rate=1 to 2.5 mL/h, Voltage=23 kV. (A) 15 wt% PUL, 20 wt% CaCAS solution (1:2); (B) 30 wt% PUL, 20 wt% CaCAS (1:4); (C) 15 wt% PUL, 20 wt% CaCAS solutions (1:1); and (D) 30 wt% PUL, 20 wt% CaCAS solution (1:2).

Egg albumen

Egg albumen is one of the globular proteins and has over 50 % of the total egg proteins. In the electrospinning process, globular proteins have too little or no interaction with each other which constrain the molecular entanglement of protein chains necessary for the elongation and stretching of jet under the electric field. Without a carrier polymer or using solvents other than water, egg albumen produced submicron particles on the collector. In a study, electrospun fibers were produced from egg albumen in formic acid

solutions by using PEO as a carrier (Wongsasulak et al., 2007). Formic acids interfere with the protein interactions by denaturing its globular structure and PEO increases the protein chain entanglements and viscosity of the solution by forming hydrogen bonds (Wongsasulak et al., 2007). When egg albumen blended with PEO at ratios of 1:10, 3:10, and 6:10 produced uniform, thinner fibers with a diameter of 188± 21 nm. As increasing PEO in the blends by changing the ratio of egg albumen to PEO from 10:3 to 10:6 for the thicker fibers with diameter from 289 to 470 nm, respectively (Wongsasulak et al., 2007).

In another study of Wongsasulak et al (2010), the electrospinning of egg albumen in 50 % formic acid mixed with cellulose acetate in 85 % acetic acid produced fibers with the diameter of 265 ± 48 nm (Wongsasulak et al., 2010). A surfactant was also added to reduce the surface tension of the blended solution to improve the electrospinnability of egg albumen. The study was addressed that the nanofibers produced from this blend could have potential functionalities for controlled release of nutraceuticals applications in vivo, but its potential in foods was not addressed (Wongsasulak et al., 2010).

Gelatin

Collagen is the most abundant structural protein found in animal connective tissues including skin, bone, and tendon (Zhang et al., 2009; Nieuwland et al., 2013). It has a coiled fibril structure formed by two α1 and one α2 chain of collagen. The diameter size of fibrils is uniform and ranges from 50 to 500 nm. Each chain of collagen has an α-helix structure formed by 1000 amino acids and the molecules have a triple-helical structure via covalent bonds by repeating of three amino acids, GLY-Proline-Hydroxyproline (Buttafoco et al., 2006; Sionkowska, 2011).

Gelatin is obtained from collagen after its treatment with mild heat under acidic or alkaline conditions (Type A or B). Marine gelatins are a by-product of fish processing and used as an alternative to cow-based gelatin (Dangaran et al., 2009). Gelatins are food-grade, biocompatible, biodegradable and nontoxic protein and they have been extensively used to as a carrier for bioactive materials in biomedical applications (Manna et al., 2015; Jalaja et al., 2016; López Angulo, and do Amaral Sobral, 2016; Aldana, and Abraham, 2017; Ren et al., 2017), pharmaceuticals (Leo et al., 1997; Fraunhofer et al., 2004; Jain et al., 2008; Aewsiri et al., 2009), food industries (Babel, 1996; Baziwane and He, 2003; Karim and Bhat, 2008; Nur Hanani et al., 2014; Musso et al., 2017), and other industries (Ali et al., 2012).

The electrospinning of gelatin is difficult to form fibers due to its molecular triple-helix structure (Araujo et al., 2014). This problem can be solved by selecting a good solvent and manipulating processing parameters and ambient conditions. Many researchers have conducted experiments on the electrospun gelatin-based tissue scaffolds by dissolving gelatin in organic solvents mostly TFE (Huang et al., 2003; Zhang et al., 2006; Chong et al., 2007; Son et al., 2013; Xue et al., 2014), HFIP (Aduba et al., 2013; Xu et al., 2015; Wang et al., 2016), and acetic acid (Pant and Kim, 2012; Baiguera et al., 2014; Gomes et al., 2015).

Gelatin melts at higher temperatures than room temperature and it can electrospin from aqueous solutions at high temperature (Li et al., 2006; Zhang et al., 2009). Gelatin-based electrospun fiber mats are produced from its blends with poly(ε-caprolactone) (PCL) which is bioresorbable and biocompatible (Chong et al., 2007). In this study, cell culture embedded in the nanofibrous mats and scaffolds produced from PCL and gelatin blends,

and then is applied on a poly-urethane wound dressing. The results show that the production of a fibroblast-populated three-dimensional dermal analog is feasible to construct the thickness of the dermis before reepithelialization (Chong et al., 2007). Tonda-Tura and co-workers (2013) study on the production of stable electrospun nanofibers from gelatin dissolved in water by using γ- glycidoxypropyltrimethoxysilane (GPTMS) as a cross-linker. The gelatin crosslinked with GPTMS nanofiber mats maintain the in vitro adhesion, proliferation, and survival of neonatal olfactory bulb ensheating cells (NOBECs) (Tonda-Turo et al., 2013). Gelatin was used as a carrier polymer to electrospin the sodium caseinate, WPI, soy protein isolate (SPI), ovalbumin and BSA and uniform nanofibers were obtained from WPI-gelatin mixture dissolved in water (Nieuwland et al., 2013).

Li et al (2006) studied the electrospinning of gelatin in HFIP solvent and produced fibers with mean diameters from 140 to 350 nm and the diameter increased as increasing gelatin concentration. For example, electrospinning of the solution concentration below 7.5 wt% and above 12.5 wt% produced beaded and few large fibers, respectively. As decreasing the concentration of gelatin solution from 8.3 to 2 wt%, the fibers diameters decreased from 485±185 nm to 77±41 nm (Li et al., 2006). Song and coauthors (2008) reported that gelatin dissolved in a mixture of ethyl acetate and acetic acid produced fibers with diameters ranging from 47 to 145 nm. (Song et al., 2008). As mentioned an approach, the electrospinnability of gelatin were studied to improve by adding other polymers in the gelatin solution. Yang et al (2007) used PVA as a carrier aid to facilitate the electrospinning of gelatin in formic acid at the ratio of PVA to gelatin of 0:1 to 1:0 (Yang et al., 2007). They obtained the fibers with diameters increased from 133±28 nm (from neat gelatin

solution) to 447±129 nm from the blend of gelatin and PVA solution. Also, the tensile properties of the fibers were improved by increasing PVA in the blends.

2.4.3.2 Plant-based Proteins

Zein

Zein protein is the main storage protein derived from corn and holds between 44 and 79 wt% of endosperm proteins depending upon the corn variety (Shukla and Cheryan, 2001). It is composed of glutamic acid (21-26 %), leucine (20 %), proline (10 %) and alanine (10 %). It is soluble in aqueous alcohol solutions, urea, and higher alkali conditions, but insoluble in water. The types of zein are characterized as α-, β-, γ-, or δ- based on its solubility properties and α-and β-zein proteins are the two major fractions. The α-zein is soluble in 95 % ethanol and accounts for approximately 80 % of the total prolamine in corn. Unlike the β-zein, α- fraction comprises less histidine, arginine, proline, and methionine (Shukla and Cheryan, 2001). The high quantities of non-polar amino acid residues favor zein to have unique aqueous alcohol solubility. However, it has poor mechanical properties in aqueous solution because it consists of roughly 1/3 hydrophilic and 2/3 hydrophobic amino acid residues in its primary structure.

Zein protein has been used to electrospin from a variety of solvents including dimethyl formamide (DEF.) (Jiang et al., 2007), aqueous ethanol (Yao et al., 2007; Selling et al., 2007), and methanol, isopropanol, and acetic acid (Selling et al., 2007) for potential application rather than foods. Different electrospun morphologies were obtained from these studies. For example, ribbon-like, bead-free fibers were produced from the 30–50 wt% zein dissolved in 70 wt% aqueous ethanol due to the rapid evaporation of ethanol. The fibers diameter size increased from 1 to 6 μm with increasing the zein concentrations

(Yao et al., 2007). Zein electrospun nanofibrous mats were crosslinked by hexamethylene diisocyanate (HDI) to improve the mechanical properties and the mats from a 40 % (w/v) zein concentration showed the highest tensile strength, 4.24 MPa (Yao et al., 2007). Additionally, Selling et al (2007) also produced ribbon-like zein fibers with the diameters ranging from 1 to 8 μm from the zein dispersions in 60–90 wt% ethanol, whereas the beads were produced by using 60 wt% acetone or 60– 90 wt% acetic acid to prepare a 27 wt% zein dispersion (Selling et al., 2007). Also, the use of DMF, 8 M urea, and 10 % NaOH did not promote the electrospinning of 40, 20, and 10 wt% zein solutions, respectively (Selling et al., 2007). However, Jiang and coauthors (2007) reported the production of bead-free, uniform nanofibers from the zein solutions (55-60 wt%) dissolved in DMF. Poly (ε-caprolactone) (PCL) was used as an inner layer for the zein electrospun nanofibers (outer layer) by carrying out a core-shell electrospinning method and produced nanofibers by the one-step coaxial electrospinning. It was concluded that the elongation stress and the strain at break increased with the PCL content, but the hydrated outer zein shell was ruptured by the elongated PCL fibers, meaning that the inner PCL fiber predominated the mechanical properties of the core-shell fibrous membrane (Jiang et al., 2007).

Researchers have studied on the encapsulation of the bioactive compounds by the electrospinning and electrospraying of zein proteins for potential applications (Shin, 2008; Fernandez et al., 2009; Torres-Giner et al., 2010; Jiang and Yang, 2011; Moomand and Lim, 2014, 2015). For example, Moomand and Lim (2014) produced electrospun nanofibers from the zein protein dissolved in the aqueous mixtures of ethanol and isopropanol solvents to encapsulate fish oil to protect it from a quick degradation (Moomand and Lim, 2014). The electrospun zein fibers had a diameter size of 300 nm. The

fibers with an increased diameter size of 500 nm were obtained by adding 30 % (w/w) fish oil to the zein solution. The electrospun zein nanofibers provided a better protection from the oxidation of the oil than the non-encapsulated fish oil.

Zein fibers via electrospinning were crosslinked to improve the fiber morphology and the release properties of the polyphenolic compounds due to the limited use of non-crosslinked porous zein fibers in applications (Erdogan et al., 2015). Oleuropein, derived from olive leaf (OLE) is the major phenolic in olive trees. In this study, it was studied as a natural crosslinker for the electrospun zein nanofibers. 70 % aqueous ethanol solution was used to dissolve 30 % (w/v) of zein, and then the solution was electrospun with OLE. The results of the OLE addition not only improved the mechanical integrity of the zein nanofibers but also reduced the diameter sizes of the fibers by 27 %. FTIR results showed a NH bending because OH- groups of the polyphenols interacting with NH and other bands resulted from the OLE and zein interactions (Erdogan et al., 2015).

Amaranth

Amaranth (Amaranthus hypochondriacus) is a traditional underutilized Mexican crop with highly nutritional grains and leaves. The seed and leaves are rich in protein 17 and 28-49 %, respectively, as well as unsaturated oil (45 % linoleic acid), dietary fiber (11 to 23 %), and minerals such as potassium, iron, magnesium, and calcium (Martínez and Añón, 1996). The proteins in amaranth mainly consist of albumins, globulins, and glutelins, which are identified based on their solubility and their amino acid compositions are reviewed in the literature by Segura-Nieto et al (1994).

Aceituno-Medina and co-workers (2013a) focused on the ability to create nanofibers from amaranth protein isolates (API) in organic solvents including glacial acetic

acid, sodium hydroxide, and HFIP under different pH conditions due to its low solubility property in aqueous solution. In the study, capsule structures occurred under extreme pH values of 2 and 12 and were produced from the proteins in formic acid solutions. Fiber-like morphologies were obtained from API dissolved in HFIP solvent which provided the formation of random coil structures and enabled protein chains to entangle (Aceituno-Medina et al., 2013a).

A few studies used PUL as a carrier polymer to promote the formation of amaranth proteins-based electrospun nanofibers to encapsulate quercetin and ferulic acid (Aceituno-Medina et al., 2015a) and folic acid as antioxidants (Aceituno-Medina et al., 2015b). Quercetin and ferulic acid were encapsulated within the API-pullulan blend electrospun nanofibers to test the loading capacity and the morphology. Also, the thermal stability of the encapsulated fiber structures was tested (Aceituno-Medina et al., 2015a). The results show that the incorporation of up to 10 and 20 wt% of quercetin and ferulic acid within the API-based fibers is feasible, respectively. In comparison to non-encapsulated compounds, the release profile during *in vitro* digestion study indicated that the release lasts longer which increases the antioxidant efficacy (Aceituno-Medina et al., 2015a).

Blanco-Padilla et al (2015) also studied the API-pullulan blend electrospun nanofibers to encapsulate curcumin. The concentrations of curcumin (0.05 and 0.075 %) were blended into fiber –making API-pullulan blend solutions and produced fibers with diameters of approximately 224.5-248.6 nm. The results showed that the encapsulation efficiencies of curcumin varied between ~73 % and ~93 % for both loadings and fiber constituents. The nanofiber structures extended the antioxidant release which occurred in

a controlled manner as tested under simulated gastrointestinal environments (Blanco-Padilla et al., 2015).

Soy protein

Soy protein is composed of globular proteins distinguished as 2S, 7S, 11S, and 15S dependent upon their molecular weights (Wolf, 1970). Soy protein isolates (SPI), which accounts for ~37 % of soy proteins, with molecular weight of 140-170 kDa consist of about 18 amino acids with the combinations of polar groups –OH, –COOH, and $–NH_2$, allowing the protein suitable for chemical and enzymatic modifications for specific requirements of biomedical applications. For example, different soy-based morphologies including membranes, microparticles, and thermoplastics were used as drug delivery vehicles for external use in wound dressings and for internal use for oral and nasal applications (Vaz et al., 2003).

Studies have been conducted for the electrospinning of SPI by using various carriers and solvents for applications including encapsulation of antimicrobial materials (Vega-Lugo, Cristina, and Lim, 2009), tissue regeneration (Ramji and Shah, 2014), and biodegradable air filtration membrane (Fang et al., 2016). Cho et al (2010) produced soy-based electrospun nanofibers in the presence of PVA as a carrier with water (Cho et al., 2010) and PEO as a carrier with water (Ramji and Shah, 2014). Fang and co-researchers (2016) produced electrospun SPI nanofibrous membranes using PVA as a carrier with a solvent mixture 80:20 (v/v) glacial acid and deionized water. As the weight ratio of SPI to PVA in the blends was increased from 1:1 to 1.5:1 and 2:1, the diameter size of fibers was decreased from 152 to 140 and 132 nm, respectively. The microporous structure of the membranes became more uniform along with a narrower diameter distribution (Fang et al.,

2016). To date, edible soy-based electrospun nanofiber produced for food use have not been reported.

Wheat Protein

Wheat gluten is a polydisperse plant storage protein which accounts for 85 % wheat protein. It has a polymeric glutenin with a molecular weight ranging from 80 to several thousand kDa and monomeric gliadin with a molecular weight less than 50 kDa (Singh et al., 1990; Hamer and Vliet, 2000). Wheat gluten has been extensively used in foods to improve dough quality and protein textures, as well as the formation of high-quality bio-based films and plastics (Gennadios and Weller, 1990) due to its ability to form disulfide bonds and chain entanglements (Edwards et al., 2001). Some studies focused on the electrospinning of wheat gluten to produce nanofibers (Woerdeman et al., 2005; Woerdeman, Shenoy, and Breger, 2007; Castro-Enríquez et al., 2012; Wang and Chen, 2012a). However, edible ultrafine fibers from wheat proteins have not yet been reported by using the electrospinning process.

Woerdeman and co-researchers (2005) electrospun wheat gluten dissolved in 5 % w/v HFIP after extracting wheat protein fraction by using acetic acid and produced fibers only at the concentration above 10 wt% (Woerdeman et al., 2005). The fibers were produced with different morphologies including circular, flat, and ribbon-like with a wide range of diameters from 25 nm to 5 μm, and increasing concentration increase the formation of ribbons. Woerdeman et al (2007) reported the electrospinning of wheat protein dissolved in HFIP by using PVA as a carrier. With increasing PVA content in the system, the strength and elongation of fibrous mats were improved (Woerdeman et al.,

2007). Also, another study reported that wheat glutenin increased the elasticity of neat PVA fibers due to the synergy between wheat gluten and PVA (Han and Chen, 2013).

Castro- Enríquez et al (2012) produced fibrous mats from electrospinning of wheat gluten-based materials by using acetic acid and/or ethanol. Fibrous mats had a thickness of 40 μm and were employed as controlled-release of fertilizer, urea, to prevent its loss (Castro-Enríquez et al., 2012).

Wang and Chen (2012b) evaluated the feasibility of electrospinning of various plant-based proteins including extracted from barley, gliadin from wheat and zein from corn dissolved in an acetic acid or its combination with water solutions and the biocompatibility of the electrospun fibers in vitro cell culture (Wang and Chen, 2012b). Electrospun nanofibers were produced from hordein, gliadin, and zein with average diameters of 184±70, 192±61, and 186±69 nm at their optimum processing concentrations, respectively. Due to higher glutamic acid contents of gliadin, it produced the strongest nanofibers. The fibers can be used as biomaterials in vitro cell culture (Wang and Chen, 2012b).

2.4.4 Polysaccharides-based Biopolymers

2.4.4.1 Plant-based Biopolymers

Sodium Alginate

Alginate is a naturally occurring linear anionic polysaccharide extracted from marine brown sea algae. It consists of (1–4) linked β-D-mannuronic acid (M) and α-L-glucuronic acid (G) units in various composition and sequence and exists in many species of brown seaweeds as sodium, calcium, magnesium, strontium, and barium salts in gelled form. Alginate is insoluble in water and water-soluble sodium alginate (SA) are produced

by converting alginate to alginic acid via an acid treatment which is followed by an alkali treatment with either NaOH or Na_2CO_3 (Dangaran et al., 2009). Due to its nontoxicity, unique tissue compatibility, and biodegradability, SA has been focused extensively for tissue engineering applications (Bouhadir et al., 2001). However, aqueous SA cannot be readily electrospun and its electrospinning requires an electrospinnable carrier polymer such as PEO (Lu et al., 2006; Alborzi, Lim, and Kakuda, 2010, 2012, 2014; Saquing et al., 2013) and PVA (Lee et al., 2009).

Nie and coworkers (2008) attempted to electrospin SA with the addition of a strong polar cosolvent (glycerol) and produced bead-free fibers. They reported that glycerol addition increased the viscosity of SA but decreased the surface tension and electrical conductivity. Glycerol, when added to water, promoted the alginate chain entanglements via its plasticizing property, beadless and smooth fibers with an average diameter of 200 nm (Nie et al., 2008). Bhattarai et al (2007) used the combination of DMSO organic solvent and nonionic Triton X-100 surfactant for the alginate: PEO blend, which allowed to produce nanofibers with a main diameter of 75 nm from 80 wt% alginate in the blends (Bhattarai and Zhang, 2007).

Saquing and co-researchers (2013) focused on the carrier polymer, PEO, and explaining its role in terms of entanglement and viscosity for the electrospinning of SA (Saquing et al., 2013). They obtained the concentration dependence of viscosity for an alginate−PEO system with a 70:30 mixing ratio. The $\eta_{sp} \sim c^{0.85}$ for the semidilute unentangled region, $\eta_{sp} \sim c^{2.37}$ for the semidilute entangled region and $\eta_{sp} \sim c^{3.45}$ for the concentrated region were reported, whereas for pure alginate solutions, the $\eta_{sp} \sim c^{0.79}$, $\eta_{sp} \sim c^{1.6}$, and $\eta_{sp} \sim c^{3.3}$, respectively. Their results showed that the proportion of η_{sp} changed

from $c^{0.85}$ to $c^{2.37}$ for the semidilute entangled region by replacing PEO with 30 % of alginate, shifting the alginate solution dynamics to more like a synthetic polymer behavior (Saquing et al., 2013).

2.4.4.2 Microorganism-based Biopolymers

Stijnman et al (2011) reported that the only food-grade polysaccharides capable of forming nanofibers from aqueous solutions were dextran (15 %), pullulan (15 %), and Glucidex DE 2 (50 %). The percentages in parentheses are of the polysaccharide concentration in the aqueous solution. Glucidex DE 2 was reported to form an irregular jet (Stijnman et al., 2011). Only dextran and pullulan are profiled below

Dextran

Dextran, a water-soluble, bacterial-derived polysaccharide, consists of α-l,6-linked D-glucopyranose residues with some α–l,2–, α–l,3–, or α–l,4–linked side chains (Jiang et al., 2004; Mendes et al., 2017). It can solubilize in both water and organic solvents and has been extensively used for biomedical applications due to its biodegradability and biocompatibility.

Jiang and coauthors (2004) investigated the effect of solvents (water, DMSO/water, and DMSO/dimethylformamide (DMF)) and concentrations (0.5 to 1.0 g/mL) on the electrospinning of dextran with a molecular weight in the range of 64-76 kDa (Jiang et al., 2004). They reported that uniform fibers with diameters of 100 nm were produced from aqueous solutions of 0.75 g/mL, and no beads occurred at c≥ 0.75 g/mL. The aqueous dextran solution at the concentration of 0.5 g/mL produced spherical beads with diameters of 0.5-6 μm as the fibers with spindle-like were produced at the concentration of 0.65 g/mL (Jiang et al., 2004). Also, Ritcharoen et al (2008) studied the effect of the solution

concentration and applied voltage on the electrospinning of the aqueous dextran solution and the resultant fiber morphology. They concluded that the beaded fibers were produced from the solution at the concentration up to a critical concentration of 0.9 g/mL, and the average fiber diameter size increased from 290 to 1950 nm with increasing its concentration in the range 0.7 to 1.3 g/ mL. However, the concentration of 1.3 g/ mL made the solution have a high viscosity (> 4.4 Pa. s). Increasing the electric field from 9 to 15 kV/cm increased the diameter size of dextran fibers from 520 to 1760 nm. Dextran was also crosslinked by using glutaraldehyde to improve the usefulness of electrospun dextran fiber mats in aqueous media (Ritcharoen et al., 2008).

Pullulan

Pullulan is a water-soluble fungal exopolysaccharide, which consists of α–1,6 glycosidic linked maltotriose connected to three glucose units bonded by α–1,4 glycosidic linkages which associate with randomly ordered chains (Shingel, 2004; Kristo and Biliaderis, 2007). Due to the distinctive linkage pattern of PUL, it has unique physical properties including high water solubility, biodegradability, high-water-absorbing capability, and the capability to form strong films and nanofibers (Li et al., 2011; Tomasula et al., 2016; Li et al., 2017). PUL is also capable of forming hydrogen bonds with proteins (Gounga, Xu, and Wang, 2010), which can make it as a good candidate for electrospinning carrier polymer.

PUL has been used to produce electrospun PUL fibrous mats or as a carrier polymer for food-based biopolymers which cannot be electrospun. Electrospun PUL nanofibers have been investigated for several biomedical applications, including targeted drug and gene delivery (Rekha and Sharma, 2009), wound dressing (Li et al., 2011). Pullulan

nanofibers were produced from aqueous solutions with diameters ranging from 100–700 nm (Sun et al., 2014) and by using 95% formic acid (Aceituno-Medina et al., 2013). PUL as a spinning aid, was used to produce API-based nanofibers with diameters in the range of 200 to 310 nm depending on the mixing ratio of API with PUL. The PUL: API nanofibers were produced and used for the encapsulation of folic acid. The fibrous structure was used to improve the thermal stability of folic acid and protected it from degradation after UV light exposure (Aceituno-Medina et al., 2015). Also, pectin-based (Liu et al., 2016), caseinates-based (Tomasula et al., 2016) and WPI-based (Drosou, Krokida, and Biliaderis, 2018) edible electrospun nanofibers were produced by using PUL as a carrier polymer.

Li et al (2017) studied the electrospinning of aqueous PUL solution containing sodium chloride (NaCl) or sodium citrate ($Na_3C_6H_5O_7$) at different concentrations to determine the effect of salt addition on the fiber morphology (Li et al., 2017). They reported that a lower concentration of PUL solution of 8 % (w/v) showed a Newtonian fluid behavior with a weak shear thinning behavior with an apparent viscosity of 0.03 Pa. s, whereas a higher concentration of PUL solution at the concentration of 15 % (w/v) showed a shear thinning behavior with an apparent viscosity ~0.25 Pa. s at the shear rate of 15 s^{-1} (Li et al., 2017).

Bead-free electrospun PUL fibers with diameters of 124±34 and 154±36 nm were produced from PUL solution 8%, (w/v) in the presence of a 0.20 M NaCl and 0.05 M $Na_3C_6H_5O_7$, respectively. PUL solutions with a salt concentration (NaCl or $Na_3C_6H_5O_7$) of 1 M or more produced thick fibers with defects and salt crystals adhering on the surfaces of fibers, as shown in Figure 8 (Li et al., 2017).

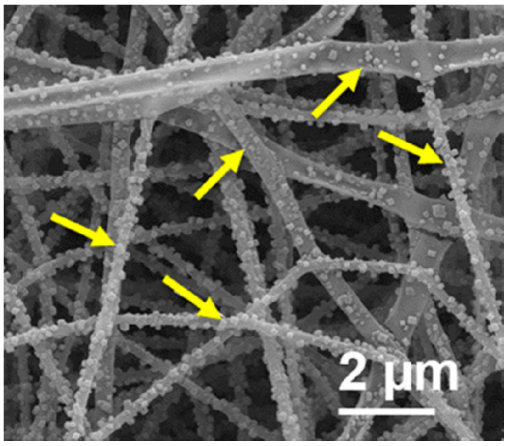

Figure 8: SEM image of PUL fiber (15 % PUL, 1.0 M NaCl) at high magnification (25,000×). Crystals of NaCl are seen on the fiber surfaces.

Liu et al (2016) produced nanofibers and nanofibrous mats from aqueous PUL and pectin (PEC) blend solution by using PUL as a processing aid (Liu et al., 2017). They reported that the c_e of pure PUL solution and the mixture of PEC and PUL were 5.8 and 4.3 wt%, respectively. The blends of 3 wt% PEC and 15 wt% PUL produced fibers with diameters of 140 nm and increasing PEC content in its blend with PUL decreased the fiber diameters from 140 to 38 nm with increasing bead formations. (Liu et al., 2017). The nanofibrous mats obtained from this blend were used to encapsulate a probiotic bacteria *Lactobacillus rhamnosus* GG (LGG) to test its viability. Since the initial loading of LGG, 8.26 $\log_{10}$, was decreased to that of 7.4 $\log_{10}$ in the nanofibrous mats, as shown in Figure 9A (Liu et al., 2016). The fibrous mats were crosslinked by calcium chloride ($CaCl_2$), which decreased pore size and changed the fibers morphology, and LGG bacteria were spread within the nanofibrous mats (Liu et al., 2016), as shown Figure 9B.

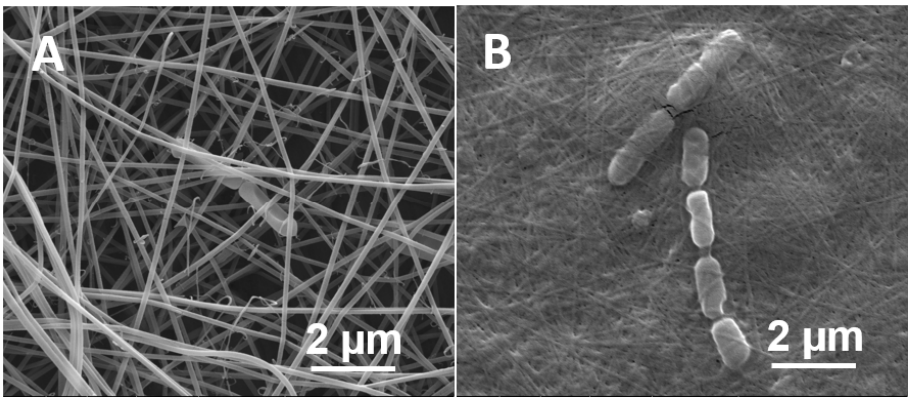

Figure 9: SEM images of electrospun LGG incorporated in PEC/PUL fibrous mats prior to cross-linking (A) and embedded in cross-linked mats (B).

Drosou et al (2018) used PUL as electrospinning aid for whey protein isolates (WPI) and produced continuous fibers with average diameters of 231 nm from aqueous WPI: PUL blends at weight mixing ratios of 20:80, 30:70, and 50:50. Also, uniform bead-free nanofibers were obtained from the WPI: pullulan blend solution at a ratio of 50:50, containing 10 wt% PUL. This could be attributed to improved molecular entanglement which PUL promotes by interacting with the protein (Drosou et al., 2018).

CHAPTER 3

The Objectives of the Thesis

The main goal of this study is to establish a fundamental work of edible caseinate and pullulan ultrafine fibers and fibrous mats for future studies by using the novel electrospinning technology. To achieve this goal, the study was pursued through the following specific objectives.

Objective 1: Evaluate the feasibility of electrospinning of milk-based proteins by evaluating the concentration regions and concentration dependence of viscosity for pure pullulan (PUL), nonfat dry milk (NFDM), calcium caseinate (CaCAS), and sodium caseinate (NaCAS) in aqueous solutions.

Sub-objective 1a: Determine the dependence of viscosity on aqueous PUL concentration, c, to identify the entanglement concentration, c_e, the point at which the polymer chains begin to entangle and the c regions where the formation of nanofibers occurred.

Sub-objective 1b: Determine the dependence of viscosity on aqueous NFDM, CaCAS, and NaCAS concentrations to identify the c_e and c regions and how these are related to fiber formation.

Hypothesis 1a-b: If the entanglement concentration of polymer is a determinant factor for polymers to be electrospun, then protein concentrations exceeding the c_e would be required for their electrospinning.

Objective 2: Investigate the effect of PUL carrier on the concentration dependence of viscosity and the c_e of NFDM and CAS solutions by identifying the c regions and c_e of their blend solutions.

Sub-objective 2a: Study the incorporation of PUL carrier into aqueous NFDM and CAS solutions by varying concentrations and mixing ratios to determine the role of carrier polymer on the c_e in fiber formation.

Hypothesis 2a: PUL can facilitate the molecular entanglements for caseinate proteins by affecting the concentration dependence of viscosity, concentration regions, and c_e to produce bead-free caseinate-based nanofibers.

Sub-objective 2b: Evaluate the incorporation of Lactobacillus Rhamnosus GG within fibrous mats to investigate the viability of the loaded probiotic as a model application.

Hypothesis 2b: Due to the higher surface area of fibrous mats, the bioactive compound would be embedded within the fibrous mats which may protect its viability from its surrounding conditions.

Objective 3: Investigate the effect of protein conformation on fiber morphology obtained from aqueous CAS solutions in the presence of PUL.

Sub-objective 3a: Evaluate the effect of higher pH on the concentration dependence of viscosity and the c_e of the CAS: PUL blended solutions and how they affect the morphology and mechanical properties of edible nanofibrous mats.

Hypothesis 3a: Increasing pH of fiber-making caseinate solutions would affect the entanglement of protein chains and improve the electrospinnability of milk proteins blended with PUL. Increase in protein content of fiber-making CAS-based solutions would increase the viscosity which promotes the protein chain entanglement and improves the fiber morphology. An improved morphology can likely improve the mechanical properties of the nanofibrous mats.

CHAPTER 4

Materials and Methods

4.1 Materials

Nonfat dry milk (NFDM) was obtained from Dairy Farmers of America (DFA Reading, PA, USA). NFDM contains 0.43 % fat, 3.1 % moisture, and 35.9 % protein provided by the manufacturer. Calcium caseinate (CaCAS) and sodium caseinate (NaCAS) were obtained from the American Casein Co. (AMCO Proteins, Burlington, NJ). CaCAS contains 90 % protein, 5.3 % moisture, 1.0 % fat, 4.1 % ash and less than 1 % carbohydrate while NaCAS has 88 % protein, 6 % moisture 1.8 % fat, 4.2 % ash and 1.0 % carbohydrate which are provided by the manufacturer. Pullulan (PUL) was obtained from TCI America (Portland, OR). 50 % liquid NaOH and $Ca(OH)_2$ powders were purchased from Sigma Aldrich (Saint Louis, MO) to use in pH adjustment. De-ionized (DI) water produced by Milli-Q Synthesis water purification system (Millipore, Billerica, MA, USA) was used to prepare the solutions. A plasticizer such as glycerol was ACS grade and obtained from Sigma-Aldrich (St Louis, MO, US) (will be used in the future experiments).

To compare PUL with other common carrier polymers used to electrospin the polymers which are not electrospinnable alone, a water-soluble polymer and food-grade biopolymer were briefly tested to observe their flow curves and concentration dependence of viscosity. Poly(ethylene oxide) (PEO) with 900 kDa was obtained from Sigma-Aldrich (Sigma-Aldrich, St Louis, MO) and gelatin from porcine skin, Type A (Gel) (G2500) was purchased from Sigma-Aldrich (Sigma-Aldrich, St Louis, MO). PEO at the concentrations ranging from 0.1 to 5.0 wt% were mixed with DI water for 2-4h at RT, but Gelatin Type A at the concentrations from 1.0 to 20.0 were prepared with DI water by mixing with a

magnetic stirrer (Cole-Parmer, Vernon Hills, IL) in a water bath at 45 ºC for 2-4h. Only gelatin solutions were run both rheology and electrospinning testing at 45 °C due to its gelation at 20 °C.

4.2 Methods

This section will cover the solution preparation, the rheological properties of biopolymer solutions, their electrospinning process and the analysis of fiber morphology.

4.2.1 Solution Preparation

4.2.1.1 Preparation of neat protein and polysaccharide solutions

All solutions containing NFDM, CaCAS, NaCAS, PUL and their blends were prepared with DI water by mixing with a magnetic stirrer (Cole-Parmer, Vernon Hills, IL), for 2-4h at 20 ºC at various concentrations (Table 2) by following the same procedure used in the lab (Dairy & Functional Foods Unit, Agricultural Research Unit Service, ERRC, USDA, Wyndmoor, PA). The solutions were refrigerated overnight at 4 ºC to remove air bubbles prior to electrospin (Tomasula et al., 2016). All the solution concentrations are expressed in % (w/w) and all solutions were measured at 20 °C unless any other temperature values were reported.

Table 2: Pure NFDM, CaCAS, NaCAS, and PUL solutions at various concentrations.

	Concentration of NFDM (wt%)	Concentration of CaCAS (wt%)	Concentration of NaCAS (wt%)	Concentration of PUL (wt%)
Neat solutions	1	1	1	1
	2	2	2	2
	3	3	3	3
	5	5	5	5
	7	7	7	7
	8	8	8	8
	9	9	9	9
	10	10	10	10
	11	11	11	11
	12	12	12	12
	13	13	13	13
	14	14	14	14
	15	15	15	15
	20	NA	NA	NA
	30	NA	NA	NA
	35	NA	NA	NA
	40	NA	NA	NA
	45	NA	NA	NA
	50	NA	NA	NA

4.2.1.2 Preparation of blend solutions

At neutral pH

NFDM, CaCAS, and NaCAS compounds with a concentration ranging from 1 to 25 wt% for NFDM and 1 to 20 wt% for both CAS were dissolved completely. Then, they were mixed with 15 wt% PUL wet solution at a pre-determined weight ratio for 2 h at 20 ºC under continuous mixing, as shown in Table 3, 4, and 5, respectively.

In our preliminary data, bead or defect-free and continuous fibers were produced from 15 wt% PUL than those with below 15 wt%. Therefore, 15 wt% PUL solution was used for its blends with NFDM, CaCAS, and NaCAS as a spinning aid. NFDM dissolved

in DI-water up to 50 wt% at 20 ºC, whereas CaCAS and NaCAS dissolved in DI-water up to 20 wt% under the same conditions. Then, to obtain fibrous mats the experiments were carried on with 15 wt% both NFDM and CAS and in blends with PUL at various mixing ratios of 30:70, 50:50, 67:33, 70:30, and 75:25 by increasing the protein content in the mixture solutions.

pH adjustment

After the characterization of solution compositions and fiber morphology, NFDM, CaCAS and NaCAS solutions at various concentrations (1, 3, 5, 9, 11, 13, 15, and 17 wt%) blended with 15 wt% PUL will be used to continue this study further. In the case, the pH of protein solutions was adjusted to pH 8, 9, and 10 before blending proteins with polysaccharide carrier. To study the effect of pH and increased protein content on the fiber morphology, the solutions were prepared from 15 wt% protein and 15 wt% polysaccharide with various weight ratios. Later part of the thesis used both pH 6.7 and 7.0 as a neutral pH.

Table 3: Concentration of NFDM and PUL solutions and their blends with a 50:50 weight mixing ratio and their zero shear viscosity at the shear rate of 10 s^{-1} at different pH of the solutions. pH adjustment was made with NaOH solution before blending with PUL.

Concentration of NFDM solution (wt%)	Concentration of PUL solution (wt%)	Weight ratio of blend solutions	Total blend concentration (wt%)	η_0 at shear rate of 10 s^{-1}, Pa. s
				pH 6.7
0	15	50:50	7.5	0.046
1	15	50:50	8.0	0.066
5	15	50:50	10.0	0.079
9	15	50:50	12.0	0.092
11	15	50:50	13.0	0.102
15	15	50:50	15.0	0.121
20	15	50:50	17.5	0.197
25	15	50:50	20.0	0.283

Table 4: Concentration of CaCAS and PUL solutions and their blends with a 50:50 weight mixing ratio and their zero shear viscosity at the shear rate of 10 s^{-1} at different pH of the solutions. pH adjustment was made with NaOH solution before blending with PUL.

Concentration of CaCAS solution (wt%)	Concentration of PUL solution (wt%)	Weight ratio of blend solutions	Total blend concentration (wt%)	η_0 at shear rate of 10 s^{-1}, Pa. s			
				pH 6.7	pH 8.0	pH 9.0	pH 10.0
0	15	50:50	7.5	0.046	NA	NA	NA
1	15	50:50	8.0	0.059	0.067	0.059	0.059
5	15	50:50	10.0	0.081	0.093	0.090	0.084
9	15	50:50	12.0	0.108	0.131	0.127	0.1172
11	15	50:50	13.0	0.137	0.167	0.157	0.1484
15	15	50:50	15.0	0.244	0.232	0.289	0.223
		67:33	15.0	0.149	0.218	0.469	0.378
		75:25	15.0	0.137	0.267	0.500	1.025
20	15	50:50	17.5	0.302	NA	NA	NA

Table 5: Concentration of NaCAS and PUL solutions and their blends with a 50:50 weight mixing ratio and their zero shear viscosity at the shear rate of 10 s^{-1} at different pH of the solutions. pH adjustment was made with NaOH solution before blending with PUL.

Concentration of NaCAS solution (wt%)	Concentration of PUL solution (wt%)	Weight ratio of blend solutions	Total blend concentration (wt%)	η_0 at shear rate of 10 s^{-1}, Pa. s			
				pH 6.7	pH 8.0	pH 9.0	pH 10.0
0	15	50:50	7.5	0.046	NA	NA	NA
1	15	50:50	8.0	0.060	0.06	0.06	0.06
5	15	50:50	10.0	0.080	0.09	0.09	0.09
9	15	50:50	12.0	0.106	0.14	0.12	0.12
11	15	50:50	13.0	0.129	0.16	0.15	0.15
15	15	50:50	15.0	0.193	0.286	0.280	0.280
		67:33	15.0	0.247	0.326	0.329	0.356
		75:25	15.0	0.318	0.442	0.470	0.536
20	15	50:50	17.5	0.480	NA	NA	NA

4.2.2 Solution Rheological and Physical Properties

4.2.2.1 Solution viscosity

Before the viscosities, electrical conductivities, surface tensions of the solutions were measured at 20 ºC on the next day. They were taken from the refrigerator, left outside, and mixed for 20 min to reach RT. All measurements were conducted at 20 ºC, each sample was examined for at least 5 times, and an average was taken.

The shear viscosities of the solutions were investigated using a rheometer equipped with a 27.4 mm inside diameter cup and a 25 mm outside diameter bob (Kinexis Lab+; Kinexus Instruments, Worcestershire, UK).

4.2.2.2 Solution pH, conductivity, and surface tension

The pH and electrical conductivities of NFDM, CaCAS, NaCAS, PUL, and their blend solutions were measured using a conductivity meter (IQ270G; Scientific Instruments, Loveland, CO) with built in a temperature sensor and automatic temperature correction (reference temperature = 25 ºC).

Surface tension is a measure of the tendency of a liquid to minimize its surface area due to interactions among the molecules (Steffe, 1996). The surface tensions of these solutions were determined using rate-hart Advanced Automated Goniometer equipped with automated tilt, dispensing and DROPimage advanced (rate-hart Instruments, Succasunna, NJ).

4.2.3 Electrospinning

The electrospinning process was run by using similar conditions with a few modifications that Tomasula et al (2016) studied. Each polymer solution was fed into a 3 mL disposable plastic syringe fitted with a tubeless spinneret in an electrospinning unit

consisted of a syringe pump, a high voltage generator, and a grounded rotating cylinder receptor (NaBond Technologies, Hong Kong, China). The pump delivered the solution to the spinneret at a flow rate. The voltage source connected to the needle with a range of 0 to 50 kV and the fiber was collected on the rotating cylinder covered (10.2 cm diameter) with an aluminum foil (Tomasula et al., 2016).

All samples were electrospun at 20 ºC under constant operating parameters: distance from the needle tip to the receptor of 12 cm; flow rates ranging from 1.0 to 3.0 mL/h; voltages varying from 11 to 20 kV and the rotating speed of the collector of 80-84 rps. The fibrous mats with an average dimension of 20, 10, and 0.01 cm as width, length, and thickness were produced by using 3 mL of each solution, which resulted in the mats with 2.5 g with an average porosity of 50%, measured by ImageJ software. The dimensions depend upon both solution and processing parameters, as well as the amount of polymer solutions used for the electrospinning.

The collected samples of fibers on the counter electrode were cut in a small strip for SEM analysis. These conditions were acquired from the preliminary data obtained from the resultant fibers in triplicate. When the solution was viscous, the whipping motion visually became narrower. Also, an increase in the applied voltage decreased the radius of whipping motion due to the increase in electrostatic force, which shortens the travel time of jet under the electric field. Resultant fibers and fibrous mats were characterized by scanning electron microscopy (SEM) for morphology, as shown in Figure 10, and Fourier transform infrared spectroscopy (FT-IR) for chemical structure.

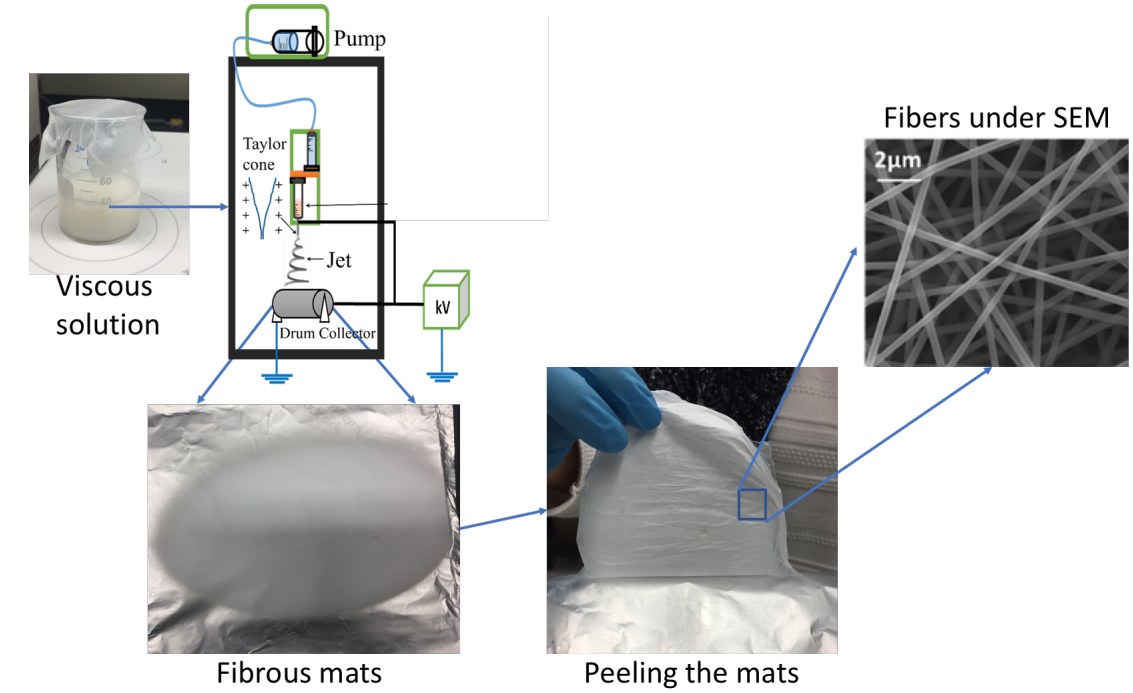

Figure 10: The short graphical picture of the process.

4.2.4 Scanning Electron Microscopy (SEM) Analysis

SEM (FEI, Hillsboro, OR) was used to examine the samples of the fibrous mats coated with a thin gold film. At an accelerating voltage of 10 kV, the high-vacuum secondary electron imaging modes with the distance of 12.5 mm were applied. Fiber diameter sizes for the fibrous mat samples were measured using the ImageJ software with Diameter J plugin to construct a diameter histogram and pore size or space among fibers, as shown in Figure 11. OriginLab software (2018b OriginLab Corporation, Northampton, MA) was used to plot the flow curves of the solutions, nanofiber diameter histograms, and its statistical analysis plugin to compare the significance of the results.

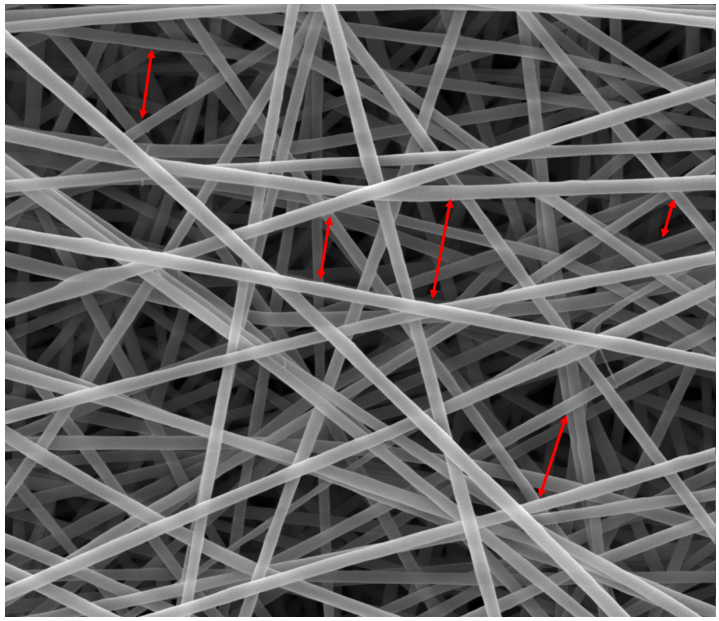

Figure 11: SEM image of 15 wt% NaCAS blended with 15 wt% PUL with a 67:33 mixing percentage. The fibers diameter size and the spaces or pore size among the fibers that red arrows pointed are measured by the ImageJ software with DiameterJ plugin.

4.2.5 Fourier Transform Infrared Spectroscopy (FT-IR) Analysis

FT-IR spectra were recorded on a Thermo Scientific IS50 FTIR (Madison, WI) for liquid samples in a scanning range of 1111-4000 cm^{-1} for 128 scans at a spectra resolution of 4 cm^{-1}. CaF_2 windows were used to dry the liquid solutions under vacuum before testing. Solid samples were recorded on the same FT-IR system coupled with IS50 ATR accessory in a scanning range 400-4000 cm^{-1} for 128 scans at the same resolution.

4.2.6 Tensile Properties of Nanofibrous Mats

The viscoelastic properties of electrospun CAS: PUL blend nanofibrous mats under a controlled RH were measured via dynamic mechanical analysis (DMA-Q800, TA Instruments, New Castle, PA) with a closed unit to control RH by an external RH generator linked to the RH sensor in the cabinet and kept RH constant, 50 ± 0.5 %.

The fibrous strips were cut with a height of 20 mm and length of 5.3 mm. The thickness of each strip was measured at 10 different points with a Mitutoyo absolute

thickness gage with a precision of 0.01 mm (Mitutoyo Corp., Kanagawa, Japan) and averaged before mounting them in DMA unit. The strip of the fibrous mat was loaded vertically onto a tensile grips clamp with a 15 mm gauge length, and stress-strain curves were recorded 5-6 strips of each fibrous mat tested by applying an oscillatory displacement (strain). The testing was begun with the equilibrium to the 50 % RH for 1h. Then, a static force increase of 0.01 N/min was employed until the rupture of the fibrous mats. The various tensile properties were obtained by using the stress-strain curves. They are Young's modulus, E (MPa) defined as the initial slope of the linear curve; tensile strength, TS (MPa) was taken the value from the curve which corresponds to the point of maximum stress; and elongation-at-break, EB (%) was attributed to the value of the strain (%) at which rapidly decreases depending upon the rupture of mat.

4.2.7 Bacteria Strain and Media

Lactobacillus rhamnosus GG (ATCC 53103) was maintained in deMan Rogosa and Sharpe (MRS) broth (Difco Laboratories, Detroit MI) at 37 °C. Prior to inoculation of CaCAS-based solutions, *L. rhamnosus* GG was grown overnight in 25 mL of MRS broth, which reached a cell density of 4×10^9 colony forming units (CFU) mL^{-1}. The culture was centrifuged at 2990×g and washed three times in 0.1 % peptone water, and then resuspended in 10 mL of 15 wt% of CaCAS blended with 15 wt% PUL solution. The suspension *L. rhamnosus* viability was analyzed by plating on MRS agar immediately after resuspension in the CaCAS: PUL blend solution. The solutions with a bioactive bacteria were electrospun under the same conditions, as mentioned in Section 5.2.3. A fibrous mat with a weight of 2.5 g was obtained and a sample piece was cut for SEM analysis. To determine the viability of *L. rhamnosus* GG within the nanofibrous mats, 1 g of the mats

were dissolved in 9 mL of peptone water by shaking at 2200 rpm for 1h at RT and then plated on MRS agar for 2 days at 37 °C.

CHAPTER 5

Electrospinning of Pure Pullulan, Nonfat Dry Milk, and Caseinates

This Chapter will cover Objective 1 and attempt to explore the importance of viscosity on the molecular chain entanglements of pure PUL, NFDM, CaCAS, and NaCAS and their ability to electrospin alone and establish a correlation between the chain entanglements and the ability of fiber formation. The c_e and the c regions were identified for these biopolymer solutions.

As mentioned before in Section 2.3, a stable jet is required for a successful electrospinning. The stable jet is only formed when sufficient chain entanglements (numbers of entanglement ≥2.5) occur, and the occurrence of such entanglements depends upon the viscosity which is a function of concentration and molecular weight of the polymers (Shenoy et al., 2005). The increase in the polymer concentration stabilizes the jet and then promotes continuous electrospun nanofiber formation. Therefore, chain entanglement increased with increasing the polymer concentration when the molecular weight is above entanglement molecular weight have been considered to correlate to electrospinnability of polymers and fiber morphology. Because the electrospinning of NFMD and CAS solutions was difficult, it is anticipated that their solutions can be electrospun when the concentrations are above the c_e.

The objective of this Chapter was to study the feasibility of electrospinning of a polysaccharide and milk-based proteins by evaluating the c and the c dependence of the viscosity of pure PUL, NFDM, CaCAS, and NaCAS in aqueous solutions and the relationships between the solution rheology and electrospinnability of these biopolymers without using any organic solvents, acids, or carrier polymers.

5.1 Overview

To investigate the relationship between the viscosity and polymer chain entanglement, we investigated the onset of the chain entanglement for PUL and NFDM and its derivatives, CaCAS and NaCAS, in aqueous solutions with varying concentrations and weight mixing ratios. The changes in the solution properties such as electrical conductivity, viscosity, and surface tension were also determined to have a better understanding of the electrospinning process for food-grade biopolymers.

5.2 Preliminary results for aqueous NFDM and CAS dispersions

As increasing the concentration of CaCAS, it started to swell under a continuous mixing and then reverts to a liquid form 20 min later, whereas NaCAS was required to disperse first to dissolve by adding the powder slowly in DI-water. The swelling is most probably due to the submicelles structures which can reversibly interact with Ca^{2+} and trap the water at the beginning of mixing in CaCAS solutions. NaCAS solutions had translucent (non-milky) appearance while NFDM and CaCAS solutions appeared turbid (opaque and white). This is expected due to the polymerization characteristics of caseins because the proteins without calcium remain as protein strands and small agglomerates (McMahon and Oommen, 2013). CaCAS has a lower viscosity than NaCAS solutions at the same solid concentration. It results from linear polymeric rods and weakly branched chains formed by self-assembly of caseins in sodium caseinates in the absence of calcium (Thomar et al., 2012). The η_0 of NFDM ranged from 0.05 to 0.28 Pa. s at the shear rate of 10 s^{-1} as the neat protein concentration increased from 0.15 to 3.75 wt% in blend solutions, as shown in Table 3. NFDM is less viscous than both CAS at the same solid concentration because NFDM and CAS contain proteins by about 30 % and 90%,

respectively, which influence the viscosity of the solutions (McMahon and Oommen, 2013).

5.3 Control PUL, NFDM, CaCAS, and NaCAS

Flow curves were built from shear viscosity versus shear rate data obtained with the shear rate changing from 0.01 to 1000 s^{-1} for all solutions prepared from NFDM, CaCAS, NaCAS, and PUL. Then, shear viscosity at 10 s^{-1} was used to calculate the specific viscosity (η_{sp}) to plot it against to the concentration, c, to determine the overlap concentration, c^*, the entanglement concentration, c_e, and the concentrated regime, c^{**}. The c^*, c_e, and c^{**} were determined from the intercepts of the fitted lines in the semidilute unentangled, semidilute entangled, and concentrated regimes. The η_{sp} was calculated by using Equation 4, as mentioned in Section 2.3.1.

In this chapter, control solutions were prepared from neat PUL, NFDM, CaCAS, and NaCAS. NFDM solutions in the concentration range from 1 to 50 wt% were prepared and CaCAS, NaCAS, and PUL in the concentration range from 1 to 20 wt% were prepared at 20 ºC. Then, each protein solution was blended with 15 wt% PUL with a 50:50 weight ratio with total solids concentrations also ranging from 1 to 20 wt%. Three regions, the semidilute unentangled ($c<c^*$), the semidilute entangled ($c_e<c$), and the concentrated entangled ($c^{**}<c$) regimes were identified in the plot of the concentration dependence of the viscosity for neat PUL, NFDM, CaCAS, and NaCAS.

5.3.1 Pullulan (PUL)

Rheological Properties and Determination of Concentration Regimes

The concentration regimes for neat PUL solutions were determined using solution rheology measurements. Viscosity directly depends on the concentration of the solution

and molecular weight of the polymer. These parameters of the solution influence the ability of electrospinning of the polymer solutions. The chain entanglements and concentration regions can be determined to evaluate the fiber formation, which is reported in the literature (Colby et al., 1991; McKee et al., 2004; Shenoy et al., 2005). Figure 12 shows a plot of shear viscosity as a function of shear rate for PUL solutions at various concentrations. Even though the shear rate involved in electrospinning is much higher than the highest shear rate in our rheological tests, the shear rate ranges from 0.01 to 1000 s^{-1} were performed on the solutions ranging from 1 to 20 wt% in aqueous solutions at 20 ºC.

PUL solutions at the lower concentration showed Newtonian behavior and their viscosities increased from 0.007 to 0.2 Pa. s as increasing concentration ranging from 1 to 10 wt%. However, shear thinning behavior occurred at the higher concentration than 10 wt% at a higher shear rate. In the range of shear rates less than 100 s^{-1}, the shear viscosity of 15 wt% PUL solution, 1.0 Pa. s, was about 10 times higher than that of 8 wt% PUL, 0.09 Pa.s. This finding is consistent with the previously reported data by Deitzel et al (2001) who found that a mixture of fibers and beads were obtained from the electrospinning of PEO (400 kDa) when the solution viscosity was below 1 Pa. s (Deitzel et al., 2001). Even though the PUL solutions at the concentrations ranging from 11 to 15 wt% showed shear thinning behavior, the influence of shear rate on the shear viscosity was still very light at the shear rates below 100 s^{-1}. These results are consistent with the findings by Li et al (2017) that reported that the viscosity of 15 % PUL solutions was 8 times higher than that of 8 % PUL solution in the range of low shear rates.

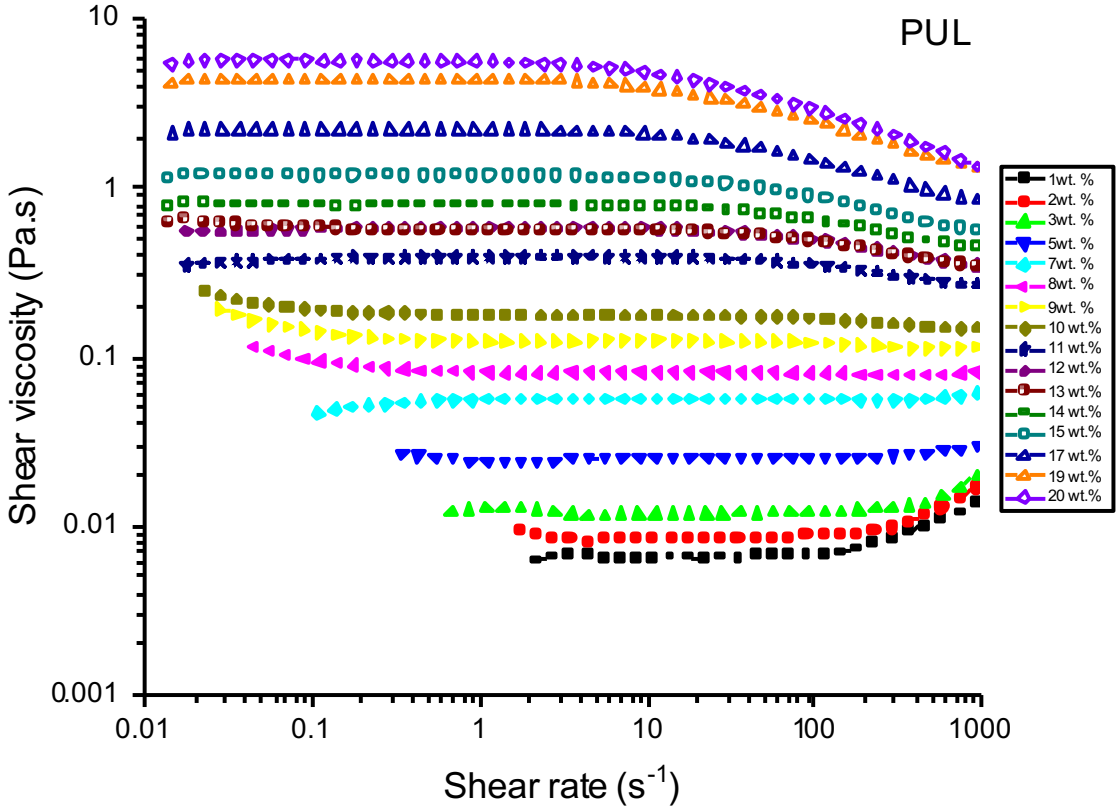

Figure 12: Dependence of shear viscosity (Pa. s) on shear rate (s^{-1}) for PUL at the concentrations ranging from 1 to 20 wt% in aqueous solutions.

Figure 13 shows the concentration dependence of specific viscosity for aqueous PUL solutions. The η_0 obtained from flow curves at the shear rate of 10 s^{-1} and used to calculate η_{sp}. η_0 increased from 0.006 to 4.789 Pa. s as the concentration of PUL solutions was increased from 1 to 20 wt%. PUL polysaccharide contribution to the η_0 was studied by calculating the η_{sp} in Equation 4 to plot the dependence of η_{sp} on the solution concentration. The slope changes marked the beginning of the semidilute unentangled, semidilute entangled, and concentrated regimes. The dilute region was not determined since the rheology measurement was not performed on PUL solutions less than 1 wt%. The c^*, c_e, and c^{**} were determined following the method employed by Colby et al (1991). They were 4.0, 5.5, and 12 wt%, respectively.

In aqueous dispersion of PUL, the c_e was observed 5.5-6.0 wt%. This is close to reported values for PUL in aqueous solutions which were, 5.33 (Kong and Ziegler, 2014) and 5.8 (Liu et al., 2016). In the semidilute unentangled regime ($c<c_e$), the η_{sp} was proportional to $c^{0.61}$, which is similar to the reported values for PUL in water ($\eta_{sp}\sim c^{0.95}$) (Kong and Ziegler, 2014). However, our finding is a little lower than the theoretical values ($\eta_{sp}\sim c^{1.4}$) for random coil polysaccharides including dextran, locust bean gum, guar gum, and hyaluronate in dilute solutions at low pH and high ionic strength (Morris et al., 1981) and the theoretically predicted value ($\eta_{sp}\sim c^{1.25}$) for neutral, linear polymers in semidilute unentangled regime in a good solvent (Daoud and De Gennes, 1979). This little difference can be due to the solution properties including types of solvents, their viscosities, pH, ionic strength, and temperature. For example, water with a viscosity of 0.001 Pa. s at 20 $^{\circ}$C was used in this study as a solvent to calculate the η_{sp} of all solutions. In the semidilute entangled regime ($c_e< c$), η_{sp} was proportional to 2.85 to 4.76 for aqueous PUL dispersion, which is similar to theoretically predicted values for random-coil polysaccharides from 2.0 to 3.3 (Morris et al., 1981) and the theoretical prediction for linear and random coil polymers, 3.4 (Wool, 1993). Daoud and De Gennes (1979) predicted the similar values that $\eta_{sp}\sim c^{1.25}$ in the semidilute unentangled regime, $\eta_{sp}\sim c^{4.8}$ in the semidilute entangled regime, and $\eta_{sp}\sim c^{3.6}$ in the concentrated regime for neutral and linear polymers in a good solvent (Daoud and De Gennes, 1979).

An increase in polymer concentration results in the following transition of the fiber morphology: (1) beads only, (2) beads with incipient fibers, (3) beaded fibers and (4) fibers only. The morphology of resultant PUL fiber at different concentrations, 5, 11, and 15 wt%, was evaluated by SEM, as shown in Figure 15. When the c is in the range of semidilute

unentangled regime, which is less than c_e, beads with incipient fibers were produced from aqueous PUL solution. The fibers with beads and defects were formed as the concentration of aqueous PUL solution was increased to the range of semidilute entangled region, as shown in Figure 13. As the concentration was increased to 7 wt% above the c_e, beaded nanofibers were formed with diameters less than 100 nm (Figure 14b). More uniform, fully-formed nanofibers were obtained from PUL solutions with the concentrations ranging from 11 to 16 wt%, is similar to the results reported (Kong and Ziegler, 2014). Also, Liu et al (2016) reported that the beads with incipient fibers from PUL solutions were obtained at the concentration of 5.8 wt%, which is consistent with our result of the c_e ranging from 5.5 to 6 wt% (Liu et al., 2016).

In addition to the shear viscosity and concentration regimes, other solution properties including electrical conductivity and surface tension are important parameters for the nanofiber formation through the electrospinning process. Table 1 shows the electrical conductivity, surface tension, and shear viscosity at the shear rate of 100 s^{-1} measured for PUL solutions at various concentrations at 20 ºC.

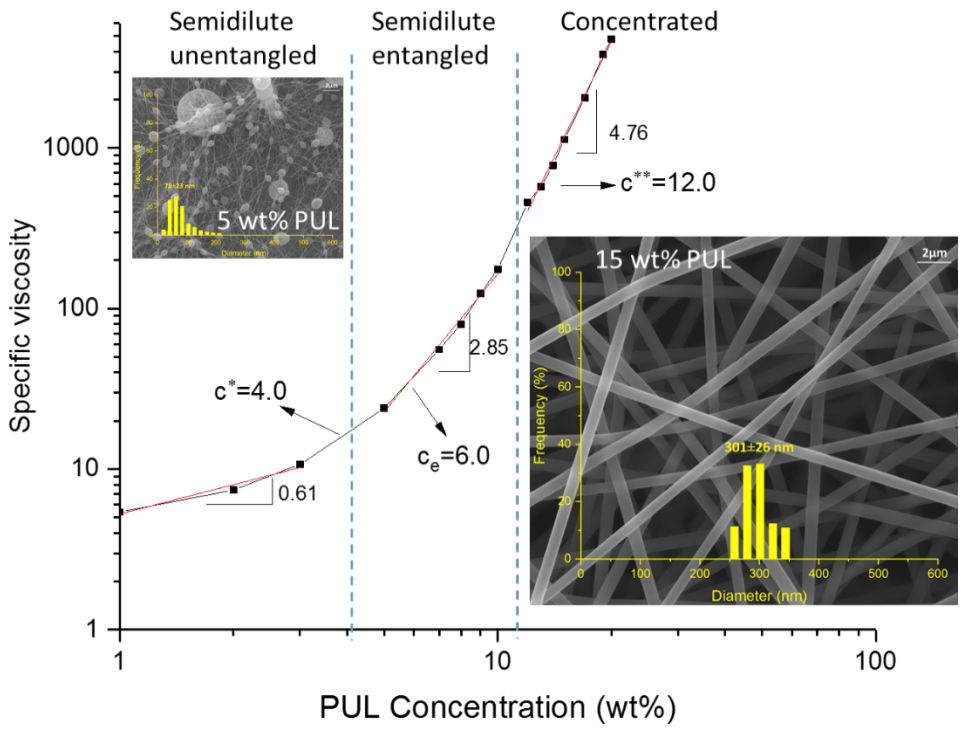

Figure 13: Dependence of specific viscosity on concentration for PUL solutions. c* is overlap concentration; ce is the entanglement concentration; c** is concentrated regime.

The values of surface tension of the PUL solutions slightly decreased from 73.17 to 67.57 mN/m with increasing PUL concentration from 1 wt% to 15 wt%, whereas the electrical conductivities were very low < 0.1 mS/cm, as shown in Table 6 and Figures 27 and 28. These results are close to the reported conductivities of 0.02, 0.03 and 0.05 mS/cm for PUL solutions at the concentrations of 5, 8, and 15 wt%, respectively (Tomasula et al., 2016). A slight difference in their results could attribute to the different processing conditions, which is temperature of 50 ºC higher than the processing temperature (20 ºC) in this study. For instance, the surface tension was measured as 61.8 mN/m and the electrical conductivity was reported as 0.0499 mS/cm in aqueous PUL solution at the concentration of 15 wt% at 50 ºC. All PUL dispersions (in water) showed a shear viscosity at 100 s^{-1} in the range of 0.4 to 1.0 Pa. s (Table 6), which is similar to the reported range from 0.06 to 2.2 Pa. s and 0.2 to 2.2 Pa. s for PUL and starch in dimethyl sulfoxide (DMSO)

solvent, respectively (Kong and Ziegler, 2012; 2014). DMSO lowered the concentration dependence of viscosity for PUL dispersion, enabling the electrospinning of high viscous PUL solution (Kong and Ziegler, 2014).

Table 6: Physical properties of neat PUL solutions and fiber morphology.

	Concentration (wt%)	Electrical conductivity (mS/cm)	Surface tension (mN/m)	Shear viscosity at 100 s^{-1} (Pa. s)	Morphology
PUL	1	0.01±0.00	73.17±0.03	0.007	No fiber
	2	0.02±0.00	70.58±0.03	0.009	No fiber
	3	0.01±0.00	70.12±0.03	0.012	No fiber
	5	0.02±0.00	69.31±0.04	0.025	No fiber
	7	0.03±0.00	70.36±0.02	0.057	Beaded fibers
	8	0.02±0.00	71.21±0.02	0.080	Beaded fibers
	9	0.03±0.00	70.87±0.02	0.122	Beaded fibers
	10	0.02±0.00	70.70±0.03	0.170	Beaded fibers
	11	0.04±0.00	70.17±0.03	0.353	FIBERS/ 160±26 nm
	12	0.03±0.00	69.75±0.03	0.484	FIBERS/ 230±22 nm
	13	0.04±0.00	69.77±0.03	0.495	FIBERS/ 342±24 nm
	14	0.03±0.00	69.74±0.02	0.650	FIBERS/ 315±26 nm
	15	0.05±0.00	67.57±0.07	0.885	FIBERS/ 301±26 nm
	16	0.06±0.00	65.12±0.09	1.004	FIBERS/ 416±23 nm
	17	NA	NA	1.481	NA at 20 °C
	19	NA	NA	2.511	NA at 20 °C
	20	NA	NA	2.990	NA at 20 °C

Electrospinning of Pullulan Solutions

PUL samples were electrospun from aqueous solutions. PUL was dissolved in DI water, but it was required to keep a certain distance between the tip of the needle and

grounded collector to allow the solvent evaporation during electrospinning due to the lower vapor pressure (2.43 kPa at 20 ºC) of water. The distance of 12 cm was used to electrospin PUL solutions. The electrospinning process was run under the flow rate of 3 mL/h and the applied voltage ranging from 15 to 20 kV.

Figure 14 shows SEM micrographs of electrospun nanofibers from PUL solutions at various concentrations and the distribution of fiber diameter size. Bead-free fibers were not obtained from neat PUL solutions with the concentration lower than 10 wt%. The FDS increased with increasing PUL concentrations and the fibers became bead- and defect-free at the concentration of 15 wt%. The results are consistent with the previous studies (Kong and Ziegler, 2014; Tomasula et al., 2016; Liu et al., 2016; Li et al., 2017).

At 16 wt% PUL (Figure 14), the fibers showed the highest FDS of 416±23 nm and were more uniform as the fibers from 15 wt% PUL produced with the diameter of 301±26 nm under the same processing conditions; the flow rate of 3 mL/h, the applied voltage of 20 kV and the temperature of 20 °C. Increasing concentration up to 16 wt% produced thicker fibers than the concentration less than 11 wt%. Mean fiber size was plotted against to PUL concentration to determine the dependence of diameter size on the concentration, as shown in Figure 14-l. The relationship between diameter size and concentration fitted in a linear equation, $y=1.64x+0.61$, with R^2 of 0.79. As increasing the PUL concentration from 9 to 16 wt%, the diameter size of resultant fibers increased and showed a distribution with a less standard deviation.

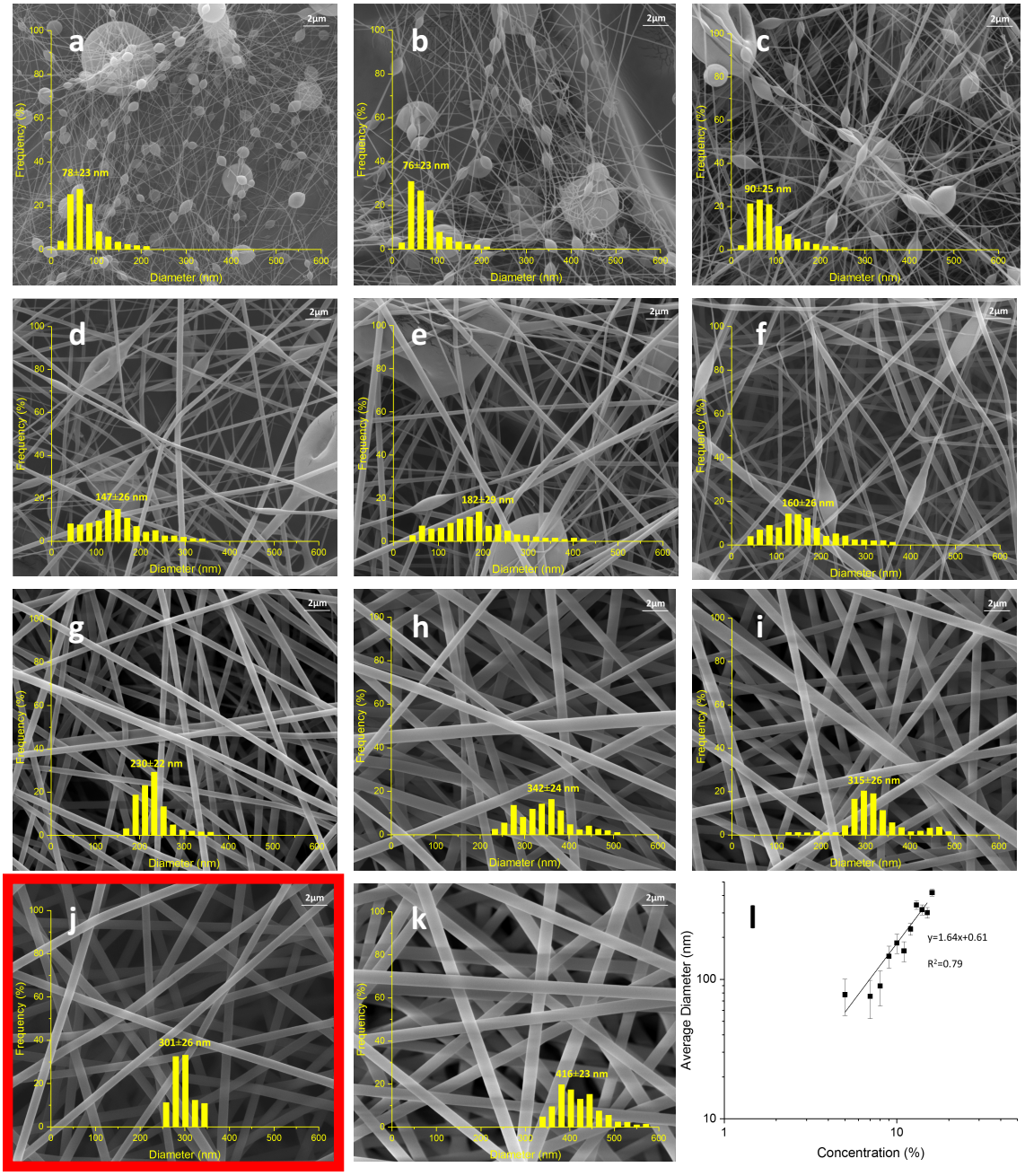

Figure 14: SEM images of electrospun nanofibers from PUL solutions at various concentrations and the distribution of fiber diameter size: (a) 5 wt.% PUL, 78±23 nm, (b) 7 wt.% PUL, 76±23 nm (c) 8 wt.% PUL, 90±25 nm (d) 9 wt% PUL, 147±26 nm (e) 10 wt% PUL, 182±29 nm, (f) 11 wt% PUL, 160±26 nm, (g) 12 wt% PUL, 230±22 nm, (h) 13 wt% PUL, 342±24 nm, (i) 14 wt% PUL, 315±26 nm, (j) 15 wt% PUL, 301±26 nm, (k) 16 wt% PUL, 416±23 nm, (l) dependence of mean diameter on PUL concentration, y=1.64x+0.61 R^2=0.79.

Figure 15 shows the SEM images of fibrous mats produced from three different concentration of PUL solutions at 4 different magnifications. Under the scale of 500 μm, the fibrous mats had some spotted black regions because of electrospraying, spotted white regions resulted from jet breakups and smooth surface for 5, 11, and 15 wt% PUL solutions, respectively. As the magnification increased, the fibrous mats with smooth surface showed a uniform, well-formed fiber structure at a high concentration of PUL solution. This result was confirmed the relationship between the solution rheological properties and concentration regions.

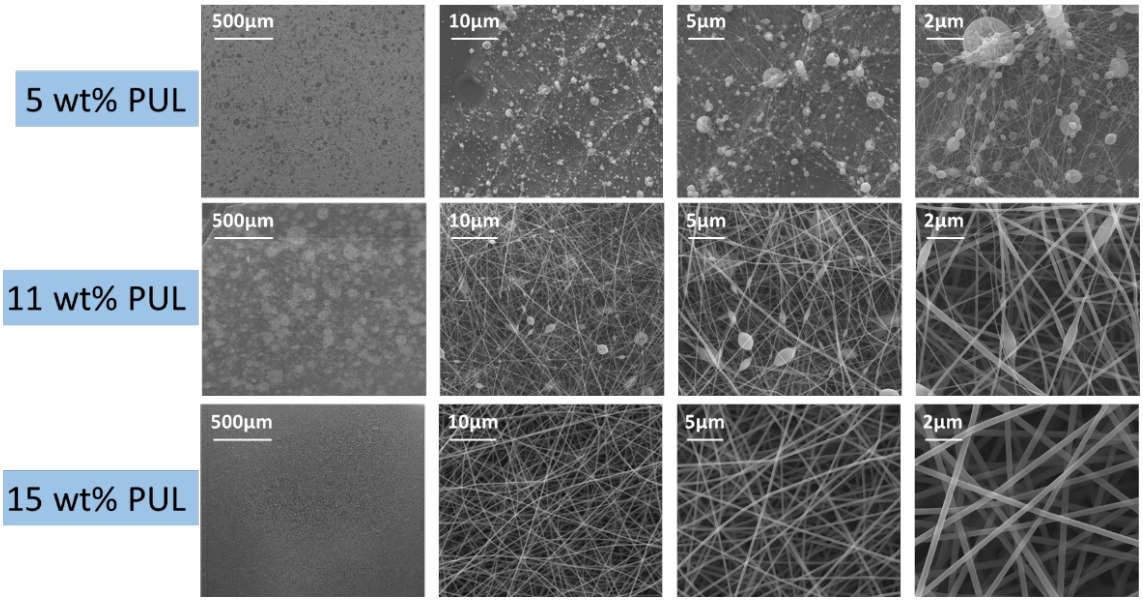

Figure 15: Electrospun fibrous mats from 5, 11, and 15 wt% PUL at the magnifications of 100×, 5,000×, 10,000× and 25,000×.

The dependence of the electrospun fiber diameter on η_0 for PUL solutions is shown in Figure 16. Three different fiber morphologies were identified based on the η_0 of the solutions. The PUL solutions with a η_0 less than 0.02 Pa. s produced polymer droplets when electrospun, as the solutions with a η_0 between 0.03 and 0.45 Pa. s produced electrospun fibers with beads, as shown in Figure 16. The fiber-forming solutions with a

η_0 greater than 0.45 Pa. s generated defect-free and uniform fibers. Moreover, the mean fiber diameter size correlated with η_0 by the relationship below

$$\text{Diameter (nm)} = 323.7\eta_0^{0.44} \qquad \text{Equation 5}$$

An increase in the zero shear rate viscosity (η_0) indicated a larger number of polymer chain entanglement, leading to form thicker electrospun fibers.

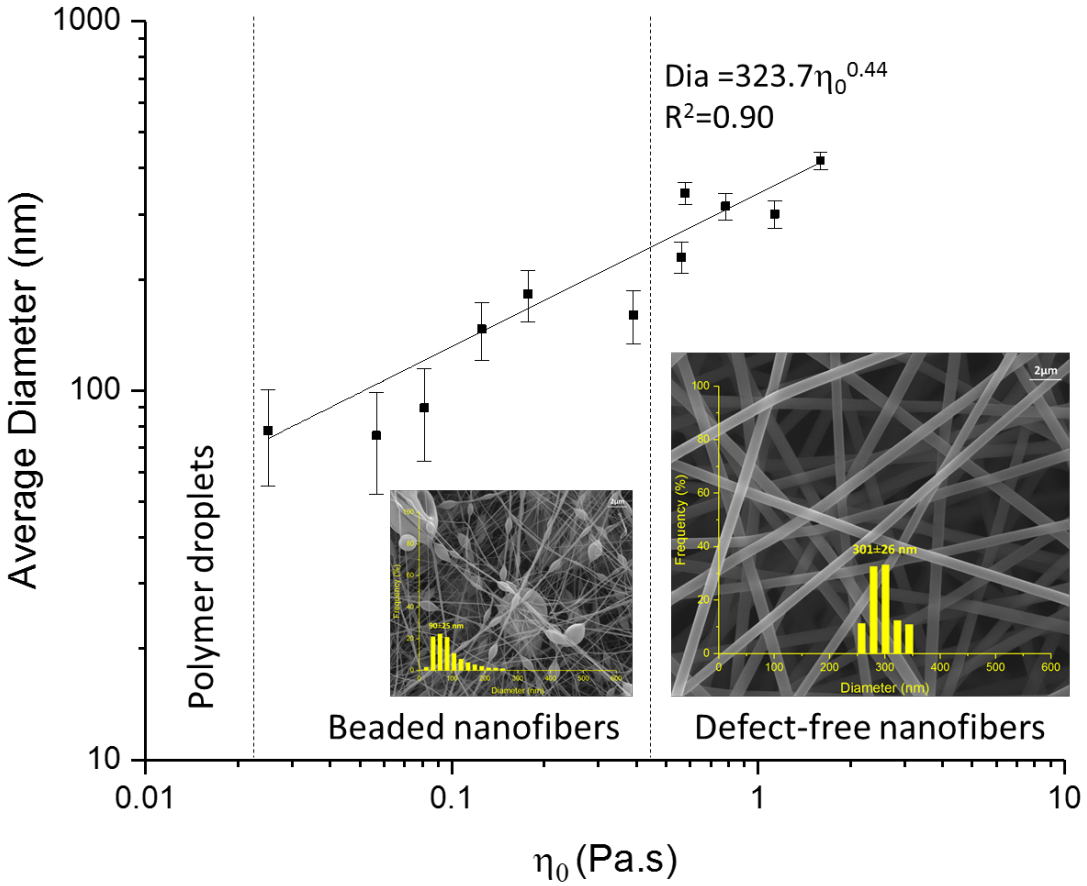

Figure 16: Dependence of electrospun fiber size on the η_0 for PUL solutions. Three distinct regimes of morphology were determined based on the η_0: polymer droplets, beaded nanofibers, and defect-free fibers.

Figure 17 shows that the solution of each PUL concentration was normalized with its respective c_e value to evaluate the dependence of fiber diameter on normalized solution

concentration for PUL solution series. The electrospun PUL fiber diameter scaled with the normalized concentration as

$$\text{Diameter (nm)} = 74.7\ (\frac{c}{c_e})^{1.6} \qquad \text{Equation 6}$$

where c is the polymer concentration in the solution and c_e is the entanglement concentration. In Figure 17, the shaded region shows 2-2.5 times c_e, which was the minimum concentration required to electrospin fully-formed and defect-free fibers. Equation 6 was estimated based on the plot of η_{sp} versus concentration data for the concentration regions to predict $c \sim \eta_{sp}^{3.8}$. Then, this relationship was substituted into the Equation 5 obtained from the plot of average diameter versus η_0, it was predicted as the $\text{diameter (nm)} = c^{1.67}$, which is identical to the equation obtained from Figure 17. The formation of smooth and defect-free fibers required that PUL concentration 1.7 to 2.7 times c_e, which is a wider range than the reported concentration 1.88 to 2.25 times c_e for PUL in DMSO solvents (Kong and Ziegler, 2014).

In this study, our lab used PUL as an edible carrier polysaccharide to electrospun casein-based proteins due to its properties to interrupt the 3D structure of proteins and favor them to entangle and stretch under an electric field. This strategy was extensively used for fiber production for non-food applications by adding PEO or PVA carriers. Xie and Hsieh (2003), for instance, used PEO and PVA to electrospun casein proteins in aqueous triethanolamine.

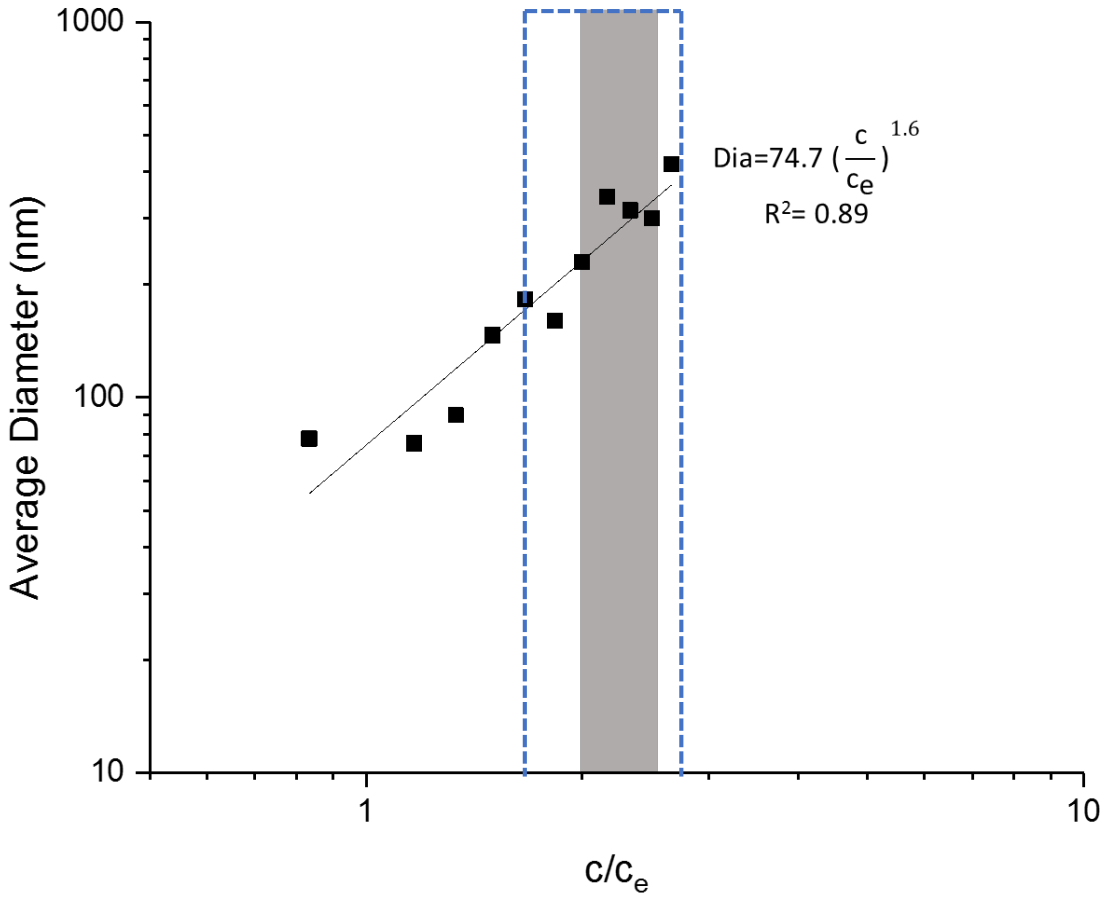

Figure 17: Dependence of fiber diameter on the normalized concentration for PUL solutions. The blue dashed region corresponds to fully-formed PUL fibers at the concentration of 1.7-2.7 times c_e and grey shaded area represents 2.0-2.5 times c_e for the defect-free fiber formation from neutral polymers (McKee et al., 2004).

Casein-based fibers with the diameter of 100-500 nm were obtained, but this nanofiber cannot be applied in foods because of the use of non-food carrier polymers and organic solvents (Xie and Hsieh, 2003). Also, non-food carrier polymer must be used as low as possible to produce fibers from proteins. Various PUL concentration ranging from 1 to 20 wt% were analyzed to evaluate their fiber morphologies and optimize the minimum concentration that allows the casein-based proteins to electrospin.

5.3.2 Milk Proteins

Electrospinning of pure proteins especially caseinates from aqueous solutions is difficult to produce fibers due to the reasons that are protein complex structure and the presence of Ca^{2+} and Na^{1+} ions in caseinate dispersions which constrain the electrostatic forces created by the voltage (Alborzi et al., 2010; Nieuwland et al., 2013). In addition, for electrospinning to occur, the compounds should dissolve completely with a random coil structure in solvents, as mentioned in Section 2.3.1. CaCAS with increasing concentration is not fully soluble and micellar fragments from denatured casein can interact with Ca^{2+} ions, which hinders the random coil structure (Khaoula et al., 2004). As CaCAS concentration increases, it becomes less soluble especially above the concentration of 10 % reported by Khaoula et al (2004). Electrospinning was not possible to proceed because the higher viscosity, which is a function of concentration, caused the formation of droplets at the spinneret or needle tip to initiate Taylor cone formation (Fong et al., 1999; Ramakrishna, 2005; Greiner and Wendorff, 2007; Nieuwland et al., 2013; Liu et al., 2016; Tomasula et al., 2016).

The dependence of shear viscosity on the shear rate for pure NFDM, CaCAS, and NaCAS in aqueous solutions were studied. Shear viscosity was plotted against to shear rate ranging from 0.01 to 1000 s^{-1} to obtain flow curves. Then, shear viscosity at 10 s^{-1} was used to calculate the specific viscosity by using Equation 4 to obtain the c_e and determine concentration regions; semidilute unentangled, semidilute entangled and concentrated regions.

The c_e of pure NFDM, CaCAS, and NaCAS viscosity were 21, 9, and 8 wt%, respectively. Electrospraying took place below these critical concentration limits and

generated only droplets due to the insufficient molecular entanglement, which provides jet stability during the spinning process (Fong et al., 1999; Ramakrishna, 2005; Greiner and Wendorff, 2007; Karim et al., 2009; López-Rubio et al., 2012). Above these limits up to 20 wt% (except for NFDM), enough viscosity was met to maintain jet stability due to the molecular entanglement and stretches under the applied voltage (Tomasula et al., 2016).

5.3.2.1 Nonfat dry milk (NFDM)

NFDM, as defined by FDA/CFR is produced by removing water from pasteurized skim milk. Typical NFDM contains protein of 34-37 %, lactose of 49.5-52.0 %, fat of 0.6-1.25 %, ash of 8.5 %, and moisture of 3.5 %, reported by Reference Manual for U.S. Milk Powders (2005).

Figure 18 shows the flow curves of NFDM at the concentrations ranging from 1 to 50 wt%. In the plot, the shear viscosity was obtained at 20 ºC as the shear rate is employed from 0.01 to 1000 s^{-1}. NFDM solutions at lower concentrations from 1 up to 30 wt% showed Newtonian behavior over the range of the shear rates used and their viscosities increased from 0.006 to 0.020 Pa. s. For the dilute solutions, a reduction in the viscosity with increasing the shear rate is relatively minor. The solutions with the concentrations of 35 and 40 wt% slightly showed shear thinning behavior over the same range of shear rates. However, a strong shear thinning behavior occurred for aqueous NFDM solutions beyond 40 wt%. A further increase in concentration increased the dependence of shear viscosity on the shear rate, as shown in Figure 18.

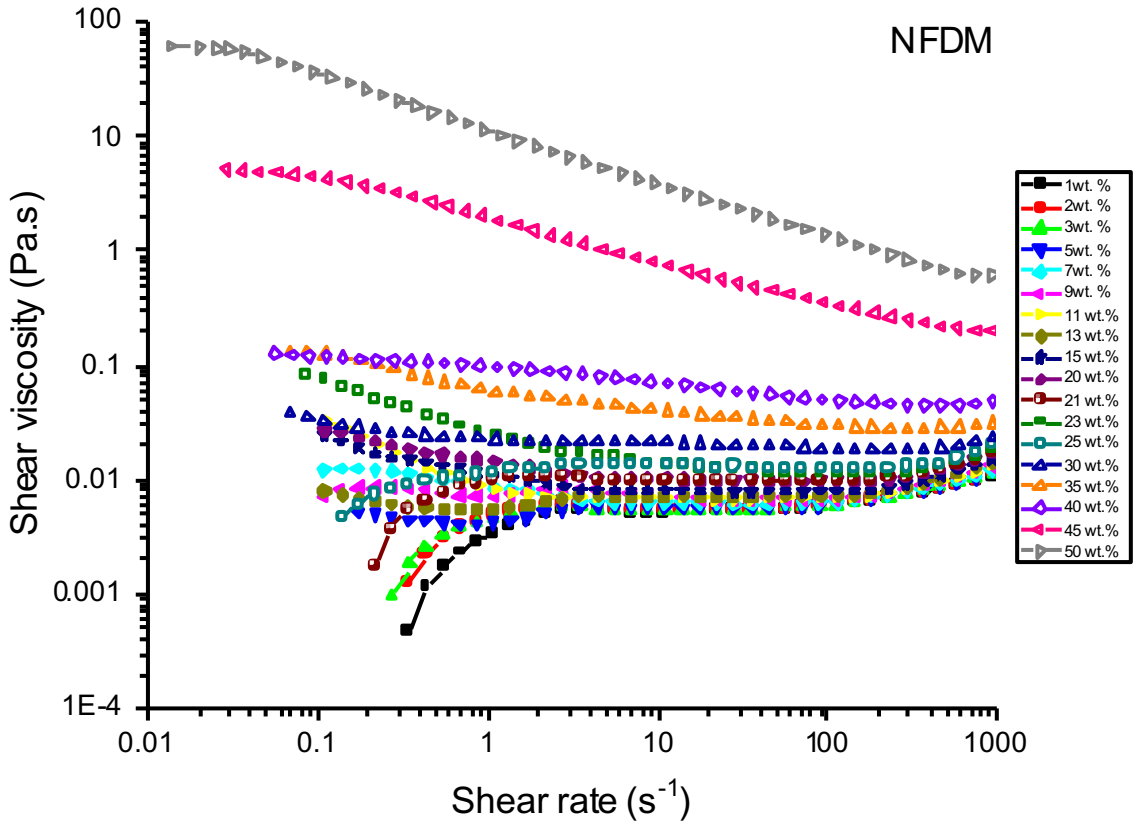

Figure 18: Dependence of shear viscosity on the shear rate for NFDM at various concentrations.

Figure 19 shows the plot of η_{sp} as a function of NFDM concentration to determine the c regimes by using η_0 values obtained from the flow curves (Figure15) at the shear rate of 10 s^{-1}. The c^*, c_e, and c^{**} were determined from the intercepts of fitted lines in the semidilute unentangled, semidilute entangled regimes and concentrated regimes, as shown in Figure 19. The c^*, c_e, and c^{**} were calculated as 9.0, 21.0 and 31 wt%. In the semidilute unentangled regime ($c<c_e$), the η_{sp} was proportional to $c^{0.08}$ which is less than the reported date for some biopolymers and synthetic polymers (Reneker et al., 2000; McKee et al., 2004a). In the semidilute entangled regime ($c>c_e$) was proportional to $c^{1.0}$ for NFDM solutions. These findings are less than the reported data in the literature for neutral and linear synthetic polymers in a good solvent, $\eta_{sp}\sim c^{1.0}$ in the dilute regime, $\eta_{sp}\sim c^{1.25}$ in the

semidilute unentangled regime. After the point of c_e, the slope had a sharp increase, 11.34, meaning that the concentration dependence of viscosity increased. It is probably due to increased protein contents, which have polymerization (aggregation) behavior. It is dependent upon the calcium-mediated interactions via nanoclusters of phosphoserine groups, interactions via hydrophobic regions, interactions with water via their hydrophilic structure, hydrogen bonding and electrostatic interactions such as calcium bridging between negatively charged sites and ion pairing (Swaisgood, 2003). These interactions lead the caseins to interact with themselves, each other and minerals, as well as hydrophobic and ionic interactions with other proteins (Dalgleish and Parker, 1979), which cause a sharp increase in viscosity after a certain concentration.

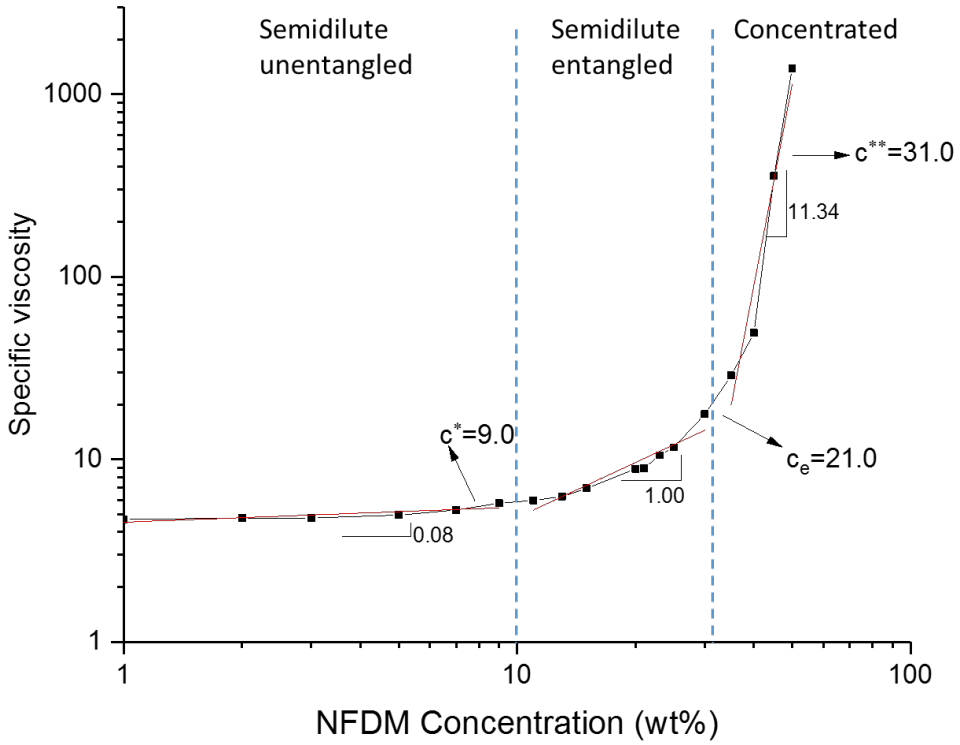

Figure 19: Dependence of specific viscosity on concentration for NFDM solutions with the values of c*; c_e; and c**.

Table 7 shows the electrical conductivity, surface tension, and the shear viscosity at the shear rate of 100 s^{-1} measured for NFDM solutions at various concentrations at 20 °C. The value of surface tension for the solutions slightly decreased from 53 to 45 mN/m with increasing concentration from 1 to 40 wt%, whereas the electrical conductivities increased from 0.8 to 9.0 mS/cm, as also shown in Figure 27. The electrical conductivities of NFDM suspensions is higher than CAS. Also, the viscosity values for NFDM are lower than CaCAS and NaCAS solutions over the same solid concentrations. The reason is due to its composition which consists of approximately 35 % protein including native casein and whey proteins, lactose and minerals such as calcium, magnesium, potassium, etc. (Reference Manual for U.S. Milk Powders, 2005), whereas CAS contains about 90% protein which predominantly responsible for viscosity and protein chain entanglements.

Instead of forming fibers, small beads and spherical structures were precipitated on the grounded collector, as shown in Figure 20. This is expected because the proteins in NFDM are composed of casein and whey proteins and casein exists in micellar structure with the size ranging from 20 to 300 nm (Oommen, 2004; Rebouillat and Ortega-requena, 2015). Due to less protein content of NFDM (~35 %) and the globular structure of proteins, protein chain entanglement is not enough to form fibers under the electric field.

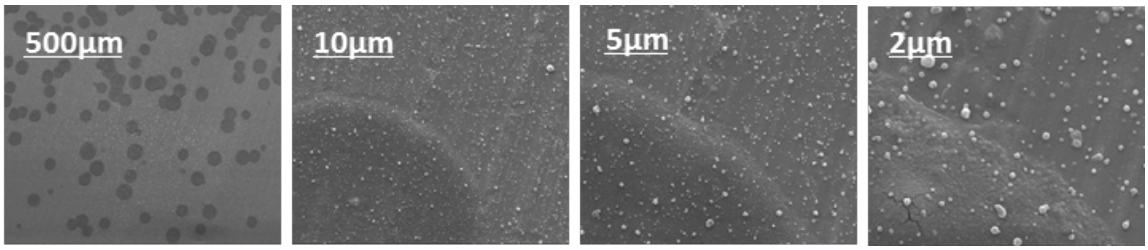

Figure 20: SEM images of the electrospun structure of 15 wt% NFDM at the magnifications of 100×, 5,000×, 10,000× and 25,000×.

Table 7: Physical properties of NFDM solutions.

	Concentration (wt%)	Electrical conductivity (mS/cm)	Surface tension (mN/m)	Shear viscosity at 100 s^{-1} (Pa.s)	Morphology
NFDM	1	0.81±0.00	52.79±0.11	0.0058	No Fiber
	2	1.45±0.00	50.39±0.04	0.0059	
	3	2.05±0.00	50.04±0.02	0.0059	
	5	3.17±0.00	50.28±0.03	0.0060	
	7	4.16±0.01	47.47±0.06	0.0063	
	8	4.52±0.01	49.10±0.02	0.0065	
	9	5.00±0.01	49.70±0.12	0.0068	
	10	5.35±0.01	49.20±0.04	0.0069	
	11	5.76±0.01	48.63±0.08	0.0070	
	12	6.05±0.01	48.41±0.03	0.0071	
	13	6.45±0.01	48.42±0.04	0.0073	
	14	6.66±0.01	47.84±0.02	0.0076	
	15	6.97±0.01	47.14±0.05	0.0080	
	20	8.05±0.01	44.53±0.04	0.0099	
	30	8.92±0.01	44.33±0.04	0.0187	
	35	8.71±0.01	44.39±0.06	0.0296	
	40	8.47±0.01	45.49±0.08	0.0499	

5.3.2.2 Calcium (CaCAS) and Sodium Caseinates (NaCAS)

CaCAS

The viscosities of CaCAS dispersions increased with increasing concentrations. The NaCAS solutions were viscous than the CaCAS at the same concentrations due to the formation of the dense caseinate domains caused by the presence of Ca^{+} ions, which reduces the effective volume fraction (Grabowska, Van der Goot, and Boom, 2012; McMahon and Oommen, 2013; Thomar et al., 2013). CaCAS solution was Newtonian fluid at lower shear rates and exhibited slightly shear thinning behavior at higher shear rates with increasing concentrations. At the concentrations of 1, 3, 5, 7, and 9 wt% CaCAS, the solutions showed shear thinning behavior as the samples at the concentrations of 11 and 13

wt% showed Newtonian behavior with the shear viscosities around 0.03 and 0.06 Pa. s, respectively. CaCAS solutions below the concentration of 9 wt%, electrospraying or drops occurred due to the insufficient viscosity, which provides less molecular entanglement of polymer chains. Without enough chain entanglement, it is impossible to sustain jet stability which plays an important role to produce continuous and defect-free fibers. At the higher concentrations of CaCAS above 13 wt%, the solutions showed shear thinning behavior, as shown in Figure 21. For example, the viscosities of CaCAS solutions above 15 wt% drastically decrease over a higher shear rate.

Figure 21 shows the dependence of shear viscosity on the shear rate for neat CaCAS solutions at various concentrations. Shear viscosity was measured based on the range of shear rate from 0.01 to 1000 s^{-1} for the CaCAS solutions at the concentration ranging from 1 to 17 wt% in aqueous solutions at 20 °C. CaCAS solutions at the lower concentrations below 14 wt% followed a Newtonian fluid behavior over the shear rate ranging from 1 to 100 s^{-1}. Their viscosities slightly increased from 0.006 to 0.06 Pa. s at the shear rate of 100 s^{-1} while the viscosities at the concentrations of 14 and 15 wt% were 0.243 and 0.210 Pa.s. With increasing shear rate, the protein molecules reaggregate or self-associate themselves to rearrange the proteins into colloidal particles due to the changes in hydrophobic interactions (McMahon and Oommen, 2013). This results in a sudden change in viscosity at the shear rate above 10 s^{-1} at higher protein concentrations, as shown in Figure 21. Stijnman et al (2011) reported that the polysaccharides with a strong shear thinning behavior at lower shear can only form a jet and/or droplet and no fibers (Stijnman et al., 2011). The viscosity changes occurred due to the attractive interactions in CaCAS are

employed by Ca^{2+} ions and induce the formation of domains of casein particles as increasing its concentrations (Thomar et al., 2013).

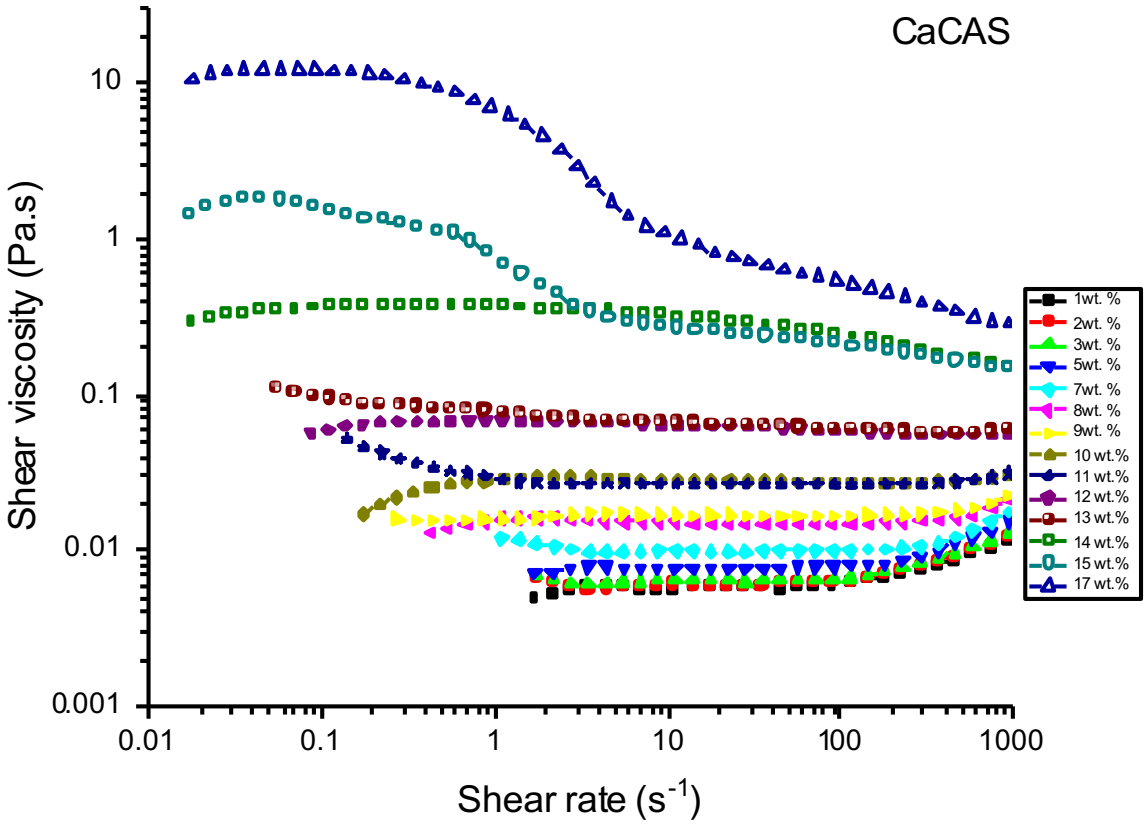

Figure 21: Dependence of shear viscosity on the shear rate for CaCAS at various concentrations.

Figure 22 shows the concentration regimes and c_e of CaCAS solution and its c_e is 9 wt%. According to McKee et al (2004), the concentration of polymer solutions should be at least 2-2.5 times c_e for neutral polymers to form fibers from polymer solutions via electrospinning. Therefore, CaCAS solutions at the concentrations above 9 wt% may produce fibers. In Figure 22, the viscosities in semidilute unentangled ($c<c_e$), semidilute entangled ($c^{**}>c>c_e$) and concentrated regimes ($c>c^{**}$) are proportional to $c^{0.16}$, $c^{1.40}$, and $c^{7.48}$, respectively. The slope in the semidilute entangled is not close to theoretical prediction for the formation of bead-free fibers from linear polymers in a good solvent

(η_{sp}~$c^{4.8}$) (Daoud and De Gennes, 1979) and the other random coil polysaccharides, including dextran and lambda-carrageenan, η_{sp}~$c^{3.3}$ (Morris et al., 1981). As discussed in more depth below, aqueous CaCAS cannot form nanofibers under the conditions used in this study.

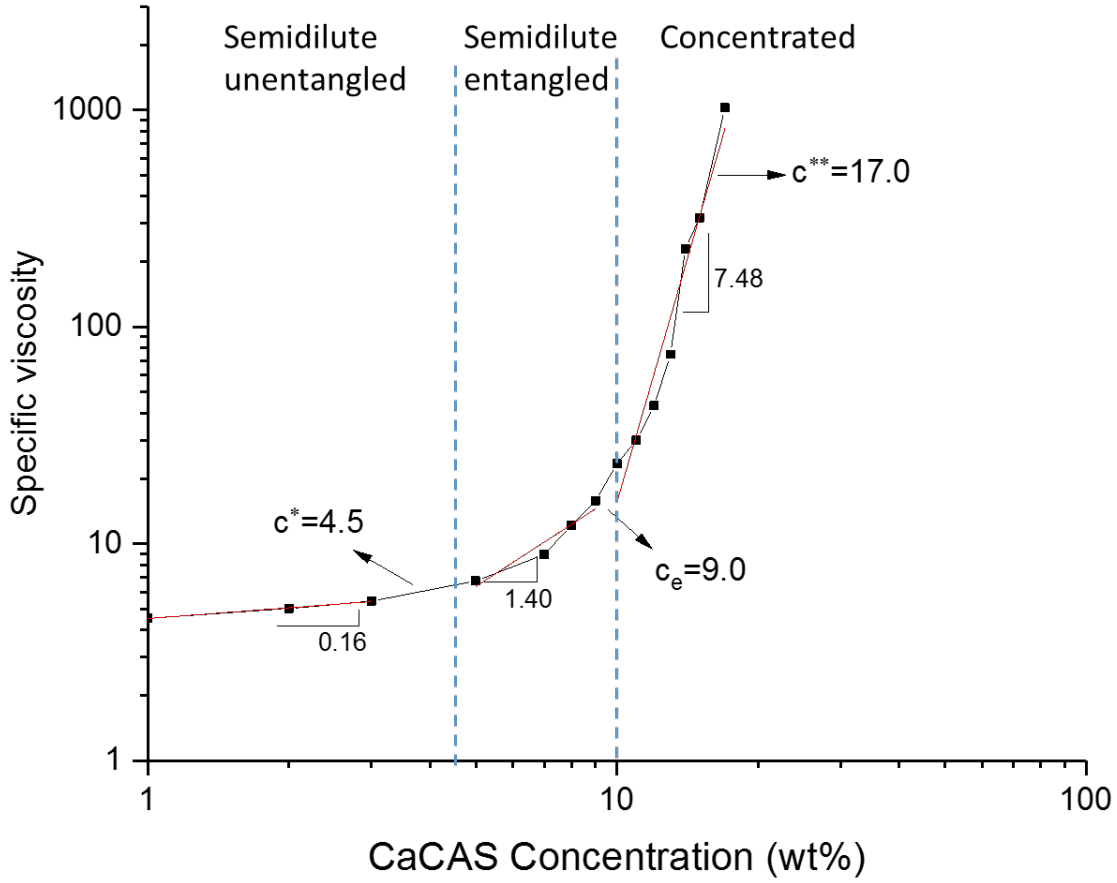

Figure 22: Dependence of specific viscosity on the concentration for CaCAS solutions with the values of c*, c_e, and c**.

Besides the shear viscosity and concentration regimes, other solution properties including electrical conductivity and surface tension are important parameters for the nanofiber morphology through the electrospinning process. Table 8 shows the electrical conductivity, surface tension, and the shear viscosity at the shear rate of 100 s^{-1} measured for CaCAS solutions at various concentrations at 20 °C.

The value of surface tension for CaCAS solution was constant by about 45 mN/m with increasing concentration from 1 to 15 wt%, whereas the electrical conductivities increased from 0.2 to 1.4 mS/cm, as shown in Table 8. These results are similar to the conductivities of aqueous CaCAS solutions reported 1.0 and 1.76 mS/cm at the concentrations of 5 and 10 wt%, respectively (Tomasula et al., 2016). In the same study, the surface tension of CaCAS solutions ranged from 45 to 50 mN/m over the concentrations ranging from 5 to 20 wt% which is similar to our findings, as shown in Table 8.

Based on the plot of the concentration dependence of the η_{sp}, the results showed the slope of the concentration regimes were lower than the theoretical predictions for the synthetic polymers and biopolymers (Daoud and Daoud and De Gennes, 1979; Morris et al., 1981; Reneker et al., 2000; McKee et al., 2004). The reasons could be due to caseinates' heterogeneous molecular size and structure due to calcium bindings and high electron density (McMahon and Oommen, 2013) which both may hinder the solubility and random coil structure as well as entanglement of protein chains, which is an important requirement for the electrospinning. Even at concentrations approximating 2.5 times c_e, bead-free nanofibers cannot be achieved from aqueous CaCAS solutions, as shown in Figure 23.

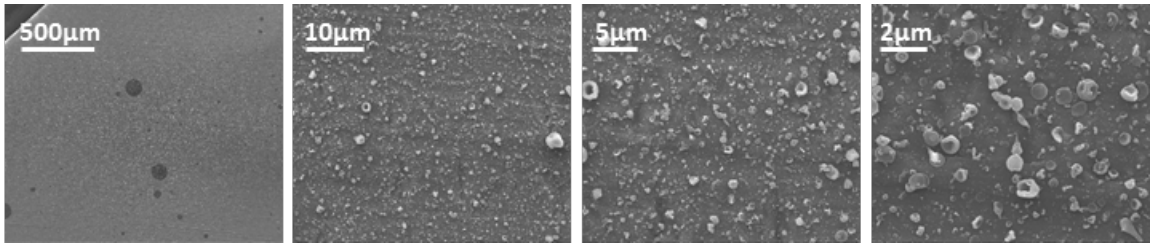

Figure 23: SEM images of the electrospun structure of 15 wt% CaCAS at the magnifications of 100×, 5,000×, 10,000×, and 25,000×.

Table 8: Physical properties of CaCAS solutions.

	Concentration (wt%)	Electrical conductivity (mS/cm)	Surface tension (mN/m)	Shear viscosity at 100 s^{-1} (Pa.s)	Morphology
CaCAS	1	0.19±0.00	45.47±0.04	0.006	**No fiber**
	2	0.36±0.00	47.80±0.08	0.006	
	3	0.46±0.01	47.73±0.08	0.007	
	5	0.67±0.01	45.33±0.10	0.008	
	7	0.86±0.01	47.18±0.10	0.010	
	8	0.94±0.00	45.39±0.02	0.015	
	9	1.03±0.01	45.12±0.08	0.017	
	10	1.10±0.00	45.06±0.02	0.027	
	11	1.18±0.01	45.68±0.07	0.026	
	12	1.25±0.00	44.21±0.01	0.059	
	13	1.31±0.02	46.57±0.06	0.060	
	14	1.36±0.00	45.55±0.04	0.210	
	15	1.42±0.01	46.76±0.05	0.243	

Instead of forming fibers, small beads and spherical CaCAS structures were collected on the collector. This is expected because CaCAS have large colloidal particles (~300 nm diameter) and small particles of 10 to 20 nm diameter, which have a spherical appearance similar to native micelles in milk (Oommen, 2004). They also have electron density which result from a combination of higher concentration protein in colloidal particles or high level of calcium binding to casein particles (Thomar et al., 2013; McMahon and Oommen, 2013), which may affect both carrying the positive charges and the amount of solutions withdrawn from needle to the collector under the electric field.

NaCAS

Figure 24 shows the dependence of shear viscosity on shear rate ranging from 0.01 to 1000 s^{-1} for NaCAS solutions. The solutions with the concentrations of 1, 2, 3, 5, 7, 8, 9, 10, 11, 12, and 13 wt% showed Newtonian fluid behavior at the shear rates less than 100 s^{-1} while the solutions with the concentrations above 15 wt% reverted to shear thinning

behavior. The shear viscosity increases from 0.06 to 3.00 Pa. s with the solution concentrations ranging from 1 to 15 wt%, as shown in Figure 24. This finding is consistent with previously reported data that dense suspensions of NaCAS at the concentration above 10 wt% have a viscoelastic behavior and its viscosity increases with an increased concentration (Thomar et al., 2013). The changes in viscosity are attributed to the jamming of dense small casein particles in NaCAS proteins (Pitkowski et al., 2008).

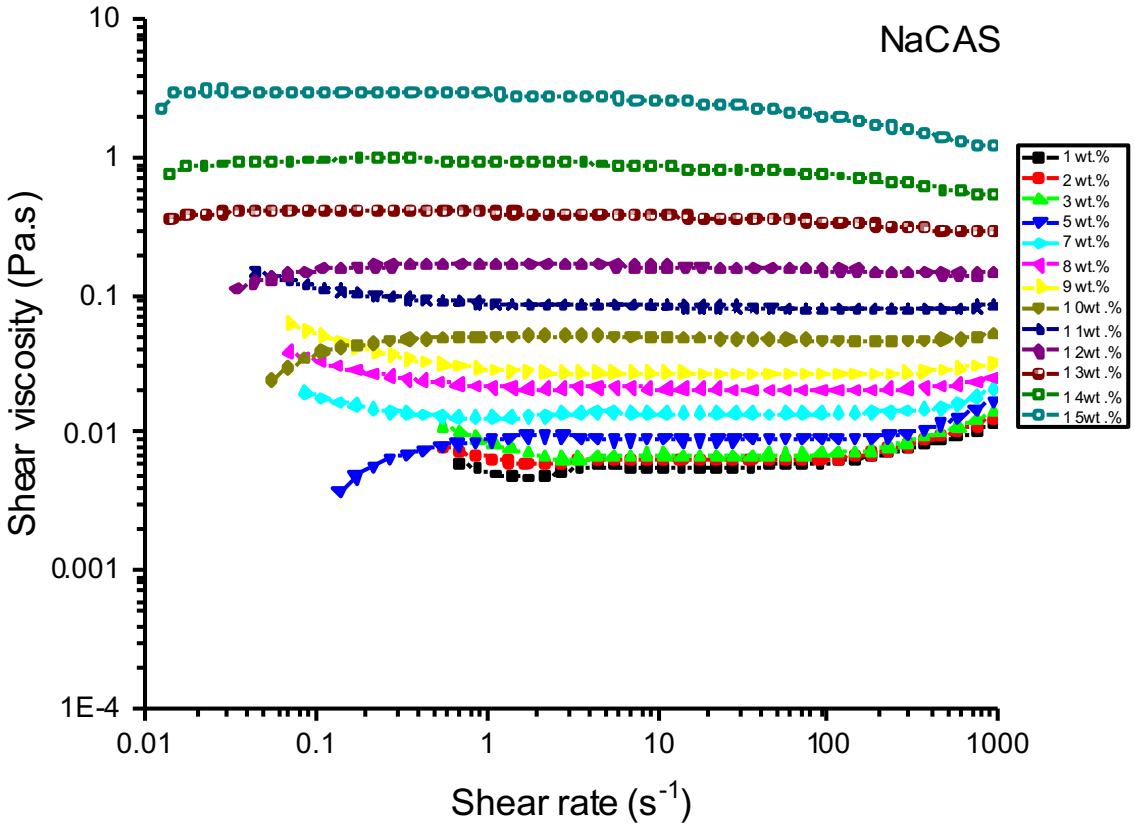

Figure 24: Dependence of shear viscosity on the shear rate for NaCAS at various concentrations.

Figure 25 shows the concentration regimes and c_e of NaCAS solution and its c_e is 8 wt%. The viscosities in the semidilute unentangled, semidilute entangled, and concentrated regimes are proportional to $c^{0.19}$, $c^{1.75}$, and $c^{8.38}$, respectively. Even though the slope in the semidilute entangled is lower than the slopes for electrospinnable synthetic and natural

polymers, which were reported as 3.5 for neutral and linear polymers (Colby et al., 1991; Wool, 1993) and 4.8 for polysaccharides such as dextran (Morris et al., 1981).

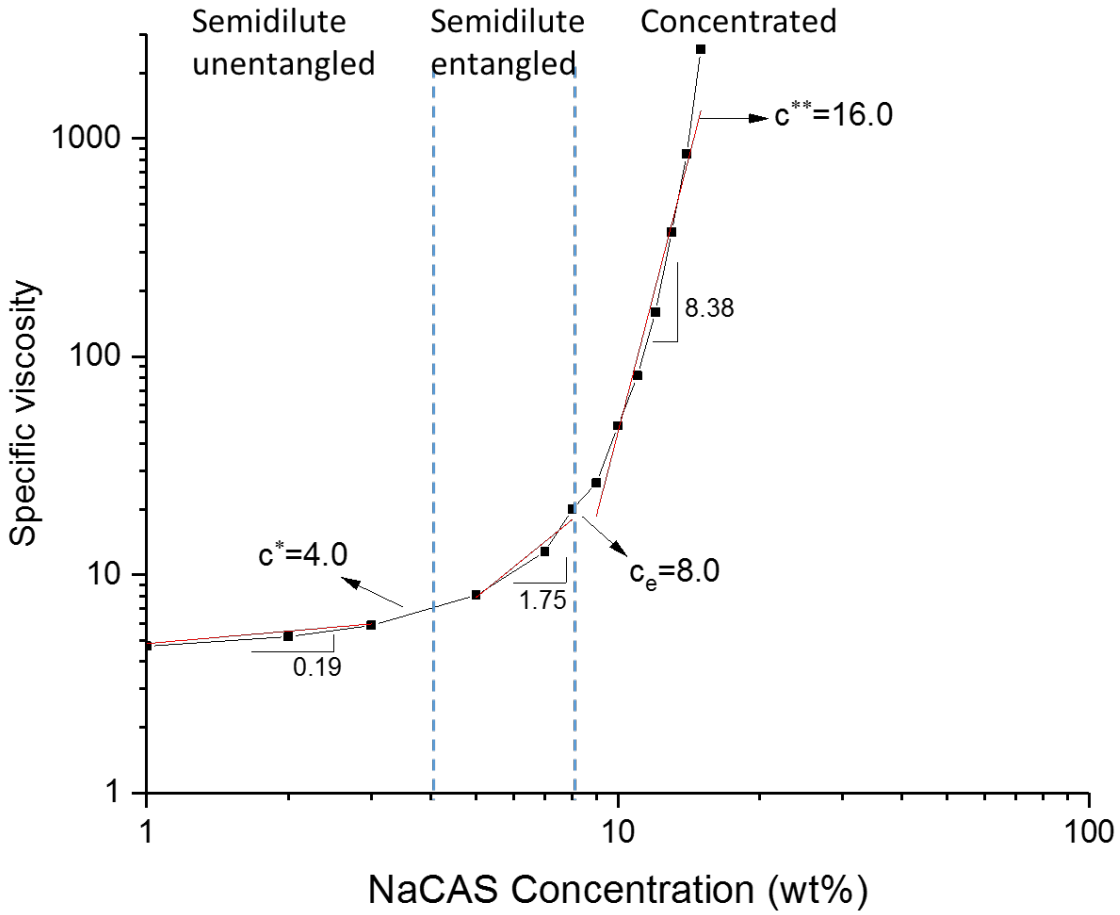

Figure 25: Dependence of specific viscosity on the concentration for NaCAS solutions with the values of c*, c_e, and c**.

Table 9 shows the electrical conductivity, surface tension, and shear viscosity at the shear rate of 100 s^{-1} measured for NaCAS solutions at a various concentration at 20 °C. The value of surface tension for NaCAS solution slightly decreased from 50 to 47 mN/m with increasing concentration from 1 to 15 wt%, whereas the electrical conductivities increased from 0.3 to 3.3 mS/cm, as also shown in Figures 27 and 28. These results are similar to the conductivities of aqueous NaCAS solutions reported 1.0 and 1.76 mS/cm at the concentrations of 5 and 10 wt%, respectively (Tomasula et al., 2016). In the same study,

the surface tension of CaCAS solutions ranged from 45 to 50 mN/m over the concentration range from 5 to 20 wt% which is similar to our findings, as shown in both Table 8 and Figure 28.

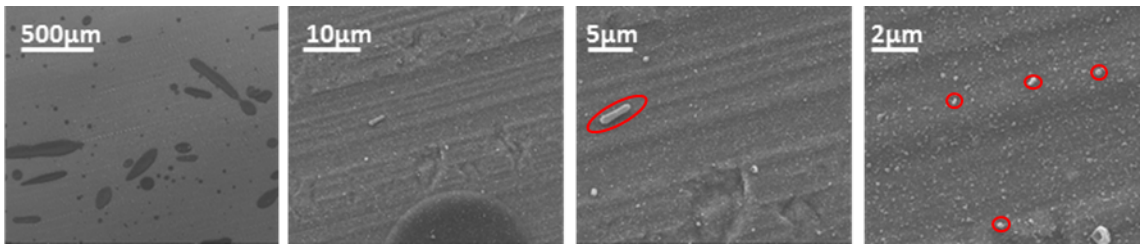

Figure 26: SEM images of the electrospun structure of 15 wt% NaCAS at the magnifications of 100×, 5,000×, 10,000×, and 25,000×.

Table 9: Physical properties of NaCAS solutions.

	Concentration (wt%)	Electrical conductivity (mS/cm)	Surface tension (mN/m)	Shear viscosity at 100 s^{-1} (Pa.s)	Morphology
NaCAS	1	0.34±0.00	49.26±0.04	0.006	**No fiber**
	2	0.72±0.00	49.62±0.05	0.006	
	3	0.86±0.01	49.87±0.03	0.007	
	5	1.33±0.01	48.75±0.03	0.009	
	7	1.74±0.01	47.40±0.04	0.014	
	8	2.09±0.02	47.73±0.05	0.020	
	9	2.24±0.00	47.69±0.06	0.027	
	10	2.42±0.02	48.16±0.04	0.047	
	11	2.64±0.01	47.71±0.04	0.079	
	12	2.72±0.02	47.44±0.03	0.152	
	13	2.88±0.01	47.70±0.06	0.339	
	14	2.92±0.05	47.56±0.03	0.746	
	15	3.32±0.00	47.16±0.03	1.994	

Even though the concentration of NaCAS was at least 2.0-2.5 times the c_e, which fits in the reported values for the electrospinnable synthetic and natural polymers, and its viscosity (above 0.1 Pa. s) was adequate for the processing, the nanofibers were not produced, as shown in Figure 26. Instead, electrospun dried powder particles were formed.

This could be due to the lack of molecular entanglement properties of CAS resulting from their complex protein structures, including large colloidal particles and interactions of monovalent and/or divalent ions with casein proteins (Oommen, 2004; McMahon et al., 2009).

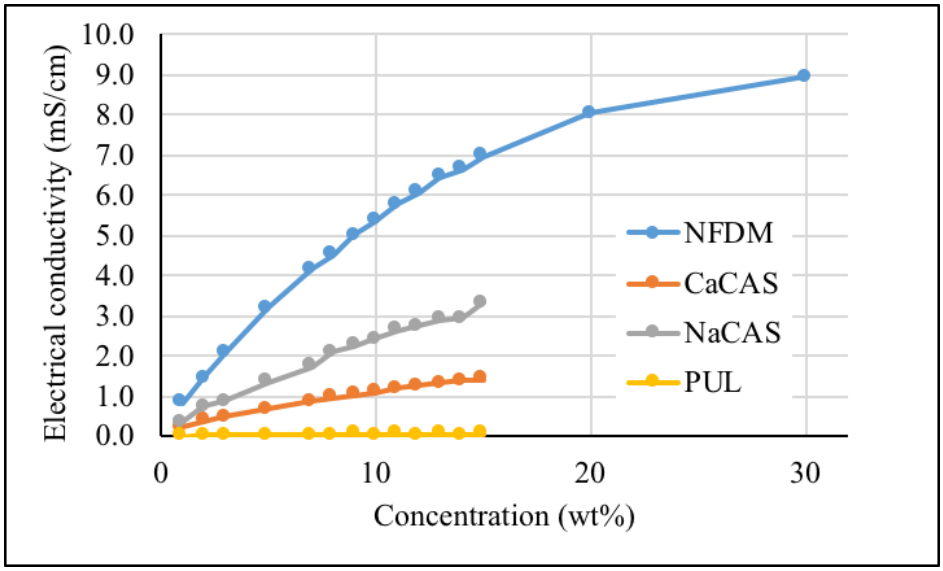

Figure 27: Electrical conductivities of NFDM, CaCAS, NaCAS, and PUL as a function of solution concentration (wt%) at 20 ºC.

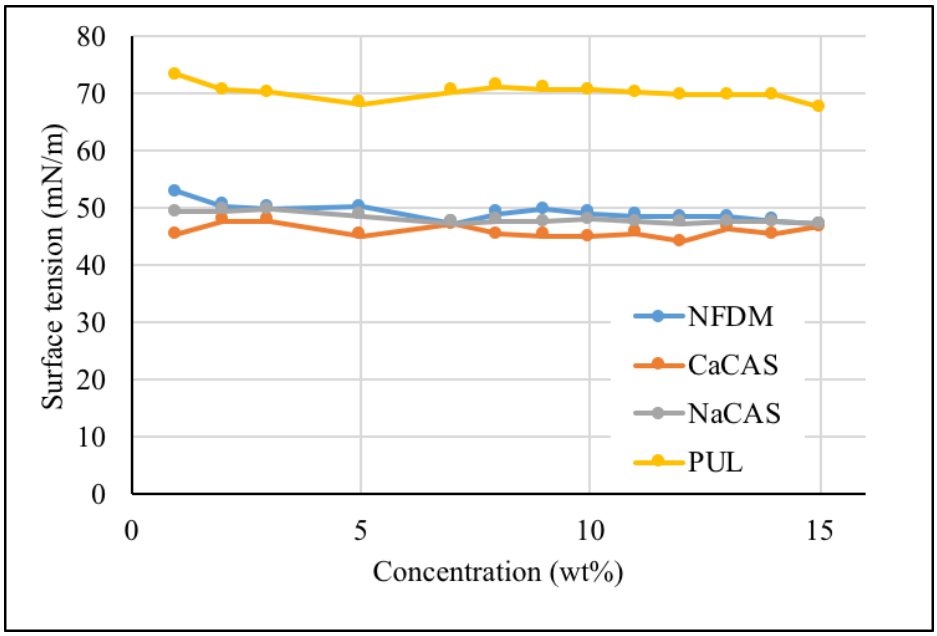

Figure 28: Surface tension of NFDM, CaCAS, NaCAS, and PUL solutions as a function of solution concentration (wt%) at 20 °C.

5.4 Summary

This chapter focused on the c and shear rate (s^{-1}) dependence of η for pure and aqueous PUL, NFDM, CaCAS, and NaCAS solutions and their influence on the electrospinning of these biopolymers without using any organic solvents, acids, and carrier polymers in the solutions.

- The transition from the semidilute unentangled to both the semidilute entangled and concentrated regimes occurs at the c_e of 5.5 wt% for aqueous PUL solutions which is similar to the reported c_e (4.0 wt%) for random coil polysaccharides dissolved in salt solution (0.5 M, NaOH) (Morris et al., 1981). The η_{sp} varies as $c^{0.61}$ for the semidilute unentangled, $c^{2.85}$ for the semidilute entangled, and $c^{4.76}$ for the concentrated PUL solutions. Below the c_e, it formed only beads due to insufficient viscosity causing only electrospraying. The lower and upper viscosity limits were determined as 0.3 Pa. s and 1.0 Pa. s to produce PUL fibers at 20 °C, respectively, but the viscosity at beyond 0.3 Pa. s (10 wt%), bead-free, uniform PUL nanofibers were produced.
- Based on the data in this section, the c_e of aqueous NFDM, CaCAS, and NaCAS were found as 21.1, 9.0, and 8.0 wt%. McKee et al (2004) determined that the formation of uniform, bead-free fibers is required the solution concentration 2.0-2.5 times the c_e for neutral polymers (McKee et al., 2004). In the case of NFDM and CAS, we anticipated that the solutions at the concentrations above the c_e may produce fibers, but their aqueous solutions were not able to form nanofibers via electrospinning at RT (20±1 °C).
- NFDM contains 35 wt% proteins consisting of micellar native casein and whey proteins and casein micelles and globular structure of whey proteins lack the molecular

interactions and restrict the chain entanglements, which is a necessity for the electrospinning process, as discussed in previous sections.

- CaCAS solutions up to 15 wt% showed lower shear viscosities compared to the 10 or 15 wt% PUL solutions. The solutions did not produce fibers, nor did solutions of 20 wt% CaCAS because of their high viscosities causing the accumulation of gel-like caseinates at the needle tip.
- In the presence of Ca^{2+} ions, colloidal and/or subunit structure occurs via calcium bridges formed by hydrophobically linked phosphoserine groups in CaCAS during its conversion from acid casein to soluble CaCAS. It may also form too dense protein chains, causing the lack of protein chain entanglements (Tomasula et al., 2016).
- Even though the concentration dependence of specific viscosity profile of NaCAS solution was similar to such of PUL, the η_{sp} of NaCAS solution was proportional to $c^{8.72}$, which is higher than the reported value of 3.3 for random coil polysaccharides (Morris et al., 1981) and theoretically predicted data of 3.5 for neutral and linear polymers (Wool, 1993). NaCAS exists in small protein strands and agglomerates of caseinate proteins which affect adversely the molecular chain entanglements and electrospun fiber formation.

CHAPTER 6

Effect of PUL as Carrier Polymer on Electrospinning of NFDM and Caseinate Proteins

Producing edible ultrafine fibers via electrospinning from NFDM and CAS was required an incorporation of an edible and electrospinnable polymer, PUL since the aqueous NFDM and both CAS solutions cannot produce ultrafine fibers and ultrafine fibrous mats through the electrospinning process, as discussed before in Chapter 4.

As mentioned in Section 2.3.1, previous studies have been reported empirically that the fiber formation via electrospinning is strongly influenced by the amount of polymer chain entanglements in solutions (c/c_e) for neutral polymers (Colby et al., 1991; McKee et al., 2004; Shenoy et al., 2005). Molecular weight or concentration dependence of viscosity relationships can be applied for a measure of polymer chain entanglements which plays a crucial role for successful fiber formation. Colby et al (1991) identified three different concentration regions including the dilute and the semidilute unentangled, the semidilute entangled and the concentrated regimes from the concentration dependence of viscosity for the linear polymers in good solvents (Colby et al., 1991; Krause et al., 2001). McKee et al (2004) reported that neutral copolyester with molecular weights above the entanglement molecular weight, c_e was the minimum concentration necessary for the formation of beaded fibers, whereas the formation of uniform, bead-free fibers was required a minimum concentration as 2.0-2.5 times the c_e (McKee et al., 2004).

Nieuwland et al (2013) proposed a mechanism for the electrospinning of the proteins either with an ideal solvent or a carrier polymer, as shown in Figure 29 (Nieuwland et al., 2013). Route A shows the use of an ideal solvent for the electrospinning of proteins

by denaturing protein to promote the dissolution and random coil structure. However, it sometimes causes the aggregation of denatured protein pieces and organic solvents (except ethanol) are not for food use. Based on the aim of this study, we need to form edible nanofibrous mats from the milk proteins. Therefore, Route B is the option which depicts the application of a processing aid to electrospin milk-based proteins that are impossible to electrospin in aqueous solutions (Nieuwland et al., 2013).

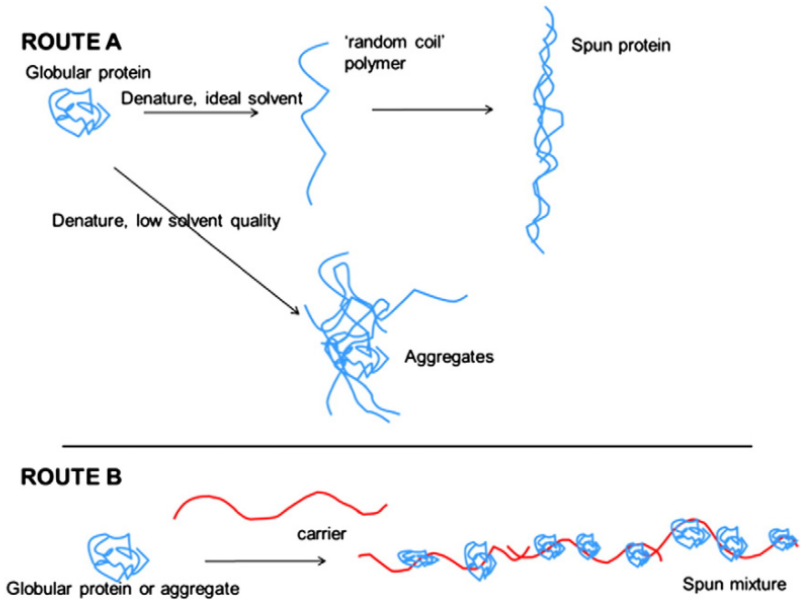

Figure 29: A mechanism for the electrospinning of proteins. Route A shows the use of an ideal solvent to denature proteins aggregates and Route B depicts the use of a processing carrier to electrospin protein (Nieuwland et al., 2013).

In the mixture of polysaccharide and protein compounds, their complexes can interact each other by forming intermolecular hydrogen bonds due to the interactions between hydroxyl groups from polysaccharides and amino groups from proteins, which likely promotes the molecular entanglements for the electrospinning process (Tomasula et al., 2016). Other interactions can occur between water molecules and hydroxyl residues of the polymer chains, provind more flexibility to the polymer chains. In the case of this study, we can interpret that PUL can introduce more flexibility within dense protein chains of

caseinate structures, allowing bending of the protein chains due to PUL molecular structure with α-(1-6) linkages associated with randomly ordered chains (Kristo and Biliaderis, 2007; Aceituno-Medina et al., 2013). Unlike NFDM or native casein and whey proteins, CAS proteins do not have disulfide linkages due to their low amount of cysteine, nor globular structure, which allows forming stable polysaccharide-protein complexes. Also, it contains a large number of proline residues, which can allow the bending of protein chains by preventing the formation of secondary structures (Gennadios et al., 1994). Due to these characteristics of CAS proteins may be well-suited to incorporate with PUL for electrospinning process better than NFDM or whey proteins in the absence of organic solvents.

The objective of this Chapter was to investigate the effect of PUL carrier on the viscosity and chain entanglements of NFDM and CAS solutions by identifying the c regions and c_e of their blended solutions.

6.1 Overview

A systematic investigation is presented to understand why aqueous NFDM, CaCAS, and NaCAS can only be electrospun into fibers through a blend with another polymer, specifically pullulan (PUL) used in this study. To examine and understand the role of PUL as a processing aid, this section covers the effects of concentration and viscosity on the NFDM and caseinate-based ultrafine fibers.

In this section, NFDM, CaCAS, and NaCAS blended with PUL in aqueous solutions were electrospun to characterize the effect of PUL on their electrospinning. The onset of chain entanglement in aqueous milk protein solutions in the presence of PUL and the role of PUL on chain entanglement and fiber morphology were determined. Other

solution properties including electrical conductivity, shear viscosity, and surface tension were also determined to find out the relationship between the electrospinning process and solutions properties.

6.2 Preliminary results

To compare PUL with both a neutral (PEO) and protein carriers (gelatin), a water-soluble polymer (PEO, 900 kDa) and a food-grade polymer (Gelatin Type A, 50-100 kDa) were tested to determine their shear rate dependence of shear viscosity and concentration dependence of specific viscosity briefly in comparison to PUL (PUL, ~500 kDa), which is used as a carrier polymer throughout this study.

Figures 30, 31, and 32 show the shear rate dependence of the shear viscosity and the concentration dependence of the η_{sp} of pure PEO and gelatin in aqueous solutions to compare their flow curves and the concentration regimes for the electrospinning process. Flow curves were built from shear viscosity versus shear rate data obtained with the shear rate ranging from 0.01 to 1000 s^{-1}. Then, shear viscosity at 10 s^{-1} was used to calculate the specific viscosity to obtain the c_e, which is an onset concentration for molecular chain entanglements. Even though Figure 32 shows the plots of the flow curve and concentration dependence of η_{sp} for PUL, the discussion will not be presented here because the details have been already discussed and explained in Section 5.3.1. It was only mentioned here again (Figure 32) to compare it with the rheology of PEO and gelatin solutions.

The viscosities of PEO and gelatin solutions increased with increasing concentrations as shown in Figures 30a and 31b. PEO showed a strong shear thinning behavior at the shear rate above 20 s^{-1}, as shown in Figure 30a. However, aqueous gelatin solutions at the concentrations ranging from 1 up to 20% showed Newtonian flow behavior

less than 0.2 Pa. s at the shear rate ranging from 0.1 to 100 s^{-1}. This difference could be attributed to the processing temperature which was 45 °C higher than the processing temperature (20 °C) for PEO and PUL polymers.

The c_e of aqueous PEO and gelatin solutions was 1.1 and 5.9 wt%, as shown in Figures 30b and 31b, respectively. At $c < c_e$, electrospraying took place for both polymers and aqueous PEO solution at the concentration of 1 wt% produced the beads with incipient fibers, while gelatin at the concentration of 5 wt% was unable to produce fibers. This is due to the insufficient molecular entanglement, which provides jet stability during the spinning process (Fong et al., 1999; Greiner and Wendorff, 2007; Karim et al., 2009).
At the $c > c_e$, 17 wt% gelatin solution produced smooth, bead-free fibers with a diameter of 380 nm, as shown in Figure 31b, whereas 3 wt% PEO produced uniform, well-formed fibers with a diameter of 170 nm, as shown in Figure 30b.

The η_{sp} of PEO was proportional to $c^{3.99}$ at the $c > c_e$, which is little lower than the theoretical prediction of $c^{4.8}$ (Daoud and Daoud and De Gennes 1979), but similar to the PUL results, 4.34, as shown in Figure 32. The lower and upper viscosity limit for PEO solutions were observed as 0.4 to 1.0 Pa. s for electrospinning of PEO, whereas such viscosity range for PUL was from 0.06 to 1.0 Pa. s, as shown in Figure 32a. However, the η_{sp} of gelatin was proportional to $c^{2.01}$ at the $c > c_e$, which is lower than the theoretical prediction of $c^{4.8}$ (Daoud and De Gennes 1979).

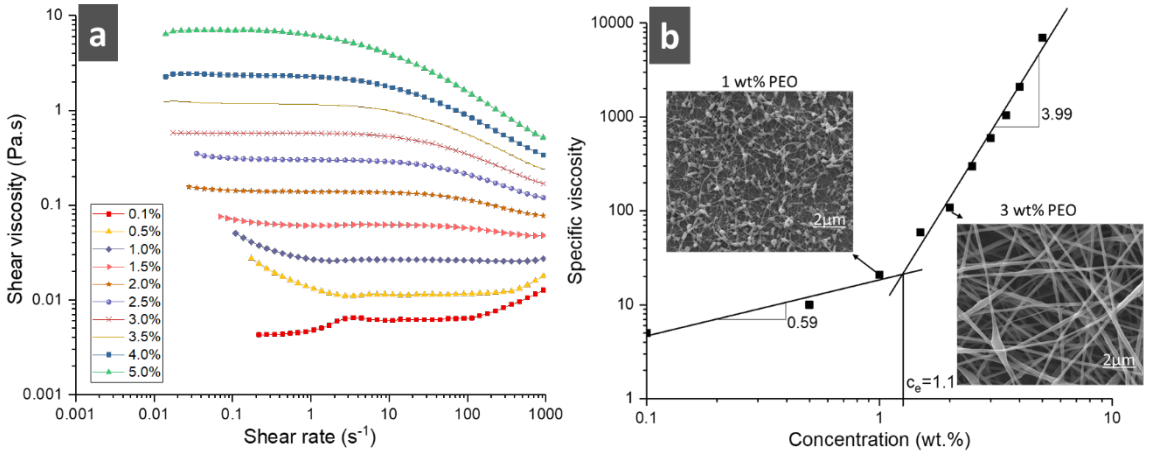

Figure 30: Dependence of shear viscosity on the shear rate for PEO at the concentration in the range from 0.1 to 5.0 wt% (a); concentration dependence of η_{sp} for PEO solutions (b). The c_e is 1.1 wt%.

Even though PEO and gelatin are an excellent electrospinnable polymer, PEO was not used as a carrier polymer due to its ineligibility for food products, and gelatin was not used because it requires a high temperature processing (~40 °C). However, all analysis and electrospinning were employed at 20 °C and RT in this study. In this case, PUL is a good candidate for the electrospinning of proteins because it is a water-soluble, food-grade, and electrospinnable polysaccharide at RT.

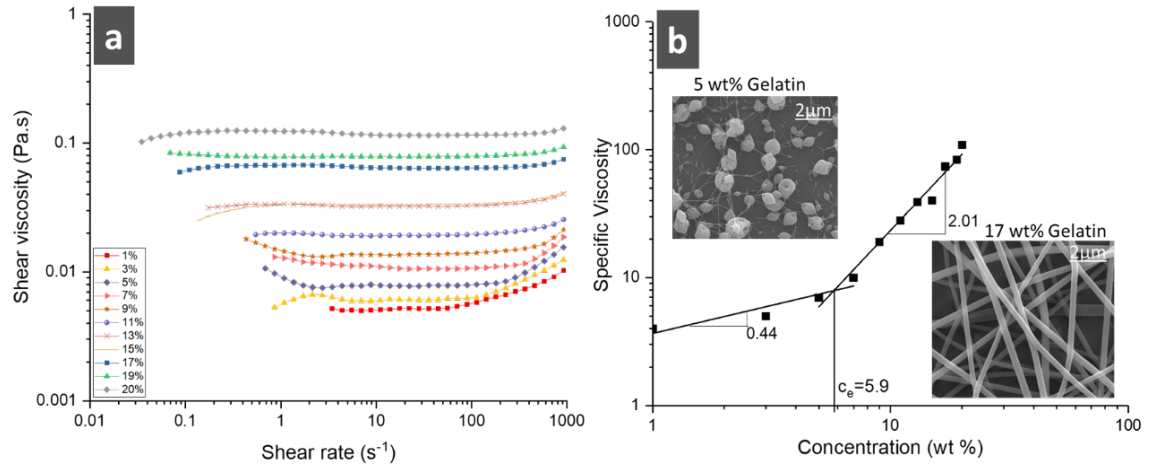

Figure 31: Dependence of shear viscosity on the shear rate for gelatin at the concentration in the range from 1 to 20 wt% (a); concentration dependence of η_{sp} for gelatin solutions (b). The c_e is 5.9 wt%. Only gelatin solutions were prepared and tested at 45 °C.

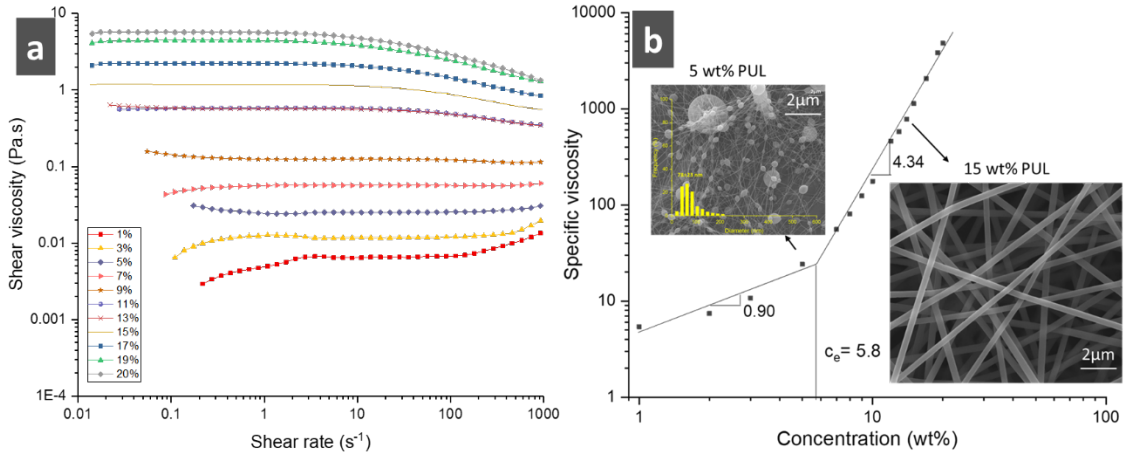

Figure 32: Dependence of shear viscosity on the shear rate for PUL at the concentration in the range from 1 to 20 wt% (a); concentration dependence of η_{sp} for PUL solutions (b).The c_e is 5.8 wt%.

Figure 33 shows that electrospun 15 wt% PUL fibers and electrospun NFDM, CaCAS, and NaCAS structures to demonstrate their electrospun structures before beginning the details in the study. The minimum concentration of 1.7-2.7 times the c_e needed to obtain uniform, defect-free fibers from neat PUL solutions, as mentioned in Section 5.3.1, which fits the theoretical model for the concentration regimes (Morris et al., 1981; Wool, 1993). Unlike PUL, milk proteins in the absence of carrier polymer and organic solvents cannot form fibers via electrospinning due to the reasons mentioned in detail in Section 5.3.2. Therefore, PUL, excellent food-based, electrospinnable polymer, was used to electrospin the milk proteins by making use of natural protein-polysaccharides interactions without adding any non-food compounds or applying harsh treatments.

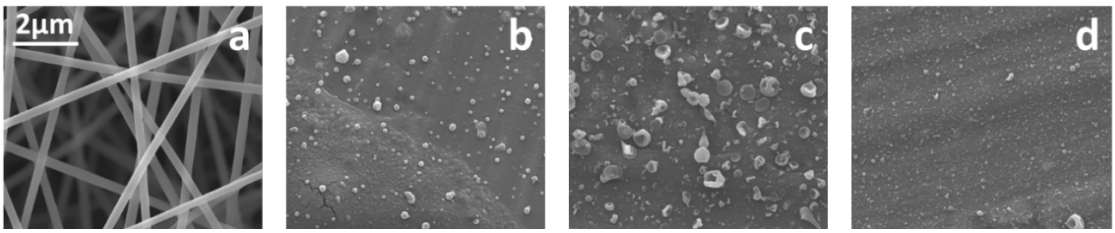

Figure 33: Electrospun structures from 15 wt% PUL, NFDM, CaCAS, and NaCAS in aqueous solutions. (a) PUL fibers from its fibrous mats and (b) electrospun NFDM, (c) CaCAS and (d) NaCAS structures.

6.3 Increasing PUL concentration in the blends with 15 wt% NFDM and CAS

To understand the effect of PUL in electrospinning milk-based proteins electrical conductivity, surface tension and shear viscosity were measured by increasing PUL concentrations ranging from 1 to 15 wt% in the solutions and keeping the NFDM, CaCAS and NACAS concentrations constant, 15 wt%, as shown in Table 10. When 15 wt% PUL mixed with 15 wt% NFDM, CaCAS, and NaCAS with a 50:50 weight ratio, PUL viscosity decreased from 0.885 to 0.12, 0.19, and 0.19 Pa. s at the shear rate of 100 s^{-1}, as shown in Table 10. Since NFDM has fewer proteins with micellar and globular structure, it causes a weak interaction between protein chains and a dilute solution, which made the viscosity of PUL solution decrease.

In a protein and a polysaccharide mixing in aqueous solution, the interaction of two biopolymers attributes either segregative or associative. In very dilute solutions, protein and polysaccharides are stable and co-soluble because mixing entropy dominates (Kruif and Tuinier, 2001). Thus, the blend solution viscosity in dilute solutions showed a little change and had a Newtonian fluid behavior at the shear rate of 100 s^{-1}. However, increasing PUL concentration in the blends with proteins at an increased shear rate made them follow shear thinning behavior, as shown in Figures 37, 43, and 49 in the following sections.

Table 10: Solution properties of NFDM, NFDM: PUL, CaCAS, CaCAS: PUL, NaCAS, and NaCAS: PUL. Concentrations of NFDM, CaCAS, and NaCAS were kept constant, 15 wt%. The blends were prepared from 15 wt% NFDM and CAS mixed with PUL at the concentrations ranging from 1 to 15 wt% with a 50:50 mixing ratio. Shear viscosity is at 100 s^{-1} (Pa. s).

Solution Composition	Total polymer concentration (wt%)	Electrical Conductivity (mS/cm	Surface Tension (mN/m)	Shear Viscosity at 100 s^{-1} (Pa. s)
15 % PUL	15	0.05±0.0	67.6±0.1	0.89
15 % NFDM	15	7.0±0.0	47.1±0.1	0.01
NFDM: 1 % PUL	8	4.3±0.0	47.9±0.0	0.07
NFDM: 5 % PUL	10	4.1±0.0	46.4±0.1	0.02
NFDM: 9 % PUL	12	3.9±0.0	48.5±0.1	0.04
NFDM: 11 % PUL	13	3.8±0.0	48.6±0.0	0.05
NFDM: 15 % PUL	15	3.6±0.0	48.7±0.1	0.12
15 % CaCAS	15	1.4±0.0	46.8±0.0	0.24
CaCAS: 1 % PUL	8	0.9±0.0	37.0±0.6	0.01
CaCAS: 5 % PUL	10	0.8±0.0	38.0±0.0	0.03
CaCAS: 9 % PUL	12	0.8±0.0	44.2±0.2	0.06
CaCAS: 11 % PUL	13	0.7±0.0	45.0±0.3	0.09
CaCAS: 15 % PUL	15	0.7±0.0	46.8±0.0	0.19
15 % NaCAS	15	3.3±0.0	47.2±0.0	1.99
NaCAS: 1 % PUL	8	1.8±0.0	50.0±0.3	0.02
NaCAS: 5 % PUL	10	1.7±0.0	50.7±0.3	0.03
NaCAS: 9 % PUL	12	1.6±0.0	50.0±0.3	0.07
NaCAS: 11 % PUL	13	1.5±0.0	50.0±0.3	0.10
NaCAS: 15 % PUL	15	1.4±0.0	47.8±0.0	0.19

Increasing PUL in the blend solutions both increases the viscosity of the solutions and favors NFDM, CaCAS, and NaCAS to produce uniform, defect-free nanofibers. When the concentration of blend solutions increased up to 15 wt%, the fibers become beadless and more uniform, as shown in Figure 34. Minimum viscosity (~0.1 Pa. s) was reached by increasing the solid concentration and such concentration with the help of PUL carrier. This could be attributed to increased molecular interaction and/or polymer chain

entanglement of NFDM and CAS in the presence of PUL with increasing concentrations. PUL addition to the solutions made from NFDM, CaCAS, and NaCAS reduced the conductivities of the solutions from 7.0 to 3.6, 1.4 to 0.7, and 3.3 to 1.4, respectively, which enabled the molecules to carry positive charges resulting in stretching the jet to form ultrafine fibers. This result is consistent with the SEM micrographs of the fibers obtained from fibrous mats in this study, as shown in Figure 34. When the viscosity increases with increasing PUL content in the blend solutions from 0.5 to 7.5 wt%, the fibers became more uniform and defect-free for the blended solutions made from 15 wt% NFDM, CaCAS and NaCAS with 15 wt% PUL with a 50:50 mixing weight ratio, as shown in in Figures 34e, j, and o.

Figure 35 shows the SEM images of fibrous mats produced from three different concentration of 15 wt% PUL and 15 wt% NFDM, CaCAS, and NaCAS blended with 15 wt% PUL solutions with a 50:50 ratio at 4 different magnifications which are 100×, 5,000×, 10,000×, and 25,000×. They produced fibers with diameters 301±18, 163±22, 217±15, and 215±22 nm, respectively. Even though all the fibrous mats had smooth surface under a scale of 500 μm, 15 wt% NFDM: 15 wt% PUL (50:50) showed breakups and defects in fiber structure under the scale of 2 μm which are indicated by red arrows in Figure 35. The fibers obtained from 15 wt% CaCAS: 15 wt% PUL (50:50) showed small defects but mostly uniform while the NaCAS: PUL fibrous mats with smooth surface showed a uniform, well-formed fiber structure as the magnification increased.

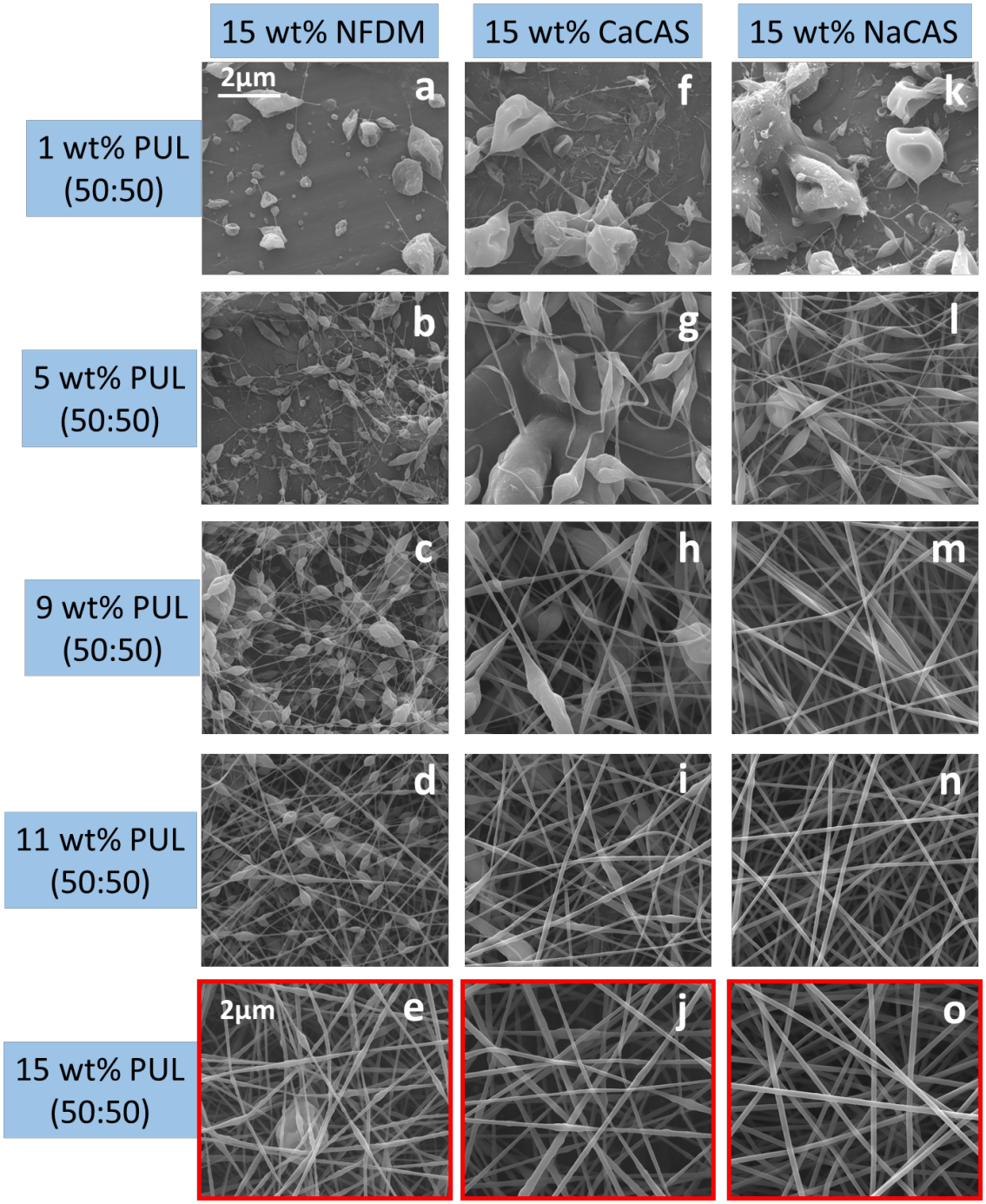

Figure 34: SEM images of electrospun nanofibers from neat 15 wt% NFDM, CaCAS and NaCAS and their blends with 1, 5, 9, 11 and 15 wt% PUL solutions with a 50:50 mixing ratio (a) 15 wt% NFDM: 1 wt% PUL (50:50), (b) 15 wt% NFDM: 5 wt% PUL (50:50), (c) 15 wt% NFDM: 9 wt% PUL (50:50), (d) 15 wt% NFDM: 11 wt% PUL (50:50), (e) 15 wt% NFDM: 15 wt% PUL (50:50), (f) 15 wt% CaCAS: 1 wt% PUL (50:50), (g) 15 wt% CaCAS: 5 wt% PUL (50:50), (h) 15 wt% CaCAS: 9 wt% PUL (50:50), (i) 15 wt% CaCAS: 11 wt% PUL (50:50), (j) 15 wt% CaCAS: 15 wt% PUL (50:50), (k) 15 wt% NaCAS: 1 wt% PUL (50:50), (l) 15 wt% NaCAS: 5 wt% PUL (50:50), (m) 15 wt% NaCAS: 9 wt% PUL (50:50), (n) 15 wt% NaCAS: 11 wt% PUL (50:50), (o) 15 wt% NaCAS: 15 wt% PUL (50:50).

The blend of NaCAS: PUL produced thinner fibers with the diameters of 215±22 nm than the one from PUL with 301±18 nm over the same processing conditions, a flow rate of 3 mL/h and an external voltage of 20 kV. It is because 15 wt% PUL has a higher viscosity of 0.885 Pa. s at a shear rate of 100 s^{-1} than its blend with 15 wt% NaCAS which reduced the viscosity of PUL to 0.186 Pa. s at the same shear rate, as shown in Table 10. This result is consistent with literature reports that fiber diameters increase significantly with higher viscosities which is a function of polymer concentration as thinner fibers are formed at lower viscosities (Greiner and Wendorff, 2007; McKee, Elkins, and Long, 2004).

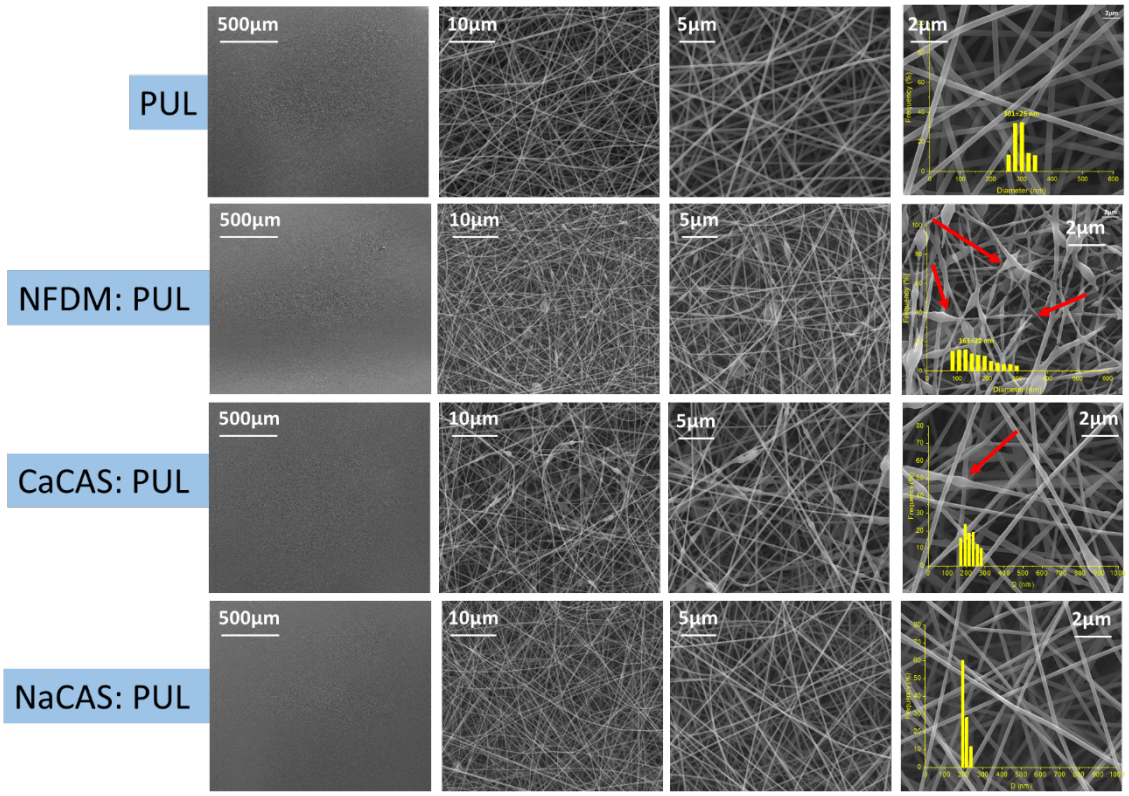

Figure 35: Electrospun fibrous mats from 15 wt% PUL and its blends with 15 wt% NFDM, CaCAS and NaCAS with a 50:50 weight ratio at various magnifications, vertically 100×, 5,000×, 10,000×, and 25,000×. Fiber diameter size of PUL, NFDM: PUL, CaCAS: PUL and NaCAS: PUL are 301±18, 163±22, 217±15, and 215±22 nm from up to down, respectively. Red arrows show the breakups and defects within fiber structure.

6.4 NFDM with PUL blends

Figure 36 shows the dependence of shear viscosity on the shear rate of aqueous NFDM solutions in the concentration range blended with 15 wt% PUL with a 50:50 weight mixing ratio. The concentrations of NFDM solutions range from 1 to 25 wt%. Due to the molecular structure of proteins in NFDM, there is a lack of the protein chain entanglements under the electric field. The shear rate was employed from 0.01 to 1000 s^{-1} were performed on the concentrations of NFDM blended with PUL solutions ranging from 8.0 to 20.0 wt% in aqueous solutions at 20 ºC. Blend solutions at the lower concentration showed Newtonian behavior and their viscosities increased from 0.007 to 0.28 Pa. s as increasing NFDM concentrations ranging from 1.0 to 17.5 wt%. However, shear thinning behavior occurred at the higher total solid concentration more than 17.5 wt%. The dependence of shear thinning behavior on concentration increased at the total solid concentration of 20 wt%. As shown in Figure 36, 15 wt% PUL showed a higher viscosity dependence on concentration compared to its blend with NFDM. This is due to the higher lactose content of NFDM (Reference Manual for U.S. Milk Powders 2005), causing lack of chain to chain interactions, which is a function of protein content, to promote a higher viscosity.

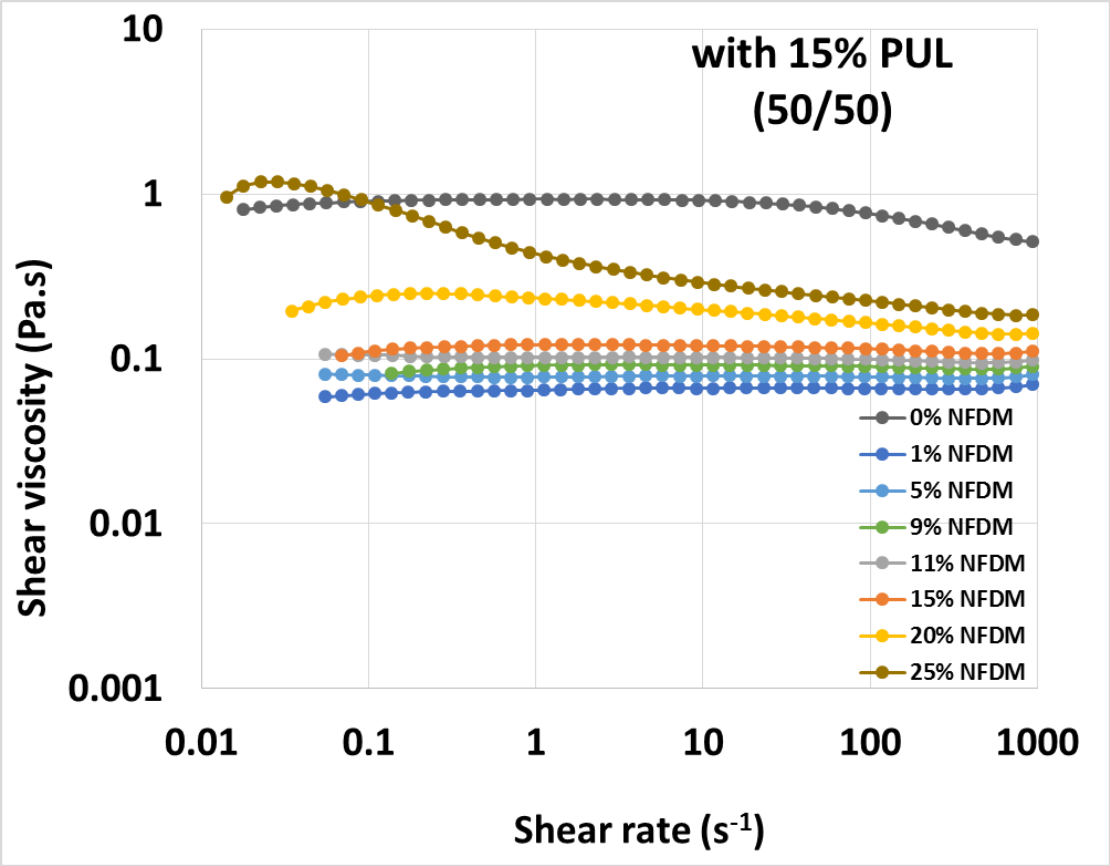

Figure 36: The dependence of shear viscosity on the shear rate of aqueous NFDM solutions at a range of concentrations blended with 15 wt% PUL with a 50:50 weight mixing ratio. The concentrations of NFDM solutions range from 1 to 25 wt%. Neat protein content in blend solutions increases 0 to 4.5 % because NFDM contains 35.9 % protein.

Table 11 summarizes the concentration of NFDM and PUL solutions and their blends with a 50:50 weight mixing ratio and their zero shear viscosity at the shear rate of 10 s^{-1}, which is used to calculate specific viscosity by using Equation 4. The η_0 increased with increasing NFDM content in the mixed solutions from 0.066 to 0.283 Pa. s at the shear rate 10 s^{-1}. Compared to CAS blended with PUL, the viscosity values were lower because of the less protein content which is correlated to viscosity (McMahon and Oommen, 2013).

Table 11: Concentration of NFDM and PUL solutions and their blends with a 50:50 weight mixing ratio and their zero shear viscosity at the shear rate of 10 s^{-1}.

Concentration of NFDM solution (wt%)	Concentration of PUL solution (wt%)	Weight mixing ratio	Total blend concentration (wt%)	η_0 at shear rate of 10 s^{-1} (Pa.s)
0	15	50:50	7.5	0.046
1	15	50:50	8.0	0.066
5	15	50:50	10.0	0.079
9	15	50:50	12.0	0.092
11	15	50:50	13.0	0.102
15	15	50:50	15.0	0.121
20	15	50:50	17.5	0.197
25	15	50:50	20.0	0.283

The dependence of η_{sp} on the concentration for NFDM blended with 15 wt% PUL with a 50:50 ratio is shown in Figure 37. The blue lines with blue scatter data are the blend of NFDM and PUL solutions by keeping PUL concentration constant, 15 wt%, and increasing NFDM content in the blends so that increasing the total solid concentration. Three SEM images show the electrospun structures in Figure 37; PUL fibers with a diameter of 301±26 nm, NFDM powders and/or pieces and NFDM: PUL blend fibers with the diameter of 210±17 nm. With the improvement of electrospinnability of NFDM through the addition of PUL, Figure 37 shows the viscosity concentration relationships, varying the different ratios of NFDM and PUL from 0% to 100% NFDM content. A shift in the c_e of the blend system from 5.5 wt% for neat PUL to 21.1 wt% for the pure NFDM, with the NFDM: PUL (50:50) blend 12.0 wt% indicated the influence of PUL in overall solution behavior which decreased the c_e of the blend solution as the c_e of pure PUL is lower than NFDM due to its less protein content. PUL increase the viscosity of NFDM in the blends of 0.1 Pa. s at the blend concentration of 15 wt% blend concentration compared

to the viscosity of pure 15 wt% NFDM, 0.01 Pa.s. Therefore, the addition of PUL enhanced chain entanglement needed for fiber formation. As mentioned before in Section of 2.3, enough viscosity is required to maintain the jet formation to elongate and stretch under an electric field for a successful fiber formation. This change of viscosity dependence was similar to that of a blend of pectin and PUL fibers (Liu et al., 2016) formed from the blend solution which had the c_e of 4.3. PUL decreased the PEC viscosity as well as its c_e from 6.1 wt% to 4.3 wt%. In comparison with the c_e of neat NFDM (21.1 wt%), the blends of NFDM: PUL entangled at relatively lower concentrations somewhere around 12 wt%, as shown in Figure 37.

More importantly, the viscosities differ at higher concentrations and viscosity power-law behavior was affected by the addition of PUL. Table 12 summarizes the power law exponents and non-linear regression equations in the semidilute unentangled, semidilute entangled, and concentrated regimes as well as the c_e for the two polymers and their blend in aqueous solutions. The concentration dependence of viscosity obtained for NFDM: PUL blend with a weight ratio of 50:50 were $n_{sp}\sim c^{1.18}$ for the semidilute unentangled region and $n_{sp}\sim c^{2.98}$ for the semidilute entangled region. These results showed that the incorporation of PUL to NFDM solution affected the n_{sp} compared to the pure NFDM solutions at the semidilute unentangled as evident by the change in the slope from 0.08 to 1.18. The power law exponent for the blend of NFDM and PUL was found to 1.18 in the semidilute unentangled, which is in good agreement with theoretical prediction ($\eta_{sp}\sim c^{1.25}$) for neutral and linear polymers in a good solvent. However, the concentration dependence of the blend was found as 2.98 in the semidilute entangled region, which is a weaker dependence compared to the theoretical predictions of 4.8 for linear polymers in a

good solvents (Daoud and De Gennes, 1979), and some reported values for biopolymers ($\eta_{sp}\sim c^{6.0}$) for chitosan in a mixture solvent of acetic acid- water (Klossner et al., 2008) and ($\eta_{sp}\sim c^{4.0}$) for pure PUL in aqueous solution (Kong and Ziegler, 2013). However, this concentration dependence is very close to such of the other random coil biopolymers, including dextran, alginate, lambda-carrageenan, and hyaluronate, ($\eta_{sp}\sim c^{3.3}$) (Morris et al., 1981).

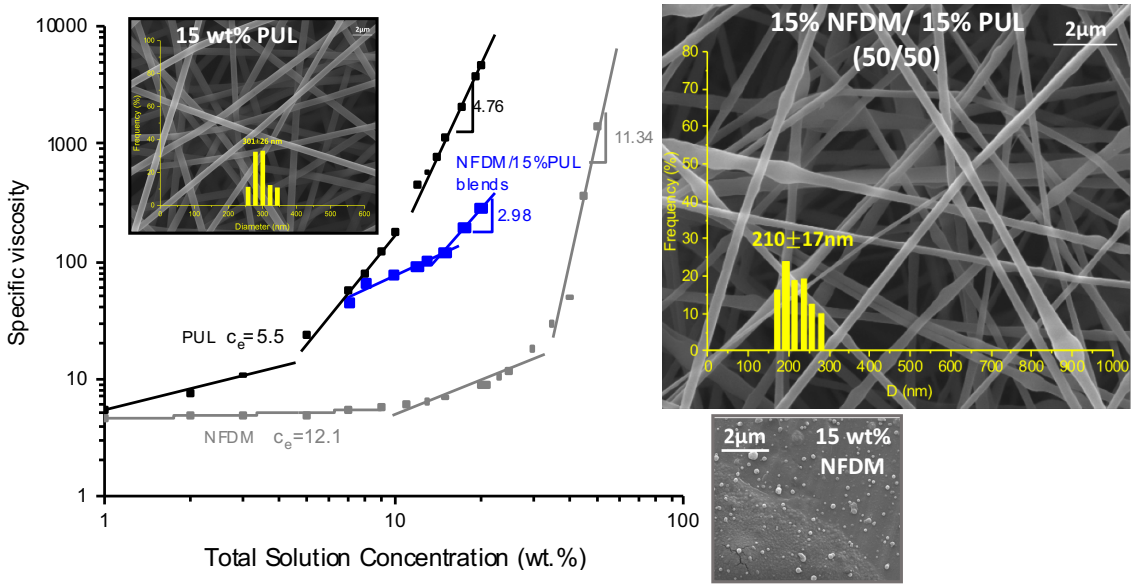

Figure 37: The dependence of specific viscosity on the solution concentration. The black lines with the black scatters are neat PUL solutions with the concentration ranging from 1 up to 16 wt%. The grey interpolated lines are neat NFDM solutions with the concentration from 1 to 45 wt%. The blue lines with the blue scatters are the blends of NFDM and 15 wt% PUL solutions by keeping the PUL concentration constant and increasing the NFDM content, so that increasing the total solid concentration. Three SEM images show the electrospun structures; 15 wt% PUL-fibers with 301±26 nm, 15 wt% NFDM-no fiber and 15 wt% NFDM: 15wt% PUL (50:50)-fibers with the diameter of 210±17 nm.

Table 12: The equations obtained by interpolating scattered data points from Figure 37. Concentration regimes were identified as the semidilute unentangled, semidilute entangled and concentrated regions obtained from Figure 37 for neat PUL, NFDM, and their blends. c_e is entanglement concentration and η_0 is zero shear viscosity at the shear rate of 10 s^{-1}.

	PUL	**NFDM**	**Blends with increasing NFDM content**
semidilute unentangled	y=0.61x+0.72 R^2=0.96	y=0.08x+0.66 R^2=0.74	y=**1.18**x+0.70 R^2=0.93
semidilute entangled	y=2.85x-0.64 R^2=0.99	y=**1.00**x-0.32 R^2=0.91	y=**2.98**x-1.42 R^2=0.99
concentrated regime	y=4.76x-2.53 R^2=0.99	y=**11.34**x-16.21 R^2=0.94	NA
c_e	5.5 wt%	21.1 wt%	12.0 wt%
η_0 (Pa. s) at 10 s^{-1}	0.04	0.02	NA

The dependence of the electrospun fiber diameter on η_0 for NFDM blended with 15 wt% PUL solutions is shown in Figure 38. Three different fiber morphologies were identified; polymer droplets, beaded nanofibers, and defect-free fibers based on the η_0 of the solutions. The blend solutions with a η_0 less than 0.02 Pa. s produced polymer droplets when electrospun, as the solutions with a η_0 between 0.02 and 0.1 Pa. s produced electrospun fibers with beads, as shown in Figure 38. The fiber-forming solutions with a η_0 greater than 0.1 Pa. s generated defect-free and fully-formed fibers. Moreover, the mean fiber diameter size was correlated with η_0 by the relationship below

$$\text{Diameter (nm)} = 492\ {\eta_0}^{0.72} \qquad \text{Equation 7}$$

An increase in η_0 indicated a larger number of polymer chain entanglement, leading to form thicker fully-formed electrospun fibers instead of producing beaded fibers.

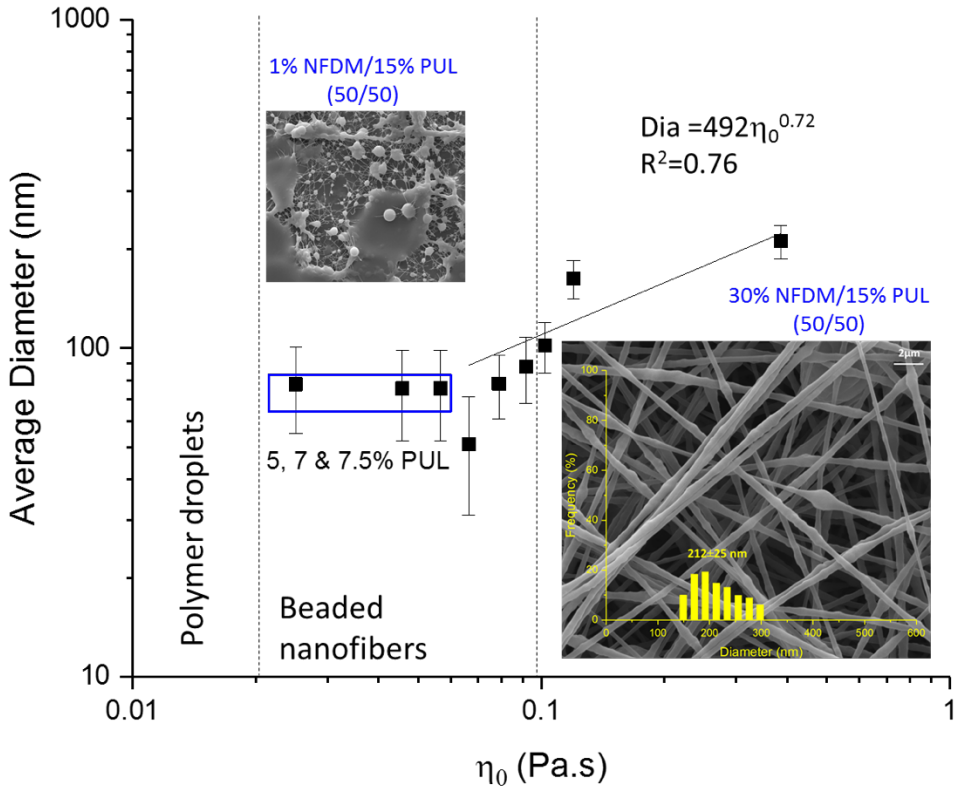

Figure 38: The dependence of the average fiber diameter (nm) on the zero shear viscosity at the shear rate of 10 s^{-1}. Three regions identified are polymer droplets, beaded nanofibers, and fibers. The SEM images show beaded nanofibers from the blends of 1 wt% NFDM and 15 wt% PUL and the fibers with the diameter of 217±25 nm from the blends of 30 wt% NFDM and 15 wt% PUL with a 50:50 mixing ratio. Blue circled area shows the beads with incipient fibers with the diameter less than 100 nm from neat PUL solutions at the concentrations of 5, 7 and 7.5 wt%. The linear line represents mean diameter trend from the blend solutions of NFDM: PUL by increasing NFDM content in the blends.

Figure 39 shows that the solution of each NFDM: PUL blend concentration was normalized with its respective c_e value to evaluate the dependence of fiber diameter on normalized solution concentration for the blend solution series. The electrospun NFDM: PUL fiber diameter scaled with the normalized concentration as

$$\text{Diameter (nm)} = 97.8\,(\frac{c}{c_e})^{1.3} \qquad \text{Equation 8}$$

Where c is the polymer concentration in solution and c_e is the entanglement concentration. As shown in Figure 39, the shaded region shows 2-2.5 times c_e, which was

the minimum concentration required to electrospin fully-formed and defect-free fibers. This equation was estimated based on a single equation fitted to the plot of η_{sp} versus concentration data for the semidilute entangled and the concentration regions to predict $c \sim \eta_{sp}^{1.6}$ (R^2=0.94). Then, this relationship was substituted into the Equation 7 obtained from the plot of average diameter versus η_0, it was predicted as the $\text{diameter (nm)} = c^{1.5}$, which is identical to the equation obtained from Figure 39. However, the precision and sensitivity of these findings should be supported by further investigation in the future.

The NFDM: PUL blend should require a concentration 1.6-2.3 times the c_e for effective electrospinning and the formation of defect-free nanofibers, as shown in Figure 39. This range is in good agreement with the reported prediction (2-2.5 times c_e), as mentioned above. The results are consistent with the SEM micrographs of electrospun NFDM: PUL nanofibers for the required concentration to obtain smooth and full-formed fibers successfully, as shown in Figure 41.

Figure 40 shows that the SEM micrographs of electrospun nanofibers from the blends of 15 wt% NFDM and 5, 11 and 15 wt% PUL solutions at various weight mixing ratios and average diameter size. With increasing NFDM content in the blends, the fibers structure becomes defected and less uniform. Since NFDM contains low proteins composed of casein and whey, it requires more solid content to form a solution with a sufficient viscosity. However, casein proteins exist in micellar structure with the size ranging from 20 to 300 nm (Oommen, 2004; Rebouillat and Ortega-requena, 2015), which causes the formation of defected and beaded fibers. Besides less protein content, the micellar structure of casein has a lower interaction with each other to favor the electrified jet to entangle and stretch during the electrospinning (Nieuwland et al., 2013). Therefore,

the more NFDM in the blends, the less uniform, smooth fibers are formed. 15 wt% NFDM blended with 15 wt% PUL with a weight ratio of 30:70 produced smoother, thinner fibers with the diameters of 205±18 nm compared to other blends, as shown in Figure 40f. This is because PUL dominated the solution characteristics such as excellent electrospinnability, high solubility, and ability to entangle, which favor the blended solution to produce smooth, defect-free fibrous mats as it is used more than NFDM.

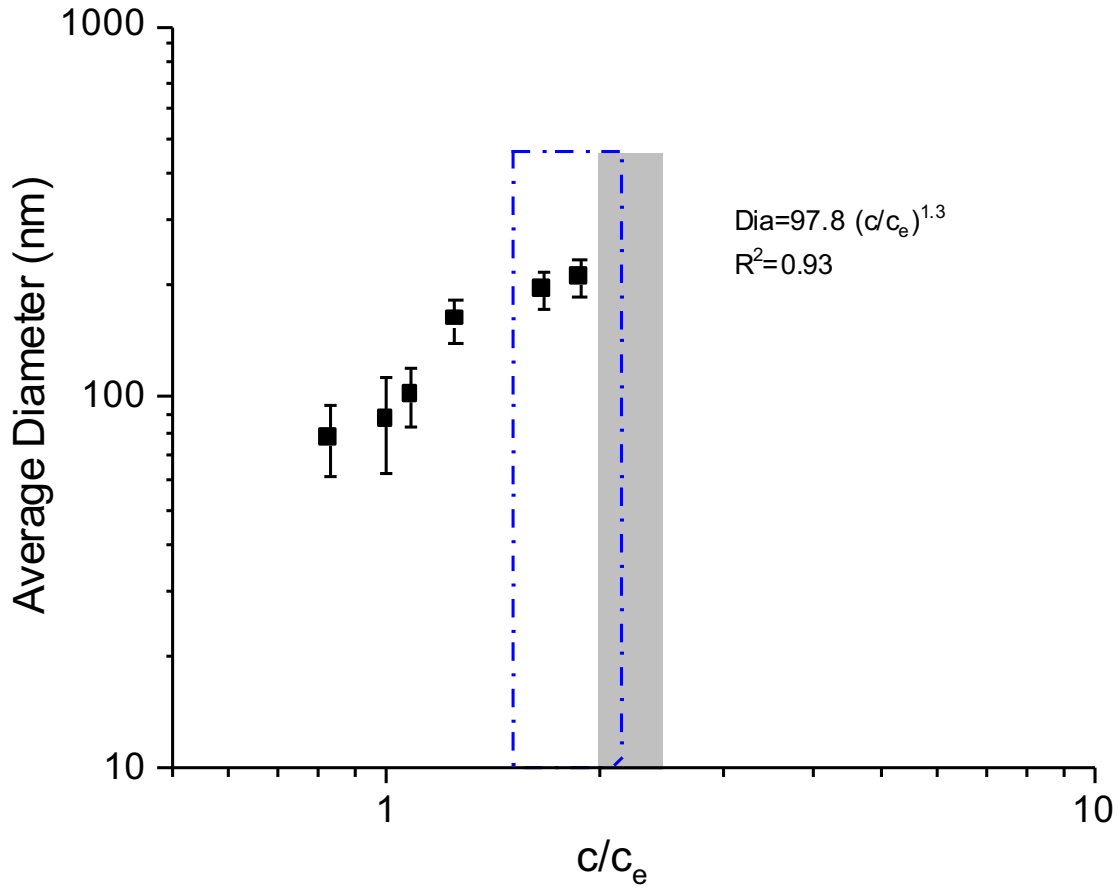

Figure 39: Dependence of fiber diameter on the normalized concentration for the solutions. The blue dashed region corresponds to the fully-formed NFDM: PUL blended fibers at the concentration of 1.6-2.3 times the c_e and the shaded area represents 2.0-2.5 times the c_e for the defect-free fiber formation from natural polymers (McKee et al., 2004).

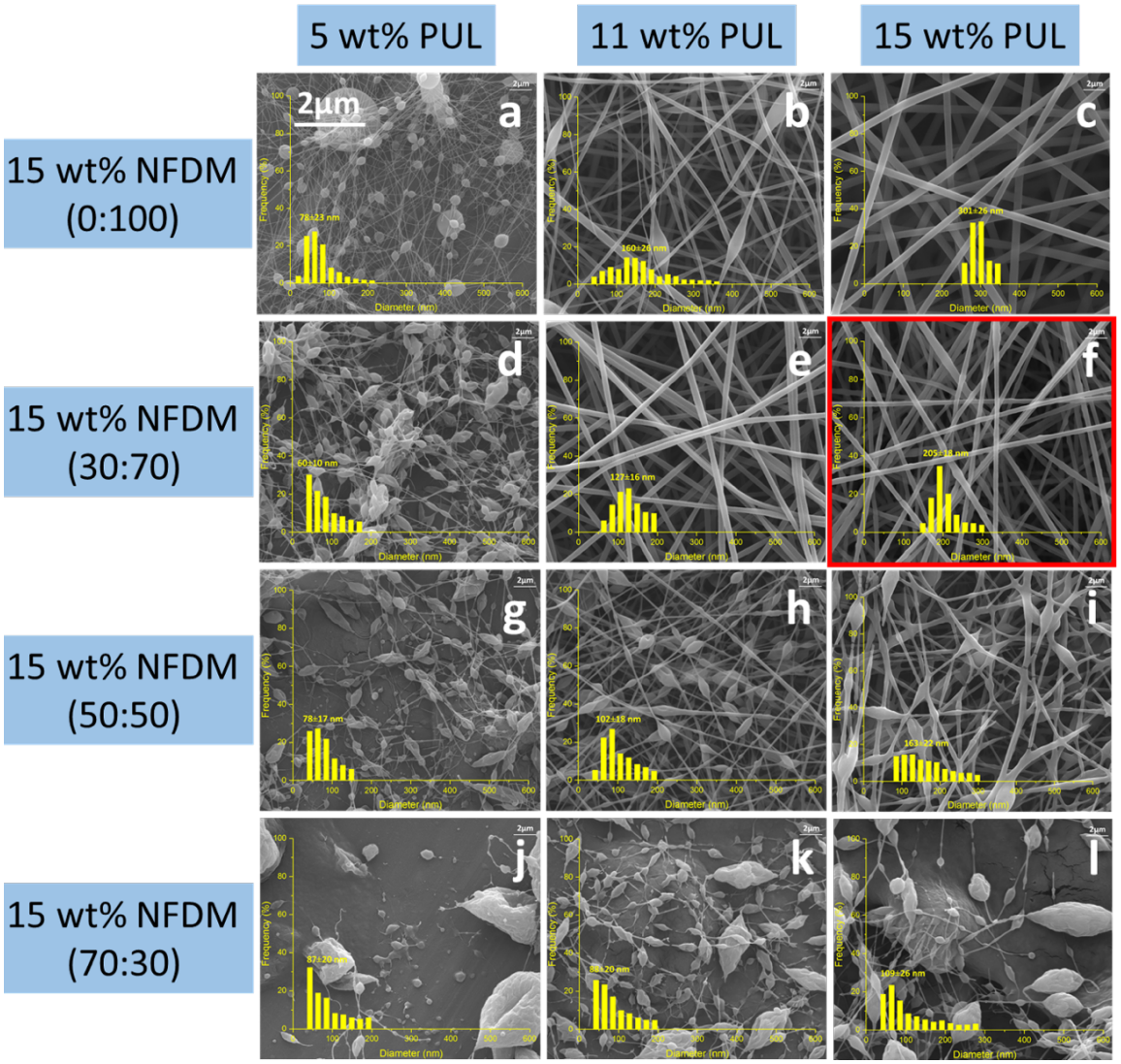

Figure 40: SEM images of electrospun nanofibers from the blends of 15 wt% NFDM and 5, 11 and 15 wt% PUL stock solutions at various weight mixing ratios and average diameter size: (a) 5 wt% PUL, beads with incipient fibers with 78±23 nm, (b) 11 wt% PUL, fibers with 160±26 nm, (c) 15 wt% PUL, fibers with 301±26 nm, (d) 15 wt% NFDM: 5 wt% PUL (30:70), beads with incipient fibers with 60±10 nm, (e) 15 wt% NFDM:11 wt% PUL (30:70), fibers with 127±16 nm, (f) 15 wt% NFDM: 15 wt% PUL (30:70), fibers with 205±18 nm, (g) 15 wt% NFDM: 5 wt% PUL (50:50), defects with incipient fibers with 78±17 nm, (h) 15 wt% NFDM: 11 wt% PUL (50:50), beaded fibers with 102±18 nm, (i) 15 wt% NFDM:15 wt% PUL (50:50), defected fibers with 163±22 nm, (j) 15 wt% NFDM: 5 wt% PUL (70:30), 87±20 nm, (k) 15 wt% NFDM: 11 wt% PUL (70:30), defected fibers with 88±20 nm, (l) 15 wt% NFDM: 15 wt% PUL (70:30), defects with incipient fibers with 109±26 nm. The magnification is 25,000×.

Figure 41 shows SEM images of electrospun fibers from 1, 5, 9, 11, 15, and 30 wt% NFDM blended with 15 wt% PUL solution with a 50:50 mixing ratio. Table 12 illustrates that the c_e for the PUL, NFDM and their blend solutions is 5.5, 21.1, and 12 wt%, respectively. The fiber morphology was dependent on the concentration regime from which the polymer solution was electrospun. As shown in Figure 41, polymer solutions electrospun from the blend solutions below the c_e, 12 wt%, did not yield fibers, and only polymer droplets and beads with incipient fibers were observed. Since there is less or no entanglements between polymer chains in blends below c_e, the jet could not withstand the force of the electric field and the surface tension, which result in jet breakups into droplets. When the concentration was close to the c_e (12 wt%), the beads with incipient fibers were observed. As the concentration was raised beyond c_e, beaded electrospun fibers were produced with an average fiber diameter of 102 nm (Figure 41). For the 15 wt% blend solution, discontinuous nanofibers with defects were generated with an average diameter of 163 nm, whereas more uniform, defect-free nanofibers with the diameter of 212 nm were produced from the blend solution at the concentration of 22.5 wt%, as shown in Figure 41. The change through the formation of fibers is from spherical beads to elongated bead from 1 up to 11 wt% NFDM blended with 15 wt% PUL. This was reported in the literature that above c_e the degree of chain overlap increases leading to chain constraint and entanglements couplings (McKee et al., 2004). Figure 41 shows that 22 wt% total solids concentration of the blended solution formed uniform, defect-free fibers with a mean diameter of 212 nm.

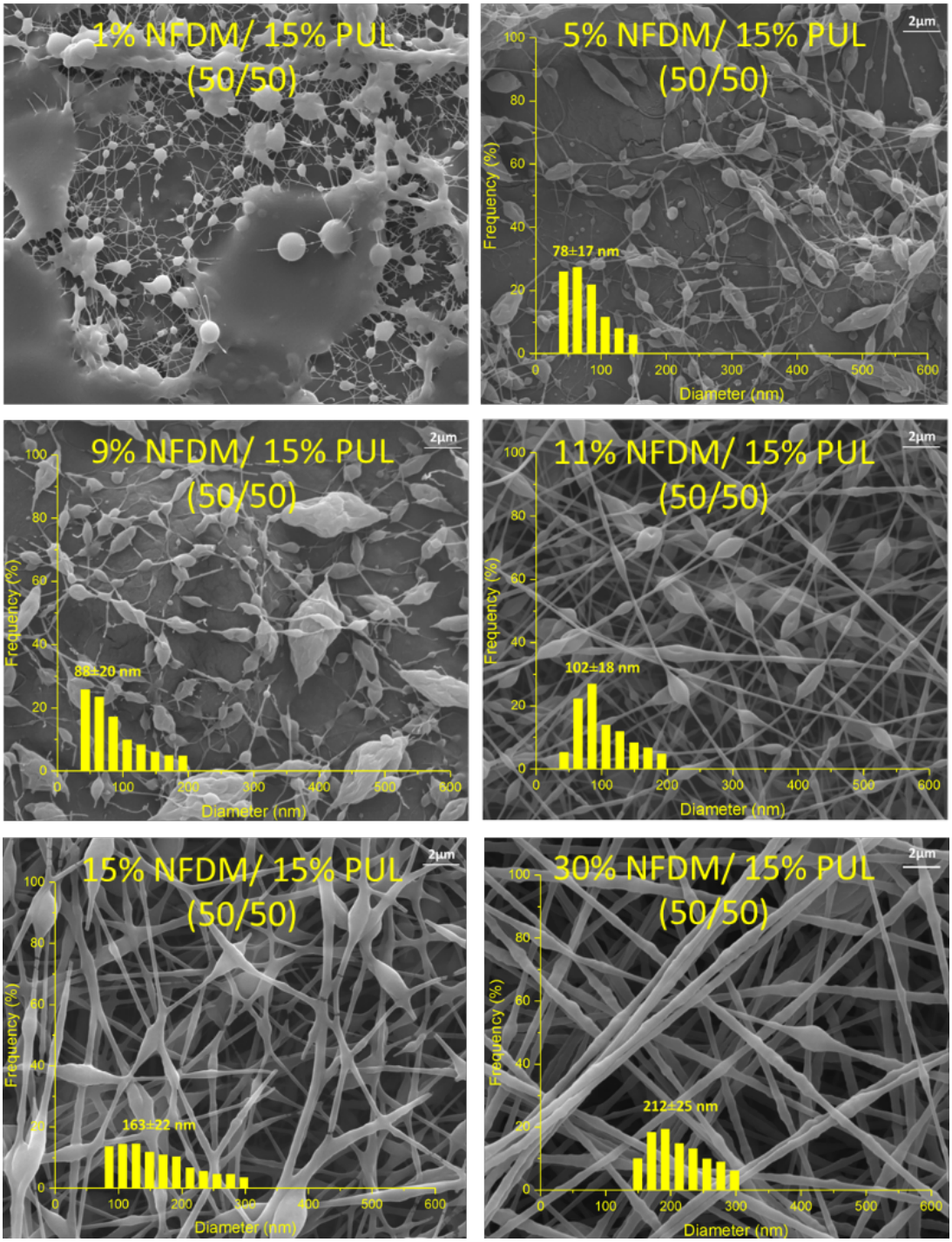

Figure 41: SEM images of electrospun nanofibers from the blends of 1, 5, 9, 11, 15 and 30 wt% NFDM and 15 wt% PUL solutions with a 50:50 weight mixing ratio and the distribution of fiber diameter size: 1 wt% NFDM: 15 wt% PUL, beads with incipient fibers; 5 wt% NFDM: 15 wt% PUL, defected fibers with 78±17 nm; 9 wt% NFDM: 15 wt% PUL, defected fibers with 88±26 nm; 11 wt% NFDM: 15 wt% PUL, beaded fibers with 102±18 nm; 15 wt% NFDM: 15 wt% PUL, defected fibers with 163±22 nm; 30 wt% NFDM: 15 wt% PUL, fibers with 212±25 nm. The magnification is 25,000×.

Figure 42 shows FTIR analysis of the PUL powder and fibers, NFDM powder, and NFDM: PUL fibers conducted to confirm that both the PUL and NFDM are present in the blend fibrous mats as well as obtaining some information related to the structure of the protein-polysaccharide complexes in the fibers. Spectrum for the NFDM: PUL blend fiber mats showed new bands at approximately 1648 cm^{-1} and 1544 cm^{-1}, compared to the PUL powder and fiber spectrums. Peaks 992 and 1015 cm^{-1} in PUL associated with C–OH bending vibrations at the C–6 positions which are attributed to the strength of the interchain interactions via hydrogen bonding. Both the decreased intensity of peak 992 cm^{-1} and the increased intensity of peak 1015 cm^{-1} may be an indication for an increase in the interchain associations of PUL molecules in both PUL and its blend with NFDM fibers. Two prominent features for protein's FTIR are Amide I band (1638 cm^{-1}) and Amide II (1537 cm^{-1}) were observed in NFDM powder sample, as shown in Figure 42. Amide I band is primarily attributed to C=O stretching vibration and Amide II band from the N–H bending and C–N stretching vibrations of peptide backbone (Haris and Severcan, 1999). Due to the shift in Amide I band in NFDM: PUL fibers to 1648 cm^{-1}, it indicated that the proteins in NFDM became unordered structure in the presence of PUL compared to proteins in NFDM powder with β-sheet structures, which is consistent the reported literature that Amide I band positions around 1633 cm^{-1} corresponding to the absorption of intramolecular β-sheet structures (Barth, 2007). Amide II band in NFDM powder shifted from 1536 to 1544 cm-1 when it blended with PUL. The shift of Amide II band toward higher wavenumbers may indicate that strong interactions occur between the hydroxyl groups of PUL and the amino groups of proteins in NFDM (Aceituno-Medina et al., 2013; Wu et al., 2013), which promotes electrospun fiber formation.

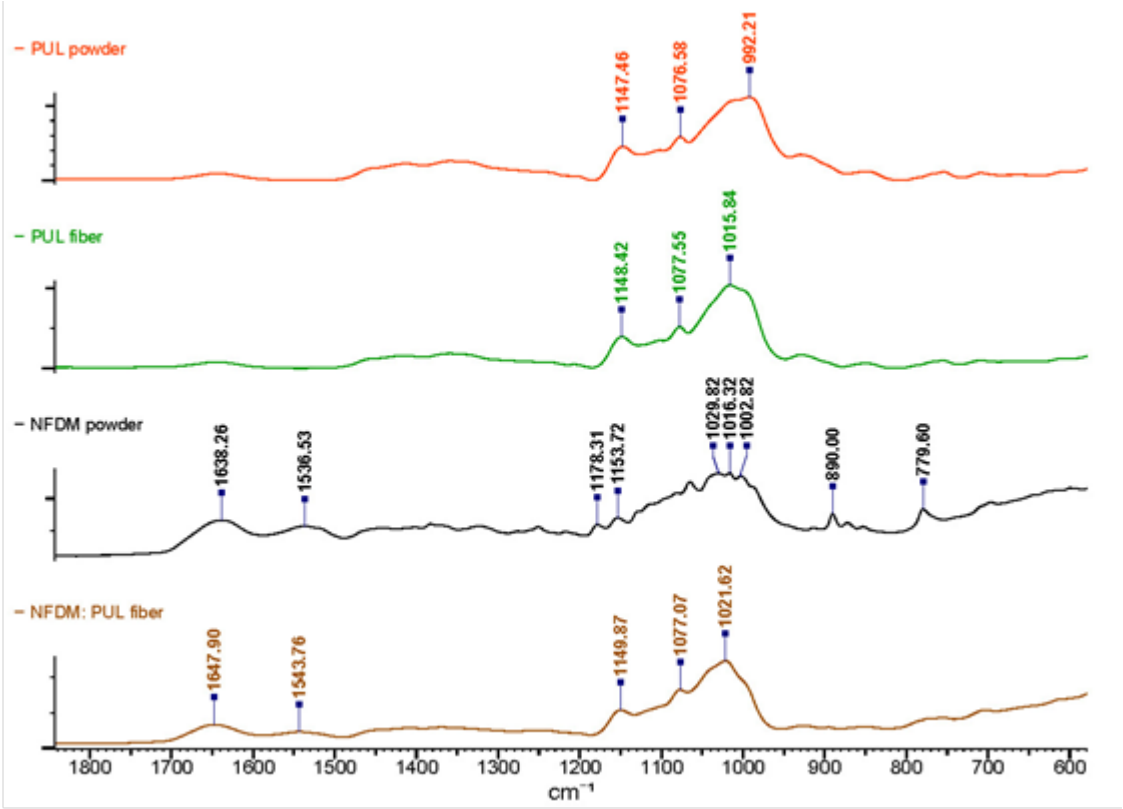

Figure 42: FTIR-ATR spectra of PUL powder and fibers, NFDM powder, and NFDM: PUL fibers from top to bottom, respectively.

Overall, the SEM images showed that PUL exerted a positive effective role in changing the morphology of the blended nanofibers towards a more uniform, continuous fiber formation as it is higher that NFDM content in the blended solution. It is strongly linked to the changes in the viscosity of the mixture solution due to the addition of PUL, which increases the viscosity to enable the molecular entanglement and fiber formation.

6.5 Electrospinning of CaCAS and NaCAS with PUL blends

6.5.1 Electrospinning of CaCAS blended with PUL

In preliminary results, after preparing CaCAS: PUL blend solutions, they were refrigerated at 4 °C overnight to remove bubbles and detect phase separation. Results indicated that the blend solutions were properly mixed, and highly stable with time;

however, some precipitation of CaCAS dispersion was observed, which is also reported that increasing concentration reduced the solubility (Swaisgood, 1993; Pitskowski et al., 2008).

To understand the effect of PUL in electrospinning CaCAS, the dependence of shear viscosity on the shear rate of aqueous CaCAS solutions at a range of concentrations from 1 to 20 wt% blended with 15 wt% PUL with a 50:50 weight mixing ratio were evaluated, as shown in Figure 43. Neat protein content in blend solutions increases 0.45 up to 9.00 % because CaCAS contains approximately 90 % protein reported by the manufacturer mentioned in Section 5.3.1. It was observed that mixing CaCAS solutions with PUL decreased the neat PUL viscosity at a higher concentration of CaCAS (15 wt%) from 0.9 (in Table 6) to 0.2 Pa. s as it was blended with 15 wt% PUL with a 50:50 weight ratio.

All blend solutions showed Newtonian behavior, and/or a weak shear thinning behavior and their viscosities increased from 0.06 to 0.30 Pa. s due to the increase in CaCAS concentration from 0.5 to 10.0 wt% in the blends, as shown in Figure 43. With increasing CaCAS in the presence of PUL, a sufficient viscosity (~ 0.1 Pa. s) and weak shear thinning behavior were met to produce continuous, smooth fibers, as shown in Figure 48. This result is in a good agreement with the reported results of polysaccharides having a minimum viscosity of 1 Pa. s and weak shear thinning behavior at the shear rates lower than 1000 s^{-1}. (Stijnman et al., 2011).

PUL, with repeating units of three glucose units connected by α-1,4 glycosidic bonded maltotriose that is linked via an α-1,6 glycosidic linkage, can interact with CaCAS by disrupting the self-association of hydrophobic groups of caseinates via cation ion, Ca^{+2},

and then forming hydrophobic interactions and/or ionic bonds (Kruif and Tuinier, 2001; McClements, 2006; Gounga et al., 2007; Aceituno-Medina et al., 2013). This may increase the flexibility of protein chains, turn CaCAS solution into more like a Newtonian fluid, and promote the entanglements of protein chains, which make the electrospinning of CaCAS possible. As shown before in Figure 21, a strong shear dependence of viscosity was observed within a wide range of shear rates (0.01-1000 s^{-1}) in aqueous neat CaCAS solutions. However, when PUL was incorporated with CaCAS solution, a typical Newtonian liquid behavior was observed over the same range of shear rates in aqueous CaCAS: PUL blend system, as shown in Figure 43. This change can also be explained in terms of the enhanced entanglement networks, which may be disturbed at higher shear rates.

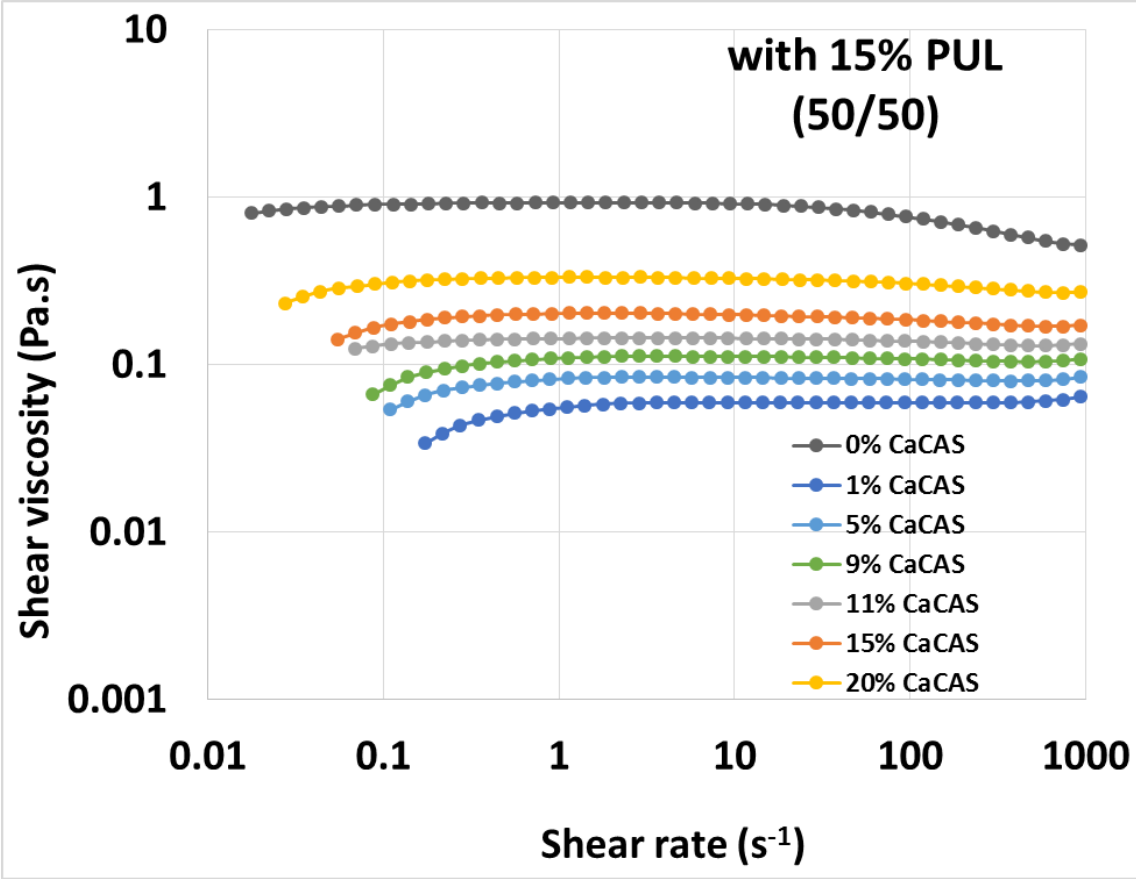

Figure 43: The dependence of shear viscosity on the shear rate of CaCAS solutions at various concentrations blended with 15 wt% PUL with a 50:50 weight mixing ratio. The concentrations of CaCAS solutions range from 1 to 20 wt%. Neat protein content in blend solutions increases 0.45 to 9.0 % because CaCAS is composed of 90 % protein.

Table 13 summarizes the concentration of CaCAS and PUL solutions and their blends with a 50:50 weight mixing ratio and their zero shear viscosity at the shear rate of 10 s^{-1}, which is used to calculate specific viscosity by using Equation 4. The η_0 increased with increasing CaCAS content in the mixed solutions from 0.059 to 0.302 Pa. s at the shear rate of 10 s^{-1}. It is difficult to measure the viscosity at 20 °C beyond 10 wt% CaCAS in the blend solution because the solution became viscous with increasing protein concentrations (McMahon and Oommen, 2013).

Table 13: Concentration of neat CaCAS and PUL solutions and their blends with a 50:50 weight mixing ratio and their zero shear viscosity at the shear rate of 10 s^{-1}.

Concentration of CaCAS (wt%)	Concentration of PUL (wt%)	Mixing weight ratio	Total blend concentration (wt%)	η_0 at shear rate of 10 s^{-1} (Pa. s)
0	15	50:50	7.5	0.047
1	15	50:50	8.0	0.059
5	15	50:50	10.0	0.081
9	15	50:50	12.0	0.108
11	15	50:50	13.0	0.137
15	15	50:50	15.0	0.183
20	15	50:50	17.5	0.302

With the addition of PUL to improve the electrospinnability of CaCAS, Figure 44 shows the concentration dependence of viscosity for aqueous CaCAS blended with 15 wt% PUL with a 50:50 ratio solution. The blue lines with blue scatter data are the blend of CaCAS and PUL solutions by keeping PUL concentration constant, 15 wt%, and increasing CaCAS content in the blends, so that increasing the total solid concentration. Three SEM images of the electrospun structures are shown in Figure 44; PUL fibers with a diameter of 301±26 nm, CaCAS powders and/or pieces and CaCAS: PUL blend fibers with a diameter of 217±15 nm. The c_e of the CaCAS: PUL (50:50) blend was determined to be 7.0 wt%, is higher than the c_e of pure PUL (5.5 wt%) and lower than the pure CaCAS solutions (9.0 wt%). This indicated the influence of PUL in overall solution behavior which decreased the c_e of the aqueous CaCAS solution and the slopes in the concentrated regime which is concentrations above c^{**} of CaCAS solution from 7.48 to 2.67, which shows a similarity with the theoretical predictions (i.e., $\eta_{sp} \sim c^{3.7}$) for neutral and linear polymers in good solvents (Daoud and De Gennes, 1979; Colby et al., 1991). However, a much weaker concentration dependence was observed in the semidilute entangled region for the CaCAS:

PUL blend (η_{sp}~$c^{1.63}$), which was attributed to the colloidal structure of casein formed via calcium bridging in the presence of calcium ions (McMahon and Oommen, 2013).

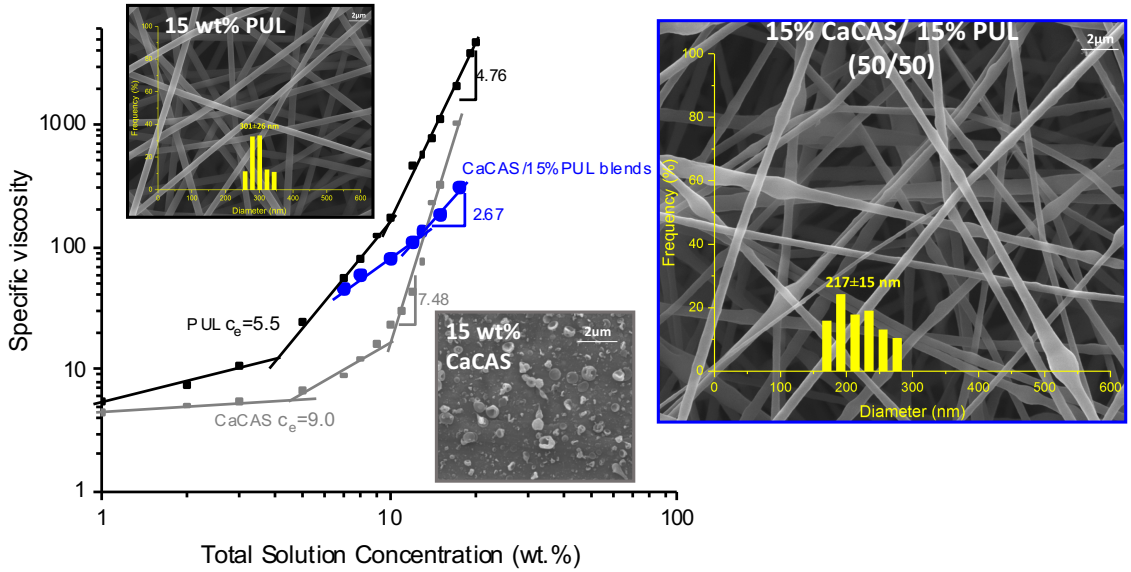

Figure 44: The dependence of specific viscosity on the solution concentration. The black lines with black scatters are neat PUL solutions with the concentration ranging from 1 up to 16 wt%. The grey interpolated lines are neat CaCAS solutions in the concentration range from 1 to 20 wt%. The blue lines with blue scatters are the blends of CaCAS and 15 wt% PUL solutions by keeping the PUL concentration constant and increasing the CaCAS content, so that increasing the total solid concentration. Three SEM images show the electrospun structures; 15 wt% PUL-fibers with 301±26 nm, 15 wt% CaCAS-no fiber and 15 wt% CaCAS: 15 wt% PUL (50:50)-fibers with the diameter of 217±15 nm from left to right.

Table 14 summarizes the power law exponents and non-linear regression equations in the semidilute unentangled, semidilute entangled, concentrated regimes, and c_e for the two polymers and their blend in aqueous solutions. The concentration dependence of specific viscosity obtained for CaCAS: PUL blend (50:50) were n_{sp}~$c^{1.63}$ for the semidilute entangled region and n_{sp}~$c^{2.67}$ for the concentrated regime.

The small exponent suggests that the caseinate molecules seemed to entangle but did not interact strongly in the semidilute unentangled regime. The formation of subunits of CaCAS could also cause to the weak dependence of specific viscosity on concentration.

As calcium increases in the solution with an increase in the addition of CaCAS, numerous calcium bridges occurred leads to form subunit structures in caseinate dispersions (McMahon et al., 2009). Calcium ions made the proteins held in close proximity, leading hydrophobically linked protein molecules with their polar groups on the surface on the casein supramolecular structure (Hokes et al., 1982).

In the semidilute entangled regime for this binary mixture, we observed that the concentration dependence of specific viscosity ranged from 1.63 to 2.67, which is lower than the theoretical scaling law exponent of 4.8 for linear polymers in a good solvents (Daoud and De Gennes, 1979), and some reported values for biopolymers ($\eta_{sp} \sim c^{6.0}$) for chitosan in a mixture solvent of acetic acid- water (Klossner et al., 2008) and ($\eta_{sp} \sim c^{4.0}$) for pure PUL in aqueous solution (Kong and Ziegler 2013). However, this concentration dependence is very close to such of the other random coil biopolymers, including dextran, alginate, lambda-carrageenan, and hyaluronate, ($\eta_{sp} \sim c^{3.3}$) (Morris et al., 1981).

Table 14: The equations were obtained by interpolating scattered data points from Figure 44. Concentration regimes identified as semidilute unentangled, semidilute entangled and concentrated regions obtained from Figure 44 for neat PUL, CaCAS, and their blends. c_e is entanglement concentration and η_0 is zero shear viscosity at the shear rate of 10 s^{-1}.

	PUL	**CaCAS**	**Blends with increasing CaCAS content**
semidilute unentangled	y=0.61x+0.72 R^2=0.96	y=0.16x+0.66 R^2=0.99	NA
semidilute entangled	y=2.85x-0.64 R^2=0.99	y=1.40x-0.18 R^2=0.93	y=1.63x+0.28 R^2=0.99
concentrated regime	y=4.76x-2.50 R^2=0.99	y=7.48x-6.29 R^2=0.96	y=2.67x-0.86 R^2=0.99
c_e	5.5 wt%	9 wt%	7 wt%
η_0 at the shear rate of 10 s^{-1}	0.04	0.02	NA

The dependence of the electrospun fiber diameter on η_0 for CaCAS: PUL blend solutions by keeping PUL content constant, 7.5 wt% in the blends, is shown in Figure 45. Three different fiber morphologies were identified; polymer droplets, beaded nanofibers, and defect-free fibers based on the η_0 of the blend solutions. The solutions with a η_0 less than 0.02 Pa. s produced polymer droplets when electrospun, as the solutions with η_0 ranged between 0.02 and 0.07 Pa. s produced electrospun fibers with beads, as shown in the fiber image embedded in Figure 45. Even though viscosity is low, 0.059 Pa. s, for the blend 1 wt% CaCAS and 15 wt% PUL with a 50:50 weight mixing ratio, this blend produced beaded fibers with diameters of 91±15 nm. This was attributed to the PUL content in the mixture which is 7.5 wt% higher than the c_e (5.5 wt%) of PUL, which refers to the onset concentration of molecular entanglements (Kong and Ziegler, 2013; Tomasula et al., 2015; Liu et al., 2016). The fiber-forming solutions with a η_0 greater than 0.07 Pa. s generated defect-free and smooth fibers and the diameter size was correlated with η_0 by the relationship below

$$\text{Diameter (nm)} = 920\,{\eta_0}^{0.75} \qquad \text{Equation 9}$$

As increasing CaCAS content in blends resulting higher viscosity, a thicker and more uniform nanofiber with a diameter of 233 nm was formed, as shown in Figure 45. However, a further increase made the fiber structure formed with defects, as well as hindering the electrospinning process of the viscous solution because the metallic needle has a small diameter of 1 mm which can be blocked by the viscous solution. As the external

voltage increases, the distortion of the accumulated gel-like solution at the tip of the needle was seen during the processing.

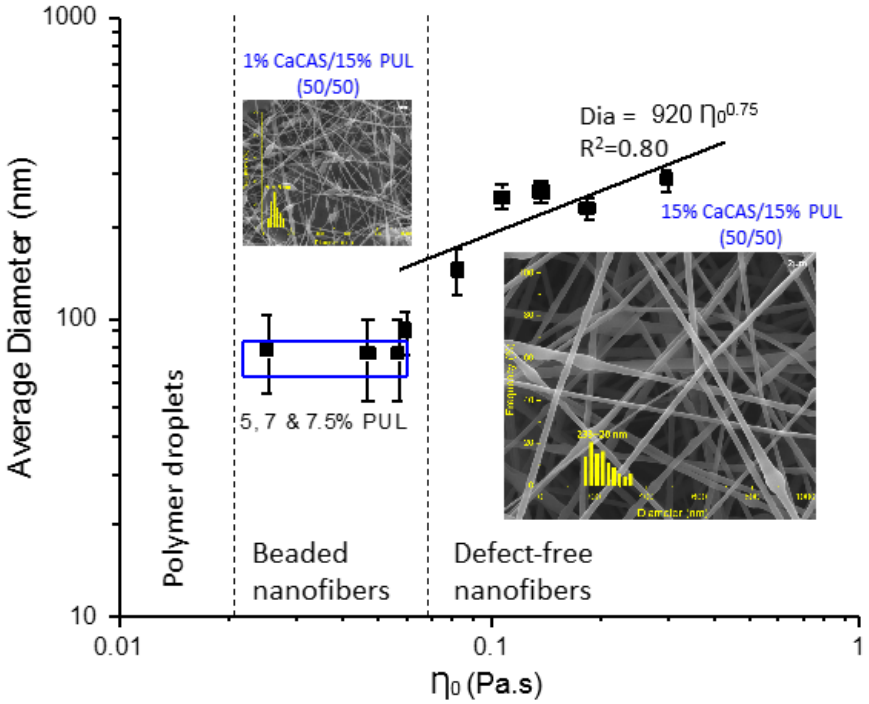

Figure 45: The dependence of the average fiber diameter (nm) on the zero shear viscosity at the shear rate of 10 s^{-1}. Three regions identified are polymer droplets, beaded nanofibers, and defect-free nanofibers. The SEM images show beaded nanofibers with the diameter of 91±15 nm from the blends of 1 wt% CaCAS and 15 wt% PUL and defect-free nanofibers with the diameter of 233±20 nm from the blends of 15 wt% CaCAS and 15 wt% PUL with a 50:50 mixing ratio. Blue circled area shows the beaded nanofibers with incipient fibers with the diameter less than 100 nm from neat PUL solutions at the concentrations of 5, 7 and 7.5 wt%. The linear line represents mean diameter trend from the blend solutions of CaCAS and PUL by increasing CaCAS content in the blends, diameter (nm) = $920\eta_0^{0.75}$ and R^2= 0.80.

Figure 46 shows that the solution of each CaCAS: PUL blend concentration were normalized with its respective c_e (7.0 wt%) to evaluate the dependence of fiber diameter on normalized solution concentration for the binary mixture series. The blend fiber diameter scaled with the normalized concentration as

$$\text{Diameter (nm)} = 88.0\ (\frac{c}{c_e})^{1.5} \qquad \text{Equation 10}$$

where c is the polymer concentration in solution and c_e is the entanglement concentration. As shown in Figure 46, the shaded region shows 2-2.5 times c_e, which is the minimum concentration required for the production of uniform, bead-free electrospun fibers (McKee et al., 2004; Klossner et al., 2008). This equation was estimated based on a single equation fitted to the plot of η_{sp} versus concentration data for the semidilute entangled and the concentration regions, predicting $c \sim \eta_{sp}^{2.0}$ (R^2=0.98). Then, this relationship was substituted into the Equation 9 obtained from the plot of average diameter versus η_0, it was predicted as $\text{diameter (nm)} \sim c^{1.5}$, which is identical to the equation obtained from Figure 46. The CaCAS: PUL blend should be at the concentration 1.3-2.5 times the entanglement concentration for effective electrospinning and the formation of defect-free nanofibers, as shown in Figure 46. This range is wider than the reported prediction (2-2.5 times c_e), as mentioned above. The results are consistent with the SEM micrographs of electrospun CaCAS: PUL nanofibers for the required concentration to obtain smooth and fully-formed fibers successfully, as shown in Figure 48.

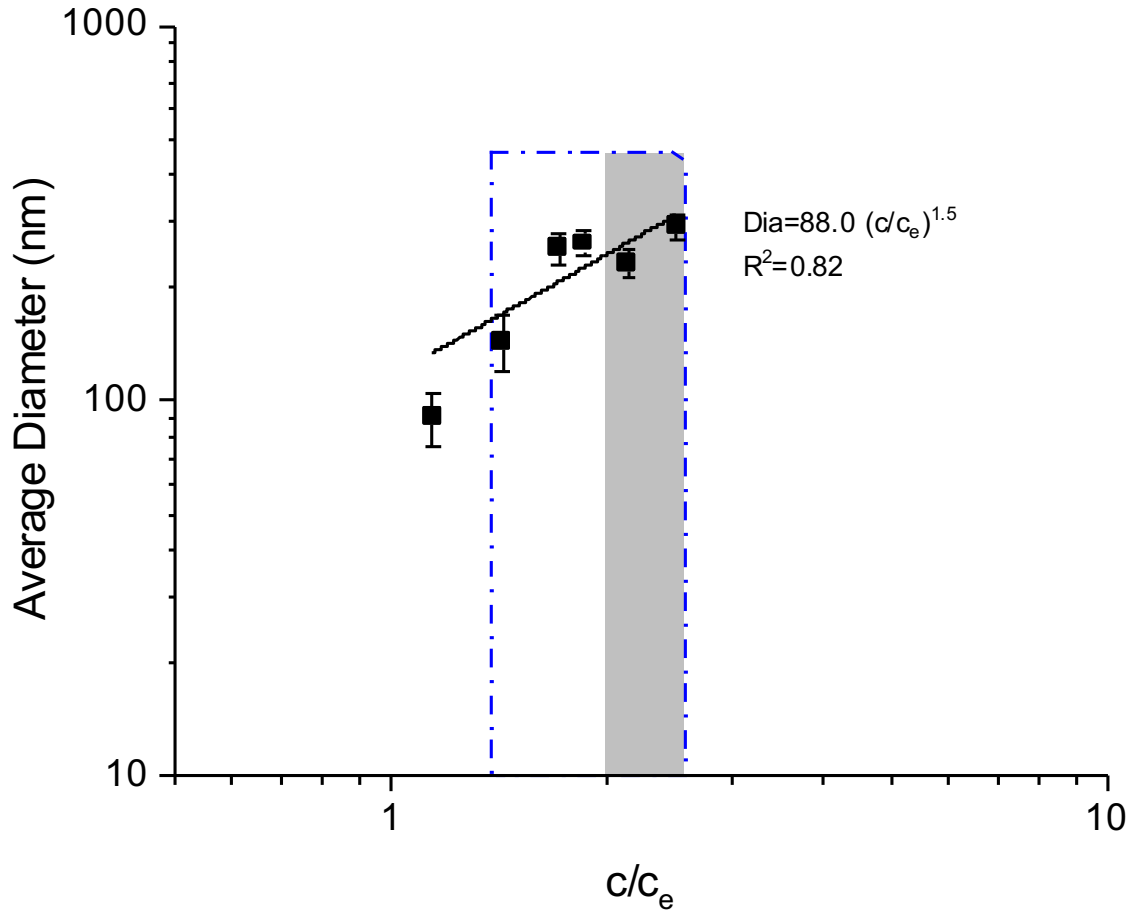

Figure 46: Dependence of fiber diameter on the normalized concentration for CaCAS: PUL blend solutions. The blue dashed region corresponds to the fully-formed fibers obtained from the blended solutions at the concentration of 1.3-2.5 times the c_e and the grey shaded area represents 2.0-2.5 times the c_e for the defect-free fiber formation from natural polymers (McKee et al., 2004).

Figure 47 shows the SEM images of electrospun nanofibers obtained from 15 wt% CaCAS blended with 5, 11, and 15 wt% PUL with weight mixing ratios of 0:100, 30:70, 50: 50, and 70:30. When CaCAS is combined with 5 wt% PUL, fibers obtained at all caseinate to PUL ratios were beaded and defected (Figures 47a, d, g, and j), and defected fibers become increased with increasing CaCAS content. However, when CaCAS is combined with PUL at the concentrations of 11 and 15 wt%., bead-free fibers were obtained at the ratios of 30 % (Figures 47e and f) and 50 % (Figures 47h and r), respectively. When 15 wt% CaCAS is mixed with 5, 11, and 15 wt% PUL with a 30:70

weight mixing ratio, the diameter of electrospun nanofibers increased from 82 to 242 nm with the increasing of PUL content in the blends, as shown in Figures 47d, e, and f. As PUL concentration increased in the solution responds to form a thicker fiber, which is consistent with the reported data (Kong and Ziegler 2014; Tomasula et al., 2016; Liu et al., 2016; Li et al., 2017). CaCAS content was increased from 30 % to 50% in the blends, and uniform, defect-free fibers with the diameters ranged from 116 to 217 nm were obtained. However, a further increase in CaCAS content caused the formation of the fibers with many defects, as shown in Figures 47j, 47k, and 47l. This is because CaCAS dominated the solution characteristics due to its complex structure via calcium bridges led the self-association of hydrophobic groups causing the lack of molecular interactions and protein chain entanglements. As increasing PUL content, PUL dominates the solution characteristics such as excellent electrospinnability, high solubility and ability to entangle, which favor the blended solution to produce smooth, well-formed fibrous mats.

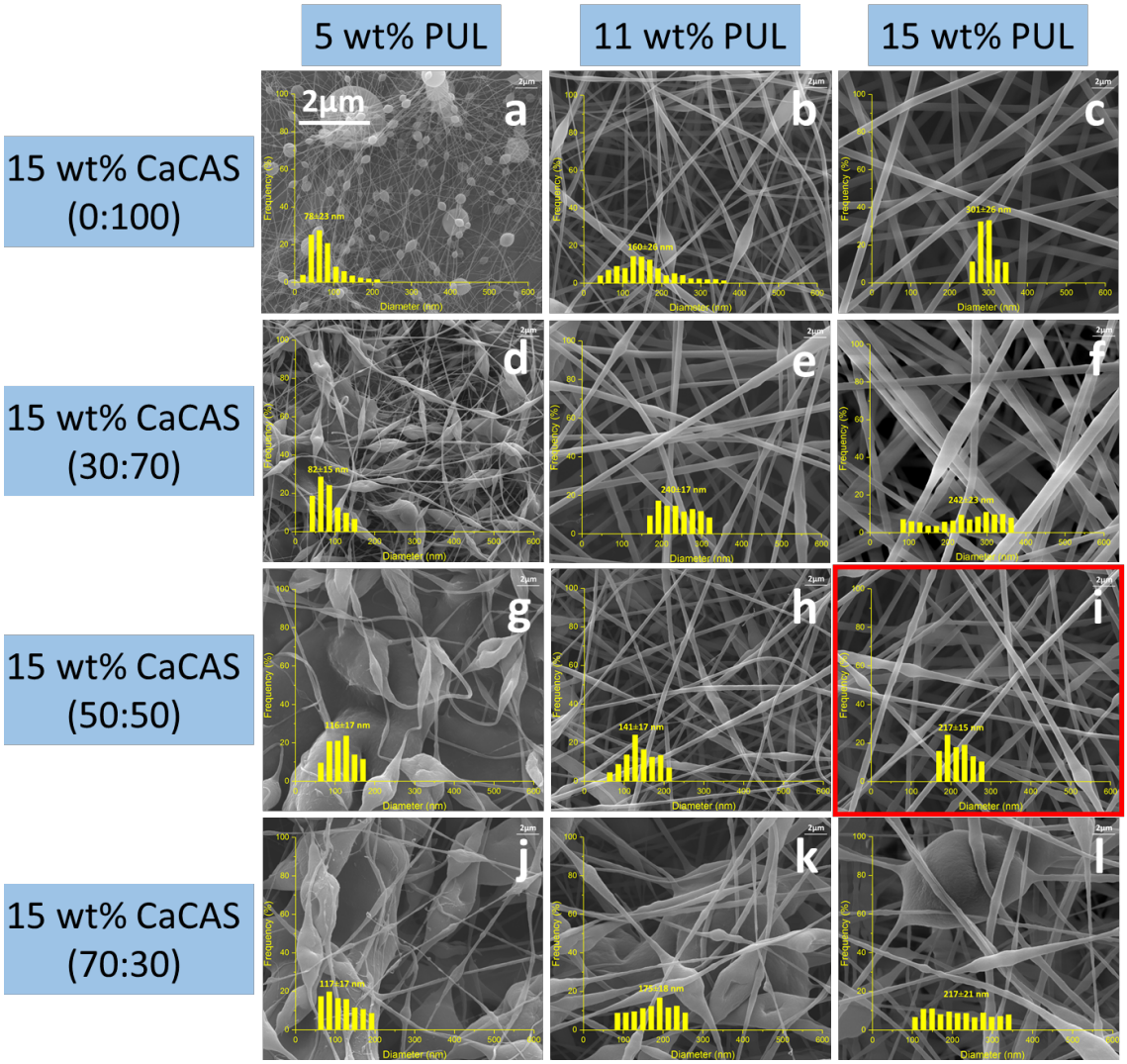

Figure 47: SEM images of electrospun nanofibers from the blends of 15 wt% CaCAS and 5, 11 and 15 wt% PUL solutions at various weight mixing ratios and the distribution of fiber diameter size: (a) 5 wt% PUL, beads with incipient fibers with 78±23 nm, (b) 11 wt% PUL, fibers with 160±26 nm, (c) 15 wt% PUL, fibers with 301±26 nm, (d) 15 wt% CaCAS: 5 wt% PUL (30:70), defected fibers with 82±15 nm (e) 15 wt% CaCAS: 11 wt% PUL (30:70), fibers with 240±17 nm, (f) 15 wt% CaCAS: 15 wt% PUL (30:70), fibers with 242±23 nm, (g) 15 wt% CaCAS: 5 wt% PUL (50:50), defects with incipient fibers with 116±17 nm, (h) 15 wt% CaCAS: 11 wt% PUL (50:50), fibers with 141±17 nm, (i) 15 wt% CaCAS: 15 wt% PUL (50:50), fibers with 217±15 nm, (j) 15 wt% CaCAS: 5 wt% PUL (70:30), defects with incipient fibers with 117±17 nm, (k) 15 wt% CaCAS: 11 wt% PUL (70:30), defected fibers with 175±18 nm, (l) 15 wt% CaCAS: 15 wt% PUL (70:30), defected fibers with 217±21 nm.

Figure 48 shows SEM images of electrospun fibers from 1, 5, 9, 11, 15, and 20 wt% CaCAS blended with 15 wt% PUL solution with a 50:50 mixing ratio. In this series of

experiments, CaCAS: PUL ratio was kept at 50:50 and PUL content was kept at 7.5 wt%. The overall solids concentrations of the blended solutions were changed from 8.0 to 17.5 wt% as increasing in CaCAS content from 0.5 to 10 wt%, as shown in Figure 48. The fibers and the spindle-like structure were observed at a low concentration of CaCAS (1 wt%) (Figure 48a) and the shape of the beaded fibers changes from the spherical to spindle-like as the CaCAS concentration is above 0.5 wt% (Figure 48b). Above the c_e of CaCAS: PUL blends (7 wt%), the fibers with beads were observed at the blend concentration of 8 wt%, as shown in Figure 48. To obtain a smooth nanofiber from CaCAS: PUL blends, the concentration was found to be 1.3 -2.5 times the c_e, as shown in Figure 46. This is in a good agreement with the results for the concentration dependence of viscosity as well, as shown before in Figure 44. At higher solid concentrations of the blended solutions from 9 to 15 wt%, smooth fibers were formed. At further concentration (17.5 wt%), the fibers became thicker and its process was difficult due to the high viscosity of the solution. As seen in Table 13, the solution viscosity increases from 0.05 to 0.30 Pa. s as the concentration of CaCAS: PUL blended solution increases. It is noted that the fiber diameter increases from 91 to 291 nm with increasing neat protein content in the blends from 0.5 to 10 wt%.

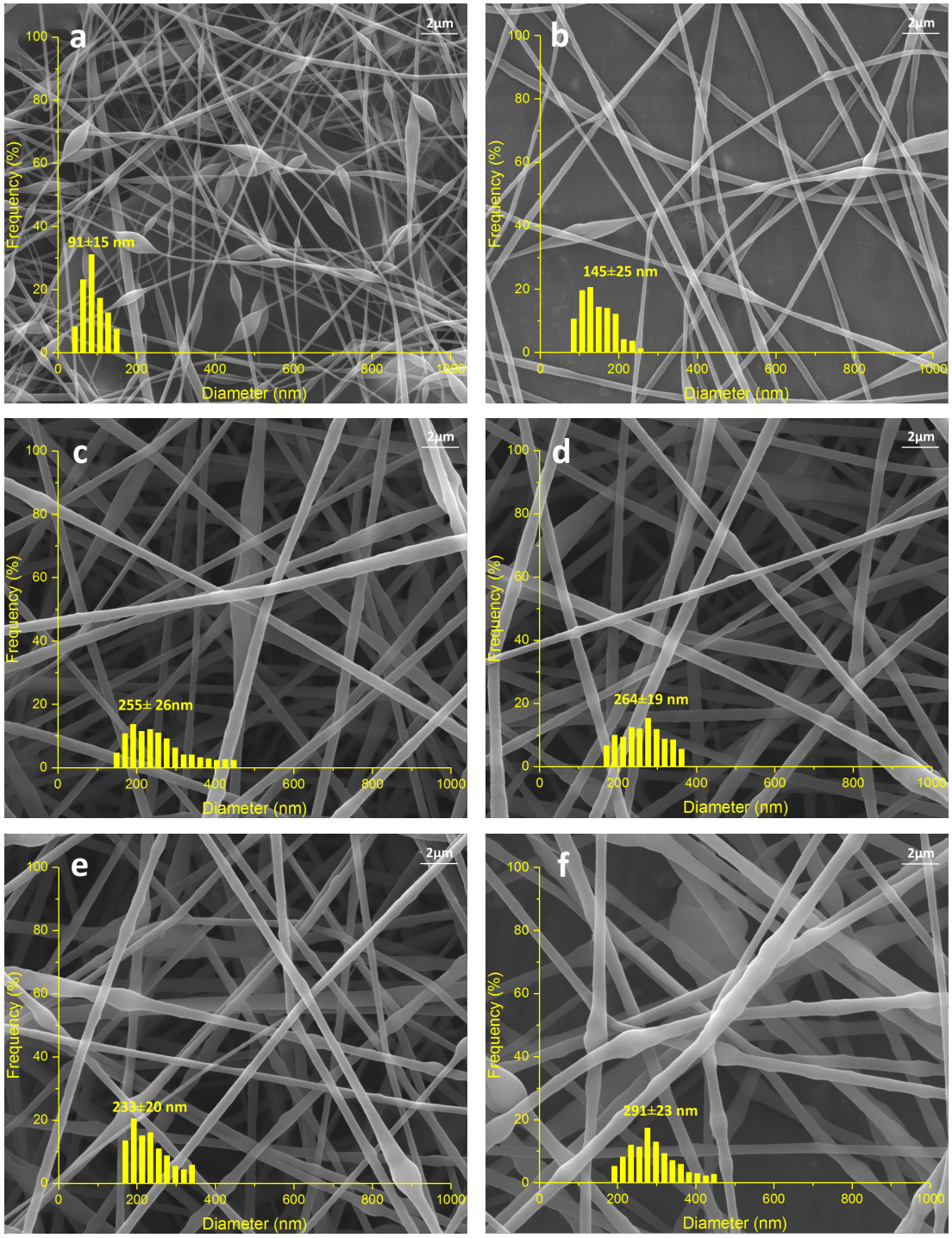

Figure 48: SEM images of electrospun nanofibers from the blends of 1, 5, 9, 11, 15 and 20 wt% CaCAS and 15 wt% PUL solutions with a 50:50 weight mixing ratio and the average of fiber diameter size: (a) 1 wt% CaCAS: 15 wt% PUL, beaded fibers with 91±15 nm, (b) 5 wt% CaCAS: 15 wt% PUL, fibers with 145±25 nm, (c) 9 wt% CaCAS: 15 wt% PUL, fibers with 255±26 nm, (d) 11 wt% CaCAS: 15 wt% PUL, fibers with 264±19 nm, (e) 15 wt% CaCAS: 15 wt% PUL, fibers with 233±20 nm and (f) 20 wt% CaCAS: 15 wt% PUL, defected fibers with 291±23 nm. The magnification is 25,000×.

6.5.2 Electrospinning of NaCAS blended with PUL

Preliminary results indicated that NaCAS protein and PUL polysaccharide blend solutions were properly mixed, translucent, and stable with time. After preparing NaCAS: PUL blend solutions, they were refrigerated at 4 °C overnight to remove bubbles and detect phase separation. The blend solution was visually translucent and there was no phase separation was detected. This might show that NaCAS form a soluble complex with PUL polysaccharide through the interactions between hydroxyl groups from polysaccharides and amino groups from proteins including hydrophobic interactions and/or ionic bonds (McClements, 2006; Gounga et al., 2007).

Figure 49 shows the dependence of shear viscosity on the shear rate of aqueous NaCAS solutions blended with 15 wt% PUL with a weight ratio of 50:50. The concentration of NaCAS ranged from 0.5 to 10 wt% in the blends and protein content in the solutions increased from 0.5 to approximately 10 wt%. The shear rate was employed from 0.01 to 1000 s^{-1} performed on the concentrations of solutions ranging from 8.0 to 17.5 wt% at 20 ºC. They showed Newtonian behavior at the concentrations (the total solids) ranging from 8 to 15 wt% and their zero shear viscosities increased from 0.05 to 0.19 Pa. s which is less than the viscosities of neat NaCAS and PUL solutions over the same range of concentrations. For example, the viscosity of neat NaCAS at the concentration of 15 wt% was 1.994 Pa. s at the shear rate of 100 s^{-1}, as shown in Table 9, whereas it was 0.885 Pa. s over the same range of the shear rate for pure 15 wt% PUL solution, as shown in Table 6. During the production of NaCAS from acid casein, the proteins remain as strands and small agglomerates of proteins in the absence of calcium (Oommen, 2004; McMahon and Oommen, 2013). Therefore, self-assembly of casein in NaCAS solutions would

attribute to produce linear polymeric rods and weakly branched chains, which might cause the formation of jamming proteins at higher concentrations. Compared to the NaCAS: PUL blended solution, neat NaCAS solution showed a higher concentration dependence of the solution viscosity, which caused a quick solidification of the viscous solution at the tip of the needle, blocking the flow of the solution during the electrospinning of neat NaCAS solution.

PUL enabled the NaCAS to entangle to form more uniform electrospun nanofibers than its blends with CaCAS. In the absence of Ca^{2+} ions, NaCAS attributes as strands or short chains which favor the blends solution to have polysaccharide-protein complex with translucent appearance (McMahon and Oommen, 2013) that PUL can form a strong interaction between its hydroxyl groups and the amino groups from the caseinate proteins Kruif and Tuinier, 2001; Aceituno-Medina et al., 2013), which could promote chain entanglements to retain jet stability under the electric field. This could also explain more uniform, bead-free nanofibers from NaCAS: PUL blended compared to CaCAS: PUL blended fibers.

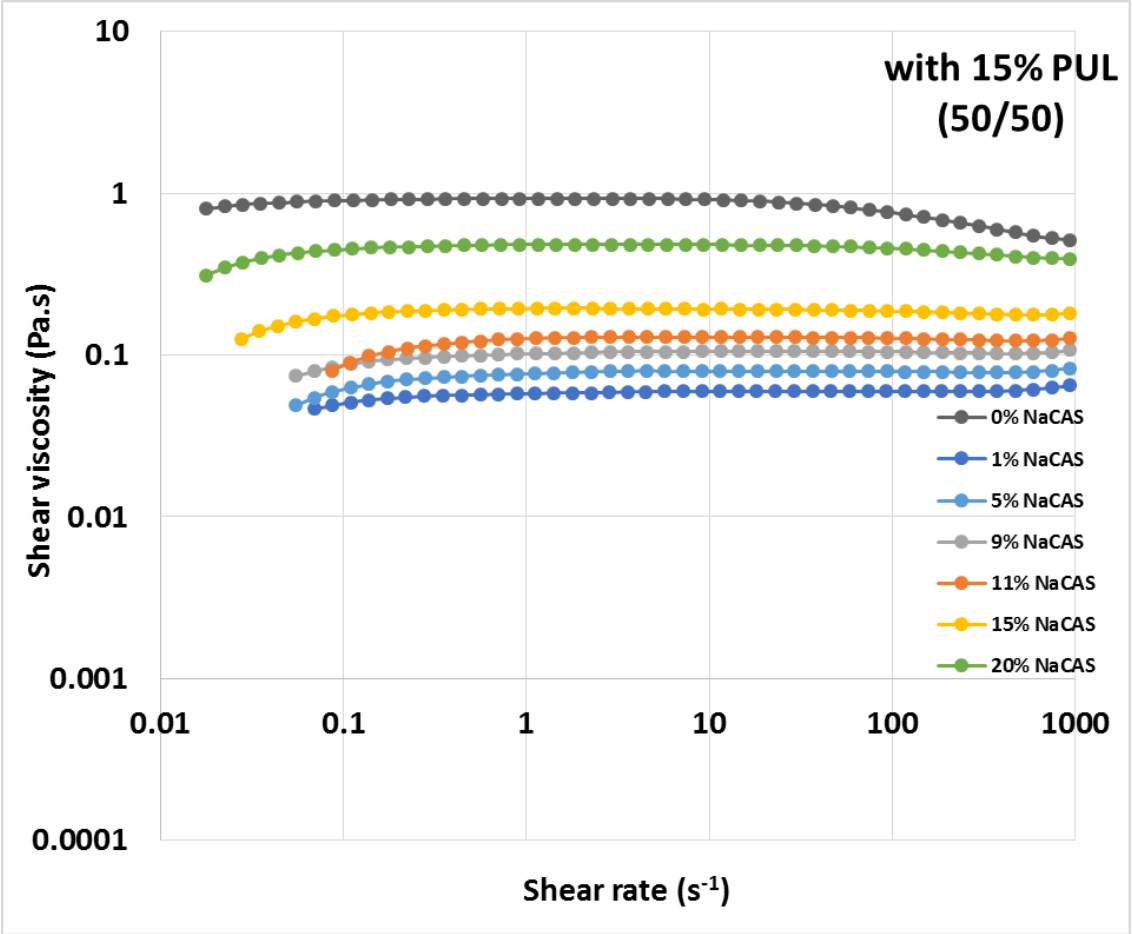

Figure 49: The dependence of shear viscosity on the shear rate of NaCAS solutions at various concentrations blended with 15 wt% PUL with a 50:50 weight mixing ratio. The concentrations of NaCAS solutions range from 1 to 20 wt%. Neat protein content in blend solutions increases 0 to 9.0 % because NaCAS is composed of 90 % protein.

Table 15 summarizes the concentration of NaCAS and PUL solutions and their blends with a 50:50 weight mixing ratio and their zero shear viscosity at the shear rate of 10 s^{-1}, which is used to calculate specific viscosity by using Equation 4. The η_0 increased with increasing NaCAS content ranging from 0.5 to 10 wt% in the mixture solutions from 0.06 to 0.480 Pa. s at the shear rate 10 s^{-1}. The viscosity of NaCAS: PUL at a higher concentration (15 wt%) values were a little bit higher than aqueous CaCAS: PUL system. This could be attributed to the molecular differences between CaCAS existed in colloidal

particles via self-association of hydrophobic groups and NaCAS composed of the short chains and weak branch structure (McMahon and Oommen, 2013; Crowley et al., 2016).

Table 15: Concentration of neat NaCAS and PUL solutions and their blends with a 50:50 weight mixing ratio and their zero shear viscosity at the shear rate of 10 s^{-1}.

Concentration of NaCAS (wt%)	Concentration of PUL (wt%)	Weight mixing ratio	Total solid concentration (wt%)	η_0 at shear rate of 10 s^{-1}
0	15	50:50	7.5	0.046
1	15	50:50	8.0	0.060
5	15	50:50	10.0	0.080
9	15	50:50	12.0	0.106
11	15	50:50	13.0	0.129
15	15	50:50	15.0	0.193
20	15	50:50	17.5	0.480

Figure 50 shows the concentration dependence of η_{sp} of aqueous NaCAS, PUL, and their blends with a 50:50 mixing ratio. The blue lines with blue scatter data represent the NaCAS: PUL blend solutions by keeping PUL concentration constant, 15 wt%, and increasing NaCAS content in the blends, and thus the total solid concentration and viscosity.

In aqueous dispersion of neat NaCAS, PUL, and their blends, the c_e was observed 8, 5.5, and 7.0 wt%, respectively, as shown in Figure 50 and Table 16. Also, three SEM images of the electrospun structures are shown in Figure 50; PUL fibers from 15 wt% solution with a diameter of 301±26 nm, NaCAS powders and/or pieces, and NaCAS: PUL blend fibers with the diameter of 215±22 nm. In the semidilute unentangled regime, the η_{sp} of NaCAS was proportional to $c^{0.19}$, which is lower than the reported values ($\eta_{sp} \sim c^{1.4}$) for random coil polysaccharides including dextran, locust bean gum, guar gum, and

hyaluronate in dilute solutions (Morris et al., 1981) and theoretical predictions (η_{sp}~$c^{1.25}$) for neutral, linear polymers in the semidilute unentangled regime in a good solvent (Daoud and De Gennes, 1979).

The influence of PUL in overall solution behavior was to decrease the c_e of the aqueous NaCAS (8 wt%) to 7.0 wt% for its blend and decrease the concentration dependence of specific viscosity for pure NaCAS solution from 1.86 to 1.56 in the semidilute entangled regime ($c>c_e$) and 8.72 to 3.98 in the concentrated regime ($c>c^{**}$). The η_{sp} of blend in the concentrated regime ($c> c^{**}$) was proportional to 3.98, which is close to theoretically predicted values for random-coil polysaccharides 3.3 (Morris et al., 1981), random coil polymers, 3.4 (Wool, 1993), neutral and linear polymers in good solvents, 3.7 (Daoud and De Gennes, 1979; Colby et al., 1991; McKee et al., 2004).

With increasing NaCAS content in the physical mixture of NaCAS and PUL polymers, the extent of chain entanglement of overlapping coils would be expected to increase with increasing concentration which is in effect raising the average molecular weight by mixing two polymers, and thus the concentration dependence of viscosity.

Table 16 summarizes the power law exponents and non-linear regression equations in the semidilute unentangled, semidilute entangled, and concentrated regimes and c_e for the aqueous NaCAS, PUL, and their mixture solution. The concentration dependence of specific viscosity obtained for NaCAS: PUL blend (50:50) were η_{sp}~$c^{1.56}$ for the semidilute entangled region and n_{sp}~$c^{3.98}$ for the concentrated regime. The result showed that the incorporation of PUL to NaCAS solution affected the n_{sp} compared to the pure NaCAS solutions in the semidilute entangled and concentrated regimes by the change in the dependence from 1.82 to 1.56 and from 8.72 to 3.98, respectively.

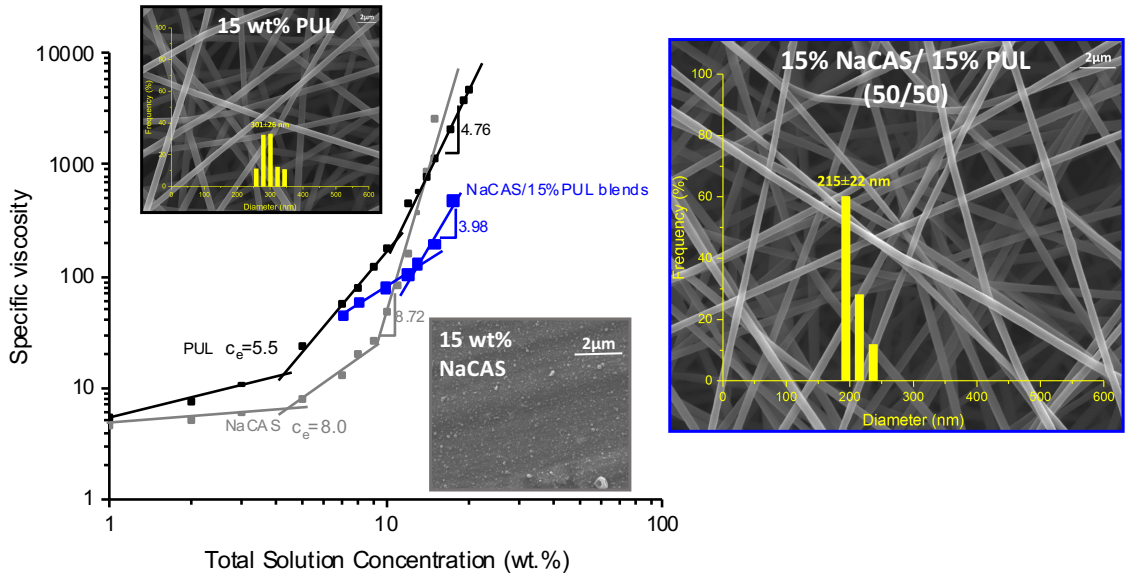

Figure 50: The dependence of specific viscosity on the solution concentration. The black lines with black scatters are neat PUL solutions at the concentration ranging from 1 up to 16 wt%. The grey interpolated lines are neat NaCAS solutions with the concentration from 1 to 20 wt%. The blue lines with blue scatter data are the blend of NaCAS and 15 wt% PUL solutions by keeping the PUL concentration constant and increasing the NaCAS content, so that increasing the total solids concentration. Three SEM images show the electrospun structures; 15 wt% PUL-fibers with 301±26 nm, 15 wt% NaCAS-no fiber and 15 wt% NaCAS: 15 wt% PUL (50:50)-fibers with the diameter of 215±22 nm.

The concentration dependence of viscosity obtained for NaCAS: PUL blend (50:50) were n_{sp}~$c^{1.56}$ for the semidilute entangled region and n_{sp}~$c^{3.98}$ for the concentrated regime, which is close to the theoretically predicted results of $c^{3.4}$ for linear synthetic polymers (Wool, 1993), reported values of $c^{3.3}$ for the other random coil polysaccharides (Morris et al., 1981), and (η_{sp}~$c^{4.0}$) for pure PUL in aqueous solution (Kong and Ziegler, 2013). The exponent, the slope of 1.82 for neat NaCAS, suggests that the caseinate molecules seemed to entangle but did not interact strongly in the semidilute entangled regime. This is due to the dissolution of NaCAS in water that possesses short protein strands and small agglomerates of protein, which restricts the molecular chain entanglement and fiber formation (McMahon et al., 2009; Tomasula et al., 2016).

Table 16: The equations were obtained by interpolating scattered data points from Figure 50. Concentration regimes were identified as the semidilute unentangled, semidilute entangled and concentrated regions obtained from Figure 50 for neat PUL, NaCAS, and their blends. c_e is entanglement concentration and η_0 is zero shear viscosity at the shear rate of 10 s^{-1}.

	PUL	**NaCAS**	**Blends with increasing NaCAS content**
semidilute unentangled	y=0.61x+0.72 R^2=0.96	y=0.19x+0.67 R^2=0.96	NA
semidilute entangled	y=2.85x-0.64 R^2=0.99	y=1.82x-0.38 R^2=0.95	y=1.56x+0.34 R^2=0.99
concentrated regime	y=4.76x-2.50 R^2=0.99	y=8.72x-7.06 R^2=0.96	y=3.98x-2.32 R^2=0.96
c_e	5.5 wt%	8 wt%	7 wt%
η_0	0.04	0.02	NA

Figure 51 shows the dependence of electrospun ultrafine fiber diameter on η_0 for NaCAS: PUL blend solutions. Three different fiber morphologies were identified; polymer droplets, beaded nanofibers, and defect-free fibers based on the η_0 of the blend solutions. The diameter dependence followed a similar trend as CaCAS: PUL blend solutions. The solutions with a η_0 less than 0.02 Pa. s produced polymer droplets when electrospun, as the solutions with η_0 ranged between 0.02 and 0.07 Pa.s produced electrospun fibers with beads, as shown in the fiber image embedded in Figure 51. Even though viscosity is low, 0.06 Pa.s, for the blend 1 wt% NaCAS and 15 wt% PUL with a 50:50 mixing, it produced beaded fibers with diameters of 107±20 nm, as shown in Figure 51. This was attributed to the PUL content in the mixture which is 7.5 wt% higher than the c_e (5.5 wt%) of PUL, which refers to the onset concentration of molecular entanglements (Kong and Ziegler, 2013; Tomasula et al., 2015; Liu et al., 2016). The fiber-forming solutions with a η_0 greater

than 0.07 Pa. s generated uniform, bead-free fibers. Moreover, the mean fiber diameter size was correlated with the η_0 by the relationship below

$$\text{Diameter (nm)} = 571\ {\eta_0}^{0.56} \qquad \text{Equation 11}$$

As increasing NaCAS content in the blends results a higher viscosity, and a thicker, more uniform nanofiber with a diameter of 244 nm was formed, as shown in the image in Figure 51. However, a further increase made the fiber structure formed with defects, as well as hindering the electrospinning process of the viscous solution because the metallic needle has a small diameter of 1 mm which can be blocked by the viscous solution. As the external voltage increases to initiate the electrospinning of the viscous solution, the solidification of the solution at the tip of the needle was observed during the processing. Compared to the blens of CaCAS: PUL, the NaCAS: PUL mixture produced more uniform, defect-free nanofibers. Due to the occurrence of the short protein strands and small agglomerates of the NaCAS protein in the aqueous solution (McMahon and Oommen, 2013), PUL can disperse easily and interact with these protein strands via the formation of hydrophobic interactions and/or ionic bonds (McClements, 2006; Gounga et al., 2007). However, it is probably too difficult for PUL to interfere with the numerous Ca bridges formed between the phosphoserine groups in CaCAS, which restrict the occurrence of the strong chain entanglements in CaCAS: PUL blended solutions (Tomasula et al., 2016), which might result less uniform fiber formation than such of the NaCAS: PUL blends.

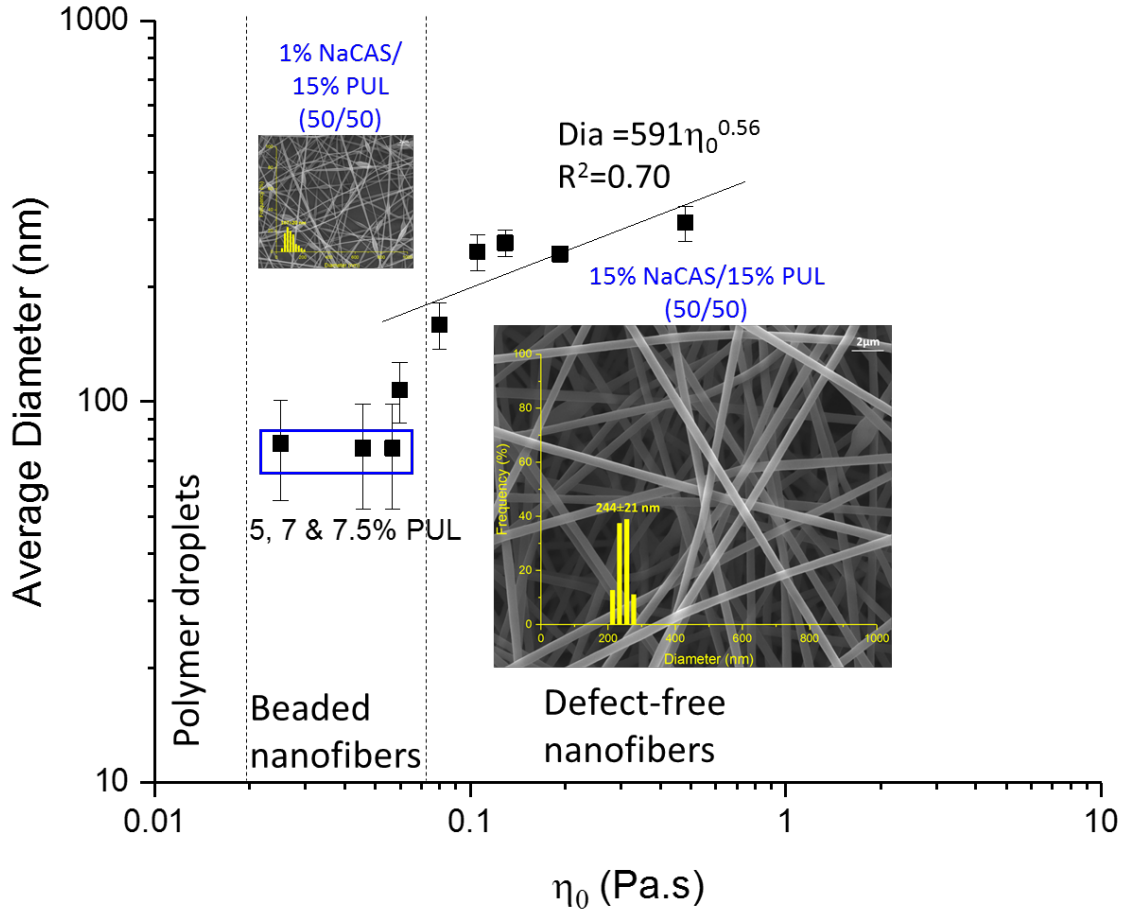

Figure 51: The dependence of the average fiber diameter (nm) on the zero shear viscosity at the shear rate of 10 s^{-1}. Three regions identified are polymer droplets, beaded nanofibers, and defect-free nanofibers. The SEM images show beaded nanofibers with a diameter of 107±20 nm from the blends of 1 wt% NaCAS and 15 wt% PUL and defect-free nanofibers with a diameter of 244±21 nm from the blends of 15 wt% NaCAS and 15 wt% PUL with a 50:50 mixing ratio. Blue rectangle shows the beads with incipient fibers with the diameter less than 100 nm from neat PUL solutions at the concentrations of 5, 7 and 7.5 wt%. Linear black line represents mean diameter trend from NaCAS: PUL blend by increasing NaCAS content in the blends, diameter (nm) = $591\eta_0^{0.56}$ and R^2= 0.70.

Figure 52 shows that the solution of each NaCAS: PUL blend concentration were normalized with its respective c_e (7.0 wt%) to evaluate the dependence of fiber diameter on normalized solution concentration for the binary mixture series. The blend fiber diameter scaled with the normalized concentration as

$$\text{Diameter (nm)} = 102.1\ (\frac{c}{c_e})^{1.3} \qquad \text{Equation 12}$$

As shown in Figure 52, the shaded region shows 2-2.5 times c_e, which is the minimum concentration required for the production of uniform, bead-free electrospun fibers (McKee et al., 2004; Klossner et al., 2008). Equation 12 was estimated when a single equation was fit to the plot of η_{sp} versus concentration of NaCAS: PUL blend solution for the semidilute entangled and the concentration regions, predicting $c \sim \eta_{sp}^{2.3}$ (R^2=0.91). Then, this relationship was substituted into the Equation 11 obtained from the plot of average diameter versus η_0, it was predicted as the $\text{diameter (nm)} \sim c^{1.3}$, which is identical to the equation obtained from Figure 52. The concentration of NaCAS: PUL blended solutions should be 1.4-2.5 times the c_e for the formation of uniform, defect-free electrospun nanofibers, as shown in Figure 52. This range is wider than the reported prediction (2-2.5 times c_e), as mentioned above. Also, the results are consistent with the SEM micrographs of electrospun NaCAS: PUL nanofibers for the required concentration to obtain smooth, full-formed fibers successfully, as shown in Figure 54.

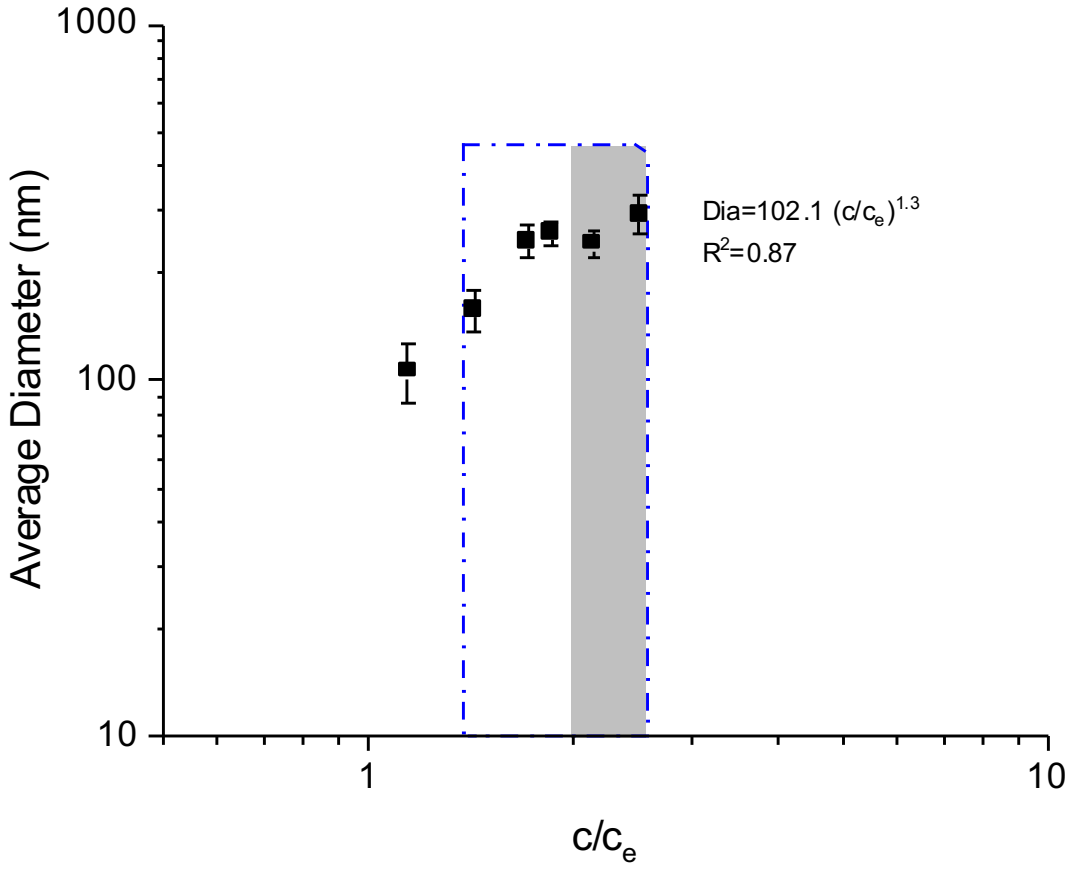

Figure 52: Dependence of fiber diameter on the normalized concentration for NaCAS: PUL blend solutions. The blue dashed region corresponds to the fully-formed blend fibers at the concentration of 1.4-2.5 times the c_e and the grey shaded area represents 2.0-2.5 times the c_e for the defect-free fiber formation from neutral polymers (McKee et al., 2004).

Figure 53 shows the SEM images of electrospun nanofibers obtained from 15 wt% NaCAS blended with 5, 11, and 15 wt% PUL with weight mixing ratios of 0:100, 30:70, 50: 50, and 70:30. As NaCAS is blended with 5 wt% PUL, fibers obtained at all caseinate to PUL ratios were beaded (Figures 53a, d, g, and j), and beaded fibers changed to ribbon-like fibers with increasing NaCAS content ranging from 0 to 10.5 wt% in the blends. However, when 15 wt% NaCAS is mixed with PUL at the concentrations of 11 and 15 wt%, bead-free and smooth fibers at all caseinate to PUL ratios were obtained, as shown in Figures 53e, f, h, I, k, and l. The diameter of the electrospun nanofibers were 229, 308, 168, 215, 175, and 216 nm, respectively. As shown in Figure 53, as 15 wt% NaCAS was

blended with 11 wt% PUL with weight mixing ratios of 30:70, 50:50, and 70:30, the fibers become more uniform and defect-free than neat PUL at the concentration of 11 wt%. As the ratio of protein to PUL concentration increased in the blend solution responds to form a thinner fiber (~216 nm) than neat 15 wt% PUL (301 nm), as shown in Figures 53f, i, and l.

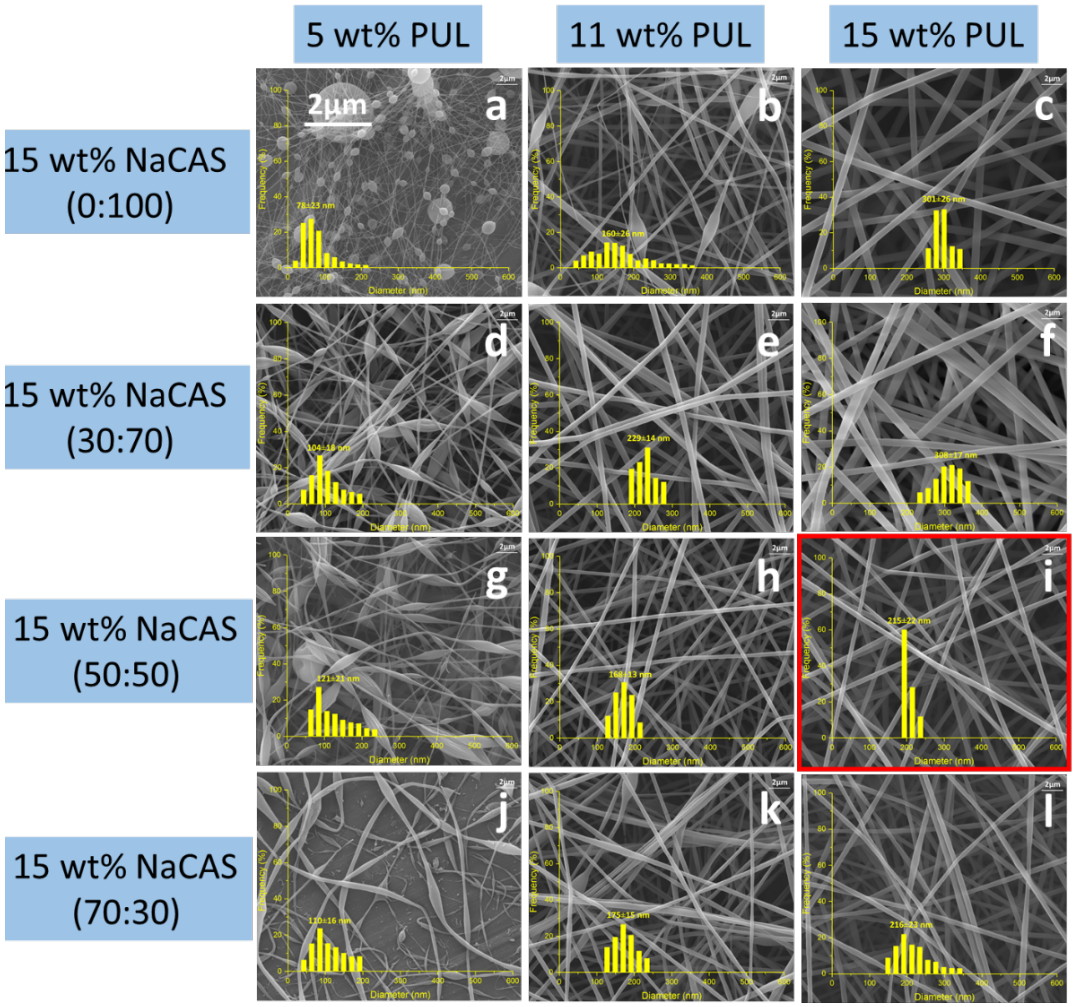

Figure 53: SEM images of electrospun nanofibers from the blends of 15 wt% NaCAS and 5, 11 and 15 wt% PUL solutions at various weight mixing ratio and the average of fiber diameter size: (a) 5 wt% PUL, 78±23 nm, (b) 11 wt% PUL, 160±26 nm, (c) 15 wt% PUL, 301±26 nm, (d) 15 wt% NaCAS: 5 wt% PUL (30:70), 104±18 nm, (e) 15 wt% NaCAS: 11 wt% PUL (30:70), 229±14 nm, (f) 15 wt% NaCAS: 15 wt% PUL (30:70), 308±17 nm, (g) 15 wt% NaCAS: 5 wt% PUL (50:50), 121±21 nm, (h) 15 wt% NaCAS: 11 wt% PUL (50:50), 168±13 nm, (i) 15 wt% NaCAS: 15 wt% PUL (50:50), 215±22 nm, (j) 15 wt% NaCAS: 5 wt% PUL (70:30), 110±16 nm, (k) 15 wt% NaCAS: 11 wt% PUL (70:30), 175±15 nm and (l) 15 wt% NaCAS: 15 wt% PUL (70:30), 216±23 nm.

Figure 54 shows SEM images of electrospun fibers from 1, 5, 9, 11, 15, and 20 wt% NaCAS blended with 15 wt% PUL solution with a 50:50 mixing ratio. In this series of experiments, NaCAS: PUL ratio was kept at 50:50 and PUL content was kept at 7.5 wt% in blend solutions. The overall solid concentrations of these solutions were changed from 8.0 to 17.5 wt% as increasing in NaCAS content from 0.5 to 10 wt%, as shown in Figure 54. Spindle-like beaded nanofibers with a diameter of 107 nm were observed at a low concentration of NaCAS (1 wt%), as shown in Figure 54a. However, above the c_e of NaCAS: PUL blend (7 wt%), bead-free and uniform electrospun nanofibers. To obtain a smooth nanofiber from NaCAS: PUL, the concentration of the solution was found as 1.4 - 2.5 times the c_e, as shown before in Figure 52. At higher solid concentrations of blend solutions from 9 to 15 wt%, smooth fibers were formed. At further concentration (17.5 wt%), the fibers became thicker and its electrospinning was difficult due to the high viscosity of the solution. As seen in Table 15, the blend solution viscosity increases from 0.06 to 0.48 Pa. s as the concentration of NaCAS: PUL blend solution increases. The fiber diameter increases from 107 nm to 295 nm with increasing neat protein content from 0.5 to 10 wt% in the blends, respectively, which is not significantly different than CaCAS: PUL blend fiber diameters ($p>0.05$).

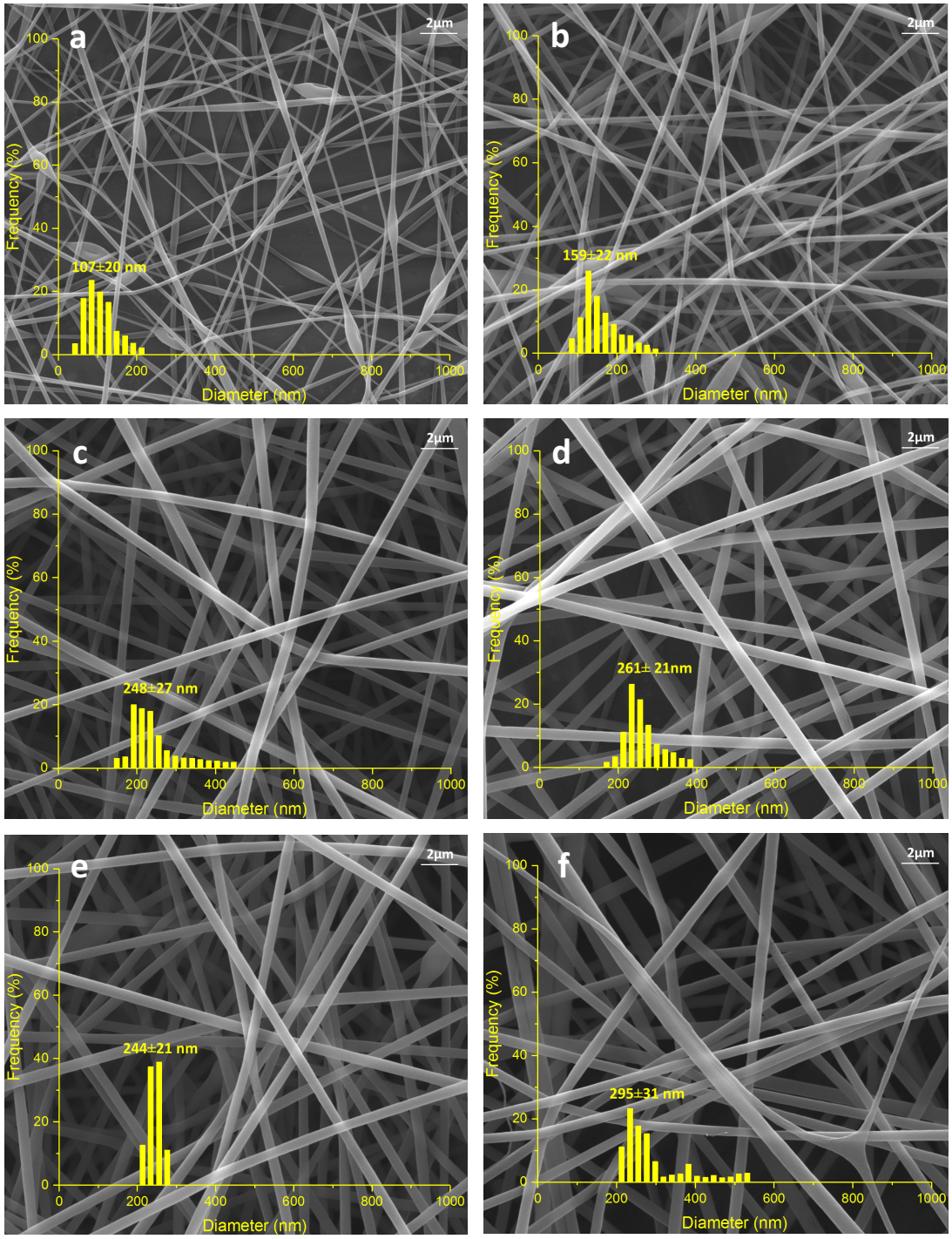

Figure 54: SEM images of electrospun nanofibers from the blends of 1, 5, 9, 11, 15 and 20 wt% NaCAS and 15 wt% PUL solutions with a 50:50 weight mixing ratio and the average of fiber diameter size: (a) 1 wt% NaCAS: 15 wt% PUL, beaded fibers with 107±20 nm, (b) 5 wt% NaCAS: 15 wt% PUL, fibers with 159±22 nm, (c) 9 wt% NaCAS: 15 wt% PUL, fibers with 248±27 nm, (d) 11 wt% NaCAS: 15 wt% PUL, fibers with 261±21 nm, (e) 15 wt% NaCAS: 15 wt% PUL, fibers with 244±21 nm and (f) 20 wt% NaCAS: 15 wt% PUL, fibers with 295±35 nm. The magnification is 25,000×.

Figure 55 shows FT-IR analysis of the PUL powder and fibers, both CAS powders, and both CAS: PUL fibers conducted to confirm that both the PUL and CAS are present in the blend fibrous mats as well as obtaining some information related to the structure of the protein-polysaccharide complexes in the fibers. Spectrum for both CaCAS: and NaCAS: PUL blend fiber mats showed new bands at approximately 1645 cm^{-1} (Amide I) and 1532 cm^{-1}, (Amide II), which are attributed to the protein existence, compared to the PUL powder and fiber spectrums. Peaks 992 and 1015 cm^{-1} in PUL associated with C–OH bending vibrations at the C–6 positions which are attributed to the strength of the interchain interactions via hydrogen bonding. Peak 992 cm^{-1} in PUL powder sample changed to 1016 cm^{-1} for PUL fibers and 1020 cm^{-1} for the blend fibers. It could be due to Ca^{2+} and/or Na^{1+} ions interrupted the hydrogen bonds of PUL molecules, which might affect the C–OH bending vibrations at the C–6 position. This result is consistent with previous findings of FT-IR results for proteins and PUL (Karim et al., 2009; Sakata and Otsuka, 2009; Stijnman et al., 2011; Liu et al., 2016). Two prominent features for protein's FTIR are Amide I band (1638 cm^{-1}) and Amide II (1537 cm^{-1}) were observed in both CAS powder samples, as shown in Figure 55. Amide I band is primarily attributed to C=O stretching vibration and Amide II band from the N–H bending and C–N stretching vibrations of peptide backbone (Haris and Severcan, 1999). Due to the shift in Amide I band in both CAS: PUL fibers to 1644 cm^{-1}, it indicated that the proteins became unordered structure in the presence of PUL, which is similar to reported value for an increase wavenumber in Amide I band to ~1640 cm^{-1} which corresponds the more unordered protein structure (Miller, Bourassa, and Smith, 2013). Amide II band in either CAS powder shifted from 1514 to 1532 cm^{-1} when it blended with PUL. The shift of Amide II band toward higher wavenumbers may indicate

that strong interactions occur between the hydroxyl groups of PUL and the amino groups of proteins (Aceituno-Medina et al., 2013; Wu et al., 2013), which may play a role in the formation of electrospun fiber.

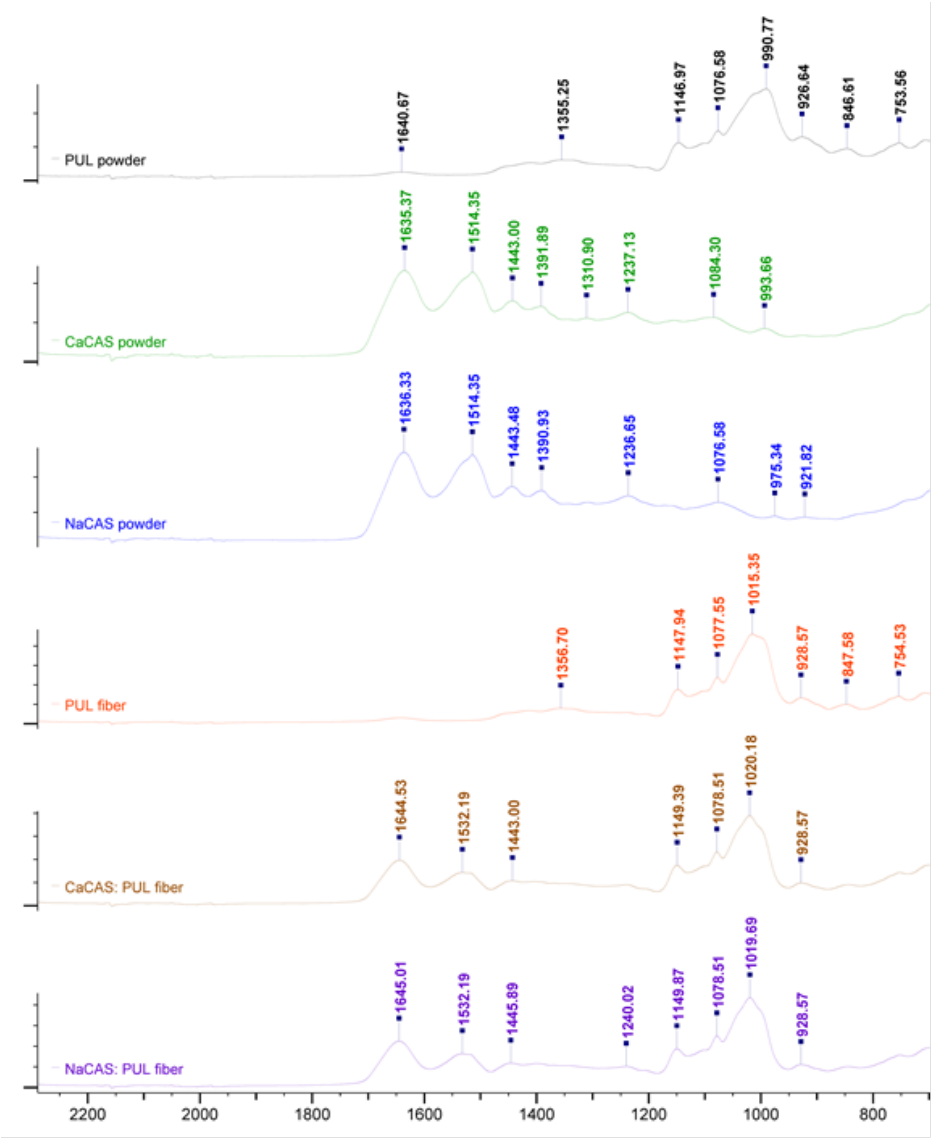

Figure 55: FTIR-ATR spectra of PUL powder and fibers, CAS powder, and CAS: PUL fibers from top to bottom, respectively.

6.6 Encapsulation of Bioactives, probiotic *Lactobacillus Rhamnosus* GG (*L. rhamnosus* GG)

Electrospun ultrafine fiber structures have been extensively used in a wide range of applications due to their unique properties including a higher porosity, the large surface area per unit mass or volume, higher permeability, and small intrafibrous pore size. However, applications of electrospun nanofibrous mats in food and agriculture industry are relatively new due to the inability to electrospin many food-grade polymers without using any organic solvents, which are not allowed to use in foods. These properties provide a new perspective on the delivery of bioactives compounds and development of composite materials for filtration and active food packaging (Drosou et al., 2017). Besides these applications, one of the potential uses for edible electrospun nanofibrous mats is to design functional foods by using it as a delivery vehicle for sensitive bioactive reagents including probiotics, vitamins, minerals, and peptides as well as flavor enhancement or texture improvement within food products.

In this study, edible electrospun nanofibrous mats were successfully produced from aqueous CaCAS blended with PUL solutions. A model application of CaCAS: PUL nanofibers were carried out by incorporating probiotic *L. rhamnosus* GG and the viability of the loaded probiotic was investigated. As shown in Figure 56 the mean diameter of electrospun CaCAS: PUL fibers were 200±31, 209±32, 228±30, 127±30, and 125±25 nm with porosities of 46, 47, 47, 42, and 48 %, respectively. These fibrous mats with an average weight of 0.38 g were obtained from only 2.5 g of aqueous CaCAS: PUL solutions.

L. rhamnosus GG bioactive cells with a length size in the range between 1.1 to 5.1 μm were spotted both within fibers, as double cell strains, and the space among the fibers,

as shown in Figure 56. The mean pore areas of these fibers were also measured as 0.26 μm^2. Inoculation of the CaCAS: PUL blend viscous solution resulted in a cell suspension which contained 10.49 $\log_{10}$ CFU g^{-1} of *L. rhamnosus* GG. The number of viable *L. rhamnosus* GG recovered from the nanofibrous mats after the electrospinning was 9.48 $\log_{10}$ CFU g^{-1}. These findings are similar to the reported data for the encapsulation of *L. rhamnosus* GG within the PEC: PUL electrospun fibrous mats and the recovery was 7.4 $\log_{10}$, which is a little less than the initial loading of 8.26 $\log_{10}$ in the blend of PEC and PUL viscous solutions. Although more extensive studies are required to determine the true potential of using the fibrous mat as a vehicle for the delivery of *L. rhamnosus* GG, these results demonstrate the potential for electrospun fibers and fibrous mats to employ this type of applications.

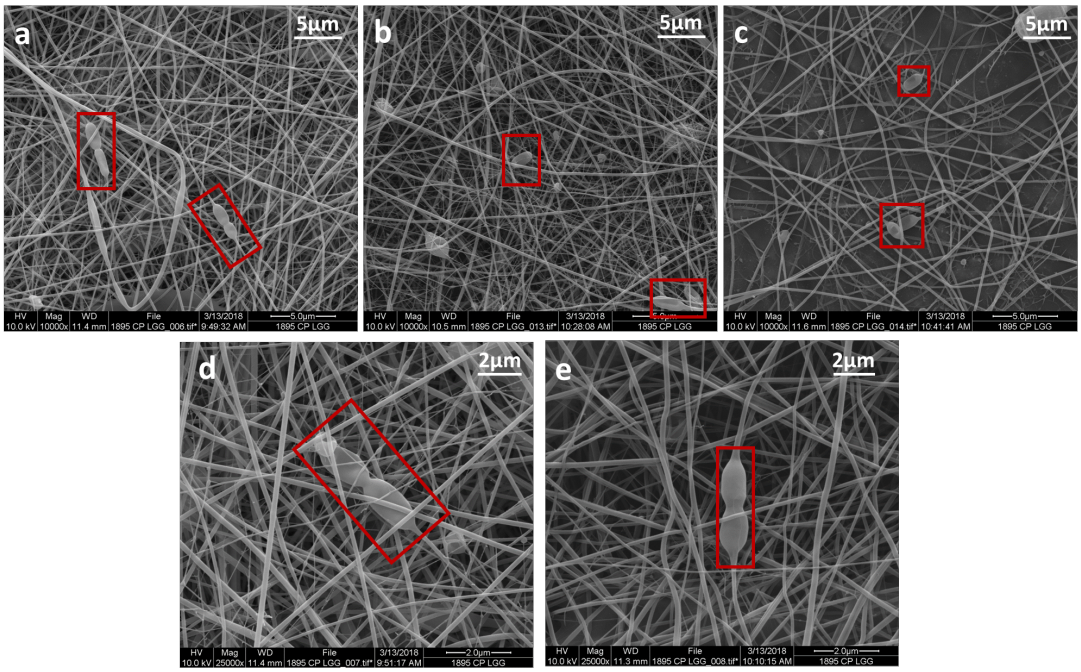

Figure 56: SEM images of electrospun *L. rhamnosus* GG incorporated in CaCAS: PUL fibrous mats. Fiber diameters are 200±31, 209±32, and 228±30 nm with porosities of 46, 47, and 47 % for a, b, and c respectively, magnified 10,000× and 127±30 and 125±25 nm with porosities of 42 and 48 % for d and e, respectively, magnified 25, 000×. These electrospun fibers were obtained from the blend solutions of 15 wt% CaCAS and 15 wt% PUL with a 50:50 weight mixing ratio.

6.7 Summary

This study is a continuous project that Tomasula et al (2016) shortly reported the first example of producing electrospun nanofibers and nanofibrous mats from the aqueous milk proteins blended with PUL. This chapter focused on the addition of PUL and its influence on the shear rate dependence of η, the concentration dependence of η_{sp}, and the c regions, for aqueous NFDM, CaCAS, and NaCAS solutions as well as electrospun fiber morphology obtained from these protein-polysaccharide blends.

- When 15 wt% NFDM, CaCAS, and NaCAS blended with 15 wt% PUL with a 50:50 weight ratio, these blends produced electrospun nanofibers with average diameters with 163±22, 217±15, and 215±22 nm, respectively, as shown in Figure 33.

NFDM: PUL blends

- The viscosity of NFDM: PUL dispersions increased from 0.07 to 0.28 Pa. s with increasing NFDM concentrations from 0.5 to 10.0 wt% in its blend with 15 wt% PUL with a 50:50 weight ratio. The inclusion of PUL promotes enough viscosity and molecular chain entanglements, which were lacking for pure NFDM suspensions due to its micellar and globular protein content. The blended solutions with a η_0 less than 0.02 Pa. s produced polymer droplets when electrospun, as the solutions with the η_0 between 0.02 and 0.1 Pa. s produced electrospun fibers with beads, as shown in Figure 38.
- The transition from the semidilute unentangled to the semidilute entangled regimes occurs at the c_e of 12.1 for aqueous NFDM: PUL blend solutions. The η_{sp} was proportional to $c^{1.18}$ in the semidilute unentangled and to $c^{2.98}$ in the semidilute entangled regions for NFDM: PUL mixtures. The NFDM: PUL blend should be at the concentration 1.6-2.3 times the c_e for effective electrospinning and the formation of

defect-free nanofibers. The fiber-forming solutions with a η_0 greater than 0.1 Pa. s generated defect-free, fully-formed fibers with an average diameter of 212 nm.

CaCAS: and NaCAS: PUL blends

The addition of PUL promotes the protein chain entanglements of CAS to make their electrospinning possible by both interrupting the formation of dense protein molecules in the presence of Ca^{2+} ions in CaCAS and the jamming of small protein strands and agglomerates in NaCAS.

- CaCAS: PUL mixtures showed Newtonian behavior and/or a weak shear thinning behavior. The η_0 of the mixtures increased from 0.06 to 0.30 Pa. s due to the increase in CaCAS concentration from 0.5 to 10.0 wt% in its blends with a constant PUL concentration, 15 wt%. The fiber diameter increases from 91 to 291 nm with increasing neat protein content ranging from 0.5 to 10 wt% in the blends.
- PUL decreased the sharp increase in viscosity of neat CaCAS solutions in the semidilute entangled region. Therefore, the proportion of η_{sp} to $c^{7.48}$ for neat CaCAS dispersions changed to $c^{2.67}$ in the semidilute entangled regions for CaCAS: PUL mixtures. The c_e of the CaCAS: PUL (50:50) blend was determined to be 7.0 wt%. The CaCAS: PUL blend should require a concentration that is 1.3-2.5 times the c_e for an effective electrospinning and the formation of defect-free nanofibers, as shown in Figure 46.
- When 15 wt% CaCAS is mixed with 5, 11, and 15 wt% PUL with a 30:70 weight mixing ratio, the diameter of electrospun nanofibers increased from 82 to 242 nm with the increasing of PUL content in the blends as shown in Figures 47d, e, and f. As CaCAS content was increased from 30 % to 50 % in the blends, uniform, defect-free fibers with an average diameter ranged from 116 to 217 nm were obtained.

- NaCAS: PUL blends also showed Newtonian behavior at the total solid concentrations ranging from 8 to 17.5 wt% and the η_0 increased from 0.05 to 0.48 Pa. s. The fiber diameter increases from 107 nm to 295 nm with increasing neat protein content from 0.5 to 10 wt% in the blends, respectively, which is not significantly different than CaCAS: PUL blend fiber diameters ($p>0.05$).
- The influence of PUL in overall solution behavior was to decrease the c_e of pure NaCAS solutions (8 wt%) to 7.0 wt% for its blends with PUL solution and decrease the concentration dependence of the η_{sp} for pure NaCAS solutions from 1.86 to 1.56 in the semidilute entangled regime ($c>c_e$) and 8.72 to 3.98 in the concentrated regime ($c>c^{**}$). The fiber-forming solutions with a η_0 greater than 0.07 Pa. s generated defect-free fibers. Also, the NaCAS: PUL blend should require a concentration 1.4-2.5 times the c_e for smooth and defect-free electrospun nanofibers, as shown in Figure 52.
- As the ratio of protein to PUL concentration increased in the blend solution responds to form a thinner fiber (~216 nm) than neat 15 wt% PUL (301 nm), as shown in Figures 53f, i, and l. The diameter of the electrospun nanofibers were 229, 308, 168, 215, 175, and 216 nm, respectively. In comparison to the electrospun fibers obtained from neat PUL at the concentration of 11 wt%, the fibers become more uniform and smoother, which obtained from 15 wt% NaCAS was blended with 11 wt% PUL with 30:70, 50:50, and 70:30 mixing ratios.

CHAPTER 7

Effect of pH Adjustment on Electrospinning of Caseinates Blended with Pullulan

This Chapter will cover Objective 3 provided below and show how changes in protein conformation by pH adjustment affect the concentration dependence of viscosity, CAS-based fiber morphology, and their mechanical properties.

The objective of this Chapter is to investigate the effect of protein conformation on fiber morphology obtained from aqueous CAS solutions in the presence of PUL and determine their c_e, and how these two contribute the fiber morphology.

7.1 Overview

In this section, further experiments in this study were carried out with adjusting the pH of only CaCAS and NACAS solutions before mixing with PUL. Even though the addition of PUL made CaCAS and NaCAS produced protein-rich, bead-free, and smooth fibers, such with NFDM produced mostly defected fibers due to its less protein content and different protein containment (i.e., native casein and whey). They possess complex and different protein structures including micelles and globular structures, causing lack of interactions and chain entanglements, which made the electrospinning of NFDM difficult to continue for now.

The pH of both CaCAS and NaCAS solutions at the concentrations ranging from 1 up to 20 wt% was adjusted to 8.0, 9.0, and 10.0 by using 1 M NaOH solutions before mixing it with a constant PUL concentration of 15 wt% with mixing ratios of 50:50, 67:33, and 75:25. The concentration dependence of specific viscosity was plotted above the c_e of both CaCAS and NaCAS blended with 15 wt% PUL with a weight ratio of 50:50. Protein

content was increased in the mixture solutions to observe the effect of protein in an increased pH on fiber morphology, as well.

7.2 Preliminary results

At the beginning of pH study, a couple of pH adjustment solutions which were 1 M $Ca(OH)_2$ for CaCAS and NaOH for NaCAS were used to change protein conformation in caseinates to observe the effects on electrospun fiber morphology obtained from their blends with PUL. Before CAS proteins wee blended with PUL, their pH was adjusted to 8.0, 9.0, and 10.0 by using 1 M $Ca(OH)_2$ for CaCAS and NaOH for NaCAS. Then, their adjusted pH solutions were electrospun under the same conditions throughout this study. However, it was unsuccessful to produce fibers, rod-like electrospun structure with many small other particles were obtained from 11 wt% NaCAS at pH 8 and 9 were observed, as highlighted in Figures 57c and 57d, whereas mostly caseinate pieces were produced from 11 wt% CaCAS at pH 8 and 9, as shown in Figures 57a and 57b. Without pH adjustment in CAS protein solutions, any electrospun structure was observed at the concentration below 15 wt% because the increases in pH made the solutions too viscous to electrospin above 13 wt%.

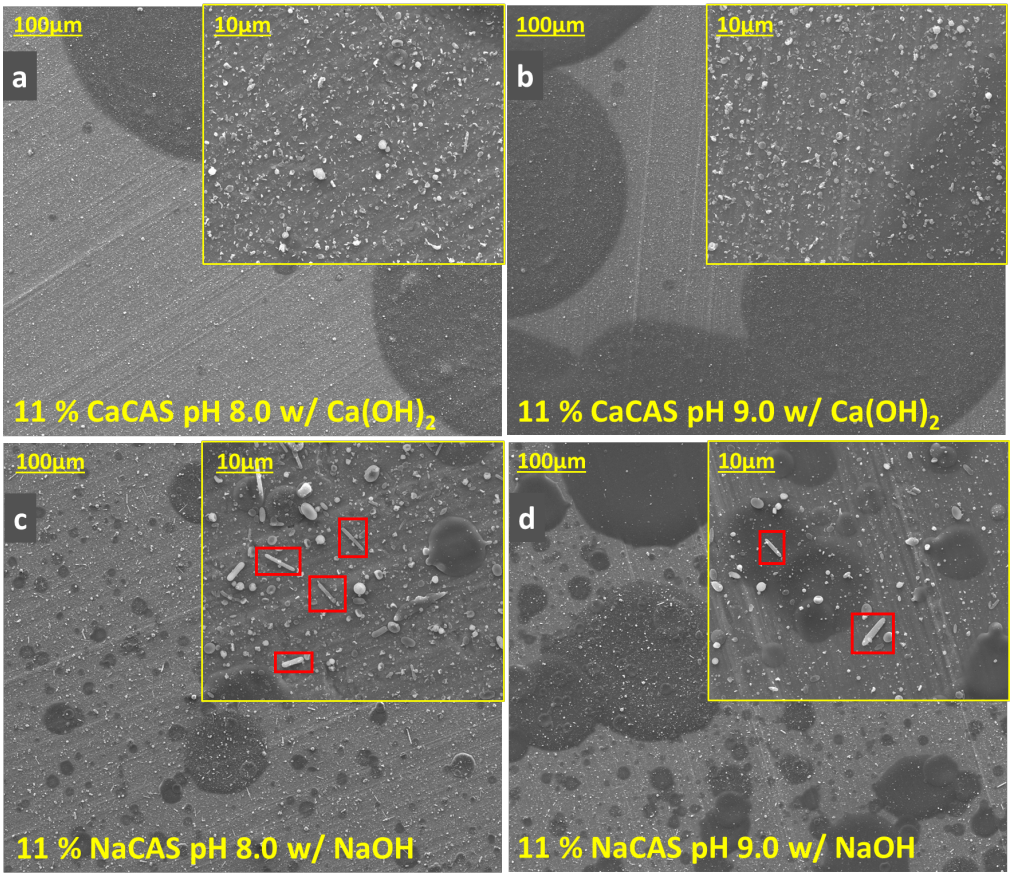

Figure 57: Electrospun pure CAS structure obtained from 11 wt % CaCAS adjusted pH to 8.0 (a) and 9.0 (b) by using 1 M $Ca(OH)_2$; 11 wt% NaCAS at pH 8.0 (c) and pH 9.0 (d) by using 1 M NaOH. Magnified 500× and 5,000×.

To observe the effect of both $Ca(OH)_2$ and NaOH adjustment on electrospun PUL fiber morphology, the pH of 15 wt% PUL was adjusted to 9.0 by using 1 M $Ca(OH)_2$ and NaOH, as shown in Figures 58b and 58c, respectively. The increase in pH of PUL solutions by $Ca(OH)_2$ produced beaded and thinner fibers with diameters of 35±16 nm and 48% porosity under the applied voltage in the range between 15-20 kV and the flow rate of 3 mL/h at 20 °C. The formation of beads within the PUL fibers indicated the occurrence of molecular interactions between Ca^{2+} ions and PUL molecules because Ca^{2+} may interrupt the existing hydrogen bondings of PUL with water molecules. In an increase in pH of PUL solutions by $Ca(OH)_2$, electrospun fibers with many beads were obtained (Unreported

results). When the pH of neat PUL solution was adjusted to 9.0 by the NaOH solution, the PUL fibers with the diameter of 74±16 nm and porosity of 49% were formed. The electrical conductivity of PUL increased when both Ca^{2+} and Na^{1+} were added, which may increase the charge density, and then elongate the PUL jet more, allowing to form thinner fibers compared to the PUL fibers at neutral pH (302 nm). Similar results were observed when a NaCl salt added to the polymer solutions (Zong et al., 2002; Ramakrishna et al., 2005; Liu et al., 2016).

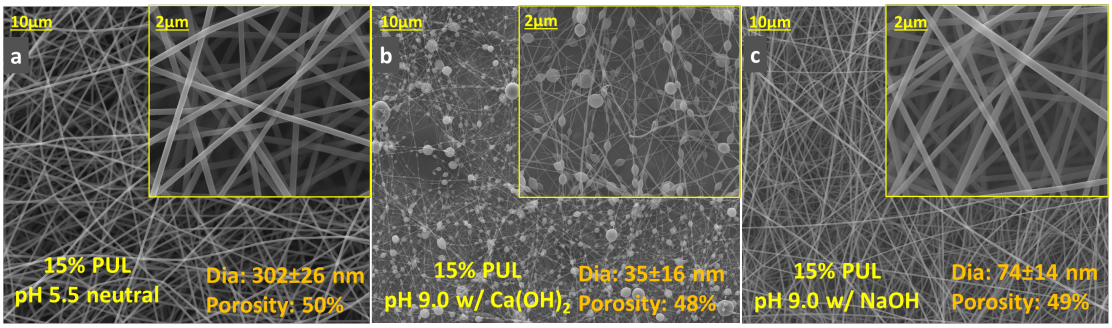

Figure 58: Electrospun pure PUL structure obtained from 15 wt % PUL (a) and its adjusted pH to 8.0 (b) and 9.0 (c) by using 1 M $Ca(OH)_2$ and 1 M NaOH, respectively. Magnified 5,000× and 25,000×.

Addition of either Ca^{2+} or Na^{1+} in CaCAS and NaCAS solutions changed the appearance and solubility of both CAS solutions. With the increase in pH by addition of $Ca(OH)_2$, a decrease in solubility of CaCAS were visually observed, whereas the translucent appearance of NaCAS solutions gradually turned into a turbid appearance with increasing Ca^{2+}, which is attributed to the formation of the micron-sized aggregates (Konstance and Strange, 1991; Swaisgood, 1993). The aggregation mainly occurs due to the calcium bindings of all casein fractions (except κ-casein), which reduces the electrostatic repulsions between protein molecules (Swaisgood, 1993). These results are also confirmed by other researchers reported the formation of close-packed protein

domains increased turbidity and influenced the solution rheology (Pitskowski et al., 2008; Pitskowski, et al., 2009; Thomar et al., 2012; McMahon and Oommen, 2013). Also, the inclusion of Ca^{2+} forms micron-sized dense protein domains, leading to agglomerate and precipitate in NaCAS dilute suspensions (Cuomo et al., 2011; McMahon and Oommen, 2013).

Based on these preliminary results, only 1 M NaOH solution was used to increase pH of both CaCAS and NaCAS up to 10, and then mix with 15 wt% PUL with weight ratios of 50:50, 67:33, and 75:25. Using $Ca(OH)_2$ causes Ca^{2+} ions in the caseinate solutions, which results in more calcium bridging via hydrophobically linked phosphoserine groups, causing the accumulation of dense protein chains (Tomasula et al., 2016). This influences the fiber morphology of CAS: PUL blends by the formation of beads. Besides the influence of Ca^{2+} on the protein conformation, it also caused beaded structure on the neat PUL electrospun fibers, as shown in Figure 58c.

7.3 Effect of pH Adjustment on Solution Rheology and Morphology of Caseinate-based Electrospun Fibers

Figures 59 and 60 show the concentration dependence of specific viscosity for neat CaCAS and NaCAS at neutral pH (~7.0), respectively, and their mixtures with 15 %wt PUL with a 50:50 weight ratio at pH 7.0, 8.0, 9.0, and 10.0, which were adjusted by 1 M NaOH. Neat CaCAS and NaCAS solutions with the concentration ranged from 8 up to 20 wt% and their pH was adjusted before mixing with PUL. The plots in Figures 59 and 60 only represent the semidilute entangled region ($c > c_e$) for both CAS and their blends with PUL because the formation of fibers requires the solution concentration above the c_e, which was extensively discussed in Chapters 4 and 5. In this regime, the η_{sp} of pure CaCAS at

pH 7.0 and its blends with PUL at pH 7.0, 8.0, 9.0, and 10.0 were proportional to $c^{7.48}$, $c^{2.16}$, $c^{2.24}$, $c^{2.32}$, and $c^{2.34}$, respectively, whereas such η_{sp} of neat NaCAS and its blends with PUL were proportional to $c^{8.38}$, $c^{2.50}$, $c^{2.01}$, $c^{2.01}$, and $c^{2.23}$, respectively.

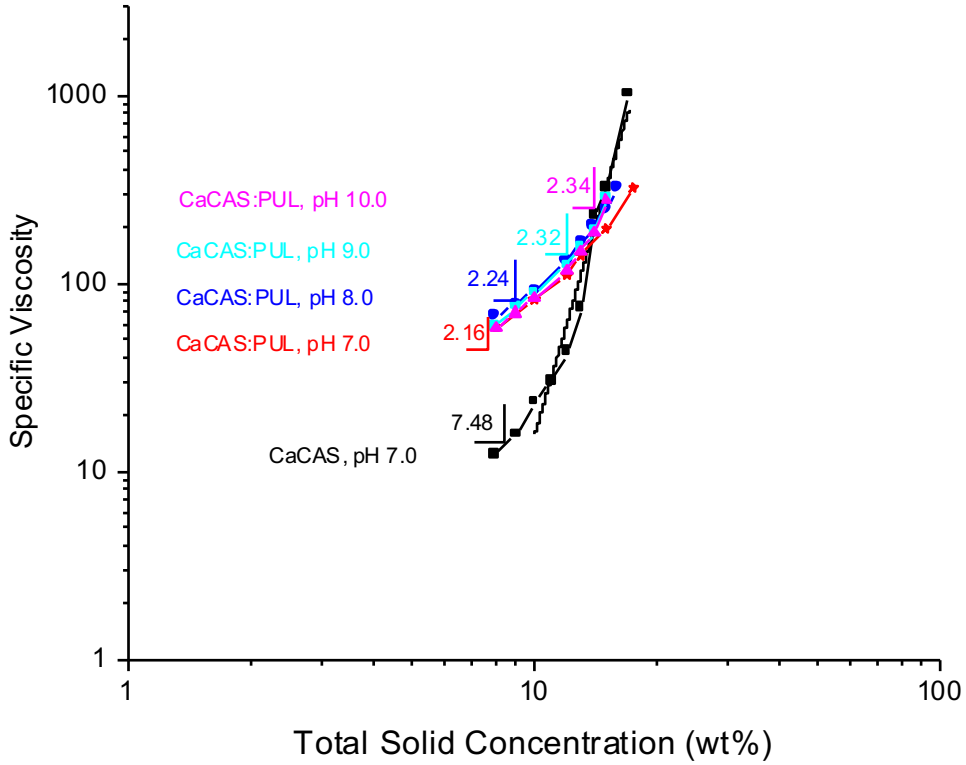

Figure 59: The dependence of specific viscosity on the solution concentration of neat CaCAS and its mixture with 15 %wt PUL with a 50:50 weight ratio. The black line with black scatters represents neat CaCAS solutions with the concentration ranging from 8 to 20 wt% at neutral pH. The red, blue, cyan, and magenta lines along with the same color scatters are the blends of CaCAS (8-20 wt%) and 15 wt% PUL solutions by keeping PUL concentration constant (7.5 wt%) and increasing CaCAS content (0.5-10 wt%) at neutral pH 7.0 (6.7) in the blends and pH 8.0, 9.0, and 10.0, respectively.

The concentration dependence continuously increased for CaCAS: PUL blends with increasing pH (in Figure 59), but it first decreased from 2.50 to 2.01 for NaCAS after its blend with PUL, and then increased to 2.23, as shown in Figure 62. These resultant exponents became closer to the theoretically predicted value of $c^{3.4}$ for neutral and linear polymers (Wool, 1993) and experimentally reported result of $c^{3.3}$ for linear and random coil polysaccharides (Morris et al., 1981). This could be due to the interruption of Na^{1+}

within calcium bridging, allowing the CaCAS proteins have more open coil structures instead of the accumulation of dense protein chains (Swaisgood, 1993; McMahon and Oommen, 2013; Tomasula et al., 2016). Therefore, the affinity of caseinate protein fractions and their interactions with hydroxyl groups of PUL probably increase (Thomar et al., 2012; McMahon and Oommen, 2013).

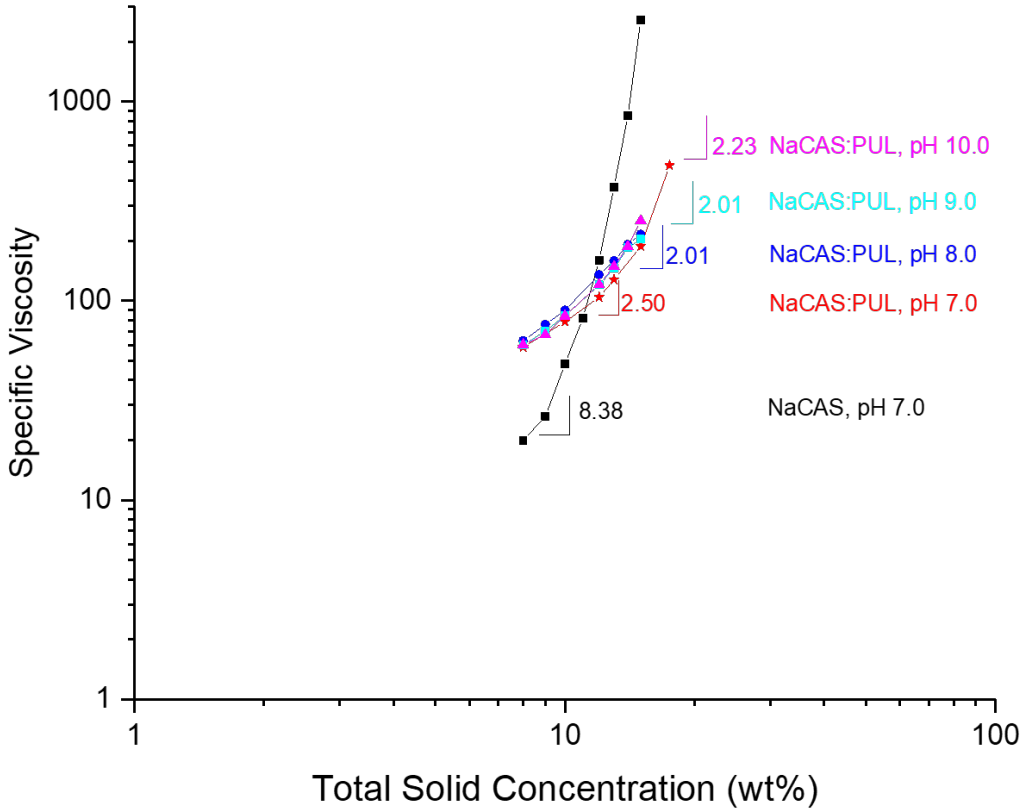

Figure 60: The dependence of specific viscosity on the solution concentration of neat NaCAS and in blends with PUL with a weight ratio of 50:50. The black line with black scatters represents neat NaCAS solutions with the concentration ranging from 8 to 20 wt% at neutral pH. The red, blue, cyan, and magenta lines with the same color scatters are the blends of NaCAS (8-20 wt%) and 15 wt% PUL solutions by keeping the PUL concentration constant (7.5 wt%) and increasing NaCAS content (0.5-10 wt%) in the blends at neutral pH and pH 8.0, 9.0, and 10.0, respectively.

Figures 61 and 62 show the shear rate dependence of shear viscosity for aqueous CaCAS and NaCAS solutions blended with 15 wt% PUL with a 50:50 mixing ratio at neutral pH 6.7, 8.0, 9.0, and 10.0 and their corresponding electrospun fiber morphology.

Both CAS blended with PUL showed an opposite relationship of shear viscosity with increasing pH in the presence of Na^{1+}. However, the opposite relationship in CaCAS and PUL blends is stronger than such in NaCAS: PUL blends, which is in agreement with the earlier data that the presence of Ca^{2+} ions (0.05-1.5 wt%) in either CAS decreased the viscosity at a temperature in the range between 30 to 50 °C (Hayes et al., 1968). Increasing pH or adding Na^{1+} ions showed a little effect on the viscosity of CaCAS: PUL (50:50) blends and all the solutions (except the one at pH 9.0) showed a weak shear thinning behavior at the shear rate less than 100 s^{-1}, as shown in Figure 61.

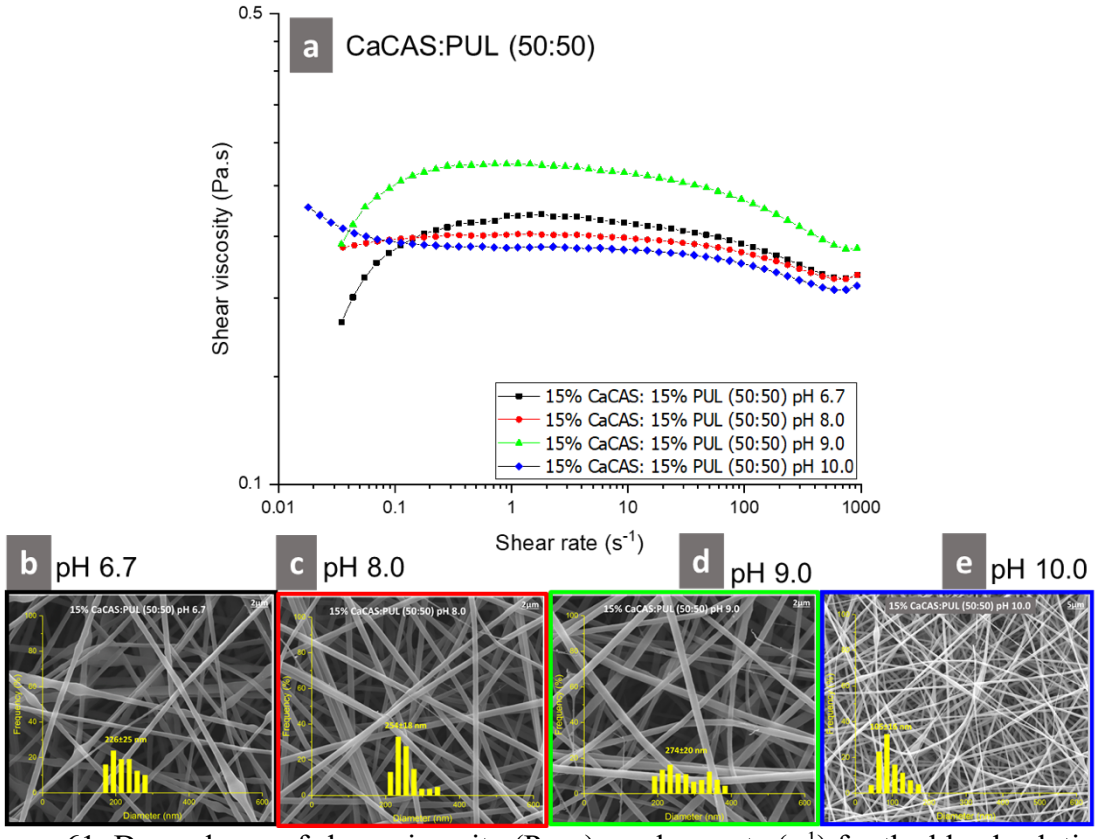

Figure 61: Dependence of shear viscosity (Pa. s) on shear rate (s^{-1}) for the blend solutions obtained from 15 wt% CaCAS and 15 wt% PUL with a 50:50 weight mixing ratio at neutral pH 6.7, 8.0, 9.0, and 10.0 (a) and electrospun CaCAS: PUL fibers with diameters of 226±25 nm (b), 254±18 nm (c), 274±20 nm (d), and 105±16 nm (e), respectively. The pH of the aqueous CaCAS solution was adjusted before mixing with PUL solution.

The viscosities of the CaCAS: PUL mixtures were about 0.2 Pa. s at pH neutral, 8.0, and 10.0 and 0.3 Pa. s at pH 9.0. However, the viscosities of NaCAS: PUL blend solutions at pH 8.0, 9.0, and 10.0 were similar, ~0.28 Pa. s, and more than the viscosity at neutral pH, 0.18 Pa. s. They also showed a weak shear thinning behavior at the shear rate below 100 s^{-1}, as shown in Figure 62.

Electrospun CaCAS: PUL fibers became thicker with increasing pH up to 9.0 and then showed a thinner structure at pH 10.0. At pH 8.0, electrospun CaCAS: PUL fibers became smoother and more uniform with an average diameter of 254±18 nm while they showed a thinner fiber structure with a diameter of 105±16 nm at pH 10.0, as shown in Figure 61. At pH 9.0, the diameter size of fibers was distributed in a wide range from 200 to 400 nm than others, which could result from a transition phase for the interruption of dense caseinate domains by Na^{1+} decreasing the size of protein domains (Pitskowski et al., 2008; Pitskowski, et al., 2009; Thomar et al., 2012; McMahon and Oommen, 2013).

The electrospun nanofibers obtained from NaCAS: PUL (50:50) at various pH only affected the fiber diameter size by increasing at pH 8.0 and 9.0, but decreased at pH 10.0, as shown in Figure 62. NaCAS: PUL (50:50) dispersions at pH 6.7, 8.0, 9.0, and 10.0 produced defect-free and uniform fibers with diameters of 215±18, 265±17, 234±16, and 188±14 nm, respectively.

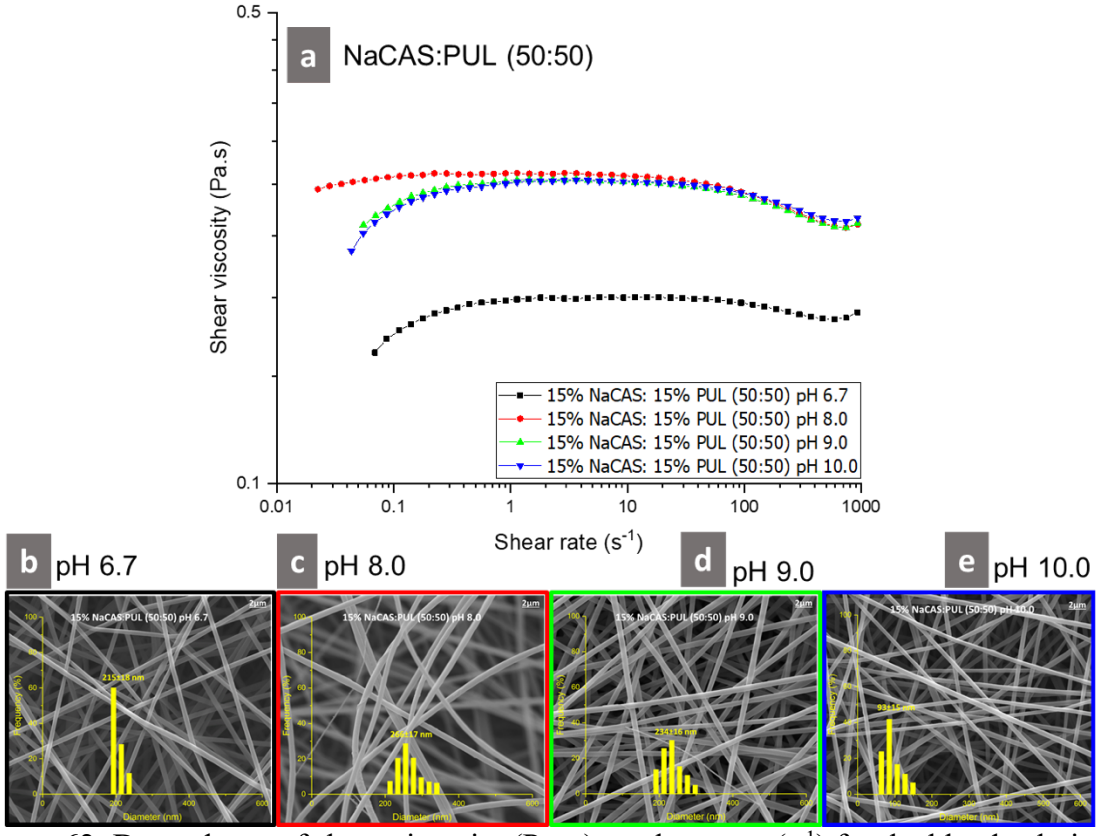

Figure 62: Dependence of shear viscosity (Pa. s) on shear rate (s^{-1}) for the blend solutions obtained from 15 wt% NaCAS and 15 wt% PUL with a 50:50 weight mixing ratio at neutral pH 6.7, 8.0, 9.0, and 10.0 (a) and electrospun NaCAS: PUL fibers with diameters of 215±18 nm (b), 265±17 nm (c), 234±16 nm (d), and 188±14 nm (e), respectively. The pH of the aqueous NaCAS solution was adjusted before mixing with PUL solution.

To observe the effect of pH along with increasing protein content in the blend solutions, Figures 63 and 64 show the shear rate dependence of shear viscosity for aqueous CaCAS and NaCAS solutions blended with 15 wt% PUL with a 67:33 mixing ratio at neutral pH 6.7, 8.0, 9.0, and 10.0. CaCAS blended with PUL showed an opposite relationship of shear viscosity at pH 9.0 (~0.5 Pa. s) and 10.0 (~0.4 Pa. s) with increasing pH in the presence of Na^{1+}, respectively, while NaCAS: PUL blends at pH 9.0 (0.3 Pa. s) and 10.0 (0.4 Pa. s), respectively. The CaCAS: and NaCAS: PUL blends at pH 9.0 and 10.0 showed a shear thinning behavior at the shear rate above of 100 s^{-1}, as shown in Figures 63 and 64. Since the shear applied on the polymer solution during electrospinning is much

higher than 1000 s^{-1}, the high shear will thin the jet more by elongating and stretching the polymer solutions (Greiner and Wendorff, 2007; Tomasula et al., 2016). The viscosities of the CaCAS: PUL (67:33) mixtures were about 0.15, 0.27, 0.47, and 0.51 Pa. s at neutral pH, 8.0, 9.0, and 10.0, respectively, while the NaCAS: PUL blended solutions showed 0.25, 0.33, 0.33, and 0.36 Pa. s, respectively. This viscosity values above the minimum viscosity for an effective electrospinning reported as 0.1 Pa. s (Morris et al., 1989; Stijnman et al., 2013).

CaCAS: PUL (67:33) dispersions at pH 8.0 produced less defected electrospun fibers with 172±20 nm while uniform, defect free fibers with a diameter of 276±21 nm were obtained the solutions at pH 9.0. The blend solutions at pH 10.0 produced a thinner and smooth nanofiber with a diameter of 95±17 nm, as shown in Figure 63d. The increase in CaCAS content in the blend solutions caused the formation of fibers with defected and less uniform, as shown in Figure 63b. This is because more Ca^{2+} ions promote the formation of dense protein agglomerates via hydrophobically linked phosphoserine groups (Pitskowski et al., 2008; Pitskowski, et al., 2009; Thomar et al., 2012; McMahon and Oommen, 2013), which probably prevent the protein molecules from the diffusion of PUL molecules in the mixtures. Therefore, the dense proteins still exist even in the presence of PUL carrier. However, adding Na^{1+} ions interrupts these formations and provide open coil structures, which may favor the CaCAS dispersions to have random coil structures and PUL can reach and spread within the protein molecules evenly.

Increasing pH had less effect on fiber diameter size obtained from NaCAS: PUL than CaCAS: PUL (67:33) fibers, as shown in Figure 64. NaCAS: PUL (67:33) dispersions at pH 6.7, 8.0, 9.0, and 10.0 produced defect-free and uniform fibers with diameters of

161±2, 164±16, 215±18, and 175±15 nm, respectively. In the absence of PUL, 15 wt% NaCAS solutions at pH 10.0 adjusted by 1 M NaOH was too high and blocked the metallic needle used in the electrospinning unit, making the process impossible (Fong et al., 1999; Paul, 2005; Greiner and Wendorff, 2007; Nieuwland et al., 2013; Liu et al., 2016; Tomasula et al., 2016). Increasing Na^{1+} ions by both the inclusion of NaOH and increasing NaCAS content in the blends with PUL dispersions may prevent small protein strands and agglomerates of CAS from jamming, which cause a sharp increase in viscosity (Thomar et al., 2012; Tomasula et al., 2016).

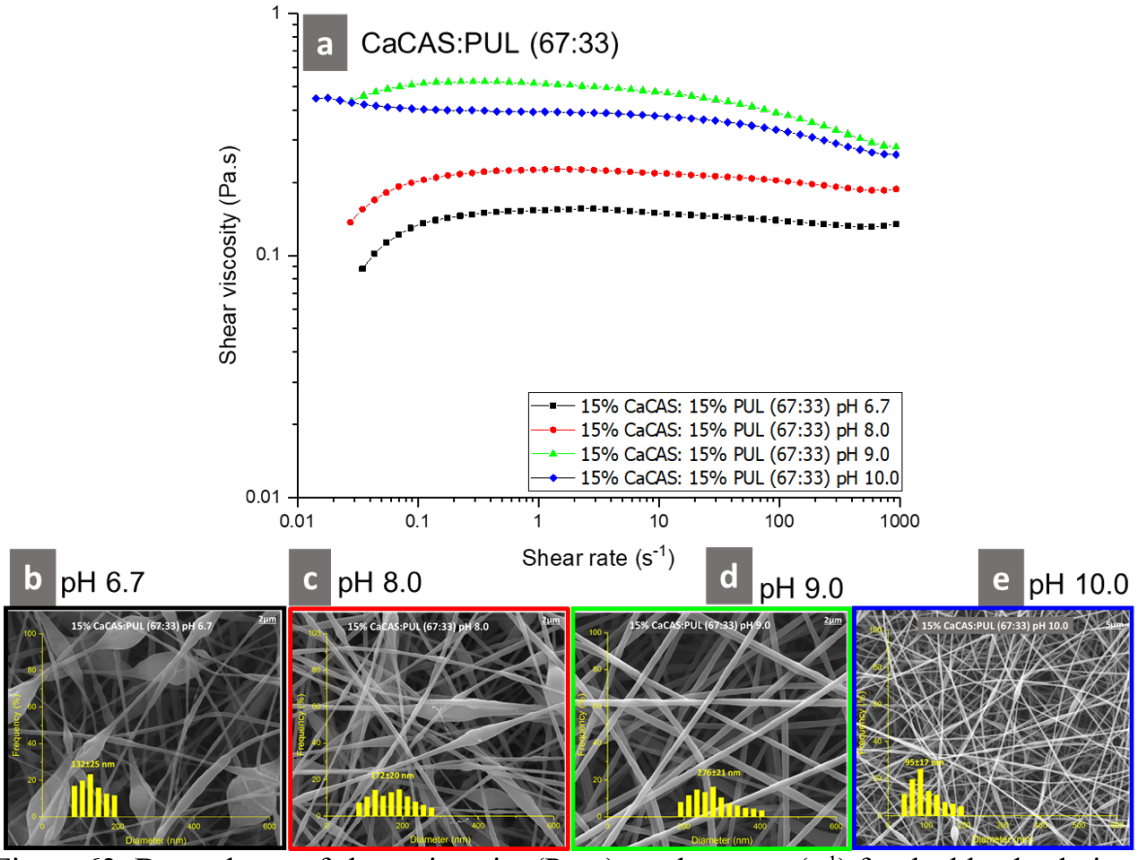

Figure 63: Dependence of shear viscosity (Pa. s) on shear rate (s^{-1}) for the blend solutions obtained from 15 wt% CaCAS and 15 wt% PUL with a 67:33 weight mixing ratio at neutral pH 6.7, 8.0, 9.0, and 10.0 (a) and electrospun CaCAS: PUL fibers with diameters of 132±25 nm (b), 172±20 nm (c), 276±21 nm (d), and 95±17 nm (e), respectively. The pH of the aqueous CaCAS solution was adjusted before mixing with PUL solution.

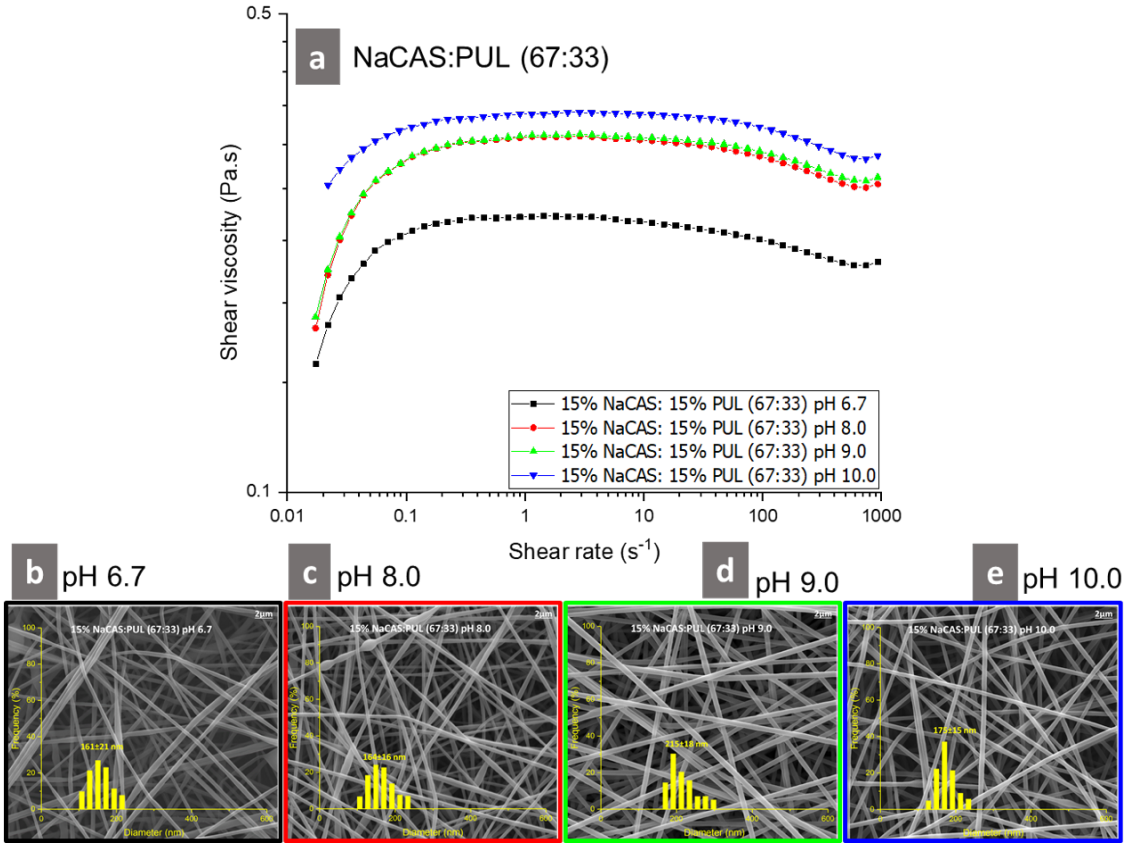

Figure 64: Dependence of shear viscosity (Pa. s) on shear rate (s^{-1}) for the blend solutions obtained from 15 wt% NaCAS and 15 wt% PUL with a 67:33 weight mixing ratio at neutral pH 6.7, 8.0, 9.0, and 10.0 (a) and electrospun NaCAS: PUL fibers with diameters of 161±21 nm (b), 164±16 nm (c), 215±18 nm (d), and 175±15 nm (e), respectively. The pH of the aqueous NaCAS solution was adjusted before mixing with PUL solution.

Figures 65 and 66 show the shear rate dependence of shear viscosity for aqueous CaCAS and NaCAS solutions blended with 15 wt% PUL with a 75:25 mixing ratio at neutral pH 6.7, 8.0, 9.0, and 10.0. The viscosity of CaCAS: PUL blends were increased due to more protein content than PUL at a higher pH, while such of NaCAS: PUL mixtures were decreased with increasing pH, especially pH 9.0 and 10.0, as shown in Figure 66a. This could be due to the molecular interactions with both Na^{1+} ions and OH^{-} with hydroxyl groups of PUL (Li et al., 2017). Also, CaCAS: PUL at a higher pH showed a strong shear rate dependence of viscosity while NaCAS: PUL dispersions followed a Newtonian behavior. The viscosity above 1.0 Pa. s made the electrospinning of the CaCAS: PUL blend

solutions difficult because the solution was jammed at the tip of needle due to the solidification of viscous solution. With increasing pH from neutral to 9.0, the fiber structures were enhanced, and the diameter size ranged from 157 to 217 nm, but the dispersions at pH 10 formed ribbon-like and defected electrospun fibers with a diameter of 95 nm, as shown in Figure 65. This may be due to a higher content of Ca^{2+} ions from CaCAS, causing the formation of dense protein chains, forming a viscous solution and blocking the process. Also, pH increase may not be effective because Na^{1+} ions from NaOH solution may not compete with a higher amount of Ca^{2+} ion in the mixture to interrupt the formation of dense caseinate protein chains (Swaisgood, 1993; Thomar et al., 2012; Tomasula et al., 2016).

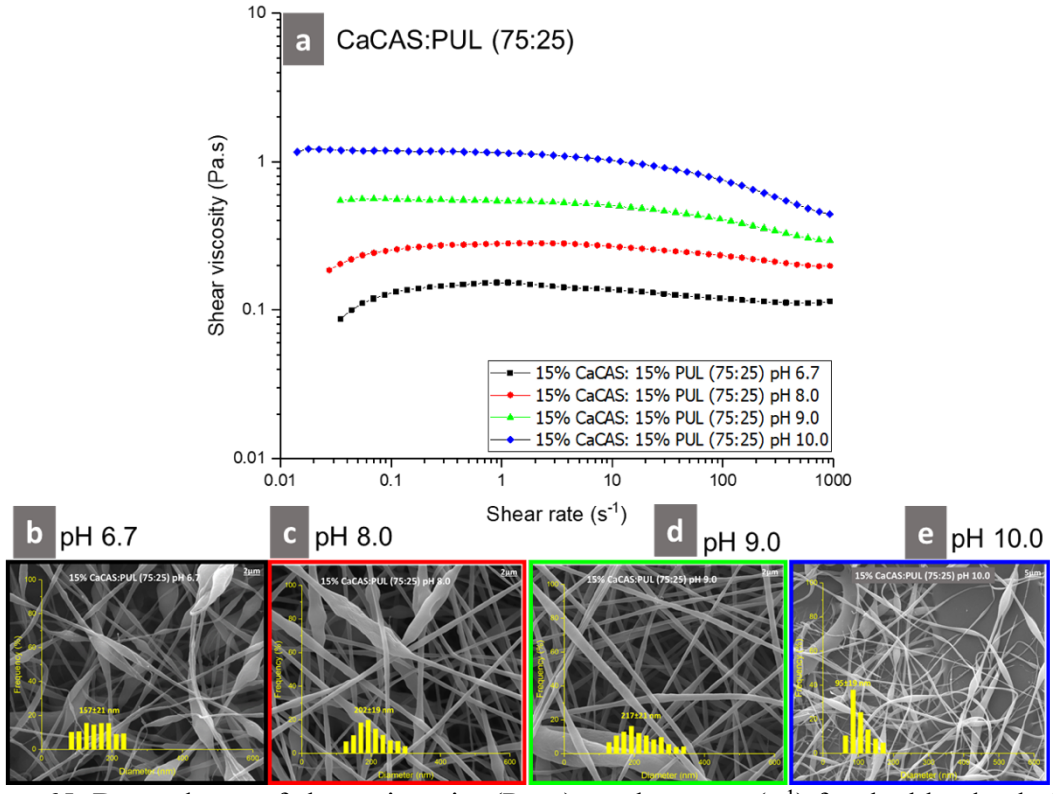

Figure 65: Dependence of shear viscosity (Pa. s) on shear rate (s^{-1}) for the blend solutions obtained from 15 wt% CaCAS and 15 wt% PUL with a 75:25 weight mixing ratio at neutral pH 6.7, 8.0, 9.0, and 10.0 (a) and electrospun CaCAS: PUL fibers with diameters of 157±21 nm (b), 202±19 nm (c), 217±21 nm (d), and 95±15 nm (e), respectively. The pH of the aqueous CaCAS solution was adjusted before mixing with PUL solution.

Increasing pH had a little effect on the fiber diameter size of electrospun NaCAS: PUL (75:25), as shown in Figure 66. NaCAS: PUL (75:25) dispersions at pH 6.7, 8.0, 9.0, and 10.0 produced defect-free and uniform fibers with diameters of 151±20, 193±19, 166±16, and 191±18 nm, respectively. These fiber diameters were thinner than the other electrospun fiber obtained from the NACAS: PUL blend with less NaCAS content, as shown in Figures 65 and 66, which is the opposite of the reported studies concluded that a higher protein content produce a thicker fiber (Stijnman et al., 2013; Nieuwland et al., 2011). Increasing Na^{1+} ions by both the inclusion of NaOH and increasing NaCAS content in blend with PUL dispersions, may prevent small protein strands and agglomerates of CAS from jamming, which may allow more elongation and stretching of polymer solution under the electric field (Thomar et al., 2012; Tomasula et al., 2016).

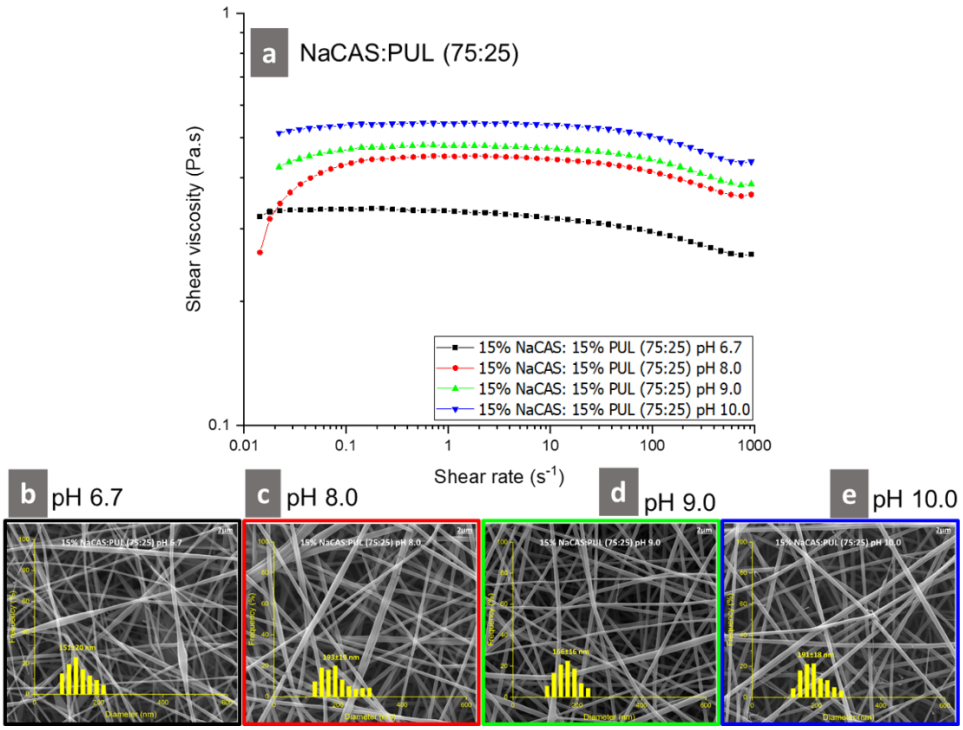

Figure 66: Dependence of shear viscosity (Pa. s) on shear rate (s^{-1}) for the blend solutions obtained from 15 wt% NaCAS and 15 wt% PUL with a 75:25 weight mixing ratio at neutral pH 6.7, 8.0, 9.0, and 10.0 (a) and electrospun NaCAS: PUL fibers with diameters of 151±20 nm (b), 193±19 nm (c), 166±16 nm (d), and 191±18 nm (e), respectively. The pH of the aqueous NaCAS solution was adjusted before mixing with PUL solution.

7.4 Mechanical Properties of CaCAS and NaCAS blended with PUL nanofibrous mats

Mechanical properties are essential to potential applications requiring structural and functional qualities of electrospun nanofibrous mats. Due to a sharp increase in development of electrospun nanofibers and their applications, the fundamental understanding of the mechanical properties of electrospun nanofibers is still lacking.

In this section, the mechanical properties of electrospun CaCAS: and NaCAS: PUL nanofibrous mats were measured under the conditions of 50 % RH within the closed cabinet at RT. The pH influence on these properties was observed as well. As mentioned in Section 4.2.3, the fibrous mats with a weight of 2.5 g and dimension of 20x10x0.01 (cm^3) were produced, and the mat strip with a dimension of 0.15x0.053x0.01 (cm^3) was used for DMA-mechanical properties. While CaCAS: PUL fibrous mats showed an opposite correlation with increasing pH, the NaCAS: PUL mats showed a positive correlation with increasing pH, as seen in Table 17. With increasing pH ranging from 6.7 to 10.0, E, TS, and EB were increased from 81, 2.7, and 4.0 to 139 MPa, 4.3 MPa, and 10 % for NaCAS: PUL fibrous mats, respectively. However, the CaCAS: PUL mats were first improved till pH 9.0 and decreased at pH 10 for CaCAS: PUL mats compared to their mats at neutral pH 6.7. For instance, TS of CaCAS: PUL first increased from 1.0 to 4.7 MPa at the pH ranging from 6.7 to 9.0, and then decreased to 1.9 Pa. s at pH 10.0 while E ranged from 45 to 117 MPa and decreased to 60 MPa, respectively, as shown in Table 17. This could be due to the conversion of CaCAS more like NaCAS with the addition of Na^{1+}, which may change the molecular structure from colloidal caseinate pieces to small protein strands and agglomerates (Thomar et al., 2012). Edible electrospun CAS: PUL mats

showed better tensile properties compared to edible gelatin fibrous mats that Zhang et al (2009) reported that E, TS, and EB for gelatin electrospun mats without crosslinking were 9.5 MPa, 1.1 MPa, and 37 % (Zhang et al., 2009). Lu and coworkers (2006) produced sodium alginate/PEO electrospun nanofibers with a mean diameter of 228 nm from their aqueous solution at the concentration of 3 %. TS and EB of sodium alginate/PEO blend electrospun mats were reported as 4 MPa and 3.4 % (Lu et al., 2006).

The fibrous mats show an improvement compared to the earlier works reported for CaCAS/Gly films even though fibrous mats and fibers are not comparable due to their different morphologies. However, using less than 0.1 g fibrous mats with 0.1 mm thickness and an average porosity of 50 % can show similar and/or better results than caseinate-based edible films. For example, some studies reported that TS values ranged from 1.6 to 7.0 MPa for CaCAS/Gly films obtained from a solution at a total solid concentration of 20 wt% with a 2.33:1 caseinate to glycerol ratio with an average thickness of 0.1 mm (Tomasula et al., 1998; Tomasula, Yee, and Parris, 2003). Bonnaillie and Tomasula (2015) reported that the CaCAS/Gly films with a 3:1 weight ratio had TS of 13.6 MPa, a high modulus, E, of 400 MPa, and EB of 20 % as testing under the conditions of 50 % RH and RT (Bonnaillie and Tomasula, 2015). Kozempel and Tomasula (2004) examined the tensile properties of CaCAS films with Gly with a 70:30 weight ratio at the concentration of 10 % and reported an average tensile strength and film thickness, 5.0 MPa and 0.136 mm (Kozempel and Tomasula, 2004), which is similar to the TS of CAS: PUL electrospun mats in this study. Additionally, Siew et al (1999) produced NaCAS/Gly films with a protein ratio to Gly of 4:1 with a thickness of 0.085 mm. TS of the films ranged from 17 to 27 MPa and EB was about 10.5 (Siew et al., 1999).

Table 17: Tensile properties of CaCAS: and NaCAS: PUL nanofibrous mats with a 50:50 weight mixing ratio at neutral pH 6.7, 8.0, 9.0, and 10.0. 1 M NaOH solution was used to adjust the pH of either CAS before mixing PUL aqueous solution.

Samples	pH	Average thickness of fibrous mats (mm)	Young's modulus, E (MPa)	Tensile strength, TS (MPa)	Elongation at break, EB (%)
15% CaCAS: 15% PUL (50:50)	6.7	0.12	44.6 ± 3.4^{a}	1.0 ± 0.0^{a}	3.6
	8.0	0.09	100.3 ± 17.9^{b}	2.9 ± 0.9^{a}	7.4
	9.0	0.09	117.2 ± 6.2^{b}	4.7 ± 0.3^{b}	8.4
	10.0	0.10	59.9 ± 7.8^{a}	1.9 ± 0.1^{a}	3.3
15% NaCAS: 15% PUL (50:50)	6.7	0.13	80.5 ± 8.1^{b}	2.7 ± 0.5^{a}	4.0
	8.0	0.08	107.2 ± 4.1^{b}	4.0 ± 0.5^{b}	9.6
	9.0	0.10	113.2 ± 4.0^{b}	4.0 ± 0.3^{b}	9.7
	10.0	0.09	138.6 ± 11.5^{d}	4.3 ± 0.7^{b}	10.1

[a-d]Means within a column with different superscripts differ ($p<0.05$).

7.5 Summary

This chapter focused on the adjusting of pH of both CAS proteins and the pH influence on the protein conformation on fiber morphology obtained from aqueous caseinates and PUL blend solutions. Also, the increase in protein ratio to polysaccharide was focused.

- In semidilute entangled regime, the η_{sp} of CaCAS blended with PUL (50:50 ratio) at pH 7.0, 8.0, 9.0, and 10.0 were proportional to $c^{7.48}$, $c^{2.16}$, $c^{2.24}$, $c^{2.32}$, and $c^{2.34}$, respectively, whereas such η_{sp} of NaCAS: PUL (50:50) blends were proportional to $c^{8.38}$, $c^{2.50}$, $c^{2.01}$, $c^{2.01}$, and $c^{2.23}$, respectively.
- At pH 8.0, electrospun CaCAS: PUL (50:50) fibers became smoother and more uniform with an average diameter of 254±18 nm while they showed a thinner fiber structure with a diameter of 105±16 nm at pH 10.0. NaCAS: PUL (50:50) dispersions at pH 6.7, 8.0,

9.0, and 10.0 produced defect-free and uniform fibers with diameters of 215±18, 265±17, 234±16, and 188±14 nm, respectively.

- Increasing pH had less effect on fiber diameter size obtained from NaCAS: PUL than CaCAS: PUL (67:33) fibers. CaCAS: PUL (67:33) dispersions at pH 8.0 produced less defected electrospun fibers with 172±20 nm compared to the fibers obtained at neutral pH 6.7. Uniform, defect free fibers with a diameter of 276±21nm were produced at pH 9.0 while a thinner nanofiber with a diameter of 95±17 nm was manufactured from CaCAS: PUL blends at pH 10.0. The dispersions of NaCAS: PUL (67:33) at pH 6.7, 8.0, 9.0, and 10.0 produced defect-free and uniform fibers with diameters of 161±2, 164±16, 215±18, and 175±15 nm, respectively.
- CaCAS: PUL (75:25) dispersion has a viscosity over 1.0 Pa. s, which made the electrospinning of the CaCAS: PUL blend solutions difficult because of fast solidification at the tip of the needle. With increasing pH from neutral to 9.0, the fiber structures were enhanced, but the dispersions at pH 10 formed ribbon-like and defected electrospun fibers with a diameter of 95 nm. Increasing pH had a little effect on the fiber diameter size of electrospun NaCAS: PUL (75:25), and the blends at the pH ranging from 6.7 to 10.0 produced defect-free and uniform fibers with diameters of 151±20, 193±19, 166±16, and 191±18 nm, respectively.
- TS of CaCAS: PUL mats first increased from 1.0 to 4.7 MPa at the pH ranging from 6.7 to 9.0, and then decreased to 1.9 Pa. s at pH 10.0 while E ranged from 45 to 117 MPa and decreased to 60 MPa, respectively. E, TS, and EB were increased from 81, 2.7, and 4.0 to 139 MPa, 4.3 MPa, and 10 % for NaCAS: PUL fibrous mats, respectively, with increasing pH ranging from 6.7 to 10.0.

- As a result, a further increase in pH allowed the fibers to become thinner because either reduction in the formation of dense protein domains or interruption dense protein structure favor more molecular interactions between hydrophobic groups of caseinates with hydroxyl groups of PUL to increase (Thomar et al., 2013). Also, more Ca^{2+} and Na^{1+} ions in the solutions increase the electrical conductivity which allows creating a higher electrostatic force and thus increase the elongation of the continuous jet, as mentioned in Section 2.3.2. The pH changes with the inclusion of Na^{1+} may disrupt the hydrogen bonds between PUL and water molecules, leading to form more interactions and molecular conformation with CAS proteins.

CHAPTER 8

Conclusion and Future Work

8.1 Conclusion

Electrospinning of the milk-based proteins in aqueous solutions is feasible to produce food-grade nanofibers and nanofibrous mats as they blend with PUL and the solution properties are optimized. Therefore, brief results along with the objectives will be concluded.

- Evaluating the relationships between the solution viscosity along with chain entanglements and electrospinnability of NFDM, CaCAS, NaCAS, and PUL solutions.

Solution rheology, particularly the chain entanglement and the viscosity of polymer solutions, is a determinant factor for polymers to be electrospun and the concentrations of the polymer solutions must exceed the entanglement concentration, c_e, which is required for a successful fiber formation. Even though the concentrations of NFDM, CaCAS, and NaCAS at above their c_e, (12, 9, and 8 wt%, respectively) were processed, their electrospinning process is not possible under the scope of the experiments conducted in this study. Therefore, PUL is used to enable the electrospinning of these proteins possible.

- Evaluating the effect of PUL carrier on the viscosity of NFDM and CAS solutions and their chain entanglements by identifying the concentration regimes and the c_e of their blended solutions.

PUL facilitated the protein chain entanglements for CAS by interrupting both the formation of the dense protein molecules in the presence of Ca^{2+} ions in CaCAS and the jamming of small protein strands and agglomerates in NaCAS. Its addition prevented the protein

solutions from a sharp viscosity increase hindering the processing and initiated the protein chain entanglements which is attributed the interactions between hydroxyl groups of PUL molecules and protein molecules. The fibrous mats were obtained from NFDM, CaCAS, and NaCAS blended with PUL and their fiber structures were uniform and bead-free with an average diameter of 200 nm. As a model application, L. *Rhamnosus* GG bioactive were successfully encapsulated within the fibrous mats by adding the cells into fiber-making solutions. L. *Rhamnosus* GG was not affected by high voltage during electrospinning the solution and recovered the amount of one-fold less than the initial loading amount. Much work must be done to generalize the carrier properties of these fibrous mats.

- Evaluating the effect of protein conformation on the fiber morphology obtained from aqueous CAS solutions in the presence of PUL and determining their c regimes and c_e, and how these contribute to the fiber formation and morphology.

Increasing the pH of fiber-making CAS solutions influenced the entanglement of protein chains and improved the electrospinnability of CAS blended with PUL. The pH adjusted by NaOH interrupted the colloidal structure of CaCAS proteins due to hydrophobically linked phosphoserine groups in the presence of Ca^{2+} ions, which allow the unordered or more randomly ordered proteins, and PUL can diffuse within the protein molecules, forming more interactions, and thus molecular entanglements. Therefore, higher pH favored the fiber morphology of CaCAS: PUL blends to have defect-free and smooth structure.

8.2 Future Work

The conclusions of this work show that milk-based proteins produced edible nanofibers and nanofibrous mats when they blended with PUL. The experiments and

results of this study can provide a groundwork to build a model to determine the factors governing the electrospinning of biopolymers with or without a carrier polymer for future studies. In future, different carrier polymers can be used to electrospin milk proteins to evaluate the effect of the carrier on the solution rheology and fiber morphology.

The 3-D fibrous nature of these mats, with smaller diameter fibers increasing the surface area-to-volume ratio and porosity between the fibers, is intriguing for their potential use in food and non-food applications. Even though more studies are required, these mats have a potential to be used as ingredient carriers in foods nutrient delivery, flavor enhancement, sensitive bioactives or volatile compounds encapsulation, or texture improvement in functional foods and beverages to meet current demands in the food industry. Milk protein-based electrospun mats can be studied to carry essential vitamins, minerals, or peptides to contribute to health-promoting foods by analyzing their loading abilities and their resistance to certain environmental conditions such as high temperature and humidity. They can be produced and used to carry antimicrobial and antioxidant compounds as a part of food packaging materials. Due to their susceptibility to humidity, it can be an opportunity to use humidity as an auto-controlled delivery system for the packaging of the fresh produce when the mats are used.

Due to the biocompatibility, biodegradability, and nanofibrous nature of the mats, they can be utilized in other applications such as tissue engineering as a biomaterial and pharmaceutical and nutraceutical as a drug or supplement carrier. The fiber morphology, mechanics, and surface chemistry of electrospun biopolymers can have an advantage over the synthetic polymers because such food-grade biopolymers are available in large amounts. However, they can be vulnerable to humidity and water, their electrospun fibers

must be strengthened by conducting more studies to make them resistant to the environmental changes.

REFERENCES

Aceituno-Medina, M., A. Lopez-Rubio, S. Mendoza, and J.M. Lagaron. 2013. Development of Novel Ultrathin Structures Based in Amaranth (Amaranthus Hypochondriacus) Protein Isolate through Electrospinning. Food Hydrocolloids 31, no. 2: 289–298. http://dx.doi.org/10.1016/j.foodhyd.2012.11.009.

Aceituno-Medina, M., S. Mendoza, J.M. Lagaron, and A. Lopez-Rubio. 2015. Photoprotection of Folic Acid upon Encapsulation in Food-Grade Amaranth (Amaranthus Hypochondriacus L.) Protein Isolate - Pullulan Electrospun Fibers. LWT - Food Science and Technology 62, no. 2: 970–975.

Aceituno-Medina, M., S. Mendoza, J.M. Lagaron, and A. López-Rubio. 2013. Development and Characterization of Food-Grade Electrospun Fibers from Amaranth Protein and Pullulan Blends. Food Research International 54, no. 1: 667–674. http://dx.doi.org/10.1016/j.foodres.2013.07.055.

Aceituno-Medina, M., S. Mendoza, B.A. Rodríguez, J.M. Lagaron, and A. López-Rubio. 2015. Improved Antioxidant Capacity of Quercetin and Ferulic Acid during In-Vitro Digestion through Encapsulation within Food-Grade Electrospun Fibers. Journal of Functional Foods 12: 332–341. http://dx.doi.org/10.1016/j.jff.2014.11.028.

Aduba, D.C., J.A. Hammer, Q. Yuan, W. Andrew Yeudall, G.L. Bowlin, and H. Yang. 2013. Semi-Interpenetrating Network (SIPN) Gelatin Nanofiber Scaffolds for Oral Mucosal Drug Delivery. Acta Biomaterialia 9, no. 5: 6576–6584. http://dx.doi.org/10.1016/j.actbio.2013.02.006.

Aewsiri, T., S. Benjakul, W. Visessanguan, J.-B. Eun, P.A. Wierenga, and H. Gruppen. 2009. Antioxidative Activity and Emulsifying Properties of Cuttlefish Skin Gelatin Modified by Oxidised Phenolic Compounds. Food Chemistry 117, no. 1 (November): 160–168. http://linkinghub.elsevier.com/retrieve/pii/S0308814609004130.

Agarwal, S., M. Burgard, A. Greiner, and J. Wendorff. 2016. Electrospinning: A Practical Guide to Nanofibers. Walter de Gruyter GmbH & Co KG.

Akkurt, S., L. Liu, and P.M. Tomasula. 2018. Electrospinning of Edible, Food-Based Polymers. Ed. Ravishankar V. Rai and Jamuna A. Bai. Nanotechnology Applications in the Food Industry. CRC Press. https://books.google.com/books?id=CM5JDwAAQBAJ.

Alborzi, S., L.-T. Lim, and Y. Kakuda. 2012. Encapsulation of Folic Acid and Its Stability in Sodium Alginate-Pectin-Poly(Ethylene Oxide) Electrospun Fibres. Journal of Microencapsulation 30, no. May 2012: 1–8.

———. 2014. Release of Folic Acid from Sodium Alginate-Pectin-Poly(Ethylene Oxide) Electrospun Fibers under in Vitro Conditions. LWT - Food Science and Technology 59, no. 1: 383–388. http://linkinghub.elsevier.com/retrieve/pii/S0023643814003600.

Alborzi, S., L.T. Lim, and Y. Kakuda. 2010. Electrospinning of Sodium Alginate-Pectin Ultrafine Fibers. Journal of Food Science 75, no. 1: 100–107.

Aldana, A.A., and G.A. Abraham. 2017. Current Advances in Electrospun Gelatin-Based Scaffolds for Tissue Engineering Applications. International Journal of Pharmaceutics 523, no. 2 (May): 441–453. http://linkinghub.elsevier.com/retrieve/pii/S0378517316308742.

Ali, J., S. Md, S. Baboota, and J.K. Sahni. 2012. Polymeric Nanoparticles, Magnetic Nanoparticles and Quantum Dots: Current and Future Perspectives. In Patenting Nanomedicines, 99–149. Berlin, Heidelberg: Springer Berlin Heidelberg. http://link.springer.com/10.1007/978-3-642-29265-1_4.

Angammana, C.J., and S.H. Jayaram. 2016. Particulate Science and Technology An International Journal Fundamentals of Electrospinning and Processing Technologies Fundamentals of Electrospinning and Processing Technologies. Particulate Science and Technology 34, no. 1: 72–82. http://www.tandfonline.com/action/journalInformation?journalCode=upst20%5Cnhttp://www.tandfonline.com/action/journalInformation?journalCode=upst20.

Anton, A., and B.R. Baird. 2001. Polyamides, Fibers. In Encyclopedia of Polymer Science and Technology. Hoboken, NJ, USA: John Wiley & Sons, Inc. http://doi.wiley.com/10.1002/0471440264.pst250.

Araujo, J., J. Padrão, J.P. Silva, F. Dourado, D.M. Correia, G. Botelho, J.L.G. Ribelles, S. Lanceros-Méndez, and V. Sencadas. 2014. Processing and Characterization of α-Elastin Electrospun Membranes. Applied Physics A 115, no. 4: 1291–1298.

Avena-Bustillos, R.J., L.A. Cisneros-Zevallos, J.M. Krochta, and M.E. Saltveit. 1994. Application of Casein-Lipid Edible Film Emulsions to Reduce White Blush on Minimally Processed Carrots. Postharvest Biology and Technology 4, no. 4: 319–329.

Babel, W. 1996. Gelatine - Ein Vielseitiges Biopolymer. Chemie in Unserer Zeit 30, no. 2 (April): 86–95. http://doi.wiley.com/10.1002/ciuz.19960300205.

Baiguera, S., C. Del Gaudio, E. Lucatelli, E. Kuevda, M. Boieri, B. Mazzanti, A. Bianco, and P. Macchiarini. 2014. Electrospun Gelatin Scaffolds Incorporating Rat Decellularized Brain Extracellular Matrix for Neural Tissue Engineering. Biomaterials 35, no. 4: 1205–1214. http://dx.doi.org/10.1016/j.biomaterials.2013.10.060.

Bak, S.Y., G.J. Yoon, S.W. Lee, and H.W. Kim. 2016. Effect of Humidity and Benign Solvent Composition on Electrospinning of Collagen Nanofibrous Sheets. Materials Letters 181: 136–139.

Barth, A. 2007. Infrared Spectroscopy of Proteins. Biochimica et Biophysica Acta (BBA)-Bioenergetics 1767, no. 9: 1073–1101.

Baumgarten, P.K. 1971. Electrostatic Spinning of Acrylic Microfibers. Journal of Colloid and Interface Science 36, no. 1: 71–79.

Baziwane, D., and Q. He. 2003. Gelatin: The Paramount Food Additive. Food Reviews International 19, no. 4 (January 11): 423–435. http://www.tandfonline.com/doi/abs/10.1081/FRI-120025483.

Beachley, V., and X. Wen. 2010. Polymer Nanofibrous Structures: Fabrication, Biofunctionalization, and Cell Interactions. Progress in Polymer Science 35, no. 7 (July): 868–892. http://linkinghub.elsevier.com/retrieve/pii/S0079670010000328.

Bellan, L.M., H.G. Craighead, and J.P. Hinestroza. 2007. Direct Measurement of Fluid Velocity in an Electrospinning Jet Using Particle Image Velocimetry. Journal of Applied Physics 102, no. 9 (November): 094308. http://aip.scitation.org/doi/10.1063/1.2799059.

Berriaud, N., M. Milas, and M. Rinaudo. 1994. Rheological Study on Mixtures of Different Molecular Weight Hyaluronates 16, no. 3: 137–142.

Berth, G., H. Dautzenberg, and M.G. Peter. 1998. Physico-Chemical Characterization of Chitosans Varying in Degree of Acetylation. Carbohydrate Polymers 36, no. 2–3: 205–216. http://www.sciencedirect.com/science/article/pii/S0144861798000290.

Bhardwaj, N., and S.C. Kundu. 2010. Electrospinning: A Fascinating Fiber Fabrication Technique. Biotechnology Advances 28, no. 3: 325–347.

Bhattarai, N., and M. Zhang. 2007. Controlled Synthesis and Structural Stability of Alginate-Based Nanofibers. Nanotechnology 18, no. 45.

Blanco-Padilla, A., A. Lopez-Rubio, G. Loarca-Pia, L.G. Gomez-Mascaraque, and S. Mendoza. 2015. Characterization, Release and Antioxidant Activity of Curcumin-Loaded Amaranth-Pullulan Electrospun Fibers. LWT - Food Science and Technology 63, no. 2: 1137–1144.

Bonino, C.A., M.D. Krebs, C.D. Saquing, S.I. Jeong, K.L. Shearer, E. Alsberg, and S.A. Khan. 2011. Electrospinning Alginate-Based Nanofibers: From Blends to Crosslinked Low Molecular Weight Alginate-Only Systems. Carbohydrate Polymers 85, no. 1: 111–119. http://dx.doi.org/10.1016/j.carbpol.2011.02.002.

Bonnaillie, L.M., H. Zhang, S. Akkurt, K.L. Yam, and P.M. Tomasula. 2014. Casein Films: The Effects of Formulation, Environmental Conditions and the Addition of Citric Pectin on the Structure and Mechanical Properties. Polymers 6, no. 7: 2018–2036.

Bosworth, L., and S. Downes. 2011. Electrospinning for Tissue Regeneration. Elsevier.

Bouhadir, K.H., K.Y. Lee, E. Alsberg, K.L. Damm, K.W. Anderson, and D.J. Mooney. 2001. Degradation of Partially Oxidized Alginate and Its Potential Application for Tissue Engineering. Biotechnology Progress 17, no. 5: 945–950.

Bueche, F. 1956. Viscosity of Polymers in Concentrated Solution. The Journal of Chemical Physics 25, no. 3: 599–600.

Buttafoco, L., N.G. Kolkman, P. Engbers-Buijtenhuijs, A.A. Poot, P.J. Dijkstra, I. Vermes, and J. Feijen. 2006. Electrospinning of Collagen and Elastin for Tissue Engineering Applications. Biomaterials 27, no. 5: 724–734.

Casper, C.L., J.S. Stephens, N.G. Tassi, D.B. Chase, and J.F. Rabolt. 2004. Controlling Surface Morphology of Electrospun Polystyrene Fibers: Effect of Humidity and Molecular Weight in the Electrospinning Process. Macromolecules 37, no. 2: 573–578.

Castro-Enríquez, D.D., F. Rodríguez-Félix, B. Ramírez-Wong, P.I. Torres-Chávez, M.M. Castillo-Ortega, D.E. Rodríguez-Félix, L. Armenta-Villegas, and A.I. Ledesma-Osuna. 2012. Preparation, Characterization and Release of Urea from Wheat Gluten Electrospun Membranes. Materials 5, no. 12: 2903–2916.

Chakraborty, A., and S. Basak. 2007. PH-Induced Structural Transitions of Caseins. Journal of Photochemistry and Photobiology B: Biology 87, no. 3: 191–199.

Cho, D., O. Nnadi, A. Netravali, and Y.L. Joo. 2010. Electrospun Hybrid Soy Protein/PVA Fibers. Macromolecular Materials and Engineering 295, no. 8: 763–773.

Choi, S.-H., D.-Y. Youn, S.M. Jo, S.-G. Oh, and I.-D. Kim. 2011. Micelle-Mediated Synthesis of Single-Crystalline β(3C)-SiC Fibers via Emulsion Electrospinning. ACS Applied Materials & Interfaces 3, no. 5 (May 25): 1385–1389. http://pubs.acs.org/doi/10.1021/am200171v.

Chong, E.J., T.T. Phan, I.J. Lim, Y.Z. Zhang, B.H. Bay, S. Ramakrishna, and C.T. Lim. 2007. Evaluation of Electrospun PCL/Gelatin Nanofibrous Scaffold for Wound Healing and Layered Dermal Reconstitution. Acta Biomaterialia 3, no. 3 SPEC. ISS.: 321–330.

Chung, H.Y., J.R.B. Hall, M.A. Gogins, D.G. Crofoot, and T.M. Weik. 2004. Polymer, Polymer Microfiber, Polymer Nanofiber and Applications Including Filter Structures 2, no. 12: 1–39. http://www.google.com/patents/US6743273.

Colby, R.H., L.J. Fetters, W.G. Funk, and W.W. Graessley. 1991. Effects of Concentration and Thermodynamic Interaction on the Viscoelastic Properties of Polymer Solutions. Macromolecules 24, no. 13: 3873–3882.

Colín-Orozco, J., M. Zapata-Torres, G. Rodríguez-Gattorno, and R. Pedroza-Islas. 2015. Properties of Poly (Ethylene Oxide)/ Whey Protein Isolate Nanofibers Prepared by Electrospinning. Food Biophysics 10, no. 2 (June 16): 134–144. http://link.springer.com/10.1007/s11483-014-9372-1.

Cooley, J.F. 1902. Apparatus for Electrically Dispersing Fluids. USA. https://patents.google.com/patent/US692631.

Corredig, M., and D.G. Dalgleish. 1996. Effect of Temperature and PH on the Interactions of Whey Proteins with Casein Micelles in Skim Milk. Food Research International 29, no. 1: 49–55.

Crowley, S. V., A.L. Kelly, P. Schuck, R. Jeantet, and J.A. O Mahony. 2016. Advanced Dairy Chemistry. Advanced Dairy Chemistry: Volume 1B: Proteins: Applied Aspects: Fourth Edition. Vol. 1. http://www.scopus.com/inward/record.url?eid=2-s2.0-84956748553&partnerID=tZOtx3y1.

Cuomo, F., A. Ceglie, and F. Lopez. 2011. Temperature Dependence of Calcium and Magnesium Induced Caseinate Precipitation in H2O and D2O. Food Chemistry 126, no. 1 (May): 8–14. http://linkinghub.elsevier.com/retrieve/pii/S0308814610012689.

Dalgleish, D.G. 1979. Proteolysis and Aggregation of Casein Micelles Treated with Immobilized or Soluble Chymosin. Journal of Dairy Research 46, no. 4: 653–661.

Dangaran, K., P.M. Tomasula, and P. Qi. 2009. Structure and Function of Protein-Based Edible Films and Coatings. In Edible Films and Coatings for Food Applications, 25–56. Springer.

Daoud, M., and P.G. De Gennes. 1979. Some Remarks on the Dynamics of Polymer Melts. Journal of Polymer Science: Polymer Physics Edition 17, no. 11: 1971–1981. http://doi.wiley.com/10.1002/pol.1979.180171113.

Deitzel, J ., J. Kleinmeyer, D. Harris, and N. Beck Tan. 2001. The Effect of Processing Variables on the Morphology of Electrospun Nanofibers and Textiles. Polymer 42, no. 1: 261–272.

deWit, J.N., and G. Klarenbeek. 1984. Effects of Various Heat Treatments on Structure and Solubility of Whey Proteins. Journal of Dairy Science 67, no. 11: 2701–2710. http://linkinghub.elsevier.com/retrieve/pii/S0022030284816288.

Dickinson, E. 2006. Structure Formation in Casein-Based Gels, Foams, and Emulsions. Colloids and Surfaces A: Physicochemical and Engineering Aspects 288, no. 1: 3–11.

Doshi, J., and D.H. Reneker. 1995. Electrospinning Process and Applications of Electrospun Fibers. Journal of Electrostatics 35, no. 2: 151–160. http://www.sciencedirect.com/science/article/pii/0304388695000418.

Drosou, C., M. Krokida, and C.G. Biliaderis. 2018. Composite Pullulan-Whey Protein Nanofibers Made by Electrospinning: Impact of Process Parameters on Fiber Morphology and Physical Properties. Food Hydrocolloids 77: 726–735. https://doi.org/10.1016/j.foodhyd.2017.11.014.

Drosou, C.G., M.K. Krokida, and C.G. Biliaderis. 2017. Encapsulation of Bioactive Compounds through Electrospinning/Electrospraying and Spray Drying: A Comparative Assessment of Food-Related Applications. Drying Technology 35, no. 2: 139–162. http://dx.doi.org/10.1080/07373937.2016.1162797.

Edwards, N.M., D. Peressini, J.E. Dexter, and S.J. Mulvaney. 2001. Viscoelastic Properties of Durum Wheat and Common Wheat Dough of Different Strengths. Rheologica Acta 40, no. 2 (March 19): 142–153. http://link.springer.com/10.1007/s003970000147.

Erdogan, I., M. Demir, and O. Bayraktar. 2015. Olive Leaf Extract as a Crosslinking Agent for the Preparation of Electrospun Zein Fibers. Journal of Applied Polymer Science 132, no. 4: 1–9.

Fang, Q., M. Zhu, S. Yu, G. Sui, and X. Yang. 2016. Studies on Soy Protein Isolate/Polyvinyl Alcohol Hybrid Nanofiber Membranes as Multi-Functional Eco-Friendly Filtration Materials. Materials Science and Engineering B: Solid-State Materials for Advanced Technology 214: 1–10. http://dx.doi.org/10.1016/j.mseb.2016.08.004.

Feng, J.J. 2003. Stretching of a Straight Electrically Charged Viscoelastic Jet. Journal of Non-Newtonian Fluid Mechanics 116, no. 1: 55–70.

Fernandez, A., S. Torres-Giner, and J.M. Lagaron. 2009. Novel Route to Stabilization of Bioactive Antioxidants by Encapsulation in Electrospun Fibers of Zein Prolamine. Food Hydrocolloids 23, no. 5: 1427–1432. http://dx.doi.org/10.1016/j.foodhyd.2008.10.011.

Ferry, J.D. 1980. Viscoelastic Properties of Polymers. John Wiley & Sons.

Fong, H., I. Chun, and D.H. Reneker. 1999. Beaded Nanofibers Formed during Electrospinning. Polymer 40, no. 16: 4585–4592.

Formhals, A. 1934. Process and Apparatus for Preparing Artificial Threads. Us 1975594: 1–7.

Fox, P.F. 2003. Milk Proteins: General and Historical Aspects. In Advanced Dairy Chemistry—1 Proteins, 1–48. Springer.

Fox, P.F., and A.L. Kelly. 2006. Chemistry and Biochemistry of Milk Constituents. Food Biochemistry and Food Processing: 425–452.

Fraunhofer, W., G. Winter, and C. Coester. 2004. Asymmetrical Flow Field-Flow Fractionation and Multiangle Light Scattering for Analysis of Gelatin Nanoparticle Drug Carrier Systems. Analytical Chemistry 76, no. 7 (April): 1909–1920. http://pubs.acs.org/doi/abs/10.1021/ac0353031.

Friedemann, K., T. Corrales, M. Kappl, K. Landfester, and D. Crespy. 2012. Facile and Large-Scale Fabrication of Anisometric Particles from Fibers Synthesized by Colloid-Electrospinning. Small 8, no. 1 (January 9): 144–153. http://doi.wiley.com/10.1002/smll.201101247.

Gennadios, A., and C.L. Weller. 1990. Edible Films and Coatings from Wheat and Corn Proteins. Food Technology.

Gennadios, A., and C.L. Weller. 1994. Moisture Adsorption by Grain Protein Films. Transactions of the ASAE 37, no. 2: 535–539.

Ghorani, B., and N. Tucker. 2015. Fundamentals of Electrospinning as a Novel Delivery Vehicle for Bioactive Compounds in Food Nanotechnology. Food Hydrocolloids 51: 227–240. http://dx.doi.org/10.1016/j.foodhyd.2015.05.024.

Gomes, S.R., G. Rodrigues, G.G. Martins, M.A. Roberto, M. Mafra, C.M.R. Henriques, and J.C. Silva. 2015. In Vitro and in Vivo Evaluation of Electrospun Nanofibers of PCL, Chitosan and Gelatin: A Comparative Study. Materials Science and Engineering C 46: 348–358. http://dx.doi.org/10.1016/j.msec.2014.10.051.

Gounga, M.E., S.-Y. Xu, and Z. Wang. 2007. Whey Protein Isolate-Based Edible Films as Affected by Protein Concentration, Glycerol Ratio and Pullulan Addition in Film Formation. Journal of Food Engineering 83, no. 4 (December): 521–530. http://linkinghub.elsevier.com/retrieve/pii/S0260877407002312.

Gounga, M.E., S. XU, and Z. Wang. 2010. Film Forming Mechanism and Mechanical and Thermal Properties of Whey Protein Isolate-based Edible Films as Affected by Protein Concentration, Glycerol Ratio and Pullulan Content. Journal of Food Biochemistry 34, no. 3: 501–519.

Grabowska, K.J., A.J. Van der Goot, and R.M. Boom. 2012. Salt-Modulated Structure Formation in a Dense Calcium Caseinate System. Food Hydrocolloids 29, no. 1: 42–47. http://dx.doi.org/10.1016/j.foodhyd.2012.02.001.

Graessley, W.W. 1974. Advances in Polymer Science. The Entanglement Concept in Polymer Rheology 16: 55.

Greiner, A., and J.H. Wendorff. 2007. Electrospinning: A Fascinating Method for the Preparation of Ultrathin Fibers. Angewandte Chemie - International Edition 46, no. 30: 5670–5703.

Gudjonsdottir, M., M.D. Gacutan, A.C. Mendes, I.S. Chronakis, L. Jespersen, and A.H. Karlsson. 2015. Effects of Electrospun Chitosan Wrapping for Dry-Ageing of Beef, as Studied by Microbiological, Physicochemical and Low-Field Nuclear Magnetic Resonance Analysis. Food Chemistry 184: 167–175.

Haider, A., S. Haider, and I.-K. Kang. 2015. A Comprehensive Review Summarizing the Effect of Electrospinning Parameters and Potential Applications of Nanofibers in Biomedical and Biotechnology. Arabian Journal of Chemistry. http://www.sciencedirect.com/science/article/pii/S1878535215003275.

Haider, S., and A. Haider. 2016. Electrospinning - Material, Techniques, and Biomedical Applications. Ed. Sajjad Haider and Adnan Haider. InTech. http://www.intechopen.com/books/electrospinning-material-techniques-and-biomedical-applications.

Hamer, R.J., and T. van Vliet. 2000. Understanding the Structure and Properties of Gluten: An Overview. In Wheat Gluten. Proceedings of the 7th International Workshop Gluten 2000, Bristol, UK, 2-6 April 2000, 125–131. Royal Society of Chemistry.

Han, Y., and H. Chen. 2013. Enhancement of Nanofiber Elasticity by Using Wheat Glutenin as an Addition. Polymer Science Series A 55, no. 5 (May 25): 320–326. http://link.springer.com/10.1134/S0965545X13050076.

Haris, P.I., and F. Severcan. 1999. FTIR Spectroscopic Characterization of Protein Structure in Aqueous and Non-Aqueous Media. Journal of Molecular Catalysis - B Enzymatic 7, no. 1–4: 207–221.

HOKES, J.C., M.E. MANGINO, and P.M.T. HANSEN. 1982. A Model System for Curd Formation and Melting Properties of Calcium Caseinates. Journal of Food Science 47, no. 4: 1235–1249.

Hongliang Jiang, †, ‡ Dufei Fang, § Benjamin S. Hsiao, § Benjamin Chu, and † and Weiliam Chen*. 2004. Optimization and Characterization of Dextran Membranes Prepared by Electrospinning. Biomacromolecules 5, no. 2: 326–333. http://dx.doi.org/10.1021/bm034345w.

Horne, D.S. 2006. Casein Micelle Structure: Models and Muddles. Current Opinion in Colloid & Interface Science 11, no. 2: 148–153.

Huan, S., G. Liu, G. Han, W. Cheng, Z. Fu, Q. Wu, and Q. Wang. 2015. Effect of Experimental Parameters on Morphological, Mechanical and Hydrophobic Properties of Electrospun Polystyrene Fibers. Materials 8, no. 5: 2718–2734.

Huang, Z.M., Y.Z. Zhang, M. Kotaki, and S. Ramakrishna. 2003. A Review on Polymer Nanofibers by Electrospinning and Their Applications in Nanocomposites. Composites Science and Technology 63, no. 15: 2223–2253.

Jain, S.K., Y. Gupta, A. Jain, A.R. Saxena, P. Khare, and A. Jain. 2008. Mannosylated Gelatin Nanoparticles Bearing an Anti-HIV Drug Didanosine for Site-Specific Delivery. Nanomedicine: Nanotechnology, Biology and Medicine 4, no. 1 (March): 41–48. http://linkinghub.elsevier.com/retrieve/pii/S1549963407002511.

Jalaja, K., D. Naskar, S.C. Kundu, and N.R. James. 2016. Potential of Electrospun Core-Shell Structured Gelatin-Chitosan Nanofibers for Biomedical Applications. Carbohydrate Polymers 136: 1098–1107. http://dx.doi.org/10.1016/j.carbpol.2015.10.014.

Jiang, H., P. Zhao, and K. Zhu. 2007. Fabrication and Characterization of Zein-Based Nanofibrous Scaffolds by an Electrospinning Method. Macromolecular Bioscience 7, no. 4: 517–525.

Jiang, Q., and Y. Yang. 2011. Water-Stable Electrospun Zein Fibers for Potential Drug Delivery. Journal of Biomaterials Science, Polymer Edition 22, no. 10: 1393–1408.

Jooyandeh, H. 2011. Whey Protein Films and Coatings: A Review. Pakistan Journal of Nutrition 10, no. 3: 293–301.

Karim, A.A., and R. Bhat. 2008. Gelatin Alternatives for the Food Industry: Recent Developments, Challenges and Prospects. Trends in Food Science & Technology 19, no. 12 (December): 644–656. http://linkinghub.elsevier.com/retrieve/pii/S0924224408002252.

Karim, M.R., H.W. Lee, R. Kim, B.C. Ji, J.W. Cho, T.W. Son, W. Oh, and J.H. Yeum. 2009. Preparation and Characterization of Electrospun Pullulan/Montmorillonite Nanofiber Mats in Aqueous Solution. Carbohydrate Polymers 78, no. 2: 336–342. http://dx.doi.org/10.1016/j.carbpol.2009.04.024.

Katti, D.S., K.W. Robinson, F.K. Ko, and C.T. Laurencin. 2004. Bioresorbable Nanofiber-based Systems for Wound Healing and Drug Delivery: Optimization of Fabrication Parameters. Journal of Biomedical Materials Research Part B: Applied Biomaterials 70B, no. 2: 286–296. http:https://dx.doi.org/10.1002/jbm.b.30041.

Kenawy, E.R., G.L. Bowlin, K. Mansfield, J. Layman, D.G. Simpson, E.H. Sanders, and G.E. Wnek. 2002. Release of Tetracycline Hydrochloride from Electrospun Poly(Ethylene-Co-Vinylacetate), Poly(Lactic Acid), and a Blend. Journal of Controlled Release 81, no. 1–2: 57–64.

Khaoula, K., P. Cristina, B. Sylvie, D. Sthane, H. Jo, K. Khwaldia, C. Perez, S. Banon, S. Desobry, and J. Hardy. 2004. Milk Proteins for Edible Films and Coatings. Critical Reviews in Food Science and Nutrition 44, no. 4: 239–251. http://dx.doi.org/10.1080/10408690490464906%5Cnhttp://www.ncbi.nlm.nih.gov/pubmed/15462128%5Cnhttp://www.ingentaconnect.com/content/tandf/bfsn/2004/00000044/00000004/art00003.

Klimov, E., V. Raman, R. Venkatesh, W. Heckmann, and R. Stark. 2010. Designing Nanofibers via Electrospinning from Aqueous Colloidal Dispersions: Effect of Cross-Linking and Template Polymer. Macromolecules 43, no. 14 (July 27): 6152–6155. http://pubs.acs.org/doi/abs/10.1021/ma100750e.

Klossner, R.R., H.A. Queen, A.J. Coughlin, and W.E. Krause. 2008. Correlation of Chitosan's Rheological Properties and Its Ability to Electrospin. Biomacromolecules.

Kong, L., and G.R. Ziegler. 2012. Role of Molecular Entanglements in Starch Fiber Formation by Electrospinning. Biomacromolecules 13, no. 8: 2247–2253.

———. 2013. Rheological Aspects in Fabricating Pullulan Fibers by Electro-Wet-Spinning. Food Hydrocolloids 38: 220–226. http://dx.doi.org/10.1016/j.foodhyd.2013.12.016.

———. 2014. Molecular Entanglement and Electrospinnability of Biopolymers. Journal of Visualized Experiments no. 91: 1–7. http://www.jove.com/video/51933/molecular-entanglement-and-electrospinnability-of-biopolymers.

KONSTANCE, R.P., and E.D. STRANGE. 1991. Solubility and Viscous Properties of Casein and Caseinates. Journal of Food Science 56, no. 2: 556–559.

Kozempel, M., and P.M. Tomasula. 2004. Development of a Continuous Process to Make Casein Films. Journal of Agricultural and Food Chemistry 52, no. 5: 1190–1195.

Krause, W.E., E.G. Bellomo, and R.H. Colby. 2001. Rheology of Sodium Hyaluronate under Physiological Conditions. Biomacromolecules 2, no. 1: 65–69.

Kriegel, C., A. Arrechi, K. Kit, D.J. McClements, and J. Weiss. 2008. Fabrication, Functionalization, and Application of Electrospun Biopolymer Nanofibers. Critical Reviews in Food Science and Nutrition 48, no. 8: 775–797.

Kristo, E., and C.G. Biliaderis. 2007. Physical Properties of Starch Nanocrystal-Reinforced Pullulan Films. Carbohydrate Polymers 68, no. 1: 146–158.

Krochta, J.M., and D.E. Mulder-Johnston. 1997. Edible and Biodegradable Polymer Films: Challenges and Opportunities. Food Technology (USA).

De Kruif, C.G., and C. Holt. 2003. Casein Micelle Structure, Functions and Interactions. In Advanced Dairy Chemistry—1 Proteins, 233–276. Springer.

De Kruif, C.G., and R. Tuinier. 2001. Polysaccharide Protein Interactions. Food Hydrocolloids 15, no. 4–6: 555–563.

de Kruif, C.G.K., H. Bhatt, S.G. Anema, and C. Coker. 2015. Rheology of Caseinate Fractions in Relation to Their Water Holding Capacity. Food Hydrocolloids 51: 503–511. http://dx.doi.org/10.1016/j.foodhyd.2015.05.026.

Lee, K.Y., L. Jeong, Y.O. Kang, S.J. Lee, and W.H. Park. 2009. Electrospinning of Polysaccharides for Regenerative Medicine. Advanced Drug Delivery Reviews 61, no. 12: 1020–1032. http://dx.doi.org/10.1016/j.addr.2009.07.006.

Leo, E., M. Angela Vandelli, R. Cameroni, and F. Forni. 1997. Doxorubicin-Loaded Gelatin Nanoparticles Stabilized by Glutaraldehyde: Involvement of the Drug in the Cross-Linking Process. International Journal of Pharmaceutics 155, no. 1 (September): 75–82. http://linkinghub.elsevier.com/retrieve/pii/S037851739700149X.

Li, C., C. Vepari, H.-J. Jin, H.J. Kim, and D.L. Kaplan. 2006. Electrospun Silk-BMP-2 Scaffolds for Bone Tissue Engineering. Biomaterials 27, no. 16: 3115–3124. http://linkinghub.elsevier.com/retrieve/pii/S0142961206000214.

Li, H., J. Yang, X. Hu, J. Liang, Y. Fan, and X. Zhang. 2011. Superabsorbent Polysaccharide Hydrogels Based on Pullulan Derivate as Antibacterial Release Wound Dressing. Journal of Biomedical Materials Research Part A 98, no. 1: 31–39.

Li, J., A. He, J. Zheng, and C.C. Han. 2006. Gelatin and Gelatin - Hyaluronic Acid Nanofibrous Membranes Produced by Electrospinning of Their Aqueous Solutions. Biomacromolecules 7, no. 7: 2243–2247.

Li, R., P. Tomasula, A. de Sousa, S.-C. Liu, M. Tunick, K. Liu, and L. Liu. 2017. Electrospinning Pullulan Fibers from Salt Solutions. Polymers 9, no. 1: 32. http://www.mdpi.com/2073-4360/9/1/32.

Librán, C.M., S. Castro, and J.M. Lagaron. 2017. Encapsulation by Electrospray Coating Atomization of Probiotic Strains. Innovative Food Science and Emerging Technologies 39: 216–222. http://dx.doi.org/10.1016/j.ifset.2016.12.013.

Lin, S.Y., and J.M. Krochta. 2006. Fluidized-Bed System for Whey Protein Film Coating of Peanuts. Journal of Food Process Engineering 29, no. 5: 532–546.

Liu, D. 2016. Electrospinning: Current Status and Future Trends. http://link.springer.com/10.1007/978-3-319-39715-3.

Liu, S., R. Li, P.M. Tomasula, A.M.M. Sousa, and L. Liu. 2016. Electrospun Food-Grade Ultrafine Fibers from Pectin and Pullulan Blends. Food Nutrition Scienceno. June: 636–646.

Livney, Y.D. 2010. Milk Proteins as Vehicles for Bioactives. Current Opinion in Colloid and Interface Science 15, no. 1–2: 73–83. http://dx.doi.org/10.1016/j.cocis.2009.11.002.

López-Rubio, A., E. Sanchez, S. Wilkanowicz, Y. Sanz, and J.M. Lagaron. 2012. Electrospinning as a Useful Technique for the Encapsulation of Living Bifidobacteria in Food Hydrocolloids. Food Hydrocolloids 28, no. 1: 159–167. http://dx.doi.org/10.1016/j.foodhyd.2011.12.008.

López Angulo, D.E., and P.J. do Amaral Sobral. 2016. Characterization of Gelatin/Chitosan Scaffold Blended with Aloe Vera and Snail Mucus for Biomedical Purpose. International Journal of Biological Macromolecules 92 (November): 645–653. http://linkinghub.elsevier.com/retrieve/pii/S0141813016307929.

Lu, J.-W., Y.-L. Zhu, Z.-X. Guo, P. Hu, and J. Yu. 2006. Electrospinning of Sodium Alginate with Poly (Ethylene Oxide). Polymer 47, no. 23: 8026–8031.

Lu, J.W., Y.L. Zhu, Z.X. Guo, P. Hu, and J. Yu. 2006. Electrospinning of Sodium Alginate with Poly(Ethylene Oxide). Polymer 47, no. 23: 8026–8031.

Lukáš, D., A. Sarkar, L. Martinová, K. Vodsed'álková, D. Lubasová, J. Chaloupek, P. Pokorný, P. Mikeš, J. Chvojka, and M. Komárek. 2009. Physical Principles of Electrospinning (Electrospinning as a Nano-Scale Technology of the Twenty-First Century). Textile Progress 41, no. 2: 59–140.

Ma, P.X., and R. Zhang. 1999. Synthetic Nano-Scale Fibrous Extracellular Matrix. Journal of Biomedical Materials Research 46, no. 1 (July): 60–72. http://www.ncbi.nlm.nih.gov/pubmed/10357136.

Manna, P.J., T. Mitra, N. Pramanik, V. Kavitha, A. Gnanamani, and P.P. Kundu. 2015. Potential Use of Curcumin Loaded Carboxymethylated Guar Gum Grafted Gelatin Film for Biomedical Applications. International Journal of Biological Macromolecules 75 (April): 437–446. http://linkinghub.elsevier.com/retrieve/pii/S0141813015000586.

Martínez, E.N., and M.C. Añón. 1996. Composition and Structural Characterization of Amaranth Protein Isolates. An Electrophoretic and Calorimetric Study. Journal of Agricultural and Food Chemistry 44, no. 9: 2523–2530. http://pubs.acs.org/doi/pdf/10.1021/jf960169p.

McClements, D.J. 2006. Non-Covalent Interactions between Proteins and Polysaccharides. Biotechnology Advances 24, no. 6 (November): 621–625. http://linkinghub.elsevier.com/retrieve/pii/S0734975006000929.

McHugh, T.H., C.L. Weller, and J.M. Krochta. 1994. Edible Coatings and Films Based on Proteins. Edible Coatings and Films to Improve Food Quality: 201.

McKee, M.G., C.L. Elkins, and T.E. Long. 2004. Influence of Self-Complementary Hydrogen Bonding on Solution Rheology/Electrospinning Relationships. Polymer 45, no. 26: 8705–8715.

McKee, M.G., G.L. Wilkes, R.H. Colby, and T.E. Long. 2004. Correlations of Solution Rheology with Electrospun Fiber Formation of Linear and Branched Polyesters. Macromolecules 37, no. 5: 1760–1767.

McMahon, D.J., H. Du, and K. Larsen. 2009. Microstructural Changes in Casein Supramolecules During Acidification of Skim Milk. Journal of Dairy Science 92, no. 2005: 5854–5867. http://dx.doi.org/10.3168/jds.2009-2324.

McMahon, D.J., and B.S. Oommen. 2008. Supramolecular Structure of the Casein Micelle. Journal of Dairy Science 91, no. 5 (May): 1709–1721. http://linkinghub.elsevier.com/retrieve/pii/S0022030208712074.

McMahon, D.J., and B.S. Oommen. 2013. Casein Micelle Structure, Functions, and Interactions. In Advanced Dairy Chemistry: Volume 1A: Proteins: Basic Aspects, 4th Edition, ed. P.L.H. McSweeney and P.F. Fox, 185–209. Boston, MA: Springer US. http://dx.doi.org/10.1007/978-1-4614-4714-6_6.

Megelski, S., J.S. Stephens, D. Bruce Chase, and J.F. Rabolt. 2002. Micro- and Nanostructured Surface Morphology on Electrospun Polymer Fibers. Macromolecules 35, no. 22: 8456–8466.

Mendes, A.C., K. Stephansen, and I.S. Chronakis. 2017. Electrospinning of Food Proteins and Polysaccharides. Food Hydrocolloids 68: 53–68. http://dx.doi.org/10.1016/j.foodhyd.2016.10.022.

Mercante, L.A., V.P. Scagion, F.L. Migliorini, L.H.C. Mattoso, and D.S. Correa. 2017. Electrospinning-Based (Bio)Sensors for Food and Agricultural Applications: A Review. TrAC Trends in Analytical Chemistry 91: 91–103. http://linkinghub.elsevier.com/retrieve/pii/S0165993617300493.

Miller, L.M., M.W. Bourassa, and R.J. Smith. 2013. FTIR Spectroscopic Imaging of Protein Aggregation in Living Cells. Biochimica et Biophysica Acta - Biomembranes 1828, no. 10: 2339–2346. http://dx.doi.org/10.1016/j.bbamem.2013.01.014.

Moomand, K., and L.-T. Lim. 2015. Properties of Encapsulated Fish Oil in Electrospun Zein Fibres Under Simulated In Vitro Conditions. Food and Bioprocess Technology 8: 431–444.

Moomand, K., and L.T. Lim. 2014. Oxidative Stability of Encapsulated Fish Oil in Electrospun Zein Fibres. Food Research International 62: 523–532. http://dx.doi.org/10.1016/j.foodres.2014.03.054.

Morr, C. V, and E.Y. Ha. 1993. Whey Protein Concentrates and Isolates: Processing and Functional Properties. Critical Reviews in Food Science and Nutrition 33, no. 6: 431–76. http://www.ncbi.nlm.nih.gov/pubmed/8216810.

Morris, E.R., A.N. Cutler, S.B. Ross-Murphy, D.A. Rees, and J. Price. 1981. Concentration and Shear Rate Dependence of Viscosity in Random Coil Polysaccharide Solutions. Carbohydrate Polymers 1, no. 1: 5–21.

Munir, M.M., A.B. Suryamas, F. Iskandar, and K. Okuyama. 2009. Scaling Law on Particle-to-Fiber Formation during Electrospinning. Polymer 50, no. 20: 4935–4943. http://dx.doi.org/10.1016/j.polymer.2009.08.011.

Musso, Y.S., P.R. Salgado, and A.N. Mauri. 2017. Smart Edible Films Based on Gelatin and Curcumin. Food Hydrocolloids 66 (May): 8–15. http://linkinghub.elsevier.com/retrieve/pii/S0268005X16307615.

Nie, H., A. He, J. Zheng, S. Xu, J. Li, and C.C. Han. 2008. Effects of Chain Conformation and Entanglement on the Electrospinning of Pure Alginate Effects of Chain Conformation and Entanglement on the Electrospinning of Pure Alginate: 1362–1365.

Nieuwland, M., P. Geerdink, P. Brier, P. van den Eijnden, J.T.M.M. Henket, M.L.P. Langelaan, N. Stroeks, H.C. van Deventer, and A.H. Martin. 2013. Food-Grade Electrospinning of Proteins. Innovative Food Science & Emerging Technologies 20: 269–275. http://linkinghub.elsevier.com/retrieve/pii/S1466856413001422.

Nur Hanani, Z.A., Y.H. Roos, and J.P. Kerry. 2014. Use and Application of Gelatin as Potential Biodegradable Packaging Materials for Food Products. International Journal of Biological Macromolecules 71 (November): 94–102. http://linkinghub.elsevier.com/retrieve/pii/S0141813014002542.

Okutan, N., P. Terzi, and F. Altay. 2014. Affecting Parameters on Electrospinning Process and Characterization of Electrospun Gelatin Nanofibers. Food Hydrocolloids 39: 19–26.

Oommen, B.S. 2004. Casein Supramolecules: Structure and Coagulation Properties. Utah State University, Logan, UT, USA.

Pant, H.R., and C.S. Kim. 2012. Electrospun Gelatin/Nylon-6 Composite Nanofibers for Biomedical Applications. Polymer International (October): n/a-n/a. http://doi.wiley.com/10.1002/pi.4380.

Parker, T.G., and D.G. Dalgleish. 1981. Binding of Calcium Ions to Bovine Beta-Casein. The Journal of Dairy Research 48, no. 1: 71–76.

Pelipenko, J., J. Kristl, B. Janković, S. Baumgartner, and P. Kocbek. 2013. The Impact of Relative Humidity during Electrospinning on the Morphology and Mechanical Properties of Nanofibers. International Journal of Pharmaceutics 456, no. 1: 125–134. http://linkinghub.elsevier.com/retrieve/pii/S0378517313007254.

Phadungath, C. 2005. Casein Micelle Structure : A Concise Review. Journal of Science and Technology 27, no. May 2004: 201–212.

Pillay, V., C. Dott, Y.E. Choonara, C. Tyagi, L. Tomar, P. Kumar, L.C. Du Toit, and V.M.K. Ndesendo. 2013. A Review of the Effect of Processing Variables on the Fabrication of Electrospun Nanofibers for Drug Delivery Applications. Journal of Nanomaterials 2013.

Pitkowski, A., D. Durand, and T. Nicolai. 2008. Structure and Dynamical Mechanical Properties of Suspensions of Sodium Caseinate. Journal of Colloid and Interface Science 326, no. 1: 96–102.

Pitkowski, A., T. Nicolai, and D. Durand. 2009. Stability of Caseinate Solutions in the Presence of Calcium. Food Hydrocolloids 23, no. 4: 1164–1168. http://dx.doi.org/10.1016/j.foodhyd.2008.07.016.

Quirós, J., K. Boltes, R. Rosal, J. Quir Os, K. Boltes, R. Rosal, J. Quirós, K. Boltes, and R. Rosal. 2016. Bioactive Applications for Electrospun Fibers. Polymer Reviews 56, no. 4: 631–667. https://www.tandfonline.com/doi/full/10.1080/15583724.2015.1136641.

Ramakrishna, S.F.K.T.W.L.T.M.Z. 2005. An Introduction to Electrospinning And Nanofibers (Google EBook). Introduction to Electrospinning And Nanofibers. Vol. 48. http://alexandria.rice.edu/uhtbin/cgisirsi/?ps=QDgPpuzYNF/FONDREN/148480076/88%5Cnhttp://books.google.com/books?id=QHkyRdb2TicC&pgis=1.

Ramji, K., and R.N. Shah. 2014. Electrospun Soy Protein Nanofiber Scaffolds for Tissue Regeneration. Journal of Biomaterials Applications 29, no. 3: 411–422. http://www.ncbi.nlm.nih.gov/pubmed/24710281.

Ramos, Ó.L., J.C. Fernandes, S.I. Silva, M.E. Pintado, and F.X. Malcata. 2012. Edible Films and Coatings from Whey Proteins: A Review on Formulation, and on Mechanical and Bioactive Properties. Critical Reviews in Food Science and Nutrition 52, no. 6: 533–552.

Rebouillat, S., and S. Ortega-requena. 2015. Potential Applications of Milk Fractions and Valorization of Dairy By-Products : A Review of the State-of-the-Art Available Data , Outlining the Innovation Potential from a Bigger Data Standpoint. Journal of Biomaterials and Nanobiotechnology 6, no. July: 176–203.

Rekha, M.R., and C.P. Sharma. 2009. Blood Compatibility and in Vitro Transfection Studies on Cationically Modified Pullulan for Liver Cell Targeted Gene Delivery. Biomaterials 30, no. 34 (December): 6655–6664. http://linkinghub.elsevier.com/retrieve/pii/S0142961209008564.

Ren, K., Y. Wang, T. Sun, W. Yue, and H. Zhang. 2017. Electrospun PCL/Gelatin Composite Nanofiber Structures for Effective Guided Bone Regeneration Membranes. Materials Science and Engineering: C 78 (September): 324–332. http://linkinghub.elsevier.com/retrieve/pii/S0928493117309724.

Reneker, D., and H. Fong. 2006. Polymeric Nanofibers: Introduction.

Reneker, D.H., and I. Chun. 1996. Nanometre Diameter Fibres of Polymer, Produced by Electrospinning. Nanotechnology 7, no. 3: 216. http://stacks.iop.org/0957-4484/7/i=3/a=009.

Reneker, D.H., and A.L. Yarin. 2008. Electrospinning Jets and Polymer Nanofibers. Polymer 49, no. 10 (May): 2387–2425. http://linkinghub.elsevier.com/retrieve/pii/S0032386108001407.

Reneker, D.H., A.L. Yarin, H. Fong, and S. Koombhongse. 2000a. Bending Instability of Electrically Charged Liquid Jets of Polymer Solutions in Electrospinning. Journal of Applied Physics 87, no. 9: 4531–4547. http://link.aip.org/link/JAPIAU/v87/i9/p4531/s1&Agg=doi.

———. 2000b. Bending Instability of Electrically Charged Liquid Jets of Polymer Solutions in Electrospinning. Journal of Applied Physics 87, no. 9 (May): 4531–4547. http://aip.scitation.org/doi/10.1063/1.373532.

Ritcharoen, W., Y. Thaiying, Y. Saejeng, I. Jangchud, R. Rangkupan, C. Meechaisue, and P. Supaphol. 2008. Electrospun Dextran Fibrous Membranes. Cellulose 15, no. 3: 435–444.

Sakata, Y., and M. Otsuka. 2009. Evaluation of Relationship between Molecular Behaviour and Mechanical Strength of Pullulan Films. International Journal of Pharmaceutics 374, no. 1–2: 33–38.

Saquing, C.D., C. Tang, B. Monian, C.A. Bonino, J.L. Manasco, E. Alsberg, and S.A. Khan. 2013. Alginate-Polyethylene Oxide Blend Nanofibers and the Role of the Carrier Polymer in Electrospinning. Industrial and Engineering Chemistry Research 52, no. 26: 8692–8704.

Schiffman, J.D., and C.L. Schauer. 2008. A Review: Electrospinning of Biopolymer Nanofibers and Their Applications. Polymer Reviews 48, no. 2: 317–352.

Segura-Nieto, M., A.P. Barba De La Rosa, and O. Paredes-López. 1994. Biochemistry of Amaranth Proteins. In Amaranth: Biology, Chemistry and Technology, 75–106. CRC Press: Boca Raton, FL.

Selling, G.W., A. Biswas, A. Patel, D.J. Walls, C. Dunlap, and Y. Wei. 2007. Impact of Solvent on Electrospinning of Zein and Analysis of Resulting Fibers. Macromolecular Chemistry and Physics 208, no. 9: 1002–1010.

Semo, E., E. Kesselman, D. Danino, and Y.D. Livney. 2007. Casein Micelle as a Natural Nano-Capsular Vehicle for Nutraceuticals. Food Hydrocolloids 21, no. 5–6: 936–942.

Shao, C., H.Y. Kim, J. Gong, B. Ding, D.R. Lee, and S.J. Park. 2003. Fiber Mats of Poly(Vinyl Alcohol)/Silica Composite via Electrospinning. Materials Letters 57, no. 9–10: 1579–1584.

Shenoy, S.L., W.D. Bates, H.L. Frisch, and G.E. Wnek. 2005. Role of Chain Entanglements on Fiber Formation during Electrospinning of Polymer Solutions: Good Solvent, Non-Specific Polymer-Polymer Interaction Limit. Polymer 46, no. 10: 3372–3384.

Shin, T.R. 2008. Properties of a Model Zein-Based Chewing Gum Investigated by Objective and Sensory Methods. University of Illinois at Urbana-Champaign.

Shin, Y., M. Hohman, M. Brenner, and G. Rutledge. 2001. Experimental Characterization of Electrospinning: The Electrically Forced Jet and Instabilities. Polymer 42, no. 25: 09955–09967.

Shingel, K.I. 2004. Current Knowledge on Biosynthesis, Biological Activity, and Chemical Modification of the Exopolysaccharide, Pullulan. Carbohydrate Research 339, no. 3: 447–460.

Shukla, R., and M. Cheryan. 2001. Zein: The Industrial Protein from Corn. Industrial Crops and Products 13, no. 3: 171–192.

Siew, D.C.W., C. Heilmann, A.J. Easteal, and R.P. Cooney. 1999. Solution and Film Properties of Sodium Caseinate/Glycerol and Sodium Caseinate/Polyethylene Glycol Edible Coating Systems. Journal of Agricultural and Food Chemistry 47, no. 8: 3432–3440.

Sill, T.J., and H.A. von Recum. 2008. Electrospinning: Applications in Drug Delivery and Tissue Engineering. Biomaterials 29, no. 13: 1989–2006.

Singh, N.K., Donovan,G. R., Batey, I. L., MacRitchie, F., I.L. Batey, G.R. Donovan, F. MacRitchie, and N.K. Singh. 1990. Use of Sonication and Size-Exclusion High-Performance Liquid Chromatography in the Study of Wheat Flour Proteins. I. Dissolution of Total Proteins in the Absence of Reducing Agents. Cereal CHem.

Sionkowska, A. 2011. Current Research on the Blends of Natural and Synthetic Polymers as New Biomaterials: Review. Progress in Polymer Science (Oxford) 36, no. 9: 1254–1276. http://dx.doi.org/10.1016/j.progpolymsci.2011.05.003.

Soffer, L., X. Wang, X. Zhang, J. Kluge, L. Dorfmann, D.L. Kaplan, and G. Leisk. 2008. Silk-Based Electrospun Tubular Scaffolds for Tissue-Engineered Vascular Grafts. Journal of Biomaterials Science, Polymer Edition 19, no. 5 (January): 653–664. http://www.tandfonline.com/doi/abs/10.1163/156856208784089607.

Son, S.-R., R.-A. Franco, S.-H. Bae, Y.-K. Min, and B.-T. Lee. 2013. Electrospun PLGA/Gelatin Fibrous Tubes for the Application of Biodegradable Intestinal Stent in Rat Model. Journal of Biomedical Materials Research Part B: Applied Biomaterials 101B, no. 6 (August): 1095–1105. http://doi.wiley.com/10.1002/jbm.b.32923.

Song, J.-H., H.-E. Kim, and H.-W. Kim. 2008. Production of Electrospun Gelatin Nanofiber by Water-Based Co-Solvent Approach. Journal of Materials Science: Materials in Medicine 19, no. 1 (January 19): 95–102. http://link.springer.com/10.1007/s10856-007-3169-4.

Steffe, J.F. 1996. Rheological Methods in Food Process Engineering. Agricultural Engineering. Vol. 23. http://linkinghub.elsevier.com/retrieve/pii/0260877494900906.

Stijnman, A.C., I. Bodnar, and R. Hans Tromp. 2011. Electrospinning of Food-Grade Polysaccharides. Food Hydrocolloids 25, no. 5: 1393–1398. http://dx.doi.org/10.1016/j.foodhyd.2011.01.005.

Subbiah, T., G.S. Bhat, R.W. Tock, S. Parameswaran, and S.S. Ramkumar. 2005. Electrospinning of Nanofibers. Journal of Applied Polymer Science 96, no. 2: 557–569.

Sullivan, S.T., C. Tang, A. Kennedy, S. Talwar, and S.A. Khan. 2014. Electrospinning and Heat Treatment of Whey Protein Nanofibers. Food Hydrocolloids 35: 36–50. http://dx.doi.org/10.1016/j.foodhyd.2013.07.023.

Sun, B., Y.Z. Long, H.D. Zhang, M.M. Li, J.L. Duvail, X.Y. Jiang, and H.L. Yin. 2014. Advances in Three-Dimensional Nanofibrous Macrostructures via Electrospinning. Progress in Polymer Science 39, no. 5: 862–890.

Swaisgood, H.E. 1993. Review and Update of Casein Chemistry. Journal of Dairy Science 76, no. 10: 3054–3061. http://dx.doi.org/10.3168/jds.S0022-0302(93)77645-6.

———. 2003. Chemistry of the Caseins. In Advanced Dairy Chemistry—1 Proteins, 139–201. Springer.

Tan, E.P.S., S.Y. Ng, and C.T. Lim. 2005. Tensile Testing of a Single Ultrafine Polymeric Fiber. Biomaterials 26, no. 13: 1453–1456.

Tan, S.H., R. Inai, M. Kotaki, and S. Ramakrishna. 2005. Systematic Parameter Study for Ultra-Fine Fiber Fabrication via Electrospinning Process. Polymer 46, no. 16: 6128–6134.

Tavares, G.M., T. Croguennec, A.F. Carvalho, and S. Bouhallab. 2014. Milk Proteins as Encapsulation Devices and Delivery Vehicles: Applications and Trends. Trends in Food Science and Technology 37, no. 1: 5–20.

Taylor, G. 1966. Studies in Electrohydrodynamics. I. The Circulation Produced in a Drop by Electric Field. Proceedings of the Royal Society of London. Series A. Mathematical and Physical Sciences 291, no. 1425: 159–166.

Taylor, T.D., and A. Acrivos. 1964. On the Deformation and Drag of a Falling Viscous Drop at Low Reynolds Number. Journal of Fluid Mechanics 18, no. 03 (March 28): 466. http://www.journals.cambridge.org/abstract_S0022112064000349.

Thomar, P., D. Durand, L. Benyahia, and T. Nicolai. 2012. Slow Dynamics and Structure in Jammed Milk Protein Suspensions. Faraday Discussions 158, no. 1: 325–339.

Thomar, P., T. Nicolai, L. Benyahia, and D. Durand. 2013. Comparative Study of the Rheology and the Structure of Sodium and Calcium Caseinate Solutions. International Dairy Journal 31, no. 2: 100–106. http://dx.doi.org/10.1016/j.idairyj.2013.02.005.

Tomasula, P.M., N. Parris, W. Yee, and D. Coffin. 1998. Properties of Films Made from CO2-Precipitated Casein. Journal of Agricultural and Food Chemistry 46, no. 11: 4470–4474.

Tomasula, P.M., A.M.M. Sousa, S.C. Liou, R. Li, L.M. Bonnaillie, and L. Liu. 2016. Short Communication: Electrospinning of Casein/Pullulan Blends for Food-Grade Applications. Journal of Dairy Science 99, no. 3: 1837–1845.

Tonda-Turo, C., E. Cipriani, S. Gnavi, V. Chiono, C. Mattu, P. Gentile, I. Perroteau, M. Zanetti, and G. Ciardelli. 2013. Crosslinked Gelatin Nanofibres: Preparation, Characterisation and in Vitro Studies Using Glial-like Cells. Materials Science and Engineering C 33, no. 5: 2723–2735. http://dx.doi.org/10.1016/j.msec.2013.02.039.

Torres-Giner, S., A. Martinez-Abad, M.J. Ocio, and J.M. Lagaron. 2010. Stabilization of a Nutraceutical Omega-3 Fatty Acid by Encapsulation in Ultrathin Electrosprayed Zein Prolamine. Journal of Food Science 75, no. 6.

Uniacke-Lowe, T., T. Huppertz, and P.F. Fox. 2010. Equine Milk Proteins: Chemistry, Structure and Nutritional Significance. International Dairy Journal 20, no. 9: 609–629.

Varesano, A., A. Aluigi, C. Vineis, and C. Tonin. 2008. Study on the Shear Viscosity Behavior of Keratin/PEO Blends for Nanofibre Electrospinning. Journal of Polymer Science Part B: Polymer Physics 46, no. 12 (June 15): 1193–1201. http://doi.wiley.com/10.1002/polb.21452.

Varnam, A., and J.P. Sutherland. 2001. Milk and Milk Products: Technology, Chemistry and Microbiology. Vol. 1. Springer Science & Business Media.

Vaz, C.M., M. Fossen, R.F. Van Tuil, L.A. De Graaf, R.L. Reis, and A.M. Cunha. 2003. Casein and Soybean Protein-based Thermoplastics and Composites as Alternative Biodegradable Polymers for Biomedical Applications. Journal of Biomedical Materials Research Part A 65, no. 1: 60–70.

Vega-Lugo, A.-C., and L.-T. Lim. 2008. Electrospinning of Soy Protein Isolate Nanofibers. Journal of Biobased Materials and Bioenergy 2, no. 3 (September 1): 223–230. http://openurl.ingenta.com/content/xref?genre=article&issn=1556-6560&volume=2&issue=3&spage=223.

Vega-Lugo, A.C., and L.T. Lim. 2012. Effects of Poly(Ethylene Oxide) and PH on the Electrospinning of Whey Protein Isolate. Journal of Polymer Science, Part B: Polymer Physics 50, no. 16: 1188–1197.

Vega-Lugo, A. Cristina, and L.T. Lim. 2009. Controlled Release of Allyl Isothiocyanate Using Soy Protein and Poly(Lactic Acid) Electrospun Fibers. Food Research International 42, no. 8: 933–940. http://dx.doi.org/10.1016/j.foodres.2009.05.005.

Walsh, M.K., and H.E. Swaisgood. 1996. Investigating the Use of the Chymosin-Sensitive Sequence of κ-Casein as a Cleavable Linker Site in Fusion Proteins. Journal of Biotechnology 45, no. 3: 235–241.

Wang, Y., and L. Chen. 2012a. Fabrication and Characterization of Novel Assembled Prolamin Protein Nanofabrics with Improved Stability, Mechanical Property and Release Profiles. Journal of Materials Chemistry 22, no. 40: 21592. http://xlink.rsc.org/?DOI=c2jm34611g.

———. 2012b. Electrospinning of Prolamin Proteins in Acetic Acid: The Effects of Protein Conformation and Aggregation in Solution. Macromolecular Materials and Engineering 297, no. 9 (September): 902–913. http://doi.wiley.com/10.1002/mame.201100410.

Wang, Y., W. Zhang, J. Yuan, and J. Shen. 2016. Differences in Cytocompatibility between Collagen, Gelatin and Keratin. Materials Science and Engineering C 59: 30–34. http://dx.doi.org/10.1016/j.msec.2015.09.093.

Weiss, J., K. Kanjanapongkul, S. Wongsasulak, and T. Yoovidhya. 2012. Electrospun Fibers: Fabrication, Functionalities and Potential Food Industry Applications. In Nanotechnology in the Food, Beverage and Nutraceutical Industries, 362–397. Elsevier.

Wendorff, J., S. Agarwal, and A. Greiner. 2012. Electrospinning. Materials, Processing, and Applications.

Woerdeman, D.L., S. Shenoy, and D. Breger. 2007. Role of Chain Entanglements in the Electrospinning of Wheat Protein-Poly(Vinyl Alcohol) Blends. Journal of Adhesion 83, no. 8: 785–798.

Woerdeman, D.L., P. Ye, S. Shenoy, R.S. Parnas, G.E. Wnek, and O. Trofimova. 2005. Electrospun Fibers from Wheat Protein: Investigation of the Interplay between Molecular Structure and the Fluid Dynamics of the Electrospinning Process. Biomacromolecules 6, no. 2: 707–712.

Wolf, W.J. 1970. Soybean Proteins : Their Functional, Chemical, and Physical Properties. J. Agr. Food Chem. 18, no. 6: 969–976.

Wongsasulak, S., K.M. Kit, D.J. McClements, T. Yoovidhya, and J. Weiss. 2007. The Effect of Solution Properties on the Morphology of Ultrafine Electrospun Egg Albumen-PEO Composite Fibers. Polymer 48, no. 2: 448–457.

Wongsasulak, S., M. Patapeejumruswong, J. Weiss, P. Supaphol, and T. Yoovidhya. 2010. Electrospinning of Food-Grade Nanofibers from Cellulose Acetate and Egg Albumen Blends. Journal of Food Engineering 98, no. 3: 370–376. http://dx.doi.org/10.1016/j.jfoodeng.2010.01.014.

Wool, R.P. 1993. Polymer Entanglements. Macromolecules 26: 1564–1569. http://www.annualreviews.org/page/help/deleted_doi.

Wu, J., F. Zhong, Y. Li, C.F. Shoemaker, and W. Xia. 2013. Preparation and Characterization of Pullulan–Chitosan and Pullulan–Carboxymethyl Chitosan Blended Films. Food Hydrocolloids 30, no. 1: 82–91.

Xie, J., and Y. Lo Hsieh. 2003. Ultra-High Surface Fibrous Membranes from Electrospinning of Natural Proteins: Casein and Lipase Enzyme. Journal of Materials Science 38, no. 10: 2125–2133.

Xu, L., N. Sheybani, S. Ren, G.L. Bowlin, W.A. Yeudall, and H. Yang. 2015. Semi-Interpenetrating Network (SIPN) Co-Electrospun Gelatin/Insulin Fiber Formulation for Transbuccal Insulin Delivery. Pharmaceutical Research 32, no. 1 (January 17): 275–285. http://link.springer.com/10.1007/s11095-014-1461-9.

Xue, J., M. He, H. Liu, Y. Niu, A. Crawford, P.D. Coates, D. Chen, R. Shi, and L. Zhang. 2014. Drug Loaded Homogeneous Electrospun PCL/Gelatin Hybrid Nanofiber Structures for Anti-Infective Tissue Regeneration Membranes. Biomaterials 35, no. 34: 9395–9405. http://dx.doi.org/10.1016/j.biomaterials.2014.07.060.

Yang, Q., Z. Li, Y. Hong, Y. Zhao, S. Qiu, C.E. Wang, and Y. Wei. 2004. Influence of Solvents on the Formation of Ultrathin Uniform Poly (Vinyl Pyrrolidone) Nanofibers with Electrospinning. Journal of Polymer Science Part B: Polymer Physics 42, no. 20: 3721–3726.

Yao, C., X. Li, and T. Song. 2007. Fabrication of Zein/Hyaluronic Acid Fibrous Membranes by Electrospinning. Journal of Biomaterials Science, Polymer Edition 18, no. 6 (January): 731–742. http://www.tandfonline.com/doi/abs/10.1163/156856207781034070.

Yördem, O.S., M. Papila, and Y.Z. Menceloğlu. 2008. Effects of Electrospinning Parameters on Polyacrylonitrile Nanofiber Diameter: An Investigation by Response Surface Methodology. Materials and Design 29, no. 1: 34–44.

Zhang, S., Y. Huang, X. Yang, F. Mei, Q. Ma, G. Chen, S. Ryu, and X. Deng. 2009. Gelatin Nanofibrous Membrane Fabricated by Electrospinning of Aqueous Gelatin Solution for Guided Tissue Regeneration. Journal of Biomedical Materials Research. Part A 90: 671–679.

Zhang, Y.Z., J. Venugopal, Z.M. Huang, C.T. Lim, and S. Ramakrishna. 2006. Crosslinking of the Electrospun Gelatin Nanofibers. Polymer 47, no. 8: 2911–2917.

Zong, X., K. Kim, D. Fang, S. Ran, B.S. Hsiao, and B. Chu. 2002. Structure and Process Relationship of Electrospun Bioabsorbable Nanofiber Membranes. Polymer 43, no. 16: 4403–4412.